

职工号： 2008114733

# 西北农林科技大学职称任职资格

## 佐 证 材 料

(教师岗位系列)

单 位 农学院

姓 名 郭东伟

现任职资格 副教授

申报资格 教 授

岗位类型 教学科研型教师

## 材料清单

一、个人基本情况

二、教学工作情况

三、科研工作

3.1 代表性论文

3.2 品种审定证书

3.3 获奖情况

3.4 项目合同

四、推广工作

博士研究生

# 毕业证书



研究生 郭东伟

性别男

一九七三年三月

七日生，于

二〇〇三年九月至二〇〇六年十二月在

作物遗传育种

专业学习，学制四年，修完博士研究生培养计划规定的全部课程，成绩合格，  
毕业论文答辩通过，准予毕业。

培养单位：

西北农林科技大学

校(院、所)长：

孙武子

证书编号：

107121200601000161

二〇〇六年

十二月二十三日



12分

# 荣誉证书

李博永、李星、范君、严圣吉、李津源：

在 2019 年参加由中国作物学会主办的第二届全国农科学子创新创业大赛“中国农业 2025”乡村振兴创业赛道西北片区复赛当中表现突出，荣获

## 二等奖

特发此证，以资鼓励。

指导老师：郭东伟

中国作物学会

二〇一九年六月



高等学校国家级实验教学示范中心  
联席会

NATIONAL DEMONSTRATION CENTER FOR EXPERIMENTAL EDUCATION

# 证书

125

为表彰第四届全国大学生生命科学创新创业大赛优秀成果  
奖获得者，特颁发此证书。

作品名称：基于互联网形式的玉米深加工项目

获奖者：李博永 李津源 李星 严圣吉 范君

学 校：西北农林科技大学

获奖等级：三等奖(创业类)

证书编号：NDC2019CXCXY01450

指导老师：郭东伟

教育部高等学校生物技术、生物工程类专业教学指导委员会

教育部高等学校食品科学与工程类专业教学指导委员会

高等学校国家级实验教学示范中心联席会

《高校生物学教学研究》编辑部

2019年7月19日





高等学校国家级实验教学示范中心  
—— 联席会 ——

NATIONAL DEMONSTRATION CENTER FOR EXPERIMENTAL EDUCATION

# 证书

**为表彰第四届全国大学生生命科学创新创业大赛优秀成果  
奖获得者，特颁发此证书。**

**作品名称：**基于互联网形式的玉米深加工项目

**指导教师：**郭东伟

**学 校：**西北农林科技大学

**获奖等级：**指导教师三等奖(创业类)

**证书编号：**NDC2019CXCXY03109

教育部高等学校生物技术、生物工程类专业教学指导委员会

教育部高等学校食品科学与工程类专业教学指导委员会

高等学校国家级实验教学示范中心联席会

《高校生物学教学研究》编辑部

2019 年 7 月 19 日

# 获奖证书



《基于互联网形式的玉米深加工项目》项目在第五届“互联网+”大学生创新创业大赛西北农林科技大学校级决赛中荣获铜奖（主赛道），特发此奖，以资鼓励。

团队成员：李博永 严圣吉 李津源 李 星 范 君

指导教师：郭东伟

共青团西北农林科技大学委员会

2019年9月学  
委员会





西北农林科技大学  
NORTHWEST A&F UNIVERSITY

## 荣誉证书

李思路 同学：

你的本科毕业论文（设计）《马铃薯  
MADS-BOX 基因家族的全基因组分析》被评为  
我校 2016 届校级优秀本科毕业论文（设计），  
特发此证。

西北农林科技大学

教务处

二〇一六年六月

地址：中国陕西杨凌示范区西农路22号 邮编：712100 电话：+86-29-87091823

Address : No. 22 Xinong Road, Yangling, Shaanxi, China Postcode : 712100 Tel : +86-29-87091823





西北农林科技大学  
NORTHWEST A&F UNIVERSITY

# 荣誉证书

张政权 同学：

你的本科毕业论文（设计）《玉米 SIM 基因的  
表达特征分析》被评为我校 2016 届校级  
优秀本科毕业论文（设计），特发此证。

西北农林科技大学

教务处

二〇一六年六月

ISSN 1003-0174  
CODEN ZLXUFO  
CN 11-2864/TS

□ ZHONGGUO LIANGYOU XUEBAO

# 中国粮油学报



JOURNAL OF  
THE CHINESE CEREALS AND OILS ASSOCIATION

2016

|第31卷 第10期|

Vol.31 No.10



主管单位

中国科学技术协会

主办单位

中国粮油学会

编辑出版

《中国粮油学报》编辑部

主 编

胡承森

执行主编

于衍霞

本期责任编辑

孟永成

编 辑

孟永成 宗英俊 李伟丽

发 行

北京报刊发行局

邮发代号

80-720

中国标准刊号 ISSN 1003-0174  
CN 11-2864/TS

地 址

北京市西城区百万庄大街 11 号

邮 编

100037

电 话

010-68357510 68357810 68357507

传 真

010-68357510

电子信箱

lyxb@ccoaonline.com

lyxuebao@ccoaonline.com

bjb@ccoaonline.com

网 址

www.ccoaonline.com

www.lyxuebao.net

印 刷

北京时捷印刷有限公司

每期定价

56.00 元

# 中国粮油学报

1986 年创刊

2016 年 10 月 25 日第 31 卷第 10 期(月刊)

美国《化学文摘》(CA)收录

## 目 次

### 小麦研究

小麦麸皮阿拉伯木聚糖体外益生活性研究

刘丽娅 赵梦丽 钟 葵 佟立涛 周闲容 王丽丽 刘兴训

蔺艳君 张梅红 周素梅

(1)

Wx 基因对小麦淀粉合成关键酶活性的影响

覃 鹏 孔治有 刘叶菊 唐永生 杨俊华(6)

### 大豆研究

高油大豆与低油大豆油脂体组成及其稳定性的研究

梁新婷 江连洲 侯俊财 王胜男(11)

### 杂粮研究

燕麦品种的品质性状及聚类分析

倪香艳 顾军强 钟 葵 佟立涛 刘丽娅 周素梅(18)

### 淀粉研究

响应面优化  $\alpha$ -淀粉酶水解制备银杏抗性淀粉工艺研究 耿敬章(25)

葛根淀粉糊流变学特性的研究

钱晶晶 杜先锋(31)

玉米直链淀粉的分离与鉴定

钟雨越 张旭东 石涵羽 刘林三 吴权明 张仁和 徐淑兔

薛吉全 郭东伟

(39)

### 蛋白研究

葡萄糖糖基化大豆分离蛋白的凝胶抗冻性研究

杜昱蒙 陈振家 施小迪 徐婧婷 郭顺堂(45)

籼米黄淀粉中蛋白质的功能性质

杨有望 高文明 易翠平 谢 涛 周素梅(50)

### 油脂研究

大豆油和菜籽油中游离脂肪酸与烟点的数学关系研究

方 冰 朱宁科 王瑛瑶 栾 霞(56)

35 个栽培牡丹品种油用特性的评价研究

罗建让 张延龙 郭丽萍 牛立新(60)

亚临界水水解脱脂高温芝麻饼粕中蛋白与糖类研究

芦 鑫 孙 强 张丽霞 宋国辉 黄纪念(66)

油橄榄鲜果中主要化合物随成熟度的变化

邓俊琳 刘 露 刘 泉 向春蓉 丁春邦 李 天 杨泽身(73)

# 玉米直链淀粉的分离与鉴定

钟雨越 张旭东 石涵羽 刘林三 吴权明 张仁和 徐淑兔 薛吉全 郭东伟

(西北农林科技大学农学院 农业部西北旱区玉米生物学与遗传育种重点实验室,杨凌 712100)

**摘 要** 以高直链玉米淀粉和普通玉米淀粉为原料,比较凝沉法等 5 种提取方法在直链淀粉提取效率及品质上的差异。结果表明:在同一提取方法下,不同淀粉原料的直链淀粉平均提取率无明显差异;利用同种淀粉原料,5 种提取方法中以蒸馏分散法和 DMSO 盐析法提取率最高,分别为 33.22% 和 34.67%;高速凝沉法提取率最低,为 16.36%。不同提取方法获得的直链淀粉在蓝值、吸收光谱、扫描电镜(SEM)、X 射线衍射(XRD)5 个纯度参数上存在差异;提取率高的方法获得的直链淀粉往往纯度偏低,提取率低的方法获得的直链淀粉纯度高。综合考虑认为,高转速凝沉法和二甲基亚砷(DMSO)分散法优于其他 3 种方法。虽然提取率略低,但纯度更高。

**关键词** 高直链玉米淀粉 直链淀粉 分离 纯度 鉴定

**中图分类号:** TS201 **文献标识码:** A

**网络出版时间:** 2016-09-30 10:48:27

**网络出版地址:** <http://www.cnki.net/kcms/detail/11.2864.TS.20160930.1048.002.html>

直链淀粉是淀粉的重要组成部分,其含量对淀粉的分子结构、物理化学性质、加工特性有着重要影响。直链淀粉在食品加工过程中形成的抗性淀粉在小肠中难以被消化,使其具有了类似膳食纤维的生理功效<sup>[1]</sup>,能选择性地促进肠内有菌(如双歧杆菌)的生长繁殖,抑制结肠癌的发生<sup>[2]</sup>。另外,高直链淀粉(直链淀粉质量分数大于 50% 的淀粉)食品能够减少餐后血糖和胰岛素响应,降低血浆胆固醇和甘油三酯的浓度,因此,是糖尿病人的理想食品,被称为“功能性食品”<sup>[3]</sup>。在食品工业领域,用高直链玉米淀粉制成的低脂食品具有很好的流变学特性及稳定性,与全脂奶油产品具有相同的口感,因此可当作冰淇淋及蛋糕中脂肪的代替物<sup>[4]</sup>。此外,直链淀粉具有较好的抗拉伸性能,可取代聚苯乙烯用来生产光降解塑料,从而应用于包装业和薄膜加工业,有助于解决目前日益严重的“白色污染”<sup>[5]</sup>。

目前,市场上的直链淀粉主要从普通淀粉中提取,提取率低,而真正商品化的高纯直链淀粉仍鲜有出售,这极大限制了直链淀粉的加工和应用。为此,

本试验以自育的高直链淀粉玉米为原料,采用凝沉法(低转速、高转速)、蒸馏法、DMSO 法(分散、盐析法)等 5 种常用方法来提取直链淀粉,并且从提取率、蓝值、碘-淀粉复合物吸收光谱、扫描电子显微镜分析、晶体特性等方面比较 5 种方法的优劣,以期直链淀粉的规模化生产提供参考。

## 1 材料与方法

### 1.1 材料

S4126 普通玉米淀粉(直链淀粉质量分数 25%)、SC-254946A 马铃薯直链淀粉:Sigma 公司;高直链淀粉玉米(直链淀粉质量分数 53%):西北农林科技大学农业部西北旱区玉米生物学与遗传育种重点实验室。

### 1.2 方法

#### 1.2.1 高直链玉米淀粉的提取

玉米籽粒去除胚芽及种皮,加水研磨成糊后,经 100  $\mu\text{m}$  尼龙网过滤至 50 mL 离心管,2 000 r/min 离心 15 min,弃上清,加 0.5% 的 NaOH 溶液 20 mL 静置 4 h,4 000 r/min 离心 10 min,NaOH 溶液重复洗涤至上清无色,沉淀加 5 mL 丙酮 4 000 r/min 离心 10 min,去上清,通风橱内自然干燥后备用。

#### 1.2.2 直链淀粉的提取

##### 1.2.2.1 凝沉分离法

参考洪雁等的方法<sup>[6]</sup>,取原料淀粉 5 g,依次加

基金项目:杨凌示范区科技计划(2014NY-01),陕西省现代农业专项(K33202135),陕西省科技统筹专项(2015KTZDNY01-01-01)

收稿日期:2015-06-30

作者简介:钟雨越,男,1993 年出生,硕士,作物遗传育种

通讯作者:郭东伟,男,1973 年出生,副教授,高直链淀粉玉米育种



入 2 mL 无水乙醇和 350 mL 0.5 mol/L 的氢氧化钠,沸水浴中搅拌 10 min,冷却至室温后置于 -20 ℃ 冷冻 24 h,8 000 r/min 高速离心 15 min, HCl 溶液中和至中性,加 10 mL 丁醇-异戊醇(3:1)混合液,沸水浴搅拌 10 min,冷却至室温,4 ℃ 静置 24 h,4 000 r/min 离心 10 min,沉淀移入丁醇饱和水溶液,加热溶解至溶液透明,冷却至室温后 4 ℃ 静置 24 h,分别以 4 000 r/min(低转速)和 8 000 r/min(高转速)离心,沉淀同法纯化 6 次后,再依次用 70 % 乙醇、95 % 乙醇和无水乙醇各洗涤 3 次,沉淀于真空冷冻干燥仪中干燥 24 h 备用。

#### 1.2.2.2 蒸馏分散法

参考 Liu 等<sup>[7]</sup>的方法,称量淀粉 5 g 于烧杯中,加蒸馏水 100 mL,沸水浴中搅拌至凝胶状,冷却到 50 ℃ 时,用磷酸缓冲液调 pH 到 6.5,于 100 ℃ 蒸煮 3 h 后在沸水浴中搅拌样品 2 h。将样品转移到 1 000 mL 圆底烧瓶并加适量正丁醇回流 1 h。当样品冷却到 50 ℃,将圆底烧瓶取出,自然冷却过夜。溶液转移到 50 mL 离心管,8 000 r/min 离心 30 min。弃上清,沉淀转移到 1 000 mL 圆底烧瓶,加正丁醇 80 mL 回流 1 h。重复离心和回流 2 次。去上清,沉淀在真空冷冻干燥机中干燥 24 h 备用。

#### 1.2.2.3 DMSO 分散法

参考杨泽敏等<sup>[8]</sup>的方法,5 g 淀粉加入适量 DMSO 后置于全温摇瓶柜中缓缓搅动 24 h,2 000 r/min 离心 15 min。取上清液注入 2 倍体积正丁醇,静置 24 h,4 000 r/min 离心 10 min。正丁醇洗涤沉淀 3 次,转入足量水中,加热至完全溶解,自然冷却至 60 ℃ 时加 8 g 百里酚,室温放置 3 d,4 000 r/min 离心 15 min。沉淀转入足量水中,加热至完全溶解,冷却后加入正丁醇 10 mL,室内静置 24 h,2 000 r/min 离心 10 min,无水乙醇洗涤 3 次,沉淀真空冷冻干燥机中干燥 24 h 获得直链淀粉。

#### 1.2.2.4 DMSO 盐析法

5 g 淀粉加入 40 mL DMSO 和 10 mL 去离子水,搅拌至乳液状转移至 60 ℃ 恒温水浴,持续搅拌 30 min 后,移除水浴,加 10 mL 正丁醇,混匀后冷却至室温,待溶液中析出细针型沉淀,2 000 r/min 离心 30 min,去上清,沉淀加 10 mL 2% NaCl,振荡混匀,缓慢加入 10 mL 正丁醇,涡旋混匀后,2 000 r/min 离心 30 min,重复结晶过程 6 次,真空冷冻干燥机中干燥 24 h 备用。

#### 1.3 直链淀粉质量测定

直链淀粉提取率 = 直链淀粉质量/原淀粉质量(干基)。

蓝值(mg/100 mL)测定:配制直链淀粉、支链淀粉和 CK 标准对照后,进行测定<sup>[9-11]</sup>。

蓝值 =  $A \times 4 / \text{样品的浓度}$

碘-淀粉复合物吸收光谱:以蓝值测定所用的标准溶液于 500 ~ 800 nm 进行连续光谱扫描分析。

晶体特性的测定:X-衍射条件:Cuka 辐射,管压 40 kV,管流 40 mA,扫描速度 4 (°)/min。淀粉样品粉碎后通过 60 目筛。

扫描电子显微镜(SEM)分析:将干燥样品充分混合,均匀黏附于样品台表面,离子溅射仪喷金固定 8 min,扫描电子显微镜(HITACHI SN3500)检测成像。

## 2 结果与讨论

### 2.1 原料及方法对提取率的影响

结果如表 1 所示,不同方法的提取率存在显著差异。以 DMSO 盐析法和蒸馏分散法最高,当分别用普通玉米淀粉和高直链淀粉为原料时,提取率依次为 22.67%、22.70% 和 46.67%、43.73%,显著高于其他 3 种方法。以高速凝沉法提取率最低,平均提取率仅 16.36%。以从普通淀粉(相对直链淀粉质量分数 25%)和高直链淀粉(相对直链淀粉质量分数 53%)实际抽提直链淀粉的量占这 2 种淀粉中总直链淀粉量(分别为 1.25、2.65 g)的百分比计算直链淀粉提取率时,普通淀粉 5 种方法的平均提取率为 63.46%,高直链淀粉为 64.88%,二者在提取率上没有明显差异。这说明高直链淀粉中,直链淀粉在淀粉粒中的分布方式可能与普通淀粉类似,这种直链淀粉含量的差异并未对直链淀粉的提取率带来明显影响。

表 1 普通玉米淀粉和高直链玉米淀粉的直链淀粉提取率

材料	质量/g	普通玉米淀粉		高直链玉米淀粉	
		提取/g	提取率/%	提取/g	提取率/%
低速凝沉法(LRP)	5.00	0.598	11.83 ± 2.3b	1.742	34.91 ± 3.7b
高速凝沉法(HRP)	5.00	0.580	11.60 ± 0.8b	1.055	21.02 ± 2.8d
蒸馏分散法(DD)	5.00	1.146	22.70 ± 2.0a	2.172	43.73 ± 3.6a
DMSO 分散法(DMD)	5.00	0.489	9.85 ± 2.8b	1.360	27.33 ± 3.2c
DMSO 盐析法(DMS)	5.00	1.153	22.67 ± 3.2a	2.269	46.67 ± 6.1a

注:所有数据均为 3 次重复的平均值。不同字母表示差异显著( $P < 0.05$ )。

### 2.2 不同提取方法对直链淀粉蓝值的影响

蓝值是表征直链淀粉纯度的重要指标之一,它体现了淀粉与碘的结合能力。通常线性聚合度越高,蓝值越高。理论上直链淀粉蓝值在 0.8 ~ 1.2 之间,本研究中,不同方法提取的直链淀粉蓝值在

0.78~1.11间,LRP法的蓝值为0.78,HRP的蓝值为0.84,DD的蓝值为0.83,DMD的蓝值为1.11,DMS的蓝值为0.91,均低于对照马铃薯直链淀粉1.19的蓝值。其中以DMSO分散法提取的直链淀粉蓝值与马铃薯标准直链淀粉的蓝值最相近,表明此法获得的直链淀粉纯度较高,以高转速凝沉法和DMSO盐析法提取的直链淀粉蓝值次之,分别达到0.94和0.91。低转速凝沉法的蓝值最低为0.78,表明此法获得的直链淀粉纯度低于其他方法。

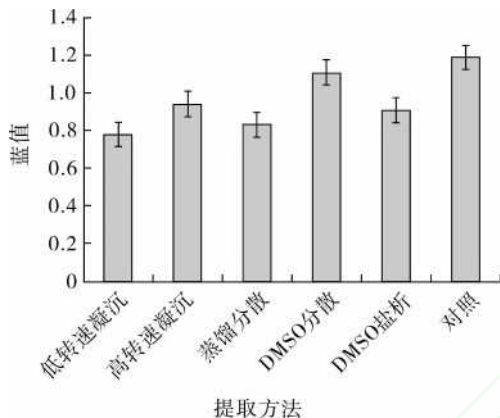
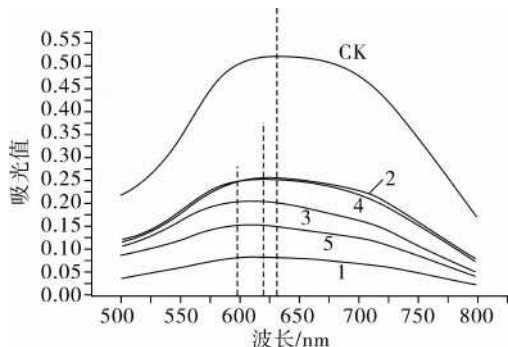


图1 不同方法提取直链淀粉的蓝值

## 2.3 不同提取方法对直链淀粉吸收光谱的影响

利用直链淀粉和支链淀粉与碘形成的复合物在紫外分光光度计扫描下形成的最大吸收波长差异也可进行直链淀粉纯度判定。研究表明,直链淀粉-碘复合物吸收峰通常在600~680 nm之间,而直链淀粉的最大吸收波长为630 nm<sup>[12-14]</sup>。图2展示了5种方法提取玉米直链淀粉及对照马铃薯直链淀粉的全波长扫描光谱图。其中对照马铃薯直链淀粉的吸收波长峰值为628 nm,最接近630 nm的标准值;其次为高转速凝沉法和DMSO分散法提取直链淀粉的吸收波长峰值,约为623 nm,表明这2种方法提取的直链淀粉纯度较高;其余3种方法获得的直链淀粉



注:1 低转速凝沉法,2 高转速凝沉法,3 蒸馏分散法,4 DMSO分散法,5 DMSO盐析法。

图2 不同方法提取直链淀粉的吸收光谱

吸收波长峰值在600 nm左右,这可能是由于这3种方法提取的直链淀粉中掺杂有支链淀粉、蛋白等杂质。

## 2.4 不同提取方法对直链淀粉晶体特性的影响

X射线衍射(XRD)是分析晶体结构的有效方法之一。淀粉颗粒的X晶体衍射图谱上在多处衍射角存在吸收峰,代表了淀粉的结晶区域,根据2 $\theta$ 角衍射峰的分布可将原淀粉的晶体结构划分为A、B和C型。当淀粉经过变性处理时,原有晶体结构被破坏并发生重结晶,晶体结构会变为V型<sup>[15]</sup>。图3的检测结果表明,提取方法及材料来源对淀粉粒的晶体类型存在显著影响,自提直链淀粉与对照马铃薯直链淀粉结晶构型均不同于原淀粉普通淀粉的A构型和高直链淀粉的B构型,属于重结晶的V构型,它们均在21°、23°、27°左右出现明显的衍射峰,而2种沉降法、蒸馏分散法和DMSO分散法4种方法提取的直链淀粉还在7°、13°附近出现明显的衍射峰,这与Bail等<sup>[16]</sup>报道的热熔淀粉的重结晶构型一致,属于Vh型晶体。

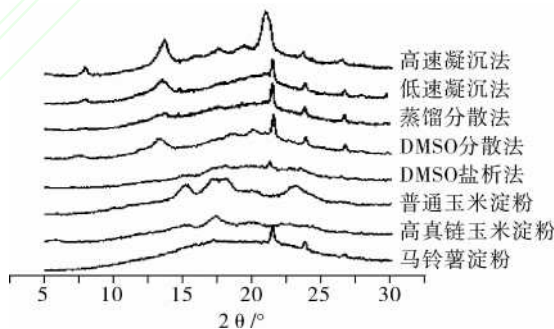


图3 5种方法提取直链淀粉的X射线衍射图谱

只有DMSO盐析法得到的淀粉构型与对照马铃薯直链淀粉的构型最接近,没有7°、13°附近的衍射峰,这说明对照马铃薯淀粉可能也是通过相同方法提取。X射线衍射图谱中衍射峰峰下区域的面积代表了晶体内非结晶区部分的比例,而峰面积代表了结晶区,因此晶体的结晶度随衍射峰的数量、宽度和高度的增高而增高<sup>[17]</sup>。根据表2的统计数据可以看出,在原淀粉中高直链淀粉的结晶度为15.48%明显低于普通淀粉的18.6%,这说明直链淀粉含量的增加和支链淀粉的减少改变了淀粉粒的构架组成,使淀粉的结晶度降低,这一结果与前人报道一致<sup>[16-17]</sup>。自提直链淀粉中以DMS法的结晶度最低仅为1.88%,也低于对照马铃薯淀粉2.34%的结晶度,其他4种方法提取的直链淀粉结晶度在18.60%~22.66%之间。

表2 不同方法提取直链淀粉的 X 晶体衍射参数

直链淀粉	2θ												晶型	结晶度
	6	7	13	15	17	18	20	21	22	23	24	26		
HRP		7.94	13.42		17.66		19.38	21.22			23.77	26.71	Vh	18.60
LRP		7.8	13.77					20.74			23.95	26.7	Vh	19.72
DD		7.66	13.47					21.22			23.95	26.72	Vh	22.66
DMD		7.49	13.12			18.62	20.09	21.52			23.77	27.20	Vh	21.18
DMS						18.31		21.52			24.01	26.66	V	1.88
NCS				15.22	16.99	18.20				23.31			A	18.60
HACS	6.18			15.72	17.88		19.89		22.73		23.94		B	15.48
PA								21.70			23.77	26.72	V	2.34

注:NCS 普通玉米淀粉;HACS 高直链玉米淀粉;PA 马铃薯直链淀粉。

2.5 不同来源直链淀粉 SEM 表观特征分析

SEM 图是表征颗粒表面形貌的有效手段,以扫描电镜观察原淀粉及提取直链淀粉颗粒的表面形貌如图 4 所示,原淀粉和提取直链淀粉颗粒的表面形貌存在很大差异,普通玉米原淀粉多呈球状(B 型颗粒直径 < 10 μm)或多面体状(A 型颗粒直径 > 10 μm),饱满,表面有蜡质光泽(图 4a)。高直链原淀粉颗粒则扭曲呈不规则形状,存在一定程度的皱缩,且在 A 型颗粒上发生的皱缩和扭曲程度似乎高于 B 型颗粒,淀粉粒表面也存在蜡质光泽(图 4b),这与前人的研究结果一致<sup>[18-19]</sup>。理论上直链淀粉以线性大

分子形式沉积于支链淀粉形成的骨架之间,当直链淀粉被析出或分散到提取体系中后,原有的淀粉颗粒结构被完全破坏,这些直链淀粉在正丁醇等凝沉剂的作用下,相互缠绕沉积成无固定形状的沉积物,经过脱水干燥等处理后,外观呈现白色的片层状颗粒,其 SEM 图片如图 4c ~ 图 4g 所示,颗粒呈现不规则形状,有明显的层状沉积痕迹,不同提取方法来源的直链淀粉颗粒仍然呈现一定程度的蜡质质感,不同提取方法间无可见差异。其结构特征均与对照马铃薯直链淀粉相似(图 4h)。

3 讨论

目前实验室中常用的直链淀粉的提取方法主要有凝沉法、分散法和盐析法,提取过程中的离心时间和速度对直链淀粉的提取质量均有较大影响。李德海等<sup>[20]</sup>以玉米淀粉为材料,用凝沉法提取直链淀粉时发现:8 000 ~ 8 500 r/min 是提取直链淀粉的最适转速,在 4 000 r/min 条件下得到的直链淀粉的蓝值仅为 0.8,远低于 8 000 r/min 的蓝值,这与本研究结果一致。蒸馏、DMSO 试剂都可以使淀粉分散。蒸馏法多适用与马铃薯直链淀粉提取,曾凡逵等<sup>[21]</sup>就以马铃薯为材料,使用蒸馏分散法得到吸收光谱峰值为 630 nm 的标准直链淀粉。杨泽敏等<sup>[8]</sup>曾用 DMSO 分散法提取水稻直链淀粉,却少见于玉米直链淀粉的提取。试验证明,DMSO 分散法适用于提取玉米直链淀粉,对蓝值、吸收光谱以及结晶度等的分析表明该方法得到的玉米直链淀粉具有很高纯度。

XRD 衍射法是检测颗粒晶体类型的常规方法,根据前人的研究原淀粉的晶体类型可分为 A、B、C 3 种,影响淀粉晶体结构的因素很多,如来源、淀粉组成、加工方式等。禾谷类作物淀粉通常为 A 型,马铃薯等块根类淀粉多为 B 型晶体,而豌豆、荸荠等淀粉为 C 型晶体;直链淀粉含量也影响淀粉的晶体结构,Norman 等<sup>[14]</sup>研究了不同直链淀粉含量的玉米淀粉

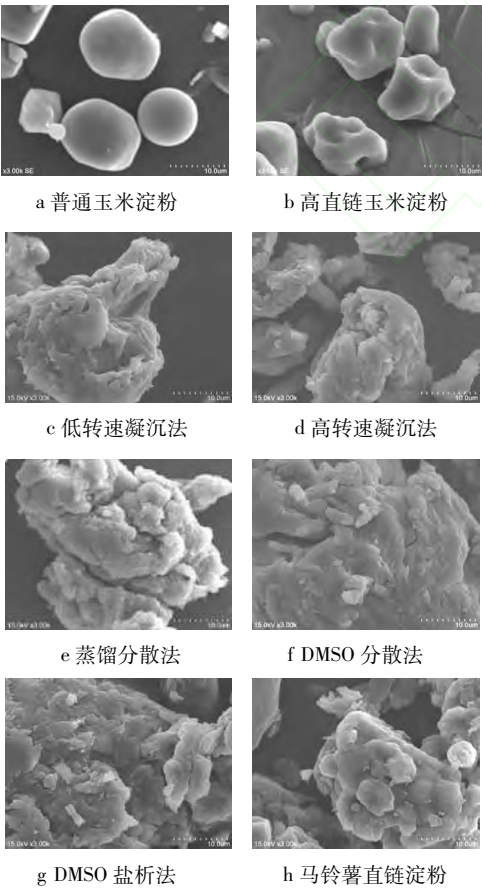


图4 提取直链淀粉 SEM 图



的 X 射线晶体衍射图谱,结果表明:随着直链淀粉含量的增加,玉米淀粉的晶体结构表现为一个由 A 型经 C 型转变为 B 型晶体的过程,当直链淀粉质量分数低于 40% 时,玉米淀粉为典型的 A 型晶体,直链淀粉质量分数超过 50%,淀粉的晶体结构为典型的 B 型。当直链淀粉被析出凝沉时,会发生重结晶,重结晶后的直链淀粉晶体结构完全不同于原淀粉的晶体结构。熊善柏等<sup>[25]</sup>测量了水稻直链淀粉的晶体特征,发现水稻直链淀粉在 2 $\theta$  角 13° 和 20° 左右存在明显衍射峰,结晶度在 24.99%~23.10% 之间,而支链淀粉只在 20° 处有明显吸收峰。这与研究结果存在一定差异,除 13° 和 20° 外,在 7° 和 23° 亦出现了吸收峰。但杜先锋等<sup>[26]</sup>的研究中,葛根的直链淀粉在 7° 和 23° 也存在吸收峰,说明直链淀粉来源对晶体特征也存在影响。

## 4 结论

不同直链淀粉含量的淀粉原料不影响直链淀粉的提取率。在 5 种提取方法中,高转速凝沉分离法和二甲亚砜(DMSO)分散法虽然提取率略低,但在蓝值、吸收波峰、电镜图像、结晶度等参数上优于其他 3 种方法。

## 参考文献

- [1] Park O J, Kang N E, Chang M J. Resistant starch supplementation influences blood lipid concentrations and glucose control in overweight subjects[J]. J Nutr Sci vitaminol (Tokyo), 2004, 50(2): 93-9
- [2] 王晓睿. 非淀粉多糖和抗性淀粉在断奶仔猪日粮中的应用研究[D]. 保定:河北农业大学, 2004  
Wang Xiaorui. Studies on Application of Non-starch Polysaccharides and resistant Starch in the Diets of Young Weaned Piglets[D]. Baoding: Agricultural University of Hebei, 2004
- [3] 吴建平. 抗消化淀粉的研究进展及其应用前景[J]. 食品与发酵工业, 1999, 25(2): 66-70  
Wu Jianping. Advances in the Research of Resist Starch and Its Prospective Uses[J]. Food and Fermentation Industries, 1999, 25(2): 66-70
- [4] 王中荣, 刘雄. 高直链淀粉性质及其应用研究[J]. 粮食与油脂, 2005(11): 10-13  
Wang Zhongrong, Liu Xiong. Study On Properties and Application of High Amylose Starch. Cereals and Oils, 2005(11): 10-13
- [5] 王振斌. 高直链淀粉玉米的应用前景及展望[J]. 科技致富向导, 2013, 11(16): 103  
Wang Zhenbin. Advances and Prospects of High Amylose Corn Starch[J]. Guide of Sci-tech Magazine, 2013, 11(16): 103
- [6] 洪雁, 顾正彪, 刘晓欣. 直链淀粉和支链淀粉纯品的提取及其鉴定[J]. 食品工业科技, 2004(4): 86-88  
Hong Yan, Gu Zhengbiao, Liu Xiaoxin. Extraction and evaluation of amylose and amylopectin[J]. Science and Technology of Food Industry, 2004(4): 86-88
- [7] Liu Q, Donner E, Tam R, et al. Advanced analytical techniques to evaluate the quality of potato and potato starch[J]. Advances in potato chemistry and technology, 2009(8): 221-248
- [8] 杨泽敏, 王维金, 蓝盛银, 等. 稻米三种淀粉成分的分离及其蒸煮前后的结构差异[J]. 电子显微学报, 2003, 22(4): 286-292  
Yang Zemin, Wang Weijin, Lan Shengyin, et al. Separation of three types of starch fractions in rice and the microstructures of endosperms before and after gelatinization[J]. Journal of Chinese Electron Microscopy Society, 2003, 22(4): 286-292
- [9] Schoch T J. Methods in carbohydrate chemistry IV starch New York and London[J]. Academic Press, 1964: 157-160
- [10] Hizukuri S J. Recent advances in molecular structures of starch[J]. Jpn starch Sci, 1988, 35(3): 185-198
- [11] Hizukuri S. Polymodal distribution of the chain lengths of amylopectins and its significance[J]. Carbohydrate Research, 1986, 147: 342-347
- [12] Krishnaswamy K G, Sreenivasan A. Separation and determination of the amylose and amylopectin fractions of starch[J]. Amylose and Amylopectin Starch Fractions, 1948, 176: 1253-1261
- [13] 谢涛, 陈建华, 谢碧霞. 橡实直链淀粉与支链淀粉的分离纯化[J]. 中南林学院学报, 2002, 22(2): 30-35  
Xie Tao, Chen Jianhua, Xie Bixia. The separation and purification of amylose and amylopectin from acorn starch[J]. Journal of Central South Forestry University, 2002, 22(2): 30-35
- [14] 张娟, 唐文凭, 王正武, 等. 芭蕉芋淀粉和直链淀粉提取、分离、鉴定及含量测定[J]. 食品科学, 2008, 9: 303  
Zhang Juan, Tang Wenping, Wang Zhengwu, et al. Extraction, purification, characterization and content determination of starch and amylose from canna edulis ker, growing in China[J]. Food Science, 2008, 9: 303
- [15] Cheetham Norman W H, Tao L P. Variation in crystalline type with amylose content in maize starch granules: an X-ray powder diffraction study[J]. Carbohydrate Polymers, 1998, 36: 277-284
- [16] Bail Le P, Bizot H, Ollivon M, et al. Monitoring the crystallization of amylose-lipid complexes during maize starch melting by synchrotron X-ray diffraction[J]. Biopolymers, 1999, 50: 99-110
- [17] 满建民, 蔡金文, 徐斌, 等. 作物淀粉晶体结构的波谱分析[J]. 作物学报, 2012, 38(4): 691-698



- Man Jianmin, Cai Jinwen, Xu Bin, et al. Spectrum analysis of crystalline structure of crop starches[J]. *Acta Agonomica Sinica*, 2012, 38(4): 691–698
- [18]李志伟, 钟雨越, 吴权明, 等. 高直链淀粉玉米淀粉的理化特性研究[J]. *西北农林科技大学学报*, 2014, 7(6): 39–43
- Li Zhiwei, Zhong Yuyue, Wu Quanming, et al. Physicochemical properties of high – amylose maize starch [J]. *Journal of Northwest A&F University*, 2014, 7(6): 39–43
- [19]陈培荣, 朱苏文, 杜先锋, 等. 高直链玉米淀粉颗粒的形貌与结构[J]. *高分子材料科学与工程*, 2009, 25(12): 100–102
- Chen Peirong, Zhu Suwen, Du Xianfeng, et al. The granule morphology and structure of high amylose maize starch[J]. *Polymer Materials Science & Engineering*, 2009, 25(12): 100–102
- [20]李德海, 马莺. 玉米淀粉组分的分离及特性[J]. *食品工业科技*, 2011, 5: 122
- Li Dehai, Ma Ying. Separation and characteristic of the component of corn starch[J]. *Science and Technology of Food Industry*, 2011, 5: 122
- [21]曾凡逵, 赵鑫, 周添红, 等. 马铃薯直链/支链淀粉的分离[J]. *现代食品科技*, 2011, 27: 12
- Zeng Fankui, Zhao Xin, Zhou Tianhong, et al. Separation of potato Amylose and Amylopectin[J]. *Modern Food Science & Technology*, 2011, 27: 12
- [22]高伟丽, 赵燕, 李建科. 丁醇沉淀法分离粗直链淀粉的研究[J]. *食品科学*, 2007, 9: 271
- Gao Weili, Zhao Yan, Li Jianke. Study on separating coarse amylose by butanol precipitation[J]. *Food Science*, 2007, 9: 271
- [23]夏慧玲, 王水兴, 潘阳. 红薯直链淀粉的分离纯化和检测[J]. *食品研究与开发*, 2006, 27(11): 47–49
- Xia Huiling, Wang Shuixing, Pan Yang. The Separation and purification of amylose from potato starch[J]. *Food Research and Development*, 2006, 27(11): 47–49
- [24]张娟, 唐文凭, 王正武, 等. 芭蕉芋淀粉和直链淀粉提取、分离、鉴定及含量测定[J]. *食品科学*, 2008, 9: 303–30
- Zhang Juan, Tang Wenping, Wang Zhengwu, et al. Extraction, purification, characterization and cogent determination of starch and amylose from canna edulis ker. growing in China[J]. *Food Science*, 2008, 9: 303–30
- [25]熊善柏, 赵思明, 张声华. 稻米淀粉的理化特性研究 II 稻米直链淀粉和支链淀粉的理化特性[J]. *中国粮油学报*, 2003, 18(2): 5–8
- Xiong Shanbo, Zhao Siming, Zhang Shenghua. Study on the physicochemical properties of rice amylose and amylopectin [J]. *Journal of the Chinese Cereals and Oils Association*, 2003, 18(2): 5–8
- [26]杜先锋, 许时婴, 王璋. 葛根直链淀粉和支链淀粉分离纯化的研究[J]. *食品与发酵工艺*, 1998, 424: 18–21
- Du Xianfeng, Xu Shiyin, Wang Zhang. Separation and purification of amylose and amylopectin from pueraria lobata ohwi starch[J]. *Food and Fermentation Industries*, 1998, 424: 18–21.

## The Isolation and Identification of Maize Amylose

Zhong Yuyue Zhang Xudong Shi Hanyu Liu Linsan Wu Quanming

Zhang Renhe Xu Shutu Xue Jiquan Guo Dongwei

(The Key Laboratory of Biology and Genetic Improvement of Maize in Arid Area of Northwest

Region, Ministry of Agriculture, College of Agronomy, Northwest A&F University, Yang ling 712100)

**Abstract** In this paper, five methods including precipitation separation, etc. were employed to isolate amylose from maize high – amylose starch and normal starch. Differences in extraction efficiency and quality were compared. The results showed that there is no obvious difference in the average extraction rate of five extraction methods between maize high – amylose starch and normal starch. Distillation dispersion method and DMSO salting out method had the highest extraction rate (33.22% and 34.67%), while high – rpm precipitation separation method had the lowest extraction rate of 16.36%. In addition, there were obvious differences in five Purity parameters: blue value, absorption spectrum, SEM and XRD of amylose derived from different isolation method. In conclusion, despite of low extraction rates by precipitation separation method and DMSO dispersion method, the purity of amylose extracted by them is higher than the purity by using remaining three methods.

**Key words** high – amylose maize starch, amylose, isolation, purity, identification



# 中国粮油学报 JOURNAL OF THE CHINESE CEREALS AND OILS ASSOCIATION

- |                          |                           |
|--------------------------|---------------------------|
| ◎ 全国食品工业类中文核心期刊          | ◎ 中国科技期刊精品数据库             |
| ◎ 中国科技论文统计源期刊 (中国科技核心期刊) | ◎ 中国期刊全文数据库全文收录期刊         |
| ◎ 中国科学引文数据库来源期刊          | ◎ 中国学术期刊综合评价数据库           |
| ◎ 万方数据库全文收录期刊            | ◎ 《中国生物学文摘》和中国生物学文摘数据库    |
| ◎ 《中国期刊网》全文收录期刊          | ◎ 中国农业核心期刊                |
| ◎ 中国学术期刊 (光盘版) 全文收录期刊    | ◎ 美国《化学文摘》(CA) 固定收录源刊     |
| ◎ 中国学术期刊综合评价数据库来源期刊      | ◎ CBST科学技术文献速报 (日) 收录源刊   |
| ◎ 中国科技论文数据库固定收录期刊        | ◎ 英国《食品科技文摘》(FSTA) 固定收录源刊 |

## 中国粮油学会《中国粮油学报》

地址: 北京市西城区百万庄大街11号粮科大厦 (100037)

电话: 010-68357510

投稿平台: <http://www.lyxuebao.net>

电子邮件: [lyxuebao@163.com](mailto:lyxuebao@163.com)

ISSN 1003-0174



邮发代号 80-720



西北农林科技大学教学改革与研究项目

结 题 证 书

编号: JY1503003

项目名称: 《植物组织与细胞培养》精品课程的建设及创新教学改革研究

项目类别: 一般

项目负责人: 李春莲

项目成员: 陈耀锋 郭东伟 徐淑兔 汪勇

验收结果: 合格

西北农林科技大学教务处

二〇一七年十二月



ISSN 1674-9324  
CN 13-1399/G4

JIADYU JIAOXUE LUNTAN

# 教育教学论坛

2019年12月  
第50期

EDUCATION TEACHING FORUM

中  
万  
维  
龙  
博

国  
方  
源

知  
数  
普  
期  
看  
刊

网  
据  
网  
网  
网

收录本刊全文

ISSN 1674-9324



9 771674 932102



50>



- 201 基于迁移学习思想的教学方法研究 ..... 潘剑寒
- 203 基于认知行为的教学案例组织与实施  
——以《机械工程测试技术》课程为例 ..... 杨 静, 李 言, 张文英
- 205 基于混合式教学模式《IT 项目管理》课程实践研究 ..... 吴清锋
- 207 基于进阶式项目驱动法的 Java 开源框架课程教学实践设计  
——以电子商城项目开发为例 ..... 杨 坤, 赵 峰, 杨延村
- 209 PBL 教学法在泌尿外科住院医师规范化培训教学中的效果分析  
..... 张江磊, 陆祺中, 张志昱, 侯建全
- 211 移动学习在大学英语词汇教学中的应用研究 ..... 陈梦华
- 213 四则运算法则在极限运算中的应用探究 ..... 李 波, 刘乃伟, 侯汝臣, 王广富
- 215 探究翻转课堂在高校电磁学课程教学中的应用 ..... 杨昕卉
- 217 混合式教学模式在经济法教学中的融合探析 ..... 高玉侠

### 教师观点

- 219 基于科学思维例谈高中生物课堂教学“示弱”策略  
..... 凤 玉, 贾红影, 姚瑞雪, 徐靖琳
- 221 给排水科学与工程专业毕业设计(论文)质量强化管理措施举要  
..... 帖靖玺, 王玉霞, 李宗喜
- 223 新形势下种业人才培养改革的思考 ..... 郭东伟, 李春莲, 刘柏林, 许盛宝
- 225 军医大学《临床心理学》课程教学设计的思考  
..... 武圣君, 史 康, 王秀超, 张玉婷, 刘旭峰
- 227 论小学数学教学中的估算 ..... 王 元
- 229 浅析科研类航空航天模型竞赛对大学生综合能力的培养  
..... 王 凯, 王道平, 王秋妍, 宁 超
- 231 浅析专业竞赛在高校人才培养过程中的功能 ..... 许淑华, 李伟峰, 乔世东
- 233 知识碎片化、课程多元化与教学系统化的探讨 ..... 谢 芳
- 235 关于高校后勤服务育人的几点思考 ..... 尹者金
- 237 民族音乐文化在高校音乐教学中的传承与发展研究 ..... 孙鹏飞
- 239 提高远程教育教学交互质量的策略探析 ..... 赵秋兰, 陆宇莺
- 241 从导师角度谈如何提升药剂学专业来华留学研究生的培养质量 ..... 韩 亮
- 243 基于核心素养的小学音乐教学研究 ..... 刘 莉
- 245 专业认证背景下《自动控制原理》教学中的几点思考 ..... 邢灿华, 徐开芸
- 247 机械类专业应用型人才培养核心能力的内涵和特征研究  
..... 宋士华, 黄 强, 张文娟, 刘 对, 张许林
- 249 教师资格证考试背景下公共教育学课堂改革探索效果思考 ..... 罗树琳
- 251 高校本科英语课堂教学质量评价存在的问题与对策研究 ..... 吴心瑜
- 253 浅谈地理科学知识在幼儿园科学教育活动中的运用 ..... 王燕华

### 职业教育

- 255 新媒体与高职学生创新能力培养 ..... 黄泽文
- 257 高职金融文秘人才产教融合培养体系创新策略探索 ..... 凌云志
- 259 强化高职社团活动 促进学生工匠精神培养 ..... 高玉环
- 261 高职英语隐性分层教学研究 ..... 邵文华
- 263 基于 PBL 教学模式高职学生学前心理学课程学习动机的激发与培养 ..... 纳 雯

### 阅读与写作

- 265 大学生英语写作课目标与语言维度  
——基于 60 篇作文和批改网作文语料的实证分析 ..... 赵 静, 桑紫林
- 267 引入分级阅读提升高职学生英语阅读素养 ..... 沈 艳

### 信息技术

- 269 信息化教学在《火控系统原理》课程中的应用 ..... 徐 艳, 杨 青, 赵 喜, 胡文华
- 271 高校思政课信息化教学的实效性分析 ..... 任占娟
- 273 会计信息化对企业财务管理的作用探讨 ..... 徐洲禹

### 实验平台

- 275 病原生物学与感染性疾病实验整合与设计 ..... 李艳娜, 沈 利, 王 飞, 闫小丽
- 277 浅谈现阶段高校设计学科摄影实验室的定位与发展 ..... 刘文韬
- 279 纳米生物学交叉学科实验教学与实践 ..... 甘牡丹, 左静蕊

### 声 明

来稿凡经本刊录用, 如无特殊声明, 即视作投稿者同意授权本刊进行信息网络传播。



# 新形势下种业人才培养改革的思考

郭东伟,李春莲,刘柏林,许盛宝

(西北农林科技大学农学院,陕西 杨凌 712100)

**摘要:**种业是国家基础性、战略性的产业,提升种业核心竞争力对确保国家粮食安全和国民经济的良性运行至关重要。文章通过分析现阶段我国种业人才培养的现状、存在问题以及种业产业发展新形势对种业人才培养的新要求,提出了进行种业人才培养改革的探索性意见,以期能够对新形势下我国种业人才培养改革提供参考。

**关键词:**种业;人才培养;改革

**中图分类号:**G642.0

**文献标志码:**A

**文章编号:**1674-9324(2019)50-0223-02

## 一、前言

种业是农业中基础性、战略性核心产业。种业的竞争核心是创新能力的竞争,归根结底是种业人才的竞争。2011年国务院颁布的《关于加快农作物种业发展的意见》以及2016年农业农村部等四部委联合发布的《关于扩大种业人才发展和科研成果权益改革试点的指导意见》,明确提出加快种业人才培养是推动我国种业发展的重点任务之一。随着我国加入WTO,种子市场的进一步开放,企业兼并重组的进行,竞争的不断加剧,对种业人才也提出了新的更高的要求。

## 二、我国种业人才培养的现状

1.我国种业人才的分布特点。与广义的种业人才其实包括了从种子培育到市场营销、管理全过程中的各类从业人员。目前,我国的种子研发人才主要集中在科研院所和大专院校,是种业创新的核心技术力量;种子生产、种子营销人员则主要集中在种业企业,这部分人员是连接种子研发和种子应用的纽带,也是实现种业科技成果转化成为生产力的关键力量;还有一部分是种业管理人才,主要集中在种子管理部门,是确保种子准入和市场有序运行的行政保障。近几年,随着国家推动商业化育种以来,相当一部分种业研发人员开始从科研院所向种业企业流动,使企业自主研发能力大幅度提升。例如,在2019年通过国家审定的548个玉米品种中,只有44个是由科研院所独立或科研单位与企业联合培育,仅占总数的8%,超过90%的玉米品种是由企业自主培育的,企业已成为作物育种的主体。

2.我国种业人才培养的特点。自1995年国家实施种子工程战略以来,种业人才培养就一直是该战略的核心任务之一,而高校则是种业人才培养的主阵地。2002年中国农业大学率先在全国设立种子科学与工

程专业,开创了我国种科专业本科教育的先河。随后,各涉农高校纷纷跟进,设立种子科学与工程专业。截至目前,全国能进行种子科学与工程专业本科及本科以上学历教育的高校已达到36个,其中能达到硕士层次的高校超过14所,博士层次的超过11所,已形成了由本科到博士的完整种业人才培养体系。其主要培养目标是:培养具备植物育种、种子加工、贮藏、种子质量检测、种子营销及其相关领域的基本理论、基本知识和基本技能,能在种子科学与工程相关部门从事教学与科研、技术推广与开发、生产经营与管理等方面的应用型高级人才;通常开设的课程主要有理论教学和实践教学两大部分,其中理论课程主要有作物育种原理、田间试验设计、作物栽培学、种子生产学、种子检验、种子生理学、公共关系学、推广学、国际贸易、市场营销、种子贮藏加工与种子经营等。

3.我国种业人才培养存在的主要问题。近年来,“育、繁、推”一体化已成为我国种业的主要发展模式。这一模式涵盖了种子产业从研发到推广的全过程,因此,种业企业对人才培养质量提出了更高的要求。但现有的种业人才主要存在四个方面的问题:(1)现有的种业人才多来自农学、园艺、植保、栽培等种业相关专业,其知识培养缺少种子从研发到推广全过程,缺少系统性,培养出的更多是“专才”而非“全才”。(2)培养组织模式、方法、环节单一,除了学校以外,科研单位、企业和市场管理部门未能有效参与到培养的过程中,多注重理论学习,对实践环节尤其是企业营销和市场管理环节重视不足,导致理论知识与实践运用脱节。(3)人才培养的质量不高。由于师资力量和办学条件等多种要素所限,各单位培养的种业人才质量参差不齐,一些掌握现代生物技术育种手段和具有国际视野、掌

收稿日期:2019-10-10

作者简介:郭东伟(1973-),男(汉族),陕西人,博士,副教授,研究方向:玉米遗传育种和细胞周期调控。



握现代企业经营管理知识和营销策略的高端人才极度缺乏。(4)培养目标、课程设置千篇一律,缺少区域特色、专业特色,人才队伍创新能力和竞争力不足。

### 三、新形势下我国种业发展对人才培养的新要求

随着经济全球化进程的加快和现代生物技术等的迅猛发展,我国种业发展空间和市场份额受到了国际种业巨头的强势挤压和挑战,要实现全面赶超和彻底突围,必须把种业科技创新摆上首要位置,而加强种业原始创新能力归根结底还要依靠种业人才质量的提高。同时,由于种业企业的兼并重组的持续推进,“一带一路”、乡村振兴、脱贫攻坚等国家倡议和新战略的实施,都促使种业市场发生了深的变革,迫切需要我们不断调整人才培养目标方向,调整培养模式和方法,以适应新形势下市场对种业人才的新要求<sup>[1-2]</sup>。这主要体现在:(1)种子企业业务的不断拓展,急需大量种业人才来开展“育、繁、加、检、销”等各个环节的工作,据统计,截至2018年底我国种业企业已超过5000家,社会对种业人才的需求量总体上会比较旺盛。但一些非科研人员的人才略有减少。对一些掌握了现代生物育种技术,如全基因组选择、基因编辑、单倍体育种、诱变育种技能的高端育种研发人员和具有国际视野,有国际种业企业履职经历的,掌握了现代企业经营管理知识以及现代资本运作技能的高端管理人才的需求将持续强劲增长。(2)用人单位更加多元化。以往我国种业人才主要流向各级种子管理等相关政府职能机构、教学、科研机构 and 种业企业,种业人才主要从事的也是种子管理、研发和销售等相关工作,但新形势下随着我国农业企业走出去和农产品贸易的不断扩大,一些植物检验检疫机构、商检机构、农资企业的涉外部门、跨境物流企业等也迫切需要有种业知识背景的工作人员,种业人才就业单位日趋多元化。(3)对种业人才的质量提出了更高要求。新形势下,由于用人单位业务范围的不拓展,专业分工的不断细化,一些种子经营管理、种子产业化、种子生物技术研发、种子物流、种子加工、种子外贸、市场宣传与媒体、种子制度与政策研究等多领域的高学历专业人才会更加紧俏。

### 四、新形势下种业人才培养改革的探索

1. 确定符合时代特色和社会需要的人才培养目标。以满足社会需求为目标,以能力培养为核心调整改革种业人才培养目标。培养目标的制订应该与产业发展的趋势和国家政策的导向相一致,与种业人才就

业单位的需求特征相吻合,在强调应用型、复合型本科人才培养的基础上加大力度开展能够突显专业特色、区域特色等差异的高学历人才的培养,又培养在“种子研发”和“营销管理”上能够提升种业企业和研发机构原始创新能力和国际竞争力的“专家”。

2. 制订科学合理的种业人才培养方案。种业人才培养方案的制订应该与种业人才培养的目标相结合,分层次、分阶段进行培养。在课程设置上对复合型、应用型“通才”培养注重知识的“广度”而非“深度”,强调课程间横向的整体协调性和系统性;尤其是在现阶段我国农产品贸易规模不断扩大、贸易争端频发的时代背景下,一些涉及知识产权保护、国际种业政策和法规、种子跨境贸易、进出口植物检验检疫制度等新知识、新理论也应作为课程予以学习和掌握;在注重理论学习的同时更注重实践教学环节,尤其是种业全产业链各个环节的实地参与和实践,应适当增加实践环节在整个教学体系中所占的比重。对创新性高学历种业研发人员“专家”的培养,在课程设置上则主要强调知识的纵向系统性,注重向“深度”延伸,尤其是增设一些近年来飞速发展的育种新技术如基因编辑技术、全基因组选择技术、分子设计育种技术等和新学科如生物信息学、计算生物学、生物组学、表观遗传学等课程的学习,人才培养的主战场应该在实验室和基地。

3. 构建多部门、多单位联动的种业人才培养模式。种业企业是种业人才需求的主体,是推动种子产业发展的核心力量,也是将种业科技成果转化为现实生产力的主要推手,因此,企业作为市场活动的一线主体,对市场需要什么样的种子和什么样的人才最清楚。所以,在种业培养模式的创新上,应主动吸引企业共同参与构建种业人才联合培养基地、联合实验室等,共同制订培养目标、培养方案,按照区域、目标的差异实行分类培养,鼓励企业接收学生参与企业的实际经营活动,适当条件下,也可以邀请企业管理层和专业技术人员开展不同形式的讲座,现身说法,激发学员的创新意识和创业精神。积极探索“四结合”、“现代学徒制”、“多元化”、“双主体育人”等多种形式的人才培养模式和机制,实现理论与实践相结合。

#### 参考文献:

- [1] 吴业卿,丁先锋.基于校企合作模式的生物技术专业实践教学改革的探讨[J].高校生物学教学研究,2014.
- [2] 王州飞,张红生.中国种业发展现状及对人才需求的变化趋势[J].中国种业,2013,(2):1-3.

#### Consideration of Reforming on Cultivation of Seed Industry Talents under New Situation

GUO Dong-wei, LI Chun-lian, LIU Bai-lin, XU Sheng-bao

(College of Agronomy, Northwest A & F University, Yangling, Shaanxi 712100, China)

**Abstract:** Seed industry is a basic and strategic industry in the country, so it is very important to improve the core competitiveness of seed industry to ensure the national food security and the healthy operation of the national economy. By analyzing the present situation, the existing problems and the new requirements of the development of the seed industry for the cultivation of talent in the seed industry, this paper puts forward the exploratory opinions on the reform of the cultivation of talent in the seed industry. In the hope of the new situation of China's seed industry personnel training reform to provide a reference.

**Key words:** seed industry; talent training; reform



JJTAOYU JJTAOXUE LUNPAN

# 教育教学论坛

网址: <http://www.jyxlzzs.com/>

电子信箱: [jyxl@jyxlzzs.com](mailto:jyxl@jyxlzzs.com)

CN 13-1399/G4

邮发代号: 18-219

定价: 40.00 元

郭东伟系陕西杨凌  
人，一九七三年三月  
七日生。在我校



作物遗传育种 学科（专业）已通过  
博士学位的课程考试和论文答辩，成  
绩合格。根据《中华人民共和国学位  
条例》的规定，授予 农学 博士  
学位。

西北农林科技大学校长

学位评定委员会主席

孙武子

二〇〇七年四月廿七日

证书编号 1071222007000026







# 聘 书

郭东伟 同志：

兹聘请您为陕西省农作物学会  
第二届理事會秘书长，聘期四年。

陕西省农作物学会

2019年12月





# 西北农林科技大学文件

校人发〔2013〕172号

---

## 关于王隼珍等 95 位同志专业技术职务 任职资格的通知

各学院（系、部、所）、处（室）、直属（附属）单位：

根据《西北农林科技大学专业技术职务评审工作实施办法》（校人发〔2011〕172号），经个人申请，单位推荐、资格审查、代表作评审、学科评议组评议、学部和学校高级专业技术职务评审委员会评审、公示，校职改领导小组审定，王隼珍等 13 位同志具有教授职务任职资格；牛文全等 7 位同志具有研究员职务任

任职资格；丁洪江等 37 位同志具有副教授职务任职资格；许向利等 7 位同志具有副研究员职务任职资格；李红霞等 5 位同志具有高级实验师职务任职资格；黄翠芳同志具有副编审职务任职资格；祝红艺同志具有副研究馆员职务任职资格；卢小三等 15 位同志具有讲师职务任职资格；王文芳等 5 位同志具有实验师职务任职资格；张琳同志具有编辑职务任职资格；杜晓燕等 3 位同志具有馆员职务任职资格。具体名单如下：

一、具有教授职务任职资格人员（13 人）（按照姓氏笔画顺序排序，下同）

王隼珍 刘雅莉 朱宏斌 权富生 陈 鹏  
陈树林 苗 芳 贺 虹 袁亚宏 康永祥  
戴 武 魏 凤 张军华

二、具有研究员职务任职资格人员（7 人）

牛文全 安韶山 张根广 李 毅 闵东红  
黄 敏 韩文霆

三、具有副教授职务任职资格人员（37 人）

丁洪江 牛 荣 王永强 王勇胜 史新娥  
白秀广 任小龙 刘文明 刘军弟 刘变芳  
孙慧敏 朱 杰 余瑞金 宋怀波 张 磊  
张宏鸣 张祖庆 李 征 李民寿 杨乙丹



杨会君 杨兆富 杨晓峰 杨新娟 汪自庆  
苏燕平 邱 立 陈俊英 段海燕 赵光辉  
赵彩平 党瑞华 凌 飞 袁茂森 郭东伟  
彭少兵 强 虹

四、具有副研究员职务任职资格人员（7人）

许向利 吴 华 吴淑芳 邱莉萍 武高林  
高 鹏 韩立荣

五、具有高级实验师职务任职资格人员（5人）

李红霞 李学俊 辛转霞 陈德育 黄雪玲

六、具有副编审职务任职资格人员（1人）

黄翠芳

七、具有副研究馆员职务任职资格人员（1人）

祝红艺

八、具有讲师职务任职资格人员（15人）

卢小三 田永刚 仲 会 刘金鼎 师燕妮  
朱红强 张华海 张瑞洁 张 璐 杜联合  
唐 英 唐 青 贾 锐 窦 龙 雷 蕾

九、具有实验师职务任职资格人员（5人）

王文芳 史晓琴 李 蓉 周晓娜 姚志凤

十、具有编辑职务任职资格人员（1人）

张 琳

十一、具有馆员职务任职资格人员（3 人）

杜晓燕 杨秀英 贾 钊

以上 95 位同志任职时间从 2013 年 1 月 1 日算起。

西北农林科技大学

2013 年 6 月 17 日

---

抄送：

---

西北农林科技大学校长办公室

---

2013 年 6 月 20 日印发





持证人：郭东伟  
性别：男  
出生年月：3/7/1973  
民族：汉族  
身份证号码：610403197303070070  
资格种类：高等教师资格  
任教学科：生物学  
证书号码：200761000700000400

根据《中华人民共和国  
教师法》及《教师资格条例》

的规定，认定 郭东伟  
具备 高等学校

教师资格。





# 留学回国人员证明

(2011) 温领 教 (文) 证字 333号

兹证明 郭东伟 男 ☒、女 ☐，系我国在 加拿大 国，

AARC - Lethbridge Research Centre 学校 (单位) 的高级研究学者 ☐、访问学者 ☒、

博士后 ☐、博士研究生 ☐、硕士研究生 ☐、本科生 ☐、大专生 ☐、其他留学人员 ☐

护照号码 G26503322 发照机关 公安部出入境管理局

在我驻外使 (领) 馆报到日期 2011 年 05 月 31 日

注册入学 (工作) 日期 2008 年 04 月 05 日

毕 (结) 业、工作结束日期 2011 年 07 月 04 日

毕 (结) 业证书名称 \_\_\_\_\_ 号码 \_\_\_\_\_

回国 (拟) 工作单位: \_\_\_\_\_

附: 毕 (结) 业证书复印件。

留学回国人员签字:

教育 (文化) 处 (组)

经 办 人 签 字: 郭东伟



教育 (文化) 处 (组)

负 责 人 签 字: 郭东伟

2011 年 06 月 16 日

第一联: 交留学回国人员

教育部国际合作与交流司 2004 年制表

## 注 意 事 项

1. 本证明只为学成回国工作的留学人员开具。
2. 本证明由我驻外使 (领) 馆教育 (文化) 处 (组) 在留学人员回国时填写, 不得涂改。
3. 本证明经使 (领) 馆教育 (文化) 处 (组) 经办人、负责人签字并在第一、第二联加盖公章方为有效。
4. 第一联由留学人员保存, 其他单位可查验原件, 收存复印件, 不得收取原件。



# 聘 书

兹聘任郭东伟同志担任 农 学 院  
植物科学与技术专业 07 级 (2) 班班主任，  
聘期 四 年。



二〇〇七年八月



## 检索报告

根据委托人宋志伟委托,通过网络检索,李思璐发表的 1 篇论文被《科学引文索引》扩展版(SCI-Expanded)数据库收录。数据库具体检索结果如下:

标题: The distribution pattern of endopolyploidy in maize  
 作者: Li, SL (Li, Silu)[ 1,2 ]; Liu, LS (Liu, Linsan)[ 1,2 ]; Li, T (Li, Ting)[ 1,2 ]; Lan, TR (Lan, Tianru)[ 1,2 ]; Wang, YH (Wang, Yahui)[ 1,2 ]; Zhang, ZQ (Zhang, Zhengquan)[ 1,2 ]; Liu, JC (Liu, Jianchao)[ 1,2 ]; Xu, ST (Xu, Shutu)[ 1,2 ]; Zhang, XH (Zhang, Xinghua)[ 1,2 ]; Zhu, JC (Zhu, Jianchu)[ 1,2 ]; Xue, JQ (Xue, Jiquan)[ 1,2 ]; Guo, DW (Guo, Dongwei)[ 1,2 ]  
 THEORETICAL AND APPLIED GENETICS 卷: 132 期: 5 页: 1487-1503  
 DOI: 10.1007/s00122-019-03294-4 出版年: MAY 2019  
 通讯作者地址: Guo, DW (通讯作者)Northwest A&F Univ, Coll Agron, Minist Agr, Key Lab Biol & Genet Improvement Maize Arid Area, Yangling 712100, Shaanxi, Peoples R China.  
 通讯作者地址: Guo, DW (通讯作者)Maize Engn Technol Res Ctr Shaanxi Prov, Yangling, Shaanxi, Peoples R China.  
 地址: [ 1 ] Northwest A&F Univ, Coll Agron, Minist Agr, Key Lab Biol & Genet Improvement Maize Arid Area, Yangling 712100, Shaanxi, Peoples R China  
 [ 2 ] Maize Engn Technol Res Ctr Shaanxi Prov, Yangling, Shaanxi, Peoples R China  
 电子邮件地址: gdwei@nwsuaf.edu.cn  
 出版商 SPRINGER, 233 SPRING ST, NEW YORK, NY 10013 USA  
 Web of Science 类别: Agronomy; Plant Sciences; Genetics & Heredity; Horticulture  
 文献类型: Article 语言: English 入藏号: WOS:000468547800016 ISSN: 0040-5752  
 Web of Science 核心合集中的 "被引频次": 0  
 第一作者李思璐,第一署名单位西北农林科技大学农学院,农业部农村部西北旱区玉米生物学与遗传重点实验室。  
 通讯作者郭东伟,署名单位西北农林科技大学农学院,农业部农村部西北旱区玉米生物学与遗传重点实验室,陕西省玉米工程技术研究中心。

2019 年公布的影响因子: 3.926, 期刊分区:

JCR® 类别	类别中的排序	JCR 分区
AGRONOMY	6/89	Q1
GENETICS & HEREDITY	43/174	Q1
HORTICULTURE	2/36	Q1
PLANT SCIENCES	25/228	Q1

2019 年中科院分区:

	学科名称	分区	Top 期刊
小类	AGRONOMY 农艺学	1	-
小类	GENETICS & HEREDITY 遗传学	3	-
小类	HORTICULTURE 园艺	1	-
小类	PLANT SCIENCES 植物科学	2	-
大类	农林科学	1	是

查证检索:

西北农林科技大学图书馆

2019 年 12 月 17 日



编号: SCIE-LY-20191217-8

# 检索报告

根据委托人宋志伟委托, 通过网络检索, 钟雨越发表的 1 篇论文被《科学引文索引》扩展版 (SCI-Expanded) 数据库收录。数据库具体检索结果如下:



标题: Short-time microwave treatment affects the multi-scale structure and digestive properties of high-amylose maize starch

作者: Zhong, YY (Zhong, Yuyue)[ 1,2,3 ]; Liang, WX (Liang, Wenxin)[ 1 ]; Pu, HQ (Pu, Hanqi)[ 1 ]; Blennow, A (Blennow, Andreas)[ 4 ]; Liu, XX (Liu, Xingxun)[ 2,3 ]; Guo, DW (Guo, Dongwei)[ 1 ]

INTERNATIONAL JOURNAL OF BIOLOGICAL MACROMOLECULES 卷: 137 页: 870-877

DOI: 10.1016/j.ijbiomac.2019.07.025 出版年: SEP 15 2019

通讯作者地址: Guo, DW (通讯作者) Northwest A&F Univ, Key Lab Biol & Genet Improvement Maize Arid Area, Minist Agr, Coll Agron, Yangling, Shaanxi, Peoples R China.

通讯作者地址: Liu, XX (通讯作者) Nanjing Univ Finance & Econ, Coll Food Sci & Engr, Collaborat Innovat Ctr Modern Grain Circulat, Nanjing 210023, Jiangsu, Peoples R China.

通讯作者地址: Liu, XX (通讯作者) Nanjing Univ Finance & Econ, Key Lab Grains & Oils Qual Control & Proc, Nanjing 210023, Jiangsu, Peoples R China.

地址: [ 1 ] Northwest A&F Univ, Key Lab Biol & Genet Improvement Maize Arid Area, Minist Agr, Coll Agron, Yangling, Shaanxi, Peoples R China

[ 2 ] Nanjing Univ Finance & Econ, Coll Food Sci & Engr, Collaborat Innovat Ctr Modern Grain Circulat, Nanjing 210023, Jiangsu, Peoples R China

[ 3 ] Nanjing Univ Finance & Econ, Key Lab Grains & Oils Qual Control & Proc, Nanjing 210023, Jiangsu, Peoples R China

[ 4 ] Univ Copenhagen, Dept Plant & Environm Sci, Copenhagen, Denmark

电子邮件地址: xliu@nufe.edu.cn; gdwei1973@126.com

出版商 ELSEVIER, RADARWEG 29, 1043 NX AMSTERDAM, NETHERLANDS

Web of Science 类别: Biochemistry & Molecular Biology; Chemistry, Applied; Polymer Science

文献类型: Article 语言: English 入藏号: WOS:000484644100094 ISSN: 0141-8130

Web of Science 核心合集中的 "被引频次": 0

第一作者钟雨越, 第一署名单位西北农林科技大学农业部农村部西北旱区玉米生物学与遗传重点实验室, 农学院。

通讯作者郭东伟, 西北农林科技大学农业部农村部西北旱区玉米生物学与遗传重点实验室, 农学院。

通讯作者刘新训, 署名单位南京财经大学食品科学与工程学院, 协同创新中心现代粮食流通, 南京财经大学国家粮油质量监督检验与控制重点实验室。

2019 年公布的影响因子: 4.784, 期刊分区:

JCR® 类别	类别中的排序	JCR 分区
BIOCHEMISTRY & MOLECULAR BIOLOGY	52/299	Q1
CHEMISTRY, APPLIED	9/71	Q1
POLYMER SCIENCE	8/87	Q1

2019 年中科院分区:

	学科名称	分区	Top 期刊
小类	BIOCHEMISTRY & MOLECULAR BIOLOGY 生化与分子生物学	3	-
小类	CHEMISTRY, APPLIED 应用化学	2	-
小类	POLYMER SCIENCE 高分子科学	2	-
大类	化学	2	否

查证检索:

西北农林科技大学图书馆

2019 年 12 月 17 日

编号: SCIE-LY-20200405-3

## 检索报告

根据委托人郭东伟委托,通过网络检索,郭东伟发表的 1 篇论文被《科学引文索引》扩展版(SCI-Expanded)数据库收录。数据库具体检索结果如下:

3✓ 标题: ZmSMR4, a novel cyclin-dependent kinase inhibitor (CKI) gene in maize (*Zea mays* L.), functions as a key player in plant growth, development and tolerance to abiotic stress  
作者: Li, FF (Li, Feifei)[ 1,2 ]; Wang, LC (Wang, Licheng)[ 1,2 ]; Zhang, ZQ (Zhang, Zhengquan)[ 1,2 ]; Li, T (Li, Ting)[ 1,2 ]; Feng, JJ (Feng, Jiaojiao)[ 1,2 ]; Xu, ST (Xu, Shutu)[ 1,2 ]; Zhang, RH (Zhang, Renhe)[ 1,2 ]; Guo, DW (Guo, Dongwei)[ 1,2 ]; Xue, JQ (Xue, Jiquan)[ 1,2 ]  
PLANT SCIENCE 卷: 280 页: 120-131

DOI: 10.1016/j.plantsci.2018.03.007 出版年: MAR 2019 文献类型: Article

通讯作者地址: Guo, DW; Xue, JQ (通讯作者) Northwest A&F Univ, Key Lab Biol & Genet Improvement Maize Arid Areas, Minist Agr, Coll Agron, Xianyang, Peoples R China.

地址: [ 1 ] Northwest A&F Univ, Key Lab Biol & Genet Improvement Maize Arid Areas, Minist Agr, Coll Agron, Xianyang, Peoples R China

[ 2 ] Maize Engn & Technol Res Ctr Shaanxi Prov, Yangling 712100, Shaanxi, Peoples R China

电子邮件地址: gdwei1973@126.com; xjq2934@163.com

出版商 ELSEVIER IRELAND LTD, ELSEVIER HOUSE, BROOKVALE PLAZA, EAST PARK SHANNON, CO, CLARE, 00000, IRELAND

研究方向: Biochemistry & Molecular Biology; Plant Sciences

Web of Science 类别: Biochemistry & Molecular Biology; Plant Sciences

语言: English 入藏号: WOS:000461262100012 ISSN: 0168-9452

Web of Science 核心合集中的 "被引频次": 0

第一作者黎飞飞, 第一署各单位西北农林科技大学农业部西北旱区玉米生物学与遗传育种重点实验室, 农学院。

通讯作者郭东伟, 署各单位西北农林科技大学农业部西北旱区玉米生物学与遗传育种重点实验室, 农学院。

通讯作者薛吉全, 署各单位西北农林科技大学农业部西北旱区玉米生物学与遗传育种重点实验室, 农学院。

2019 年公布的影响因子: 3.785, 期刊分区:

JCR® 类别	类别中的排序	JCR 分区
BIOCHEMISTRY & MOLECULAR BIOLOGY	97/299	Q2
PLANT SCIENCES	28/228	Q1

2019 年中科院分区:

	学科名称	分区	Top 期刊
小类	BIOCHEMISTRY & MOLECULAR BIOLOGY 生化与分子生物学	3	-
小类	PLANT SCIENCES 植物科学	2	-
大类	生物	2	否

查证检索: 刘媛





小类	FOOD SCIENCE & TECHNOLOGY 食品科技	4	-
大类	工程技术	4	否

### 4/ 三、标题: High-amylose starch as a new ingredient to balance nutrition and texture of food

作者: Zhong, YY 钟雨越(Zhong, Yuyue)[ 1 ]; Zhu, HY (Zhu, Heyuan)[ 1 ]; Liang, WX (Liang, Wenxin)[ 2 ]; Li, X (Li, Xu)[ 2 ]; Liu, LS (Liu, Linsan)[ 1 ]; Zhang, XD (Zhang, Xudong)[ 1 ]; Yue, HF (Yue, Huifen)[ 2 ]; Xue, JQ (Xue, Jiquan)[ 1 ]; Liu, XX (Liu, Xingxun)[ 3 ]; Guo, DW (Guo, Dongwei)[ 1 ]

JOURNAL OF CEREAL SCIENCE 卷: 81 页: 8-14

DOI: 10.1016/j.jcs.2018.02.009

出版年: MAY 2018

文献类型: Article

通讯作者地址: Guo, DW 郭东伟 (通讯作者) Northwest A&F Univ, Minist Agr, Maize Biol & Genet Lab Northwest Arid Area China, Yangling 712100, Shaanxi, Peoples R China.

通讯作者地址: Liu, XX 刘兴训 (通讯作者) CAAS, IFST, Beijing 100193, Peoples R China.

地址: [ 1 ] Northwest A&F Univ, Minist Agr, Maize Biol & Genet Lab Northwest Arid Area China, Yangling 712100, Shaanxi, Peoples R China

[ 2 ] Northwest A&F Univ, Coll Agron, Yangling 712100, Shaanxi, Peoples R China

[ 3 ] CAAS, IFST, Beijing 100193, Peoples R China

研究方向: Food Science & Technology

Web of Science 类别: Food Science & Technology

语言: English 入藏号: WOS:000437044000003

ISSN: 0733-5210

eISSN: 1095-9963

第一作者钟雨越, 第一署各单位西北农林科技大学农业部西北干旱区玉米生物学与遗传改良重点实验室。

通讯作者郭东伟, 署各单位西北农林科技大学农业部西北干旱区玉米生物学与遗传改良重点实验室。

通讯作者刘兴训, 中国农业科学院农产品加工研究所。

2018 年公布的影响因子: 2.302。期刊分区:

JCR® 类别	类别中的排序	JCR 分区
FOOD SCIENCE & TECHNOLOGY	45/133	Q2

中科院分区:

期刊全称:	JOURNAL OF CEREAL SCIENCE		
期刊简称:	J CEREAL SCI	ISSN:	0733-5210
年份:	2018 年	综述:	否

	学科名称	分区	Top 期刊
小类	FOOD SCIENCE & TECHNOLOGY 食品科技	3	-
大类	工程技术	3	否

105 ~~X~~、标题: Effects of Different Thermal Treatment Methods on Preparation and Physical Properties of High Amylose Maize Starch Based Films

作者:Zhong, YY 钟雨越 (Zhong, Yuyue)[ 1 ] ; Li, X (Li, Xu)[ 1 ] ; Lan, TR (Lan, Tianru)[ 1 ] ; Li, YB (Li, Yibo)[ 1 ] ; Liu, LS (Liu, Linsan)[ 1 ] ; Qu, JZ (Qu, Jianzhou)[ 1 ] ; Zhang, RH (Zhang, Renhe)[ 1 ] ; Liang, WX (Liang, Wenxin)[ 1 ] ; Xue, JQ (Xue, Jiquan)[ 1 ] ; Liu, XX (Liu, Xingxun)[ 2 ] ...更多内容

INTERNATIONAL JOURNAL OF FOOD ENGINEERING 卷: 14 期: 4

文献号: 20170284

DOI: 10.1515/ijfe-2017-0284

出版年: APR 2018

文献类型: Article

通讯作者地址: Guo, DW 郭东伟 (通讯作者) Northwest A&F Univ, Coll Agron, Minist Agr, Key Lab Biol & Genet Improvement Maize Arid Area, Yangling, Shaanxi, Peoples R China.

通讯作者地址: Liu, XX 刘兴训 (通讯作者) CAAS, IFST, Beijing 100193, Peoples R China.

地址: [ 1 ] Northwest A&F Univ, Coll Agron, Minist Agr, Key Lab Biol & Genet Improvement Maize Arid Area, Yangling, Shaanxi, Peoples R China

[ 2 ] CAAS, IFST, Beijing 100193, Peoples R China

研究方向: Food Science & Technology

Web of Science 类别: Food Science & Technology

语言: English 入藏号: WOS:000433248000005

ISSN: 2194-5764 eISSN: 1556-3758

第一作者钟雨越, 第一署各单位西北农林科技大学农学院农业部西北干旱区玉米生物学与遗传改良重点实验室。

通讯作者郭东伟, 署各单位西北农林科技大学农学院农业部西北干旱区玉米生物学与遗传改良重点实验室。

通讯作者刘兴训, 中国农业科学院农产品加工研究所。

2018 年公布的影响因子: 0.923。期刊分区:

JCR® 类别	类别中的排序	JCR 分区
FOOD SCIENCE & TECHNOLOGY	97/133	Q3

中科院分区:

期刊全称:	International Journal of Food Engineering		
期刊简称:	INT J FOOD ENG	ISSN:	2194-5764



编号: SCI-K-20181224-01

## 检索报告

根据委托人郭东伟委托,通过网络检索,2018年发表的6篇论文被《科学引文索引》扩展版(SCI-Expanded)数据库收录。数据库检索结果如下:

10) 5/ 一、标题: Bivariate flow cytometric analysis and sorting of different types of maize starch grains

作者: Zhang, XD 张旭东 (Zhang, Xudong)[ 1, 2 ]; Feng, JJ (Feng, Jiaojiao)[ 1 ]; Wang, H (Wang, Heng)[ 1 ]; Zhu, JC (Zhu, Jianchu)[ 1 ]; Zhong, YY (Zhong, Yuyue)[ 1 ]; Liu, LS (Liu, Linsan)[ 1 ]; Xu, ST (Xu, Shutu)[ 1 ]; Zhang, RH (Zhang, Renhe)[ 1 ]; Zhang, XH (Zhang, Xinghua)[ 1 ]; Xue, JQ (Xue, Jiquan)[ 1 ] ...更多内容

CYTOMETRY PART A 卷: 93A 期: 2 页: 213-221

DOI: 10.1002/cyto.a.23261 出版年: FEB 2018 文献类型: Article

通讯作者地址: Guo, DW 郭东伟 (通讯作者) Northwest A&F Univ, Key Lab Biol & Genet Improvement Maize Arid Area, Minist Agr, Coll Agron, Yangling 712100, Shaanxi, Peoples R China.

地址: [ 1 ] Northwest A&F Univ, Key Lab Biol & Genet Improvement Maize Arid Area, Minist Agr, Coll Agron, Yangling 712100, Shaanxi, Peoples R China

[ 2 ] Univ Hohenheim, Inst Crop Sci, Qual Plant Prod, Stuttgart, Germany

研究方向: Biochemistry & Molecular Biology; Cell Biology

Web of Science 类别: Biochemical Research Methods; Cell Biology

语言: English 入藏号: WOS:000426061500011

PubMed ID: 28976638 ISSN: 1552-4922 eISSN: 1552-4930

第一作者张旭东, 第一署各单位西北农林科技大学农业部西北旱区玉米生物学与遗传育种重点实验室, 农学院。

通讯作者郭东伟, 署各单位西北农林科技大学农业部西北旱区玉米生物学与遗传育种重点实验室, 农学院。

2018年公布的影响因子: 3.26。期刊分区:

JCR® 类别	类别中的排序	JCR 分区
BIOCHEMICAL RESEARCH METHODS	28/79	Q2
CELL BIOLOGY	100/190	Q3

中科院分区:

期刊全称:	CYTOMETRY PART A		
期刊简称:	CYTOM PART A	ISSN:	1552-4922
年份:	2018 年	综述:	否
	学科名称	分区	Top 期刊
小类	BIOCHEMICAL RESEARCH METHODS 生化研究方法	3	-

编号: SCI-K-20180921-02

## 检索报告

根据委托人渠建洲委托,通过网络检索,渠建洲发表的 1 篇论文被《科学引文索引》扩展版 (SCI-Expanded) 数据库收录。数据库检索结果如下:

标题: Evolutionary, structural and expression analysis of core genes involved in starch synthesis

作者: Qu, JZ 渠建洲 (Qu, Jianzhou)[ 1,2 ]; Xu, ST (Xu, Shutu)[ 1,2 ]; Zhang, ZQ (Zhang, Zhengquan)[ 1,2 ]; Chen, GZ (Chen, Guangzhou)[ 1,2 ]; Zhong, YY (Zhong, Yuyue)[ 1,2 ]; Liu, LS (Liu, Linsan)[ 1,2 ]; Zhang, RH (Zhang, Renhe)[ 1,2 ]; Xue, JQ (Xue, Jiquan)[ 1,2 ]; Guo, DW (Guo, Dongwei)[ 1,2 ]

SCIENTIFIC REPORTS 卷: 8 文献号: 12736

DOI: 10.1038/s41598-018-30411-y

出版年: AUG 24 2018

文献类型: Article

通讯作者地址: Xue, JQ 薛吉全; Guo, DW 郭东伟 (通讯作者) Northwest A&F Univ, Coll Agron, Key Lab Biol & Genet Improvement Maize Arid Area, Minist Agr, Yangling 712100, Shaanxi, Peoples R China.

通讯作者地址: Xue, JQ; Guo, DW (通讯作者) Maize Engn Technol Res Ctr Shaanxi Prov, Yangling 712100, Shaanxi, Peoples R China.

地址: [ 1 ] Northwest A&F Univ, Coll Agron, Key Lab Biol & Genet Improvement Maize Arid Area, Minist Agr, Yangling 712100, Shaanxi, Peoples R China

[ 2 ] Maize Engn Technol Res Ctr Shaanxi Prov, Yangling 712100, Shaanxi, Peoples R China

研究方向: Science & Technology - Other Topics

Web of Science 类别: Multidisciplinary Sciences

语言: English

入藏号: WOS:000442606500023

PubMed ID: 30143668

ISSN: 2045-2322

第一作者渠建洲, 第一署各单位西北农林科技大学农业部西北旱区玉米生物学与遗传育种重点实验室。

通讯作者薛吉全, 署各单位西北农林科技大学农业部西北旱区玉米生物学与遗传育种重点实验室。

通讯作者郭东伟, 署各单位西北农林科技大学农业部西北旱区玉米生物学与遗传育种重点实验室。

2018 年公布的影响因子: 4.122。

期刊分区:

JCR® 类别	类别中的排序	JCR 分区
MULTIDISCIPLINARY SCIENCES	12/64	Q1





中科院分区:

期刊全称: Scientific Reports

期刊简称: SCI REP-UK

ISSN: 2045-2322

年份: 2016 年

综述: 否

学科名称		分区	Top 期刊
小类	MULTIDISCIPLINARY SCIENCES 综合性期刊	3	-
大类	综合性期刊	3	否

查证检索:

西北农林科技大学图书馆

2018年9月21日

编号: SCIE-LY-20200405-1-2

## 检索报告

根据委托人郭东伟委托,通过网络检索,郭东伟发表的 2 篇论文被《科学引文索引》扩展版(SCI-Expanded)数据库收录。数据库具体检索结果如下:

- ✓ 1. 标题: Effects of extrusion treatment on physicochemical properties and in vitro digestion of pregelatinized high amylose maize flour  
 作者: Zhang, XD (Zhang, Xudong)[ 1 ]; Chen, YF (Chen, Yaofeng)[ 1 ]; Zhang, RH (Zhang, Renhe)[ 1 ]; Zhong, YY (Zhong, Yuyue)[ 1 ]; Luo, Y (Luo, Yan)[ 1 ]; Xu, ST (Xu, Shutu)[ 1 ]; Liu, JC (Liu, Jianchao)[ 1 ]; Xue, JQ (Xue, Jiquan)[ 1 ]; Guo, DW (Guo, Dongwei)[ 1 ]  
 JOURNAL OF CEREAL SCIENCE 卷: 68 页: 108-115  
 DOI: 10.1016/j.jcs.2016.01.005 出版年: MAR 2016 文献类型: Article  
 通讯作者地址: Chen, YF; Guo, DW (通讯作者) Northwest A&F Univ, Key Lab Biol & Genet Improvement Maize Arid Area, Minist Agr, Coll Agron, Yangling 712100, Shaanxi, Peoples R China.  
 地址: [ 1 ] Northwest A&F Univ, Key Lab Biol & Genet Improvement Maize Arid Area, Minist Agr, Coll Agron, Yangling 712100, Shaanxi, Peoples R China  
 电子邮件地址: chenylf3828@126.com; gdwei@nwsuaf.edu.cn  
 出版商 ACADEMIC PRESS LTD- ELSEVIER SCIENCE LTD, 24-28 OVAL RD, LONDON NW1 7DX, ENGLAND  
 研究方向: Food Science & Technology  
 Web of Science 类别: Food Science & Technology  
 语言: English 入藏号: WOS:000374361800016 ISSN: 0733-5210  
 Web of Science 核心合集中的 "被引频次": 18  
 第一作者张旭东, 第一署各单位西北农林科技大学农业部西北旱区玉米生物学与遗传育种重点实验室, 农学院。  
 通讯作者陈耀锋, 通讯单位西北农林科技大学农业部西北旱区玉米生物学与遗传育种重点实验室, 农学院。  
 通讯作者郭东伟, 署各单位西北农林科技大学农业部西北旱区玉米生物学与遗传育种重点实验室, 农学院。

2019 年公布的影响因子: 2.452, 期刊分区:

JCR® 类别	类别中的排序	JCR 分区
FOOD SCIENCE & TECHNOLOGY	42/135	Q2

2019 年中科院分区:

	学科名称	分区	Top 期刊
小类	FOOD SCIENCE & TECHNOLOGY 食品科技	3	-
大类	工程技术	3	否

- 8 ✓ 2. 标题: Transcriptome Dynamics during Maize Endosperm Development.

作者: Qu, JZ (Qu, Jianzhou)[ 1 ]; Ma, C (Ma, Chuang)[ 2 ]; Feng, JJ (Feng, Jiaojiao)[ 1 ]; Xu, ST (Xu, Shutu)[ 1 ]; Wang, L (Wang, Lei)[ 1 ]; Li, FF (Li, Feifei)[ 1 ]; Li, YB (Li, Yibo)[ 1 ]; Zhang, RH (Zhang, Renhe)[ 1 ]; Zhang, XH (Zhang, Xinghua)[ 1 ]; Xue, JQ (Xue, Jiquan)[ 1 ]; Guo, DW (Guo, Dongwei)[ 1 ]  
 PLOS ONE 卷: 11 期: 10



DOI: 10.1371/journal.pone.0163814 出版年: OCT 3 2016 文献类型:Article  
通讯作者地址: Xue, JQ; Guo, DW (通讯作者)Northwest A&F Univ, Key Lab Biol & Genet Improvement Maize Arid Area, Minist Agr, Yangling, Shaanxi, Peoples R China.  
地址: [ 1 ] Northwest A&F Univ, Key Lab Biol & Genet Improvement Maize Arid Area, Minist Agr, Yangling, Shaanxi, Peoples R China  
[ 2 ] Northwest A&F Univ, State Key Lab Crop Stress Biol Arid Areas, Coll Life Sci, Yangling, Shaanxi, Peoples R China  
电子邮件地址:xjq2934@163.com; gdwei@nwsuaf.edu.cn  
出版商 PUBLIC LIBRARY SCIENCE, 1160 BATTERY STREET, STE 100, SAN FRANCISCO, CA 94111 USA  
研究方向:Science & Technology - Other Topics  
Web of Science 类别:Multidisciplinary Sciences  
语言:English 入藏号: WOS:000385553100055 ISSN: 1932-6203  
Web of Science 核心合集中的 "被引频次": 7  
第一作者渠建州, 第一署各单位西北农林科技大学农业部西北旱区玉米生物学与遗传育种重点实验室。  
通讯作者薛吉全, 署各单位西北农林科技大学农业部西北旱区玉米生物学与遗传育种重点实验室。  
通讯作者郭东伟, 署各单位西北农林科技大学农业部西北旱区玉米生物学与遗传育种重点实验室。  
2019 年公布的影响因子: 2.776, 期刊分区:

JCR® 类别	类别中的排序	JCR 分区
MULTIDISCIPLINARY SCIENCES	24/69	Q2

2019 年中科院分区:

	学科名称	分区	Top 期刊
小类	MULTIDISCIPLINARY SCIENCES 综合性期刊	3	-
大类	综合性期刊	3	否

查证检索:

刘媛

西北农林科技大学图书馆

2020 年 04 月 05 日



# The distribution pattern of endopolyploidy in maize

Silu Li<sup>1,2</sup> · Linsan Liu<sup>1,2</sup> · Ting Li<sup>1,2</sup> · Tianru Lan<sup>1,2</sup> · Yahui Wang<sup>1,2</sup> · Zhengquan Zhang<sup>1,2</sup> · Jianchao Liu<sup>1,2</sup> · Shutu Xu<sup>1,2</sup> · Xinghua Zhang<sup>1,2</sup> · Jianchu Zhu<sup>1,2</sup> · Jiquan Xue<sup>1,2</sup> · Dongwei Guo<sup>1,2</sup>

Received: 6 June 2018 / Accepted: 24 January 2019  
© Springer-Verlag GmbH Germany, part of Springer Nature 2019

## Abstract

**Key message** We discovered that endopolyploidization is common in various organs and tissues of maize at different development stages. Endopolyploidy is not specific in maize germplasm populations.

**Abstract** Endopolyploidy is caused by DNA endoreplication, a special type of mitosis with normal DNA synthesis and a lack of cell division; it is a common phenomenon and plays an important role in plant development. To systematically study the distribution pattern of endopolyploidy in maize, flow cytometry was used to determine the ploidy by measuring the cycle (*C*) value in various organs at different developmental stages, in embryos and endosperm during grain development, in roots under stress conditions, and in the roots of 119 inbred lines from two heterotic groups, Shaan A and Shaan B. Endopolyploidy was observed in most organs at various developmental stages except in expanded leaves and filaments. The endosperm showed the highest *C* value among all organs. During tissue development, the ploidy increased in all organs except the leaves. In addition, the endopolyploidization of the roots was significantly affected by drought stress. Multiple comparisons of the *C* values of seven subgroups revealed that the distribution of endopolyploidization was not correlated with the population structure. A correlation analysis at the seedling stage showed a positive relationship between the *C* value and both the length of the whole plant and the length of main root. A genome-wide association study (GWAS) identified a total of 9 significant SNPs associated with endopolyploidy (*C* value) in maize, and 8 candidate genes that participate in cell cycle regulation and DNA replication were uncovered in 119 maize inbred lines.

## Introduction

Endoreplication, a special type of mitosis in which cells undergo many rounds of DNA replication without cell division, leads to an increase in the cellular ploidy of an organism over its lifetime, a condition termed ‘endopolyploidy’. Endopolyploidy is common among eukaryotes, and particularly among plants, where approximately 90% of herbaceous

angiosperms exhibit endopolyploidy in the majority of their tissues (Joubès and Chevalier 2000; Larkins et al. 2001).

Across flowering plants, endoreplication appears to be particularly common and it often occurs in economically important tissues, such as cereal endosperm and fruits (Shu et al. 2018). Endoreplication typically occurs in plant tissues that develop mass very quickly or that possess high metabolic activity. It has long been observed that endoreplication is positively correlated with gene expression levels and cell size. For instance, the ribosomal RNA, RNA polymerase II abundance and gene transcript levels in tomato fruits were demonstrated to increase with the endopolyploidy level (Bourdon et al. 2012), and the largest cells in the epidermal pavement and hair cells within *Arabidopsis* leaves possess the highest endopolyploidy levels (Roeder et al. 2010; Melaragno et al. 1993). However, these roles of endopolyploidy are not always true in all cases. For example, there are cases in which trichome cell size does not correlate with endopolyploidy (Schnitger et al. 1998; 2003), and it has been suggested that the relationship between cell volume and endopolyploidy depends on cell identity (Katagiri et al. 2016).

Communicated by Alain Charcosset.

**Electronic supplementary material** The online version of this article (<https://doi.org/10.1007/s00122-019-03294-4>) contains supplementary material, which is available to authorized users.

✉ Dongwei Guo  
gdwei@nwsuaf.edu.cn

<sup>1</sup> The Key Laboratory of Biology and Genetics Improvement of Maize in Arid Area of Northwest Region, Ministry of Agriculture, College of Agronomy, Northwest A&F University, Yangling 712100, Shaanxi, China

<sup>2</sup> Maize Engineering Technology Research Centre of Shaanxi Province, Yangling, Shaanxi, China



Maize (*Zea mays* L.) is a prominent food and forage crop worldwide, as well as a model to study the pattern and mechanism of specific traits in plants. In maize, the endocycle is very common and endopolyploidy exists during the development of organs throughout the life cycle. Previous studies, mainly focusing on endoreplication in the maize endosperm, have made some advances in understanding the biological significance, basic pattern and regulatory mechanism of endoreplication in maize. Endoreplication in maize endosperm begins around 8 DAP (days after pollination), starting with cells in the centre of the endosperm and slowly spreading outward. The peak of endoreplication happens at around 15 DAP, when most starchy endosperm cells have gone through at least one round of endoreplication. The mitotic activity of endosperm cells in maize gradually switches to endoreplication, so that by 15 DAP the endosperm contains a mixed population of polyploid nuclei with DNA contents ranging from 3C to 96C, and sometimes higher (Bringezu et al. 2011; Larkins et al. 2001; Sabelli and Larkins 2008; Young and Gallie 2000b). In the maize endosperm, it is proposed that endoreplication proceeds as a result of two events, induced S-phase CDK activity and inhibited M-phase CDK activity (Grafi and Larkins 1995). A number of observations are consistent with this view (Leiva-Neto et al. 2004; Sabelli et al. 2013). In addition, endoreplication in the maize endosperm correlates with the expression of cyclin-dependent kinase inhibitors (CKIs) (Dante et al. 2005), the contrasting expression and roles of different RBR proteins (Sabelli et al. 2005, 2009, 2013), and differential cyclin expression and reduced cyclin proteolysis via the ubiquitin–proteasome pathway (Dante et al. 2014b; Sun et al. 1999). In the maize endosperm, endoreplication is widely viewed as a mechanism that supports increased gene expression and the enhanced metabolic activity associated with cell enlargement and the massive accumulation of starch and storage proteins (Larkins et al. 2001; Sabelli 2014). However, some reports showed that, by perturbing the function of core cell cycle regulators, subdued endoreplication (and noticeably reduced nuclear sizes) in the maize endosperm did not result in decreased cell size, reduced gene expression or reduced storage protein accumulation (Leiva-Neto et al. 2004; Sabelli et al. 2013).

Although in recent years some endoreplication-related genes have been identified and the basic endopolyploidy pattern in the maize endosperm has been studied, lack of a detailed knowledge of the temporal and spatial occurrence of endopolyploidy in different tissues and organs has hampered the study of the physiological roles of the endocycle in maize. In addition, different environmental factors, including abiotic (e.g. light, temperature, water and soil quality) and biotic factors (e.g. herbivory and competition), have an effect on the endoreplication level of cells and tissues, and endoreplication is considered to be a plastic response

by numerous plant taxa to help them soften the effects of environmental stress or otherwise fine-tune themselves to their local conditions (Scholes and Paige 2015). The drought stress resistance of maize is important for its yield. Research on the induction of endoreplication by drought stress in maize can supplement the understanding of stress resistance development. However, few studies have investigated how endopolyploidy is affected by drought stress.

In terms of the research of endoreplication in maize, it is urgent to systematically investigate the occurrence and development of endoreplication in maize at the whole-plant level, on the basis of the endoreplication patterns of different tissues and organs rather than the endosperm solely, to provide a larger-scale view of the role and control of this special cell cycle. In this study, the endopolyploidy patterns in developing tissues and organs from seedling to maturity were finely measured; the distribution pattern of endopolyploidy among different heterotic breeding populations, as well as the effect of drought stress on endopolyploidy, was investigated; and some significant SNPs associated with endopolyploidy in maize were found. Based on this work, a more comprehensive reference for subsequent endoreplication studies in both maize and other plants is provided.

## Materials and methods

### Plant materials and field experiments

The inbred line B73 was employed to study tissue-specific and developmental stage-specific endoreplication. The standards for distinguishing the developmental stages are listed in Table 1. In the seedling stage, only the leaves and roots were analysed. The main leaf veins, leaf sheaths, internodes and nodes were added starting at the R6 (elongation) stage. In addition, staminate flowers, corn silk, cobs and ovules were tested starting at the VT (tasselling) stage. The embryos and endosperm of the seeds were tested at 10 days after pollination (DAP), 15 DAP, 20 DAP, 25 DAP, 30 DAP and 35 DAP. The seedling roots (5 days after germination (DAG)) of B73 were used to investigate endopolyploidy under stress. The seedling roots of 119 inbred lines (AM119) developed from the Shaan A and Shaan B heterotic breeding populations cultivated at Northwest A&F University (listed in Table S1) were used to investigate the distribution pattern of endopolyploidy in different inbred lines, and the leaves of the seedlings were used for SNP analysis.

The inbred line B73 was used for the ploidy analysis and the AM119 lines were used to investigate the phenotypic traits in the seedling stage; both of these lines were grown in a greenhouse (humidity maintained at 60%, 12 h light and 12 h dark, variable temperature). To investigate the agronomic traits and grain yield, 119 inbred lines

**Table 1** Distinguishing standards of maize developmental stages

Distinguishing standards of maize developmental stages	
V2 (second leaf) stage	Two leaves have grown (approximately 5 days after germination (DAG))
V3 (third leaf) stage	The third leaf of the plant grows over the leaves' hearts 2–75 px (approximately 12 DAG)
V4 (fourth leaf) stage	The plant grows its fourth leaf (approximately 15 DAG)
V5 (fifth leaf) stage	The plant grows its fifth leaf (approximately 17 DAG)
V6 (elongation) stage	Male spike elongates, total stem length is approximately 2–75 px and 6–8 leaves have grown (approximately 30 DAG)
V9 (small trumpet) stage	The female spike enters the elongation period and the male spike enters the floret differentiation period; there are 8–10 leaves (approximately 45 DAG)
V12 (big trumpet) stage	The female spike enters the floret differentiation period and the male spike enters the tetrad stage; the upper spikelet length is approximately 20 px. Three leaves shaped like a trumpet appear at this stage, and 11–13 leaves expand (approximately 50 DAG)
VT (tasselling) stage	The tip of the tassel extends the top leaf by approximately 3–125 px (approximately 60 DAG)
R1 (silking) stage	The corn silk of the female ears extends approximately 50 px from the husk leaf (approximately 62 DAG)
7 DAP	7 days after pollination

were planted in fields in Yangling (34°16'N, 108°40'E) and Yulin (38°30'N, 109°77'E) in Shaanxi Province in 2017. At each location, all inbred lines were planted in a two-row plot using a randomized experimental design, with two replications, a row length of 5 m and a distance of 0.6 m between adjacent rows. The planting density was 67,500 plants/ha. Hydroponics was used for the drought stress treatments, and polyethylene glycol (PEG) was added in a modified Hoagland's nutrient solution to establish an artificial drought environment (the formula of the modified Hoagland's nutrient solution is given in Table S2). The seedlings germinated for 8 days and were then cultivated in PEG solution for 4 more days to induce artificial drought stress.

### Sample preparation

It is vital to prepare a quality nuclear suspension for flow cytometric analysis so that limited debris and excellent staining can be ensured. The materials, including endosperm, leaves, roots and other tissues from individual plants, must be fresh and intact. Moreover, two biological replicates and three technical replicates were needed for this study. First, the material was collected and put it in a 90 mm plastic Petri dish. The materials (1–2 g) were chopped with a sharp razor blade in 1 mL of cooled

nuclear extraction buffer (10 mmol L<sup>-1</sup> MgSO<sub>4</sub>·7H<sub>2</sub>O, 50 mmol L<sup>-1</sup> KCl, 5 mmol L<sup>-1</sup> HEPES, 0.3 mmol L<sup>-1</sup> DTT, 0.25% Triton X-100, pH 7.5), and then the nuclear suspension was filtered through a 40-mm nylon sieve. Finally, a staining solution containing dye 40,6-diamidino-2-phenylindole-2HCl (DAPI) was added to the filtered nuclear suspension at a final concentration of 2 µg mL<sup>-1</sup>. The entire process was performed on ice.

### Flow cytometric analysis

The filtered nuclear suspensions were analysed via flow cytometry with a 100-mW laser, an 85-µm nozzle and an excitation wavelength of 355 nm. The thresholds were 2000 and 3000 for FSC and DAPI, respectively. The coefficient of variation (CV) of the histogram peaks was typically in the range of 2.6–7.7% and depended strongly on the tissues and organs analysed. The voltages for FSC, SSC and DAPI were 180–190, 190–200 and 170–190, respectively. In total, 10,000 events were captured to form a bivariate dot histogram for each analysis. The histograms were plotted using a logarithmic intensity scale (*x*-axis) to convert all peaks into the same width (four typical histograms, extracted from Figs. S1–S4, are shown in Fig. 1). In addition, noise derived from subcellular debris was eliminated by gating.

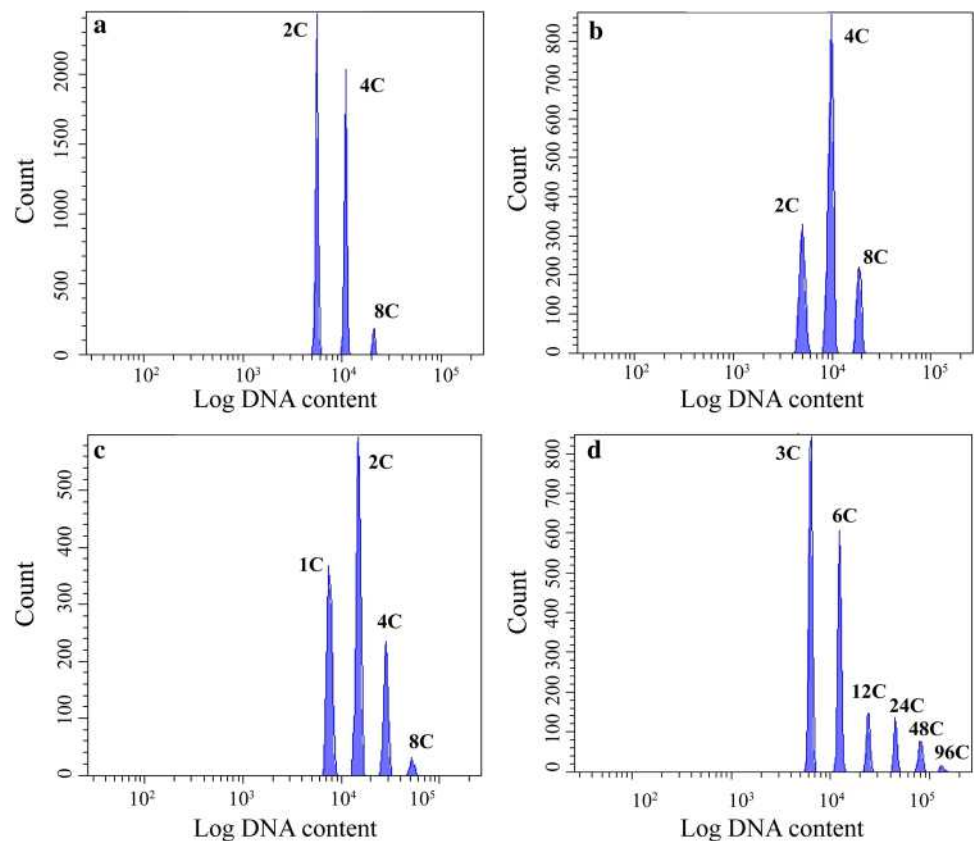
In this study, the degree of endoreplication was expressed by using the 'cycle value'. The 'cycle value' was calculated using the following formula:

$$\text{Cycle value} = \frac{(n_{2c} \times 0 + n_{4c} \times 1 + n_{8c} \times 2 + n_{16c} \times 3 + \dots)}{(n_{2c} + n_{4c} + n_{8c} + n_{16c} + \dots)}$$

where  $n_{2c}$ ,  $n_{4c}$ ,  $n_{8c}$ ... are the number of nuclei with the corresponding cycle value (Barow and Meister 2010).



**Fig. 1** Four typical logarithmic histograms. **a** Node, V6 (elongation) stage; **b** Root, VT (tasselling) stage; **c** Staminate, R1 (silking) stage; **d** endosperm, 20 DAP



### Investigation of agronomic traits and grain yield of inbred lines

The phenotypic traits of AM119 were investigated at the seedling stage (12 DAG), and the agronomic traits were investigated at maturity. The length of the whole plant and main root in the seedling stage and the plant height, ear height and leaf area in the mature stage were measured on a graduated scale. The fresh seedlings and adult plants were dried at 120 °C for the first 5–10 min and then dried to a constant weight at 60 °C. The dry weights of the seedlings and adult plants were determined with a scale. A plant stem strength tester was used to measure the stem strength, and a SPAD-502 Chlorophyll Content Meter was used to determine the chlorophyll content. The stem strength and SPAD were continuously measured for 10 plants in the middle 2 lines of each plot. Upon harvest, all ears were harvested by hand threshing, and the corresponding data, including the grain water content, total grain weight and weight of ten panicles, were recorded to calculate the grain yield per mu (kg) using the following formula:

$$\begin{aligned} \text{Grain yield (kilogram/acre)} \\ = & \text{grain weight}/10 \times (1 - \text{moisture content})/86 \\ & \times (38 - 38 \times \text{disease plant rate})/6 \times 667 \end{aligned}$$

The mean phenotypic data, the agronomic traits and mean grain yield of two replicates were calculated for the subsequent analysis (Table S3 and Table S4).

### Population structure and association analysis of endopolyploidy in 119 inbred lines

#### Genotyping by sequencing

Fresh leaves from each inbred line were collected, frozen and ground. The genomic DNA of the leaves was extracted with cetyl-trimethyl ammonium bromide (CTAB) (Doyle 1991). Fundamental qualities were evaluated by gel electrophoresis and spectrophotometry (Nanodrop2000, Thermo Scientific) in our laboratory. SNPs were identified using the genotyping-by-sequencing (GBS) method (Elshire et al. 2011; Glaubitz et al. 2014), and 48,415 SNPs were filtered for future analysis based on a minimum calling rate  $\geq 20\%$ , allele number = 2, genotype  $\geq 2$ , MAF  $\geq 1\%$ , and percent heterozygosity of 0% to  $(2 \times \text{Frequency}_{\text{allele1}} \times \text{Frequency}_{\text{allele2}} \pm 0.2\%)$ .

#### Population structure

To investigate the population structure of AM119 from Shaan A and Shaan B heterotic breeding populations, 48,415 SNPs

were imported into Admixture software V1.23 for cross-validation (Alexander et al. 2009). The optimal partitioning of subgroups (K) was determined from the mixed cross-validation error values, which were computed from the number of subpopulations (K), ranging from 2 to 10. The output of the Admixture software was imported into R to create a stacked bar chart. Furthermore, we performed principal component analysis (PCA) of AM119 using Tassel 2.5 software (Bradbury et al. 2007) and R scripts.

### Genome-wide association study (GWAS)

Based on the results of the multiple comparisons of the mean *C* value among the groups, a GWAS for endopolyploidy was performed using a general linear model (GLM) (Bradbury et al. 2007), controlling for population structure (*Q*) to avoid spurious associations. Since the strict threshold was  $2 \times 10^{-5}$  (1/48,415), and combined with the results of the population structure,  $p < 1 \times 10^{-4}$  was chosen to determine the significant SNPs for the trait. Candidate gene information was obtained from the Maize GDB (<http://www.maizegdb.org/>) genome browser based on the linkage disequilibrium (LD) decay distance of this population in a previous study (Li et al. 2018). Functional domains were searched using SMART (<https://smart.embl-heidelberg.de/>) and the CD-search service (<https://www.ncbi.nlm.nih.gov/Structure/cdd/wrpsb.cgi>).

### Statistical analysis

The software SPSS 19.0 and Duncan's test were used for data analysis. A two-way analysis of variance was used to determine the impact of the factors 'time' and 'concentration' on endopolyploidization in the drought stress experiment. The Ward method was used for the hierarchical clustering of *C* values and agronomic traits. The Tukey HSD method was used for multiple comparisons of the mean *C* value among groups. In addition, Pearson's correlation coefficient was used for correlation analysis between agronomic traits and the *C* value.

## Results

### Organ-specific patterns of endopolyploidy

The flow cytometry results showed that the somatic cells of most tested organs contained nuclei with varying ploidy, indicating that these cells had undergone several rounds of endoreplication. According to the flow cytometry typical histograms (Fig. S1–S4), almost all organs in maize, except the expanded leaves, contain three types of nuclei, namely, 2C, 4C and 8C nuclei.

The *C* values of the tested organs at all developmental stages are listed in Table 2. The *C* values of the roots

**Table 2** Cycle value (*C* value), stage and organ

Stage	Root	Leaf	Leaf sheath	Main vein	Internodes	Nodes	Husk leaf	Corn cob	Staminate	Corn silk	Ovule	Seed
V2 stage	0.88 ± 0.02a	0.54 ± 0.04b										
V3 stage	1.03 ± 0.02a	0.48 ± 0.02b										
V4 stage	0.80 ± 0.06a	0.28 ± 0.03b										
V5 stage	0.76 ± 0.08a	0.33 ± 0.03b										
V6 stage	0.81 ± 0.04a	0.14 ± 0.06d	0.55 ± 0.05b	0.54 ± 0.02b	0.32 ± 0.01c	0.54 ± 0.00b						
V9 stage	0.96 ± 0.01a	0.15 ± 0.02f	0.49 ± 0.05d	0.59 ± 0.04c	0.34 ± 0.04e	0.79 ± 0.05b						
V12 stage	1.08 ± 0.06a	0.13 ± 0.02e	0.60 ± 0.05c	0.60 ± 0.03c	0.35 ± 0.02d	0.70 ± 0.05b						
VT stage	0.93 ± 0.02a	0.16 ± 0.01 g	0.64 ± 0.06c	0.58 ± 0.06d	0.49 ± 0.01e	0.72 ± 0.02b	0.50 ± 0.02e	0.16 ± 0.01g	0.24 ± 0.01f	0.50 ± 0.05e	0.14 ± 0.01g	
R1 stage	0.90 ± 0.03b	0.17 ± 0.01 g	1.02 ± 0.04a	0.71 ± 0.02c	0.67 ± 0.01d	0.87 ± 0.02b	0.65 ± 0.04d	0.28 ± 0.01f	0.35 ± 0.01e		0.15 ± 0.01g	
7 DAP	0.90 ± 0.02ab	0.16 ± 0.03f	0.94 ± 0.01a	0.74 ± 0.05c	0.94 ± 0.02a	0.87 ± 0.01b	0.71 ± 0.07c	0.44 ± 0.06e				0.64 ± 0.03d

Mean values ± SD

<sup>abcd</sup> Different letter superscripts in the same row indicate significant differences among the samples ( $P \leq 0.01$ ), Duncan's multiple range test (DMRT)



were higher than those of the other organs at nearly every stage except the VT (tasselling) and R1 (silking) stages. Although the  $C$  values of the leaves ranged from  $0.13 \pm 0.02$  to  $0.48 \pm 0.02$ , after the V3 (third leaf) stage (Table 2), endopolyploid nuclei (8C nuclei) could not be observed in the leaves' somatic cells (Fig. S1–S4). The conditions for the ovules and corncoobs were similar to those for the leaves, and the  $C$  values of the ovules and corncoobs were the lowest of all organs. In all stages before pollination, the  $C$  values of the nodes were higher than those of the internodes; however, they were exceeded by that of the internodes at 7 DAP. This sudden increase in the  $C$  value might be related to the increasing demand for nutrient transport during this developmental stage. The endopolyploidy of the leaf sheaths and main leaf veins was maintained at a moderate level before the VT (tasselling) stage. Moreover, the differences in the  $C$  value among internodes, leaf sheaths and roots showed no significant differences ( $p > 0.05$ ) at 7 DAP. The  $C$  values of internodes in the VT (tasselling) stage were similar to those of the husk leaves and corn silk at the same stage. There was no significant difference ( $p > 0.05$ ) in the  $C$  values between the leaf sheaths and main leaf veins at the V6 (elongation) stage or the V12 (small trumpet) stage. Moreover, no significant differences ( $p > 0.05$ ) were observed among husk leaves, leaf sheaths, and leaves in their early growth stages (husk leaves at the VT stage, leaf sheaths at the V6 stage and leaves at the V2 stage). Staminate flowers were only

tested in the VT (tasselling) and R1 (silking) stages, and the  $C$  values of the flowers in these two stages were slightly higher than those of the corncoobs, ovules and leaves. The  $C$  values of the leaves and ovules showed no significant differences ( $p > 0.05$ ) at either the VT (tasselling) or R1 (silking) stages.

### Stage-specific patterns of endopolyploidy

The  $C$  values of the tested organs at various growth stages are shown in Fig. 2a–h. The  $C$  values of nearly all organs, except the leaves, increased with maturity. Two peaks are evident in Fig. 2a. The first peak in roots occurred at the V3 (third leaf) stage, while the second occurred at the V12 (large trumpet) stage. From the V4 (fourth leaf) stage to the VT (tasselling) stage, the  $C$  value dropped and then rose again. Then, the  $C$  value reached its second peak at the V12 (large trumpet) stage, which is the most vibrant stage in the maize lifecycle. After the VT (tasselling) stage, the  $C$  value of the roots decreased and remained at a constant level. In Fig. 2b, 8C nuclei were found in the leaves at the V2 (second leaf) stage and then disappeared. The  $C$  value of the leaves then decreased to its lowest level at the V6 (elongation) stage. There were no significant differences among these stages (V9 (small trumpet) stage to 7 DAP).

As shown in Table 2, the  $C$  value of the leaf sheaths ranged from  $0.55 \pm 0.05$  to  $0.60 \pm 0.05$  from the V6

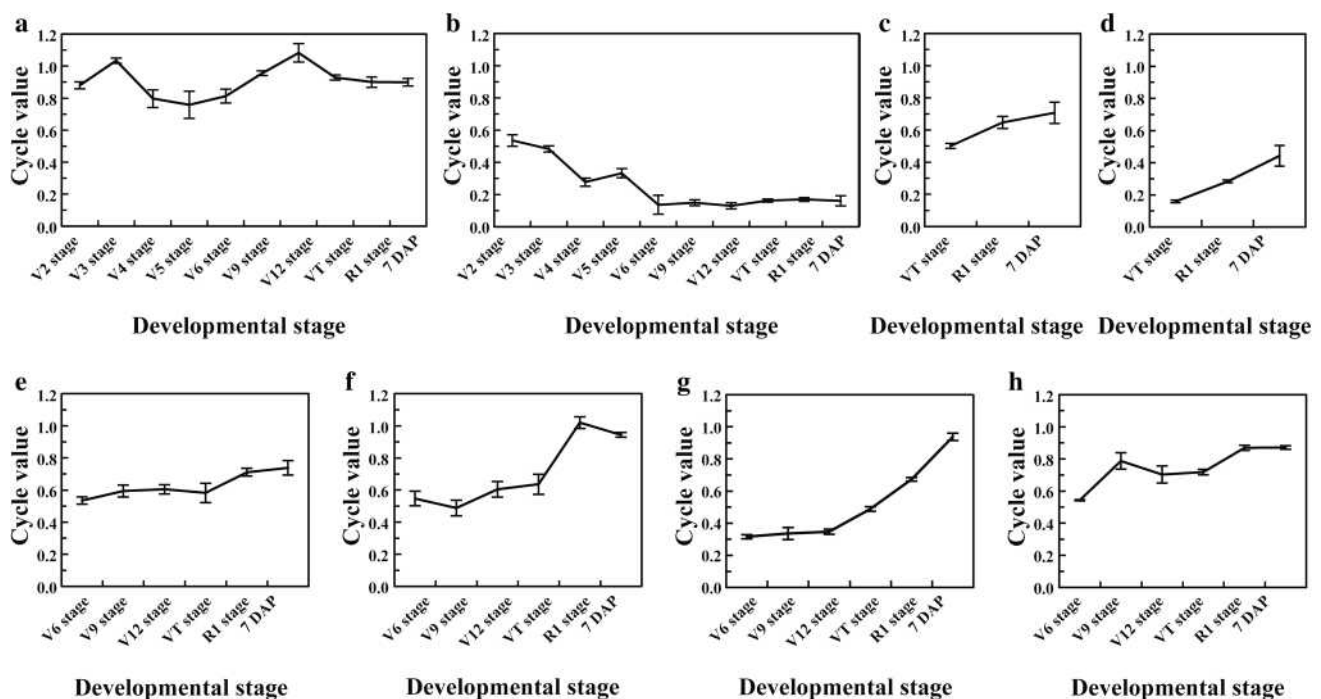


**Fig. 2** a–h Endopolyploidization within organs. Each line graph shows the trend in the variation of the cycle value in a certain organ during its growth and development. The 'cycle value' indicates the

mean number of endoreplication cycles per nucleus in an organ. **a** Root, **b** leaf, **c** Husk leaf, **d** corn cob, **e** main leaf vein, **f** leaf sheath, **g** Internodes, **h** Nodes

(elongation) to the V12 (large trumpet) stage, and there were no significant differences ( $p > 0.05$ ) among these stages. The  $C$  value of the leaf sheaths rose sharply starting at the VT (tasselling) stage and reached its peak at the R1 (silking) stage (Fig. 2f). Finally, the  $C$  value slightly decreased at 7 DAP. In Fig. 2e, a slight increasing trend in the  $C$  value was observed throughout the growth stage of the main leaf vein. Similarly, the degree of endopolyploidization of the internodes increased with increasing organ maturation (Fig. 2g). Moreover, the  $C$  value rose sharply after the V12 (large trumpet) stage and reached its maximum at 7 DAP.

As shown in Fig. 2h, the  $C$  value of the nodes increased rapidly beginning with the V6 (elongation) stage, and it reached its first peak at the V9 (small trumpet) stage. Then, the  $C$  value dropped and then rose from the V12 (big trumpet) stage to the R1 (silking) stage. The  $C$  value reached its highest level at the R1 (silking) stage and then remained at a constant level. As shown in Fig. 2c, d, the  $C$  values of the husk leaves and corncoobs increased with increasing organ maturity, which corresponds to the findings of a previous study (Galbraith et al. 1991).

### The effect of drought stress on endopolyploidy

According to a two-way analysis of variance (Table 3), the  $C$  value of roots suffering from drought stress was significantly (\*\*\*) affected by both time under stress and PEG concentration. Moreover, there was a significant synergistic effect on endopolyploidy between time under stress and PEG concentration (\*\*\*). As shown in Fig. 3, the  $C$  values changed with time under stress, and the trend in the change for each concentration was different. Prior to 12 h, the range of  $C$  values differed for different PEG concentrations. The  $C$  values for all concentrations declined from 24 h to 48 h under stress. However, after 48 h, the  $C$  values tended to increase under drought stress. By contrast, the  $C$  value of the CK continued to decline after 48 h. With 10% PEG, the  $C$  value increased, then decreased and then finally rose again. The  $C$  value with 20% PEG was higher than that with 30% throughout the stress treatment. As shown in Fig. 3, the variation in the amplitude of the  $C$  value diminished when the concentration exceeded 20%, and the  $C$  value with

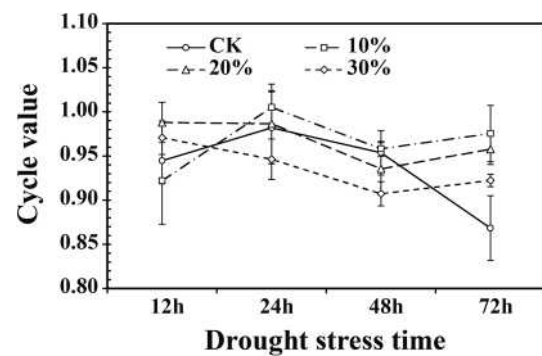


**Fig. 3** The variation in the amplitude of the  $C$  value under different PEG concentrations from 12 to 72 h. The x-axis is time, and different stress concentrations are represented by different dotted lines. Each dot on the line represents the cycle value of the root at the corresponding time and stress concentration. Different stress concentrations were represented by different polyines. Each dot on line represents the cycle value of root at the corresponding stress time and concentration

20% was the highest when the drought stress started (12 h). Twenty per cent may be a critical concentration for the drastic change in endopolyploidy under drought stress.

### Endopolyploidy in maize embryos and endosperm

Seeds are a typical model for endoreplication research in many cereal crops (Nguyen et al. 2007). In the present study, the dynamic properties of endoreplication in embryos and endosperm from 5 DAP to 35 DAP were investigated every 5 days (the whole seed was tested at 5 DAP, while the embryo and endosperm were analysed separately from 10 DAP onwards). As shown in Fig. 4a, b, at 20 DAP, endosperm contains a heterogeneous population of polyploid nuclei with DNA contents ranging from 3C to 96C, while the embryo contains no more than 3 types of polyploid nuclei. In Fig. 4a, the percentage of 2C nuclei was the highest at 15 DAP, and the percentage of 4C nuclei peaked at 10 DAP and 35 DAP. At 25 DAP, 8C nuclei were observed, and then they tended to increase. In Fig. 4b, 3c nuclei were the most abundant at 15 DAP, while 6C nuclei were the most abundant at 10 DAP. The percentages of 12C and 24C nuclei increased over time, while that of 6C nuclei showed no significant change from 20 DAP to 35 DAP ( $p > 0.05$ ). 96C nuclei were observed only at 20 DAP, but the  $C$  value of the endosperm was not the highest at this time.

As shown in Fig. 5, the  $C$  value of the endosperm was always higher than that of the embryo. The  $C$  value of endosperm cells was much higher at 10 DAP, when various starch storage processes were initiated and transcripts encoding proteins were found (Dolfini et al. 2010; Yamagata et al. 2003), than at 15 DAP. The  $C$  values of the endosperm increased again after 15 DAP and reached a peak at 35

**Table 3** Two-way analysis of variance for the impact of the factors 'PEG concentration' and 'stress time' on endopolyploidization of root under drought stress

Parameter	Degrees of freedom	F
PEG concentration	3	8.370***
Stress time	3	13.956***
PEG concentration*stress time	9	7.555***

Significance level: \*  $\leq 0.05$ , \*\*  $\leq 0.01$ , \*\*\*  $\leq 0.001$



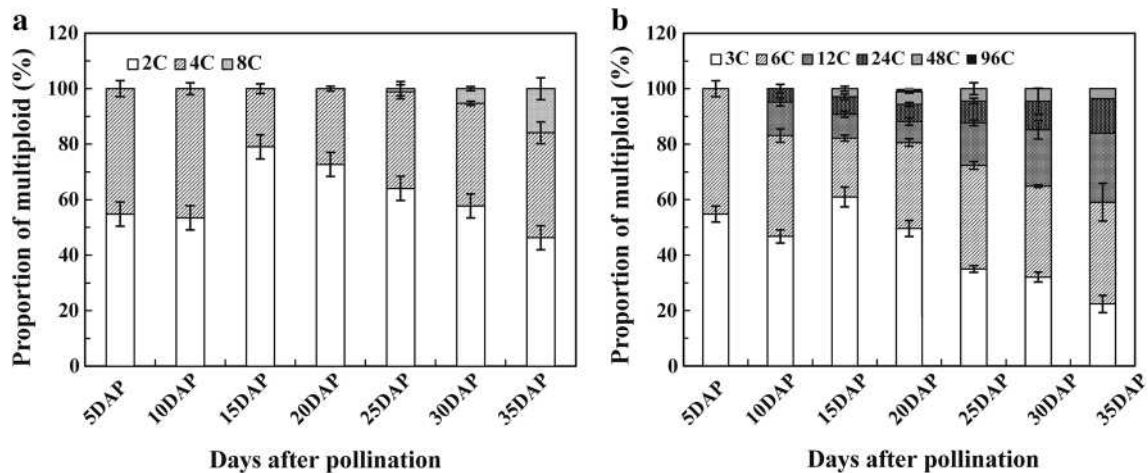


**Fig. 4** Endopolyploidy in maize embryos and endosperm. **a** Average frequency of nuclear DNA levels during grain developmental stages in the embryo. **b** Average frequency of nuclear DNA levels during

grain developmental stages in the endosperm. The data for 5 DAP for embryos and endosperm came from the whole grain

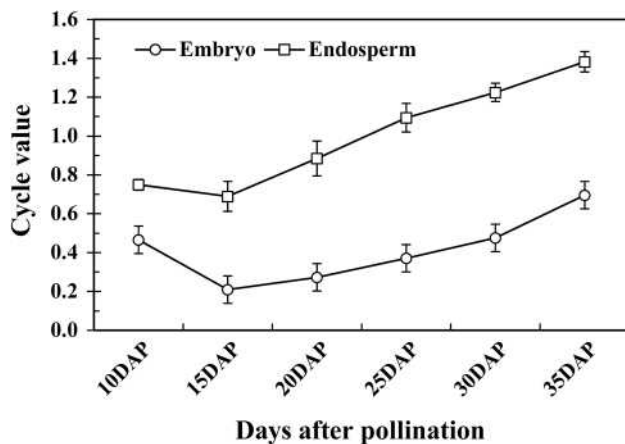


**Fig. 5** Cycle value of the embryo and endosperm during grain development (10–35 DAP)

DAP, but there were only 4 types of polyploid nuclei in the endosperm at this time. The *C* value cannot directly denote the degree of endopolyploidy. Therefore, it is appropriate to measure the level of endopolyploidy by combining the *C* value and the average percentages of nuclear DNA levels.

In this study, 20 DAP was a transition point to increase and decrease the types of polyploid nuclei. By comparing the average percentages of nuclear DNA levels with a previous study on grain filling in maize (Zhang et al. 2007), a positive correlation between the grain filling rate and the types of polyploid nuclei (Fig. 4b) could be found. In addition, the trend of increased grain dry weight was similar to the trend of the changes in *C* value.

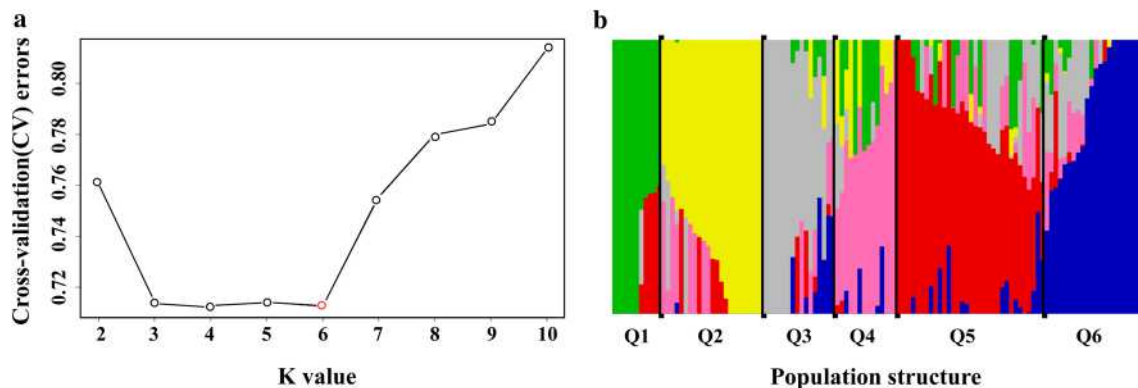
### Pattern of endopolyploidy in different maize inbred lines

The *C* values of AM119, which are listed in Table S5, could be divided into 3 classes, high-level *C* values (H), medium-level *C* values (M) and low-level *C* values (L), based on the results of hierarchical clustering (Fig. S5). The medium-level *C* value composed the majority (48.74%) of all tested materials, while the high-level *C* value represented the least (21.01%), and the low-level *C* value accounted for 30.25%. The *C* values of the inbred lines from the Shaan A group were mainly at the medium (48%) and low (44%) levels. Inbred lines with medium-level *C* values were the majority (45.74%) in the Shaan B group (Table 4). The inbred lines with the top five *C* values in AM119 were AM59×PX + A, AM43×PX09, L134428×huanggai, Z141262-2, and 4CV. Inbred lines from the two heterotic groups displayed close kinships (Li et al. 2018) and merged into connected groups in population structure analysis (Fig. 6) and PCA (Fig. 7). The AM119 were divided into six subgroups because the most significant  $\Delta K$  peak was observed when  $k=6$  (Fig. 6a) (CV errors = 0.71230 when  $k=6$ , other values are listed in Table S6). The other lines with membership probabilities < 0.6 were grouped into one cluster, which was defined as the mixed group (the seventh subgroup). The division of the population into six subgroups and a mixed group was consistent with previous studies (Li et al. 2018). In these 7 subgroups (except *Q2* and *Q6*, in which the highest percentages, 45% and 53.33%, respectively, were of low-level *C* value inbred lines), *Q1*, *Q3*, *Q4*, *Q5* and *Q7* were dominated by inbred lines with medium-level *C* values (71.42%, 66.67%, 60%, 61.54%, and 37.93%) (Table 4). However, the results of multiple comparisons showed no significant

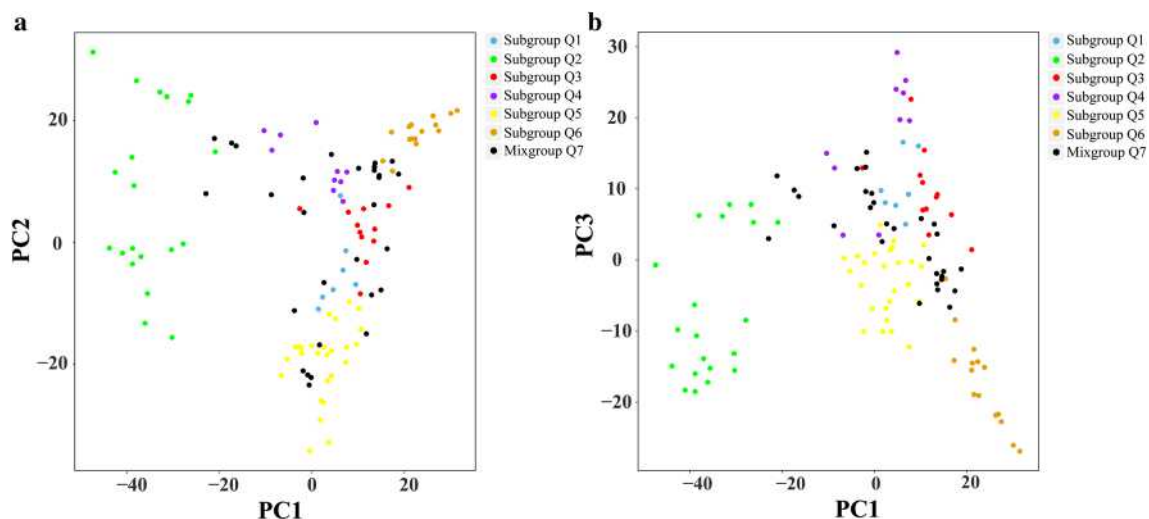
**Table 4** The percentages of H, M, L level cycle values in the Shaan A and Shaan B groups, and in the 7 subgroups

Level of cycle value	The percentages of different level cycle values								
	A (%)	B (%)	Q1 (%)	Q2 (%)	Q3 (%)	Q4 (%)	Q5 (%)	Q6 (%)	Q7 (%)
<i>H</i>	8	24.47	0	20	16.67	30	15.38	13.33	34.48
<i>M</i>	48	45.74	71.42	35	66.67	60	61.54	33.33	37.93
<i>L</i>	44	28.72	28.57	45	16.67	10	23.08	53.33	27.59

*A* the fraction of Shaan A heterotic group in the 119 inbred lines; *B* the fraction of Shaan B heterotic group in the 119 inbred lines; *Q1–Q7* 7 subgroups of the 119 inbred lines based on population structure

**Fig. 6** Population structure of 119 inbred lines. **a** Plot of LnP(D) and an ad-hoc statistic 1P calculated for  $K=1-10$ . LnP(D) is the output of STRUCTURE obtained by first computing the natural logarithm of

the probability at each step of Markov chain Monte Carlo, 1P is the difference of LnP(D) between adjacent  $K$ . **b** Population structure at  $K=6$

**Fig. 7** **a** Principal component analysis (PCA) of the first two components of AM119. **b** PCA of the first and third components of AM119. The different colours represent different clades as described in the text

differences in  $C$  values among the seven subgroups (Fig. 8), which demonstrated that the group structure had no effect on the level of endopolyploidization (the  $C$  value).

### Analysis of the correlation between $C$ value and agronomic traits

In accordance with the analysis of the correlation between the  $C$  value and the phenotypic data of AM119 at the



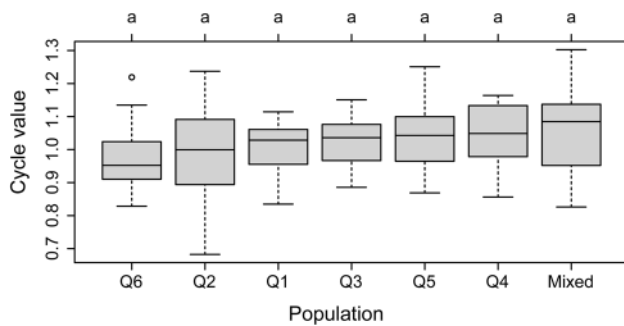


**Fig. 8** Boxplot of cycle values in the seven subgroups. The letter a indicates that there are no differences among the samples ( $p > 0.05$ )

seedling stage, weak correlations could be found between the  $C$  value and the length of the whole seedling, the length of the main root, the dry weight of the stem and leaf and SPAD (Fig. 9a). In the seedling stage, the length of the whole seedling and the length of the main root were significantly correlated with the  $C$  value at the 0.05 level ( $r = 0.213^*$  and  $r = 0.200^*$ , respectively). The correlations between the  $C$  value and the other phenotypic traits were not significant ( $r = 0.033$  for the SPAD,  $r = 0.065$  for the dry weight of the stem and leaves,  $r = -0.019$  for the dry weight of the root). A correlation analysis of the  $C$  value and each of the various agronomic traits and GY (grain yield) at the mature stages shows that the  $C$  value was not correlated with these agronomic characters or GY in AM119 (Fig. 9b).

### GWAS of maize endopolyploidy

Through tGBS sequencing, 1,133,188 sites were identified, among which 48,415 SNPs were polymorphic in AM119, with a minimum calling rate  $\geq 20\%$  and a MAF of more than 0.01. For the 48,415 SNPs, the number of SNPs per chromosome ranged from 3,418 SNPs on chromosome 10 to 6884 SNPs on chromosome 1 (Table 5). A GLM model in TASSEL2.5 software was used to perform a GWAS (the  $C$  value satisfied normality). A total of 9 significant SNPs ( $-\log_{10}(p) > 4$ ) were found to be associated with the  $C$  value in maize (Fig. 10a, b). In the population, the most significant SNPs for  $C$  value were chr9.S\_148881220 ( $p = 1.69 \times 10^{-6}$ ), chr3.S\_322376, chr4.S\_188547620, chr3.S\_322370, chr3.S\_322371, chr3.S\_231268803, chr2.S\_124468408, chr1.S\_24326912 and chr9.S\_76314578. When the  $R^2$  value was less than 0.1, the LD decay distance was about 150 kb in this population, which had been computed in a previous study (Li et al. 2018). Therefore, a 300-kb window for the significant SNPs (150 kb upstream and downstream of the lead SNP) was selected to identify the candidate genes, and a total of 99 genes were found using the genome browser ([https://www.maizegdb.org/gbrowse/maize\\_v4](https://www.maizegdb.org/gbrowse/maize_v4)). Among these 99 genes, 70 were identified to have functional domains

based on the NCBI database (<https://smart.embl-heidelberg.de/>) and the CD-search service (<https://www.ncbi.nlm.nih.gov/Structure/cdd/wrpsb.cgi>) and are listed in Table S7. Eight of these genes are related to cell cycle regulation and DNA replication (Zm00001d048046, Zm00001d048053 and Pco102965(279) on chr9; Zm00001d052376 on chr4; LOC100283338 on chr4; and Zm00001d039243, Zm00001d044536 and LOC100281587 on chr3), while the residual 29 genes were identified to have no functional domains. The 8 genes that may be associated with endoreplication are illustrated in Table 6.

## Discussion

### Endopolyploidization varies across organs in maize

In this study, ploidy is usually higher in organs with vigorous growth (i.e. root at the V3 stage and the endosperm at 20 DAP), and some highly lignified transport-associated tissues (i.e. husk leaf at 7 DAP, leaf sheath at the R1 stage and main leaf vein at 7 DAP) are prone to producing high-ploidy nuclei, which is consistent with previous reports (Larkins et al. 2001; Sabelli 2012). However, the organs with the highest ploidy differ among different plants. In cabbage, the nuclei with the highest ploidy were in the hypocotyls (Kudo and Kimura 2001), while those of maize in this study were in the grains (endosperm).

Endoreplication in plants most commonly occurs in tissues that develop mass quickly and have high metabolic activity (Edgar et al. 2014; Inzé and Veylder 2006). In this study, the high  $C$  value of roots may be closely related to their function in water metabolism. They are necessary for water acquisition and can be a significant factor in adapting to different environmental conditions (Lynch et al. 2014; Osmont et al. 2007). Endoreplication was reported to aid in maximizing the surface area needed for root hair formation and elongation, which can increase the surface area of the root, aiding plants in absorbing water and nutrients (Kondorosi et al. 2000; Lee et al. 2009). Furthermore, root hairs are important for plants to become stably rooted, and their lacking leads to instability (Menand et al. 2007). Homoplastically, endoreplication in maize roots may contribute to water metabolism by promoting root growth and structure formation.

One possible reason why the  $C$  value was the lowest in the leaves at the mature stage (V6 stage, 7 DAP) is that rapid DNA replication is no longer needed for a rapid increase in cell volume since true leaves have formed, and thus endoreplication stops at the mature stage. During the early stages of plant growth, endoreplication occurs at moderate levels in the leaf sheath and main leaf vein. There are mechanical tissues in both the leaf sheath and main leaf vein that

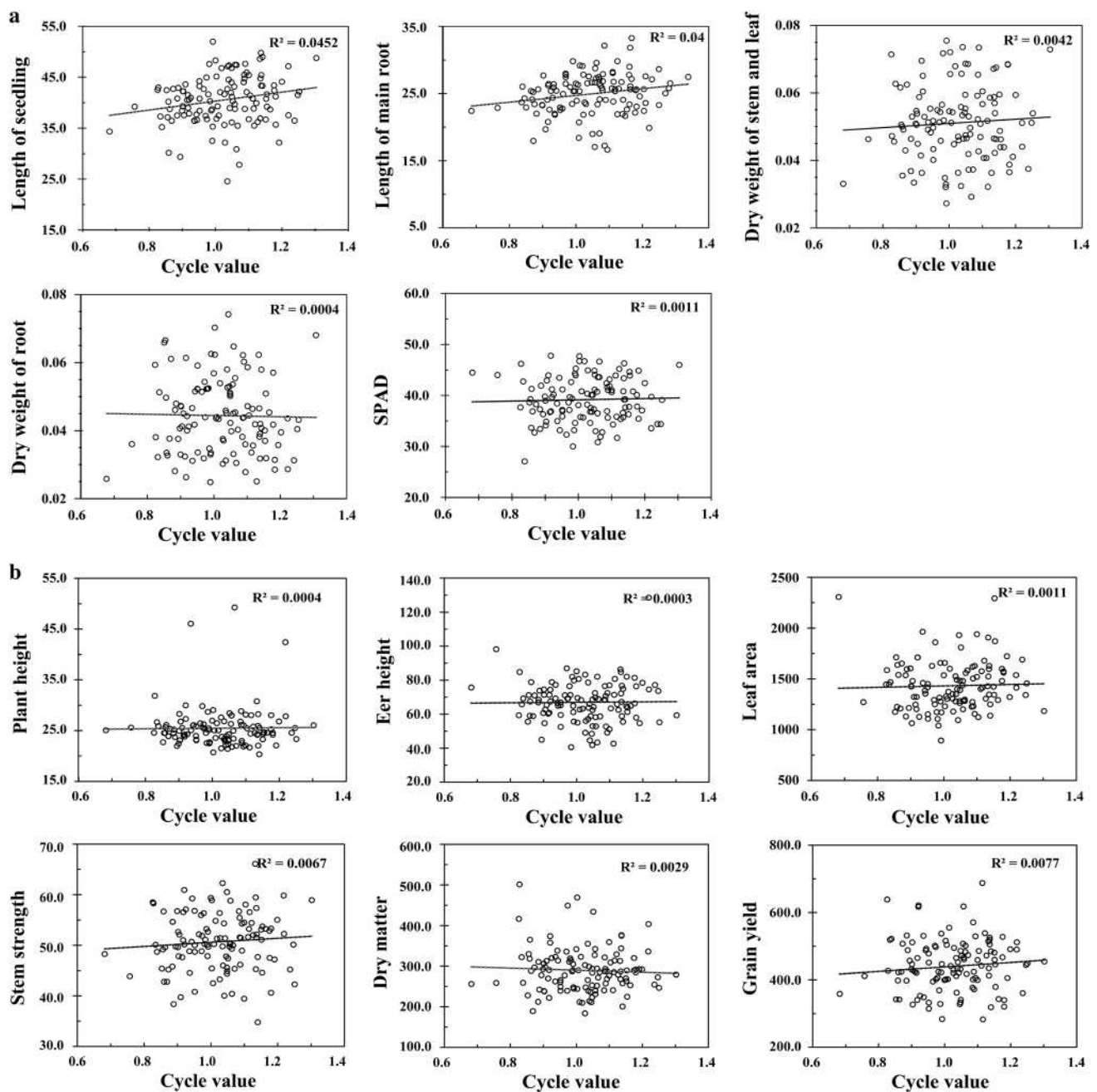


**Fig. 9** Correlation coefficient between cycle value and phenotypic traits in 119 inbred lines. **a** Correlation coefficient at the seedling stage. **b** Correlation coefficient at the mature stage

play a major role in supporting and protecting plants (Niu 2001). The degree of endopolyploidy ( $C$  value) was similar between the leaf sheath and vein because the structures and functions of these mechanical tissues are similar. The leaf sheath had the highest  $C$  value among all organs during the R1 (silking) stage due to its strengthening function. In the late growth period, the chlorophyll and soluble protein contents of the leaf sheath change dramatically (Tong and Song

2012). In stems, more endopolyploid cells were found in the nodes than in the internodes, which is consistent with previous studies (Coleman 2011; Shi et al. 2015). In addition, increased lignification in husk leaves should be the main reason why the  $C$  values of husk leaves are higher than those of leaves in the R1 (silking) stage and at 7 DAP (Guo et al. 2008; Larkins et al. 2001). Similar to the leaves, there are no 8C nuclei in corn cobs and ovules, which is important for



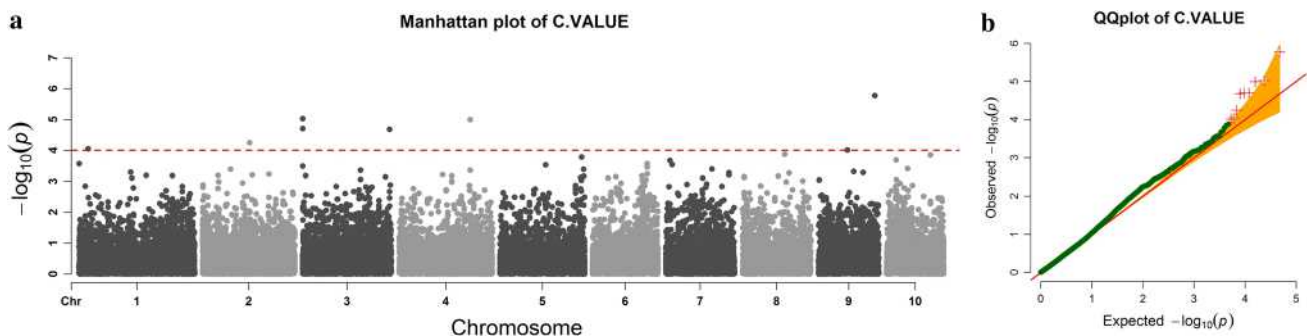
**Table 5** Chromosomal distribution and proportion of polymorphic markers used for the population structure and association analyses

Chromosome	48415 SNPs		
	No. of markers	Proportion (%)	Marker density(kb)
1	6884	14.22	44.56
2	5368	11.09	45.6
3	5988	12.37	39.35
4	5752	11.89	42.94
5	4886	10.09	45.86
6	3888	8.03	44.72
7	4177	8.63	43.66
8	4329	8.94	41.87
9	3725	7.69	42.92
10	3418	7.06	44.2
Average	4841.5	10	43.568

female flowers to avoid the generation of polyploid gametes as suggested by an early study (Galbraith et al. 1991). The 1C nuclei, which may have come from the DNA of pollen grains, appeared in the staminate flowers (Fig. S3).

## Endopolyploidization is developmental stage-specific in maize

Under normal growth conditions, the level of endopolyploidy in maize is also related to developmental stage. In all tested organs, except leaves, the level of endopolyploidy increased with organ development until reaching maturity. In the V2 (second leaf) stage, the *C* value of the roots was low because they had a simple structure and lacked root hairs in terms of cell morphogenesis (Jonathan et al. 2010). The V3 (third leaf) stage, which is also called the albumen stage, is the first important turning point in the growth of maize. Stored nutrients in seeds are depleted by this stage, during which the development of maize shifts from an autotrophic model to a photosynthetic model. During this period, roots grow vigorously at the third leaf stage to provide plenty of water and nutrients for seedling development, which might be the main reason for the *C* value of the roots being the highest in the V3 (third leaf) stage. During the V4 (fourth leaf) stage, fewer nutrients are absorbed by the roots and root metabolism weakens, which might decrease the ploidy of the roots. Between the V6 (elongation) and VT (tasselling) stage, the metabolism of the roots becomes active again.

**Fig. 10** **a** Manhattan plots of GLM for the endopolyploid traits of 119 inbred lines. **b** Quantile–quantile plots of GLM for the endopolyploid traits of 119 inbred lines**Table 6** Markers and genes significantly associated with endoreplication

Chr	Pos	<i>P</i> value	Marker <i>R</i> <sup>2</sup>	Candidate interval	Gene ID	Function domain
9	148881220	1.69E–06	0.28357	148731220–149031220	Zm00001d048046	Myb_DNA-binding
9	148881220	1.69E–06	0.28357	148731220–149031220	Zm00001d048053	Protein kinase domain; PLN00113 super family; LRRNT_2
9	148881220	1.69E–06	0.28357	148731220–149031220	Pco102965(279)	LRRNT_2; Pkinase
3	322370;322371;322376	9.50E–06	0.33381	172370–472370	Zm00001d039243	Pkinase
3	231268803	2.11E–05	0.24033	231118803–231418803	Zm00001d044536	PKc_like super family
3	231268803	2.11E–05	0.24033	231118803–231418803	LOC100281587	DNA replication licensing factor mcm4
4	188547620	1.02E–05	0.30695	188397620–188697620	Zm00001d052376	Catalytic domain of the serine/threonine kinases
4	188547620	1.02E–05	0.30695	188397620–188697620	LOC100283338	Serine/threonine-protein kinase NAK

Perhaps endoreplication is necessary to provide sufficient DNA content to sustain simultaneous vegetative and reproductive growth (Lee et al. 2009). The V12 (big trumpet) stage is the most vibrant stage in the life cycle of maize, when the *C* value reached its second highest peak during this stage. After that, plant growth was mainly reproductive, and the *C* value of the roots decreased.

In leaves, 8C nuclei only occurred at the V2 (second leaf) stage, and they disappeared at the V3 (third leaf) stage. After the V6 (elongation) stage, when the leaves had expanded, the *C* value decreased to 0.2, probably because a rapid increase in cell volume was no longer needed. Moreover, endoreplication was reported to be negatively regulated by sunlight (Gendreau et al. 1998), which might also have restrained ploidy. Active metabolism and important functions may explain why the *C* value of the leaf sheath was high throughout the developmental stages. The *C* value increased from the VT (tasselling) to the R1 (silking) stage because leaf sheaths are needed to strengthen the support capacity of the stems and conserve enough water for pollination during corn growth. For the same reasons, the extent of endopolyploidy increased from the VT stage to the R1 stage in the main leaf vein and stem. The vigorous differentiation of the stem in the V6 (elongation) stage may be an important reason for the peak *C* value of the nodes at the V9 (small trumpet) stage (Jonathan et al. 2010; Vinardell et al. 2003). Moreover, the *C* value increased during organ development, which is consistent with conclusions from previous research (Barow and Meister 2010; Galbraith et al. 1991). The higher proportion of low-ploidy nuclei in young organs may result from the organ developmental program. Cells with increased genome copy numbers may not accumulate in early development due to the high rate of cell division. In addition, some previous reports have demonstrated that those organs with a high level of lignification always have high-ploidy nuclei (Guo et al. 2008; Larkins et al. 2001), which indicates that the level of endopolyploidy increases with increasing lignification.

### Endoreplication of plants under drought stress

In this study, drought stress had an obvious impact on the degree of endopolyploidy in maize roots, which is consistent with previous studies (Barow 2006; Bhosale et al. 2018). Plants respond to water deficits and adapt to drought stress through various physiological and biochemical changes, including changes in endogenous phytohormone levels, such as hormone abscisic acid (ABA), gibberellic acid (GA), ethylene (ET), auxin, and cytokines (CKs), which have been shown to affect endopolyploidy (Bari and Jones 2009; Bradley and Crane 1955; Callebaut et al. 1982; Dan et al. 2003; Gendreau et al. 1999; Lur and Setter 1993; Mishiba et al. 2001; Mohamed and Bopp 1980; Valente et al. 1998). For instance, the accumulation of ABA can be induced by

osmotic stress signals under drought stress (Zhu 2002), and cell division, which reverses endopolyploidy, can be inhibited by ABA (Wang et al. 1998). In maize, while CKs (i.e. zeatin and zeatin riboside) are associated with the mitotic phase of development, the auxin (i.e. 3-indoleacetic acid, IAA) concentration increases at the onset of endoreplication and a positive correlation between the auxin levels and nuclear size was revealed in maize endosperm. In addition, the treatment of maize kernels with the auxin 2,4-D accelerated the switch to endoreplication, increasing the nuclear size and zein gene expression, whereas application of the antiauxin 2-(para-chlorophenoxy) isobutyric had the opposite effect (Lur and Setter 1993). These findings support an essential role for auxin in endoreplication. In this study, hormone-mediated pathways might play an important role in the resulting fluctuation in endopolyploidy in maize root.

### Prominent endopolyploidy in maize endosperm cells

Endosperm is generally used to store energy for developing seeds. A switch from the mitotic cell cycle to the endocycle occurs during endosperm formation after fertilization (Graf and Larkins 1995; Larkins et al. 2001; Leiva-Neto et al. 2004). The ploidy may be directly affected by the grain filling rate because endoreplication is often associated with processes such as cell enlargement and the accumulation of storage metabolites. Accordingly, there was a positive correlation between polysomaty and grain filling speed (Fig. 4a, b). Most types of polyploid nuclei were found at 20 DAP, which could be because the fast filling of a limited number of cells was needed. To increase the activity of endosperm cells and accumulate storage material quickly, endoreplication is activated to create many genomes over a short time (Kowles et al. 1997; Zhang et al. 2007). The increasing *C* value from 20 to 35 DAP (Fig. 5) indicates an increasing overall ploidy level of endosperm cells, for which the proportions of 12C nuclei and 24C nuclei tend to increase. Exceptionally, 96C nuclei disappeared from 20 to 25 DAP, and 48C nuclei showed a decreasing trend. These exceptions could be the result of programmed cell death (PCD), which starts at 16 DAP in endosperm cells (Young and Gallie 2000a). The number of starchy endosperm cells stops increasing after 20 DAP due to the cessation of mitosis (Nguyen et al. 2007), after which the number of cells decreases due to PCD. However, random PCD should not result in the complete disappearance of 96C nuclei, nor should it lead to a decline in 48C nuclei from 25 to 35 DAP, which indicates that PCD preferentially affects cells with high ploidy. This view might be supported by previous findings in which endoreplication and PCD were found to start from the central area of starchy endosperm cells and then



spread (Nguyen et al. 2007), indicating a potential connection between endoreplication and PCD.

### Characteristics of endopolyploidy in inbred lines and analysis of candidate genes

Although the *C* value has different distribution ratios in each genetic subgroup within the AM119, the results of multiple comparisons demonstrated that there were no significant differences in the *C* values among the 7 subgroups. Therefore, the ploidy is not affected by the group structure. The results of a correlation analysis between the *C* value and the phenotypic traits of seedlings revealed that fast-growing varieties (those with greater seedling lengths) tend to have a higher degree of endoreplication. This finding can be supported by a hypothesis suggesting an influence of endopolyploidy on plant growth and development through the larger cell volumes of endopolyploid cells in comparison with non-endopolyploid cells (Barow 2006; Melaragno et al. 1993). Moreover, endoreplication is not correlated with the GY during the mature period, which revealed that the primary effect of endoreplication may be on the rate of substance accumulation in the initial developmental stage, not the final substance levels.

Although not significant, group effects were included in the GWAS GLM model to control for a possible mild effect. Relative kinship between inbred lines was not included in the GWAS model as, consistent with previous studies (Li et al. 2018), it appeared limited: a total of 61.82% of the relative kinship values were equal to 0, 36.62% of the relative kinship values varied from 0.05 to 0.5 and only 0.15% of the relative kinship values exceeded 0.7. A total of 9 significant SNPs were detected as associated with endopolyploidy, and five candidate genes that participate in cell cycle regulation and DNA replication were identified. According to the MaizeGDB (<https://www.maizegdb.org>) description, *zm00001d048053* and *Pco102965(279)* (chr 9) produce multiple alternatively spliced transcripts. Domain analysis via SMART (<https://smart.embl-heidelberg.de/>) and the CD-search service (<https://www.ncbi.nlm.nih.gov/Structure/cdd/wrpsb.cgi>) showed that the proteins encoded by both *zm00001d048053* and *Pco102965(279)* contain two domains (LRRNT2 and Pkinase). In addition, *Zm00001d039243* on chr3 also contains a protein kinase domain. According to previous studies, the protein kinases (PKs) catalyse the transfer of the gamma phosphate from nucleotide triphosphates (often ATP) to one or more amino acid residues in a protein substrate side chain, resulting in a conformational change affecting protein function (Schenk and Snaarjagalska 1999; Stone and Walker 1995). However, protein phosphatases catalyse the reverse process and participate in cell cycle regulation.

For example, the CDKA/CYCD complexes phosphorylate and inactivate the protein retinoblastoma-related (RBR) at the G1/S transition, and thus an S-phase gene expression program is stimulated by permitting the formation of heterodimeric E2F/DP transcription factors. In addition, CDK activity is inhibited by WEE1-mediated phosphorylation at specific tyrosine residues. M-phase progression is promoted by certain B-type CDKs, whose expression is E2F/DP-dependent, through mechanisms that include the stimulation of downstream CDK activity by phosphorylating and targeting certain CKIs for proteolysis by the ubiquitin–proteasome system (UPS) and interaction with A-type cyclins (Dante et al. 2014a). *Zm00001d048046* (chr 9) contains two domains (Response\_reg and Myb\_DNA-binding). Numerous studies have reported that MYB transcription factors are involved in various developmental and physiological processes, especially in abiotic and biotic stress responses (Dubos et al. 2010). For instance, AtMYB2 functions in the ABA-mediated drought stress response (Abe et al. 2003). Moreover, the *Oryza sativa* MYB-like domain (OsMLD), which belonged to the third heterogeneous class comprised of a single or a partial MYB repeat, is involved in the control of cellular morphogenesis (Pesch and Hülskamp 2009) and plays a role in secondary metabolism (Matsui et al. 2008). Meanwhile, endoreplication is involved in the plant stress response (biological and abiotic) (Lee et al. 2009). Cell division, which reverses endopolyploidy, is inhibited by ABA, is suggested by a previous study (Wang et al. 1998). In addition, the role of polyploidy in tissue development appears to suggest that an increase in phylogenesis and endopolyploidy is an adaptive morphogenetic factor during development (Anisimov 2005). Additionally, SMART and CD-search detected a STKc\_IRAK (Catalytic domain of the Serine/Threonine kinases, Interleukin-1 Receptor Associated Kinases and related STKs) domain in a protein sequence encoded by *Zm00001d052376* (chr 4). PKs facilitate crosstalk between the cell signalling and cell cycle regulation pathways. Serine/threonine PKs, which catalyse protein phosphorylation, play an important role in DNA replication and mitosis. Protein phosphorylation at a limited number of amino acid residues is considered a general method to control protein synthesis, cell division, and the modulation of metabolic enzymes; moreover, the incorrect function of these enzymes often results in malignancies (Hunter 1987). *LOC100283338* (chr 4) is a type of serine/threonine PK called NAK. Similarly, the functional description of *Zm00001d044536* (chr 3) includes a PK catalytic domain. In addition, *LOC100281587* on chr3 encodes the DNA replication licensing factor mcm4, which plays a role in the single-stranded DNA binding activity of the complex. Mcm proteins are necessary for eukaryotic DNA replication (Chong et al. 1996; Kearsey

and Labib 1998; Kearsey et al. 1996). These 8 genes participate in cell cycle regulation and DNA replication; however, their association with endopolyploidy requires further investigation.

**Acknowledgements** This work was supported by the Shaanxi Province Comprehensive Project (Grant Number: 2015KTZDNY01-01-01) and the Yangling District Technical Plan Project (Grant Number: 2014NY-01).

**Authors' contribution statement** DWG conceived this research. SLL measured the endopolyploidy data, performed the data analyses and interpretation and drafted the manuscript. LSL edited the manuscript and assisted in the data interpretation. TL and STX performed the DNA extractions and SNP sequencing. TRL and JCL conducted the genotypic assays. YHW measured the agronomic traits in the field. JQX provided all of the plant germplasms. ZQZ, XHZ and JCZ performed the cultivation of the greenhouse and field materials. All authors read and approved the final manuscript.

## Compliance with ethical standards

**Conflict of interest** On behalf of all authors, the corresponding author states that there is no conflict of interest.

**Ethical standards** We state that all experiments in the study comply with the ethical standards in China.

## References

- Abe H, Urao T, Ito T, Seki M, Shinozaki K, Yamaguchi-shinozaki K (2003) Arabidopsis AtMYC2 (bHLH) and AtMYB2 (MYB) function as transcriptional activators in abscisic acid signaling. *Plant Cell* 15:63–78
- Alexander DH, Novembre J, Lange K (2009) Fast model-based estimation of ancestry in unrelated individuals. *Genome Res* 19:1655–1664
- Anisimov AP (2005) Endopolyploidy as a morphogenetic factor of development. *Cell Biol Int* 29:993–1004
- Bari R, Jones JD (2009) Role of plant hormones in plant defence responses. *Plant Mol Biol* 69:473–488
- Barow M (2006) Endopolyploidy in seed plants. *BioEssays* 28:271
- Barow M, Meister A (2010) Endopolyploidy in seed plants is differently correlated to systematics, organ, life strategy and genome size. *Plant, Cell Environ* 26:571–584
- Bhosale R, Boudolf V, Cuevas F, Lu R, Eekhout T, Hu Z, van Isterdael G, Lambert G, Xu F, Nowack MK, Smith RS, Vercauteren I, De Rycke RM, Storme V, Beeckman T, Larkin JC, Kremer A, Höfte H, Galbraith DW, Kumpf RP, Maere S, De Veylder L (2018) A spatiotemporal DNA endoploidy map of the Arabidopsis root reveals roles for the endocycle in root development and stress adaptation. *Plant Cell* 30:2330–2351
- Bourdon M, Pirrello J, Cheniclet C, Coriton O, Bourge M, Brown S, Moïse A, Peypelut M, Rouyère V, Renaudin JP (2012) Evidence for karyoplasmic homeostasis during endoreduplication and a ploidy-dependent increase in gene transcription during tomato fruit growth. *Development* 139:3817–3826
- Bradbury PJ, Zhang Z, Kroon DE, Casstevens TM, Ramdoss Y, Buckler ES (2007) TASSEL: software for association mapping of complex traits in diverse samples. *Bioinformatics* 23:2633–2635
- Bradley MV, Crane JC (1955) The effect of 2,4,5-trichlorophenoxy-acetic acid on cell and nuclear size and endopolyploidy in parenchyma of apricot fruits. *Am J Bot* 42:273–281
- Bringezu TGG, Sharbel TF, Weber WE (2011) Grain development and endoreduplication in maize and the impact of heat stress. *Euphytica* 182:363–376
- Callebaut A, Van OP, Van PR (1982) Endomitosis and the effect of gibberellic acid in different *Pisum sativum* L. cultivars. *Planta* 156:553
- Chong JP, Thömmes P, Blow JJ (1996) The role of MCM/P1 proteins in the licensing of DNA replication. *Trends Biochem Sci* 21:102
- Coleman LC (2011) Nuclear conditions in normal stem tissue of VICIA FABA. *Can J Res* 28:382–391
- Dan H, Imaseki H, Wasteneys GO, Kazama H (2003) Ethylene stimulates endoreduplication but inhibits cytokinesis in cucumber hypocotyl epidermis. *Plant Physiol* 133:1726–1731
- Dante RA, Sabelli PA, Sun Y, Dilkes BP, Gordon-Kamm WJ, Larkins BA (2005) Cyclin-dependent kinase inhibitors in maize endosperm and their potential role in endoreduplication. *Plant Physiol* 138:2323–2336
- Dante RA, Larkins BA, Sabelli PA (2014a) Cell cycle control and seed development. *Front Plant Sci* 5:493
- Dante RA, Sabelli PA, Hong NN, Leivaneto JT, Tao Y, Lowe KS, Hoerster GJ, Gordonkamm WJ, Jung R, Larkins BA (2014b) Cyclin-dependent kinase complexes in developing maize endosperm: evidence for differential expression and functional specialization. *Planta* 239:493–509
- Dolfini SF, Landoni M, Tonelli C, Bernard L, Viotti A (2010) Spatial regulation in the expression of structural and regulatory storage-protein genes in *Zea mays* endosperm. *Genesis* 13:264–276
- Doyle J (1991) Isolation of plant DNA from fresh tissue. *Focus* 12:13–15
- Dubos C, Stracke R, Grotewold E, Weissshaar B, Martin C, Lepiniec L (2010) MYB transcription factors in Arabidopsis. *Trends Plant Sci* 15:573–581
- Edgar BA, Zielke N, Gutierrez C (2014) Endocycles: a recurrent evolutionary innovation for post-mitotic cell growth. *Nat Rev Mol Cell Biol* 15:197
- Elshire RJ, Glaubitz JC, Sun Q, Poland JA, Kawamoto K, Buckler ES, Mitchell SE (2011) A robust, simple genotyping-by-sequencing (GBS) approach for high diversity species. *PLoS ONE* 6:e19379
- Galbraith DW, Harkins KR, Knapp S (1991) Systemic endopolyploidy in Arabidopsis thaliana. *Plant Physiol* 96:985–989
- Gendreau E, Höfte H, Grandjean O, Brown S, Traas J (1998) Phytochrome controls the number of endoreduplication cycles in the Arabidopsis thaliana hypocotyl. *Plant J Cell Mol Biol* 13:221
- Gendreau E, Orbovic V, Höfte H, Traas J (1999) Gibberellin and ethylene control endoreduplication levels in the Arabidopsis thaliana hypocotyl. *Planta* 209:513–516
- Glaubitz JC, Casstevens TM, Lu F, Harriman J, Elshire RJ, Sun Q, Buckler ES (2014) TASSEL-GBS: a high capacity genotyping by sequencing analysis pipeline. *PLoS One* 9:e90346
- Grafi G, Larkins BA (1995) Endoreduplication in maize endosperm: involvement of M phase—promoting factor inhibition and induction of S phase—related kinases. *Science* 269:1262
- Guo DW, Fei LI, Liu-Yin MA, Lian-Cheng LI, You-Zhi MA, Ri-Fei Sun (2008) Endopolyploidization phenomenon of Chinese cabbage (*Brassica rapa* ssp. *pekinensis*). *Acta Agronomica Sinica* 34:1386–1392
- Hunter T (1987) A thousand and one protein kinases. *Cell* 50:823
- Inzé D, Veylder LD (2006) Cell cycle regulation in plant development 1. *Annu Rev Genet* 40:77



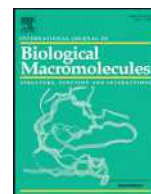
- Jonathan B, Katja W, Christina W, Farshad R, Remmy K, Larkin JC, Martin H, Arp S (2010) Endoreplication controls cell fate maintenance. *PLoS Genet* 6:e1000996
- Joubès J, Chevalier C (2000) Endoreduplication in higher plants. *Plant Mol Biol* 43:735–745
- Katagiri Y, Hasegawa J, Fujikura U, Hoshino R, Matsunaga S, Tsukaya H (2016) The coordination of ploidy and cell size differs between cell layers in leaves. *Development* 143:1120–1125
- Kearsey SE, Labib K (1998) MCM proteins: evolution, properties, and role in DNA replication. *Biochimica et Biophysica Acta (BBA)-Gene Struct Express* 1398:113–136
- Kearsey SE, Maiorano D, Holmes EC, Todorov IT (1996) The role of MCM proteins in the cell cycle control of genome duplication. *BioEssays* 18:183–190
- Kondorosi E, Roudier F, Gendreau E (2000) Plant cell-size control: growing by ploidy? *Curr Opin Plant Biol* 3:488–492
- Kowles RV, Yerk GL, Haas KM, Phillips RL (1997) Maternal effects influencing DNA endoreduplication in developing endosperm of *Zea mays*. *Genome* 40:798
- Kudo N, Kimura Y (2001) Flow cytometric evidence for endopolyploidy in seedlings of some Brassica species. *Theor Appl Genet* 102:104–110
- Larkins BA, Dilkes BP, Dante RA, Coelho CM, Woo YM, Liu Y (2001) Investigating the hows and whys of DNA endoreduplication. *J Exp Bot* 52:183
- Lee HO, Davidson JM, Duronio RJ (2009) Endoreplication: polyploidy with purpose. *Genes Dev* 23:2461
- Leiva-Neto JT, Grafi G, Sabelli PA, Dante RA, Woo YM, Maddock S, Gordon-Kamm WJ, Larkins BA (2004) A dominant negative mutant of cyclin-dependent kinase A reduces endoreduplication but not cell size or gene expression in maize endosperm. *Plant Cell* 16:1854–1869
- Li T, Qu J, Wang Y, Chang L, He K, Guo D, Zhang X, Xu S, Xue J (2018) Genetic characterization of inbred lines from Shaan A and B groups for identifying loci associated with maize grain yield. *BMC Genet* 19:63
- Lur HS, Setter TL (1993) Role of auxin in maize endosperm development (timing of nuclear DNA endoreduplication, zein expression, and cytokinin). *Plant Physiol* 103(1):273–280
- Lynch JP, Chimungu JG, Brown KM (2014) Root anatomical phenes associated with water acquisition from drying soil: targets for crop improvement. *J Exp Bot* 65:6155
- Matsui K, Umemura Y, Ohmetakagi M (2008) AtMYBL2, a protein with a single MYB domain, acts as a negative regulator of anthocyanin biosynthesis in Arabidopsis. *Plant Journal* 55:954–967
- Melaragno JE, Mehrotra B, Coleman AW (1993) Relationship between endopolyploidy and cell size in epidermal tissue of Arabidopsis. *Plant Cell* 5:1661–1668
- Menand B, Yi K, Jouannic S, Hoffmann L, Ryan E, Linstead P, Schaefer DG, Dolan L (2007) An ancient mechanism controls the development of cells with a rooting function in land plants. *Science* 316:1477
- Mishiba KI, Okamoto T, Mii M (2001) Increasing ploidy level in cell suspension cultures of *Doritaenopsis* by exogenous application of 2,4-dichlorophenoxyacetic acid. *Physiol Plant* 112:142–148
- Mohamed Y, Bopp M (1980) Distribution of polyploidy in elongating and non-elongating shoot axis of *Pisum sativum*. *Zeitschrift Für Pflanzenphysiologie* 98:25–33
- Nguyen HN, Sabelli PA, Larkins BA (2007) Endoreduplication and programmed cell death in the cereal endosperm. Springer, Berlin
- Niu Y (2001) Adapting the specialization of cell wall in the plant tissue to the functions. *J Hengshui Normal Coll* 3:49–51
- Osmont KS, Sibout R, Hardtke CS (2007) Hidden branches: developments in root system architecture. *Annu Rev Plant Biol* 58:93–113
- Pesch M, Hülskamp M (2009) One, two, three...models for trichome patterning in Arabidopsis? *Curr Opin Plant Biol* 12:587–592
- Roeder AH, Chickarmane V, Cunha A, Obara B, Manjunath BS, Meyerowitz EM (2010) Variability in the control of cell division underlies sepal epidermal patterning in *Arabidopsis thaliana*. *PLoS Biol* 8(5):e1000367
- Sabelli PA (2012) Replicate and die for your own good: endoreduplication and cell death in the cereal endosperm. *J Cereal Sci* 56:9–20
- Sabelli PA (2014) Cell cycle regulation and plant development: a crop production perspective. In: Pessaraki M (ed) *Handbook of Plant and Crop Physiology*. CRC Press, Boca Raton, FL, pp 32–61
- Sabelli PA, Larkins BA (2008) The endoreduplication cell cycle: regulation and function. Springer, Berlin
- Sabelli PA, Dante RA, Leivaneto JT, Jung R, Gordonkamm WJ, Larkins BA (2005) RBR3, a member of the retinoblastoma-related family from maize, is regulated by the RBR1/E2F pathway. *Proc Natl Acad Sci USA* 102:13005–13012
- Sabelli PA, Hoerster G, Lizarraga LE, Brown SW, Gordonkamm WJ, Larkins BA (2009) Positive regulation of minichromosome maintenance gene expression, DNA replication, and cell transformation by a plant retinoblastoma gene. *Proc Natl Acad Sci USA* 106:4042–4047
- Sabelli PA, Yan L, Dante RA, Lizarraga LE, Hong NN, Brown SW, Klingler JP, Yu J, Labrant E, Layton TM (2013) Control of cell proliferation, endoreduplication, cell size, and cell death by the retinoblastoma-related pathway in maize endosperm. *PNAS* 110:E1827
- Schenk PW, Snaarjagalska BE (1999) Signal perception and transduction: the role of protein kinases. *Biochem Biophys Acta* 1449:1
- Schnittger A, Jurgens G, Hülskamp M (1998) Tissue layer and organ specificity of trichome formation are regulated by GLABRA1 and TRIPTYCHON in Arabidopsis. *Development* 125:2283–2289
- Schnittger A, Weinl C, Bouyer D, Schöbinger U, Hülskamp M (2003) Misexpression of the cyclin-dependent kinase inhibitor ICK1/KRP1 in single-celled arabidopsis trichomes reduces Endoreduplication and cell size and induces cell death. *Plant Cell* 15:303–315
- Scholes DR, Paige KN (2015) Plasticity in ploidy: a generalized response to stress. *Trends Plant Sci* 20:165–175
- Shi H, Wang LL, Sun LT, Dong LL, Liu B, Chen LP (2015) Cell division and endoreduplication play important roles in stem swelling of tuber mustard (*Brassica juncea* Coss. var. *tumida* Tsen et Lee). *Plant Biology* 14:956–963
- Shu Z, Row S, Deng W (2018) Endoreplication: the good, the bad, and the ugly. *Trends Cell Biol* 28(6):465–474
- Stone JM, Walker JC (1995) Plant protein kinase families and signal transduction. *Plant Physiol* 108:451
- Sun Y, Flannigan BA, Setter TL (1999) Regulation of endoreduplication in maize (*Zea mays* L.) endosperm. Isolation of a novel B1-type cyclin and its quantitative analysis. *Plant Mol Biol* 41:245–258
- Tong SY, Song FB (2012) Physiological characteristic changes of leaf and leaf sheath at different stem nodes of Maize in the late growth stage. *Heilongjiang Agric Sci*
- Valente P, Tao W, Verbelen JP (1998) Auxins and cytokinins control DNA endoreduplication and deduplication in single cells of tobacco. *Plant Sci* 134:207–215
- Vinardell JM, Fedorova E, Cebolla A, Kevei Z, Horvath G, Kelemen Z, Tarayre S, Roudier F, Mergaert P, Kondorosi A (2003) Endoreduplication mediated by the anaphase-promoting complex activator CCS52A is required for symbiotic cell differentiation in *Medicago truncatula* Nodules. *Plant Cell* 15:2093–2105
- Wang H, Qi Q, Schorr P, Cutler AJ, Crosby WL, Fowke LC (1998) ICK1, a cyclin-dependent protein kinase inhibitor from Arabidopsis thaliana interacts with both Cdc2a and CycD3, and its expression is induced by abscisic acid. *Plant J* 15:501–510
- Yamagata T, Kato H, Kuroda S, Abe S, Davies E (2003) Uncleaved legumin in developing maize endosperm: identification, accumulation and putative subcellular localization. *J Exp Bot* 54:913–922

- Young TE, Gallie DR (2000a) Programmed cell death during endosperm development. *Plant Mol Biol* 44:283
- Young TE, Gallie DR (2000b) Regulation of programmed cell death in maize endosperm by abscisic acid. *Plant Mol Biol* 42:397–414
- Zhang JJ, Hu YF, Zhou H, Huang YB (2007) Starch accumulation and activities of key enzymes involved in starch synthesis in the grains of maize inbred lines with different starch contents. *J Plant Physiol Mol Biol* 33:123

Zhu J (2002) Salt and drought stress signal transduction in plants. *Annu Rev Plant Biol* 53:247

**Publisher's Note** Springer Nature remains neutral with regard to jurisdictional claims in published maps and institutional affiliations.





# Short-time microwave treatment affects the multi-scale structure and digestive properties of high-amylose maize starch

Yuyue Zhong<sup>a,b,c</sup>, Wenxin Liang<sup>a</sup>, Hanqi Pu<sup>a</sup>, Andreas Blennow<sup>c</sup>, Xingxun Liu<sup>b,\*</sup>, Dongwei Guo<sup>a,\*</sup>

<sup>a</sup> Key Laboratory of Biology and Genetic Improvement of Maize in Arid Area of Northwest Region, Ministry of Agriculture, College of Agronomy, Northwest A&F University, Yangling, Shaanxi, China

<sup>b</sup> College of Food Science and Engineering/Collaborative Innovation Center for Modern Grain Circulation and Safety/Key Laboratory of Grains and Oils Quality Control and Processing, Nanjing University of Finance and Economics, Nanjing 210023, China

<sup>c</sup> Department of Plant and Environmental Sciences, University of Copenhagen, Denmark

## ARTICLE INFO

### Article history:

Received 31 May 2019

Received in revised form 2 July 2019

Accepted 3 July 2019

Available online 4 July 2019

### Keywords:

High-amylose maize starch

Short-time microwave treatment

Multi-scale structure

Digestion properties

## ABSTRACT

Microwave processing is a suitable technology for starch-based food processing. This work investigated the changes of structures and properties of high-amylose maize starch (HAMS) during short-time microwave irradiation (1–4 min). After 1 min of treatment, short amylopectin chains (DP 6–36) and intermediate amylose chains (DP 150–2000) of HAMS were partially broken down. Compared with native HAMS, treated HAMS (1 min) had the higher relative crystallinity, the intensity of the 9 nm lamellar peak, and fluorescence intensity under CLSM. Moreover, 1-min microwaving caused the lower viscosity and higher resistant starch content of HAMS. In the 2–4 min of treatment, the crystallinity, intensity of the lamellar peak and fluorescence intensity of HAMS granules decreased significantly, but no breakdown of starch molecule chains was observed, suggesting the realignment of the crystalline region during the process. Correspondingly, the viscosity increased and resistant starch content decreased. Our study provides a deeper understanding of the mechanistic effects of short-time microwave irradiation on high-amylose starch, which is of value for the processing of HAMS to produce novel functionality and nutritional values.

© 2019 Elsevier B.V. All rights reserved.

## 1. Introduction

Microwave irradiation, *i.e.* treatment with electromagnetic waves with frequencies ranging 300 MHz to 300 GHz [1], is commonly adopted in food processing for heating, baking, enzyme deactivation, and modification, *etc.* [2]. Domestic microwave systems generally have a frequency of 2.45 GHz, and industrial microwave ovens have frequencies of 915 MHz and 2.45 GHz [3]. According to the effect of dielectric loss, microwave irradiation affects foods through high-frequency electric fields to cause micro movement and friction of molecules in foods [2]. Microwave heating can thereby convert electromagnetic energy into thermal energy and generate concurrent internal and external heating [4]. For starch modification, this heating method has been widely used due to the dielectric heating and electromagnetic polarization of hydroxyl groups of structured water and starch [5].

Native starch is a natural polysaccharide with multi-scale structures from nanometer to micrometer in scale, including amylose and amylopectin chains (~0.1 nm range), crystalline and amorphous lamellar structure (~10 nm range), alternating amorphous and semi-crystalline growth rings (~0.1 μm range) and starch granules (1–100 μm range) [6]. The multi-scale structures of starch are highly related to the

processing and degradative attributes of many starch-based foods, such as viscosity, thermal property, texture and mouth-feel [7]. Effects of microwave irradiation on fine structure and physicochemical properties have been reported for different types of starches, including rice [5], potato [8], wheat [9], corn [9], lotus [10] and barley [11]. Especially, microwave treatment can induce the rearrangement of starch molecules and the changes of crystallinity type, relative crystallinity and morphology, and thereby changing physicochemical properties, such as water absorption ability, rheological behavior, gelatinization temperature and enthalpy, swelling power and paste viscosity [12]. Existing data on microwave treatment of different starches with different amylose contents suggest that the microwave energy is preferably transmitted to amorphous region of the starch granule and the crystalline regions are affected subsequently [13,14]. Microwave heating time is an important factor affecting the physicochemical properties of starch. For instance, microwave heating time affected thermal and pasting properties of waxy and high-amylose maize starches significantly [14,15]. Some authors also documented short time microwaving treatment can improve the functionality of starches from rice [5], potato [16], and groundnut [17].

High-amylose starch (HAS) is a type of starch with high potential in industrial uses and health benefits. It has high values in different areas, such as films and coating, textiles, paper, medical devices, and biodegradable packaging [18]. In addition, due to its high resistant starch

\* Corresponding authors.

E-mail addresses: [xxliu@nufe.edu.cn](mailto:xxliu@nufe.edu.cn) (X. Liu), [gdwei1973@126.com](mailto:gdwei1973@126.com) (D. Guo).

(RS) content, HAS provides high nutritional qualities and is beneficial to patients with colorectal cancer, and high levels of plasma cholesterol or triglyceride [19].

Microwave treatment is also an effective method to physically modify HAS. The effects of microwave on HAS, include increased porosity, decreased solubility, stability, and pasting properties and higher gelatinization transition temperature [20]. The digestibility of high-amylose starch is also affected and it has been reported that, after microwave treatment, rapidly digestible starch content increased significantly and correspondingly, RS content decreased in HAS [11]. However, the precise dynamic mechanisms of structural changes of HAMS, especially molecular structure, under microwave irradiation, are still unclear.

In this study, we investigated the mechanisms of microwave heating of high-amylose maize starch (HAMS) by collecting data on multi-scale structures including molecular, crystalline, lamellar and granular structures. Viscosity and enzyme-catalyzed hydrolytic degradation are also analyzed. Our data lays a theoretical foundation to expand the further application of HAMS in the food industry.

## 2. Materials and methods

### 2.1. Materials

HAMS (51% amylose content) was obtained from Maize Genetic Breeding Laboratory in Northwest A&F University in China. Normal maize starch (NMS), pancreatin (Cat. No. P7545) and amyloglucosidase (Cat. No. A7095) were from Sigma company (St. Louis, MO, USA).

### 2.2. Microwave treatment

Microwave heating treatment of HAMS mainly followed the protocol of Yang [14]. Starch (3 g dw portions) was transferred to glass Petri dishes (diameter 15.4 cm), and distilled water was injected by a syringe to retain the moisture content of HAMS to 30% (w/w). The Petri dishes were sealed and placed in the intermediate of the microwave oven (2450 MHz, Xianou Instrument Manufacturing Co., Ltd., Nanjing, China). The output power of 1.2 kW was used. Starch (400 w/g) was put in the glass Petri dishes and then was incubated for time intervals on a minutely basis (maximum 4 min). The appearance of samples before and after treatment was shown in Fig. S1. The samples were collected and dried at 40 °C overnight for further analysis. In that condition, there was restricted mobility of starch chains partially disorganized during gelatinization, avoiding reorganization (retrogradation) of starch [21]. According to the time (X) of microwave treatment, the starch was termed as MH-X. All samples were repeated twice for all analysis. To ensure reproductivity, MH-1 and MH-4 were selected with quadruplicate and triplicate, respectively. And RVA analysis was used to detect reproductivity (Fig. S2).

### 2.3. Gel-permeation chromatography (GPC)

Weight-based chain lengths distributions (CLDs) of debranched native and treated HAMS were analyzed by Gel-Permeation Chromatography (GPC). Starch was debranched by isoamylase in sodium acetate buffer (pH 3.5). The detectors, columns, and elution procedure were the same as Li [22]. Hydrodynamic radius (Rh), the degree of polymerization (DP) and the GPC weight distributions ( $w(\log R_h)$ ) were calculated as described ([23]).

### 2.4. Fluorophore-assisted carbohydrate electrophoresis (FACE)

After debranching starches by isoamylase, freeze-drying and derivatizing by 8-aminopyrene-1,3,6-trisulfonic acid (APTS) [24], samples were analyzed with a PA-800 Plus FACE System (Beckman-Coulter, Brea, CA, Valley, USA) using a solid-state laser-induced fluorescence (LIF) detector. The excitation source was an argon-ion laser and the

analytes were separated with a carbohydrate separation buffer (Beckman-Coulter) in an N-CHO-coated capillary at 25 °C and a voltage of 30 kV. The weight-based CLDs of glucan chains with DP 6–100 and the degree of branching of amylopectin were calculated [25].

### 2.5. Wide angle X-ray scattering (WAXS) and small angle X-ray scattering (SAXS)

Equilibration of moisture content to 10% was performed before the analysis of WAXS. An Xpert PRO diffractometer (PANalytical B.V., The Netherlands), with the current of 40 mA, the voltage of 40 kV, Cu K $\alpha$  radiation, and an X-ray source of 0.154 nm. The crystallinity was also analyzed as described [26]. The analysis of the lamella structure was conducted as described [27].

### 2.6. Scanning electron microscope (SEM)

Morphology and topography of starch granules coating with gold were analyzed by a scanning electron microscope (SEM) (SU8010, Hitachi, Japanese).

### 2.7. Confocal laser scanning microscopy (CLSM)

Internal structures of the starch granules were analyzed by detection of fluorescence signals using a Confocal laser scanning microscopy (CLSM) (FLUOVIEW FV1000, Waltham, USA) [28]. The granules were labelled with APTS as described [29]. The labelled starch granules were washed at least three times before dispersing in a 1:1 water/glycerol solution. Images were recorded using a He/Ne/Ar laser, the objective lens of UPLAPO40X2 (NA: 0.95), an excitation wavelength of 488 nm, emission wavelengths between 500 and 550 nm.

### 2.8. Viscosity properties

A Rapid Visco-Analyser (RVA 4500, Perten, Hägersten, Sweden) and a standard method from AACC [30] were used to measure the pasting properties of starches.

### 2.9. In vitro digestion properties

A modified protocol was used [31]. Starch (100 mg) was mixed with water (5 mL) in a tube, and heated in boiling water bath for 1 h. After cooling down to 37 °C, 12 mL acetate buffer (0.1 M, pH 5.5) containing 18.75 mg pancreatin and 13.4  $\mu$ L amyloglucosidase was added into starch solutions. Aliquots (0.1 mL) were taken at specified time points (0, 2, 4, 6, 8, 10, 12, 14, 16, 18, 20, 24, 28, 32, 36, 40, 60, 80, 100 and 120 min). The enzyme was inactivated by 1 mL of ethanol (95%). After centrifuging the dispersion at 4,500 rpm for 10 min, Megazyme GOPOD kit was adopted to measure the glucose content. Digestible starch (DS) was defined as starch hydrolyzed for 120 min, and resistant starch content (RS) was defined as starch that was not hydrolyzed for 120 min [32].

### 2.10. Statistical analysis

All data are reported as mean  $\pm$  standard deviation (SD) ( $n = 2$ ). One-way ANOVA with Tukey's pairwise comparison was carried out using SPSS V. 22.0 software (SPSS Inc., Chicago, IL) ( $p < 0.05$ ) and all figures were drawn by Origin 2016 (OriginLab, Northampton USA).

## 3. Results and discussion

### 3.1. Molecular structure change with microwave treatment

All starches showed a typical bimodal distribution with amylopectin (AP) at DP < 100 and amylose (AM) at DP > 100 (Fig. 1A). The whole



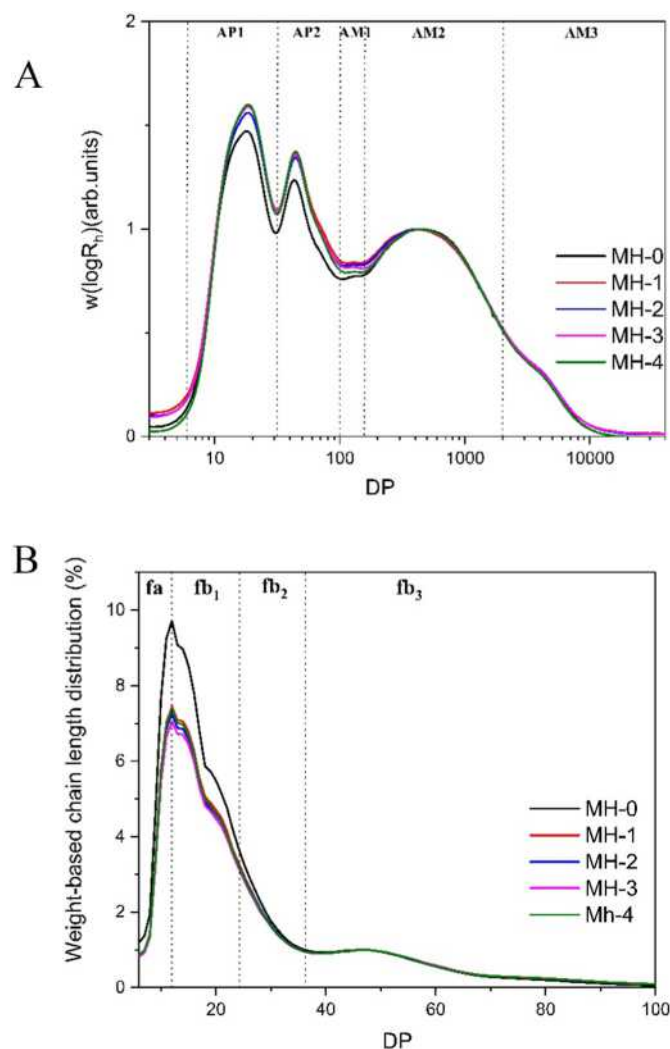


**Fig. 1.** Chain length distributions of debranched high-amylose maize starches after microwave treatment as deduced by A) GPC weight chain length distributions, normalized to the highest peak of amylose, B) FACE weight chain length distributions of amylopectin, normalized to the highest peak of fb<sub>3</sub> chain.

curve was normalized to the maximum peak of each sample. According to peaks, the amylopectin chains were divided into short (AP<sub>1</sub>, DP 6–36) and long chains (AP<sub>2</sub>, DP 36–100). Amylose chains were divided into 3 regions, AP<sub>1</sub> (100 ≤ DP < 150), AM<sub>2</sub> (150 ≤ DP < 2000), and AM<sub>3</sub> (2000 ≤ DP < 40,000), respectively, according to observed local maxima and shoulders in amylose regions (Fig. 1A). The areas of fraction X (AP<sub>1</sub>, AP<sub>2</sub>, AM<sub>1</sub>, AM<sub>2</sub>, and AM<sub>3</sub>) relative to the total eluted area under the curve (AUC) were calculated and denoted AUC<sub>x</sub> (Table 1). These parameters can be used to represent the relative contents of different AM/AP fractions [23]. AM was the sum of three amylose fractions. After 1 min of the microwave treatment (MH-1), HAMS had higher contents of

AP<sub>1</sub> and AP<sub>2</sub>, and lower contents of AM<sub>2</sub>. However, contents of AP<sub>1</sub>, AP<sub>2</sub> and Am were not significantly changed with further microwave treatment (MH-2 to MH-4).

The weight-based CLDs of amylopectin chains ranging DP 6–100 (Fig. 1B) was analyzed by FACE, aiming to obtain more details of the amylopectin of microwave-treated HAMS. Amylopectin chains can be divided into fa (DP 6–12), fb<sub>1</sub> (DP 13–24), fb<sub>2</sub> (DP 25–36) and fb<sub>3</sub> (DP > 36) chains [14]. According to the backbone model, we regard fa and fb<sub>1</sub> mainly as external chains and fb<sub>2</sub> and fb<sub>3</sub> mainly as internal chains. External chains can form double helices in crystalline lamella and internal chains are mainly found in the amorphous lamella [33]. Average chain lengths (ACLs) [34] and relative contents (same to AUC<sub>x</sub> in GPC) of different amylopectin fractions were calculated and presented in Table 2. Compared with MH-0, MH-1 exhibited higher ACLs of fb<sub>2</sub> and fb<sub>3</sub> chains, while ACLs of fa and fb<sub>1</sub> were not changed. Moreover, MH-1 had higher contents of fb<sub>3</sub>, lower contents of fa and fb<sub>1</sub>, and a lower degree of branching (DB). However, due to the limitation of FACE, we may lose the information about these very short amylopectin chains (DP < 6) cleaved from fa and fb<sub>1</sub> chains. The amylopectin structure of HAMS had not changed anymore in the next 3 min of microwave treatment.

Above data showed the main changes of molecular structures of HAMS occurred within 1 min of microwave treatment. GPC data documented the increase of AP content and the decrease of AM content. There was no reason AP content increased after the microwave treatment. Therefore, it was reasonable to attribute the increase of AP content to the breakdown of AM contents during the microwave treatment. The DP of these broken amylose chains was possibly smaller than DP 100 and thus detected as amylopectin chains by GPC. The breakdown of amylose was also found in microwave-treated potato starch [35]. Furthermore, the increase of contents of fb<sub>3</sub> chains and ACLs of fb<sub>2</sub> and fb<sub>3</sub> chains of amylopectin (FACE data, Table 2) proved this view again. The decrease of DB of amylopectin and contents of fa and fb<sub>1</sub> chains suggested the breakdown of fa and fb<sub>1</sub> of HAMS during 1 min microwave treatment. Molecular models [36] suggest that a single structural water molecule is stabilizing the branch point. When this water molecule is affected by microwave energy, the α-(1,6) glucosidic linkage can be specifically destabilized and cleaved. Such an effect has also been observed in microwave treated waxy maize starch [14].

### 3.2. Aggregation state structure

The apparent crystallinity and crystalline polymorphs, as deduced from powder wide-angle X-ray scattering (WAXS), demonstrate that both the native and the microwave-heated HAMS exhibited typical B-type crystalline structure with the strongest peak of 2θ at around 17° (Fig. 2A) [37]. All samples also showed peaks at 2θ around 20° and 22°, which are characteristic of the V-type crystalline polymorph, a single-helical structure typically found in amylose [14]. In other words, the crystalline polymorph was largely unaffected by the treatment, consistent with the unchanged proportions of fa and fb<sub>1</sub> chains (Table 2). The relative crystallinity of HAMS increased somewhat within the first minute of microwave treatment but then decreased significantly from the second minute and onwards (Table 3). We assumed

**Table 1**  
Molecular parameters of native and microwave-treated high-amylose maize starches.

Samples	AUC <sub>AP1</sub> (%)	AUC <sub>AP2</sub> (%)	AUC <sub>AM1</sub> (%)	AUC <sub>AM2</sub> (%)	AUC <sub>AM3</sub> (%)	AM
MH-0	28.2 ± 0.2 <sup>b</sup>	20.5 ± 0.0 <sup>c</sup>	5.4 ± 0.1 <sup>a</sup>	38.5 ± 0.2 <sup>a</sup>	7.6 ± 0.2 <sup>a</sup>	51.3 ± 0.3 <sup>a</sup>
MH-1	29.4 ± 0.0 <sup>ab</sup>	21.5 ± 0.0 <sup>b</sup>	5.6 ± 0.1 <sup>a</sup>	34.3 ± 0.3 <sup>b</sup>	7.5 ± 0.3 <sup>a</sup>	49.1 ± 0.00 <sup>b</sup>
MH-2	29.6 ± 0.6 <sup>a</sup>	21.5 ± 0.1 <sup>b</sup>	5.4 ± 0.0 <sup>a</sup>	36.0 ± 0.6 <sup>b</sup>	7.6 ± 0.3 <sup>a</sup>	48.9 ± 0.8 <sup>b</sup>
MH-3	29.4 ± 0.0 <sup>ab</sup>	21.4 ± 0.1 <sup>b</sup>	5.4 ± 0.0 <sup>a</sup>	36.3 ± 0.1 <sup>b</sup>	7.7 ± 0.2 <sup>a</sup>	49.2 ± 0.0 <sup>b</sup>
MH-4	29.2 ± 0.5 <sup>ab</sup>	22.1 ± 0.2 <sup>a</sup>	5.4 ± 0.0 <sup>a</sup>	36.6 ± 0.5 <sup>b</sup>	6.9 ± 0.5 <sup>a</sup>	48.7 ± 0.7 <sup>b</sup>

AUC<sub>AP1</sub>, AUC<sub>AP2</sub> and AUC<sub>AM</sub> were the ratios of the area under the curve (AUC) of AP<sub>1</sub>, AP<sub>2</sub>, and AM branches to the AUC of overall AP and AM branches in debranched starches. DB is the degree of branching of amylopectin.

All data are means ± standard deviation of two trials. Values with different letters in the same column are significantly different at  $p < 0.05$ .

**Table 2**

Weight-based chain length distribution of debranched amylopectin from native and microwave-treated high-amylose maize starches.

Time	Average chain lengths (ACLs)(DP)				Relative proportions (AUC)(%)				
	fa	fb <sub>1</sub>	fb <sub>2</sub>	fb <sub>3</sub>	fa	fb <sub>1</sub>	fb <sub>2</sub>	fb <sub>3</sub>	DB
0 min	10.3 ± 0.0 <sup>a</sup>	17.6 ± 0.0 <sup>a</sup>	27.5 ± 1.3 <sup>b</sup>	53.9 ± 1.9 <sup>b</sup>	21.9 ± 0.0 <sup>a</sup>	46.8 ± 0.3 <sup>a</sup>	14.8 ± 1.1 <sup>a</sup>	17.7 ± 0.3 <sup>b</sup>	4.2 ± 0.1 <sup>a</sup>
1 min	10.3 ± 0.0 <sup>a</sup>	17.7 ± 0.0 <sup>a</sup>	29.2 ± 0.0 <sup>a</sup>	56.6 ± 0.1 <sup>a</sup>	19.0 ± 0.0 <sup>b</sup>	44.5 ± 0.1 <sup>b</sup>	14.7 ± 0.0 <sup>a</sup>	21.8 ± 0.1 <sup>a</sup>	3.8 ± 0.0 <sup>b</sup>
2 min	10.3 ± 0.0 <sup>a</sup>	17.7 ± 0.0 <sup>a</sup>	29.3 ± 0.0 <sup>a</sup>	56.7 ± 0.1 <sup>a</sup>	18.7 ± 0.2 <sup>b</sup>	44.0 ± 0.0 <sup>b</sup>	14.8 ± 0.0 <sup>a</sup>	22.4 ± 0.2 <sup>a</sup>	3.7 ± 0.0 <sup>b</sup>
3 min	10.3 ± 0.0 <sup>a</sup>	17.6 ± 0.0 <sup>a</sup>	29.2 ± 0.0 <sup>a</sup>	55.7 ± 0.1 <sup>a</sup>	18.8 ± 0.4 <sup>b</sup>	43.9 ± 0.2 <sup>b</sup>	14.9 ± 0.1 <sup>a</sup>	22.5 ± 0.5 <sup>a</sup>	3.7 ± 0.0 <sup>b</sup>
4 min	10.3 ± 0.0 <sup>a</sup>	17.7 ± 0.0 <sup>a</sup>	29.3 ± 0.1 <sup>a</sup>	56.7 ± 0.1 <sup>a</sup>	18.9 ± 0.2 <sup>b</sup>	44.2 ± 0.2 <sup>b</sup>	14.7 ± 0.2 <sup>a</sup>	22.3 ± 0.4 <sup>a</sup>	3.9 ± 0.1 <sup>b</sup>

All data are means ± SD of two trials. Values with different letters in the same column are significantly different at  $p < 0.05$ .

DB: degree of branching.

the increase of the crystallinity in MH-1 was related to the cleavage of unpacked fa and fb<sub>1</sub> chains in the crystalline lamella and crystallization of these cleaved linear chains. It has been reported unpacked fa and fb<sub>1</sub> chains are crystalline defects [38]. The cleavage of these chains was reasonable to the increase of crystallinity. Moreover, these cleaved linear chains may aggregate and induce crystallization. From FACE and GPC data, we already knew there were no changes in molecular structures at longer treatment times. Therefore, we assumed the reorganization of crystalline was responsible for the decrease of crystallinity during this period. With further rapid heating by microwave treatment, higher

mobility of moistened HAMS molecules [39] and loosened double helices [5] as demonstrated for starch subjected to rapid heating, allowing for the reorganization of crystalline regions.

Small-angle X-ray scattering (SAXS) reveals the lamellar structure of starch granules by the appearance of a scattering intensity at typically  $q = 0.68 \text{ nm}^{-1}$  arising from a distinct electron density contrast between the crystalline lamellae and the amorphous lamellae in the starch granule [5]. A major scattering peak around the  $q$  value of  $0.6\text{--}0.7 \text{ nm}^{-1}$  was identified in both the native starch and the microwave-heated starch samples (Fig. 2B). The intensity of scattering peak in MH-1 was much higher than the native starch, MH-0 (Fig. 2B). This effect may be related to the cleavage of unpacked fa and fb<sub>1</sub> as well. Slightly higher lamellar ordering was also reported in rice starch after short-time microwave treatment due to the effects of rapid heating on packing unpacked double helices [5]. However, the scattering peak intensities of MH-3 and MH-4 were somewhat lower than for MH-0 supporting deterioration of the crystalline lamellae for longer treatments. The lamellar thicknesses ( $d = 2\pi/q$ ) of MH-3 and MH-4 were both 10.26 nm, which was lower than both MH-0 and MH-1 (11.04 nm) verifying partial reorganization of the crystalline lamellae and partial collapse of the lamellar structure [37].

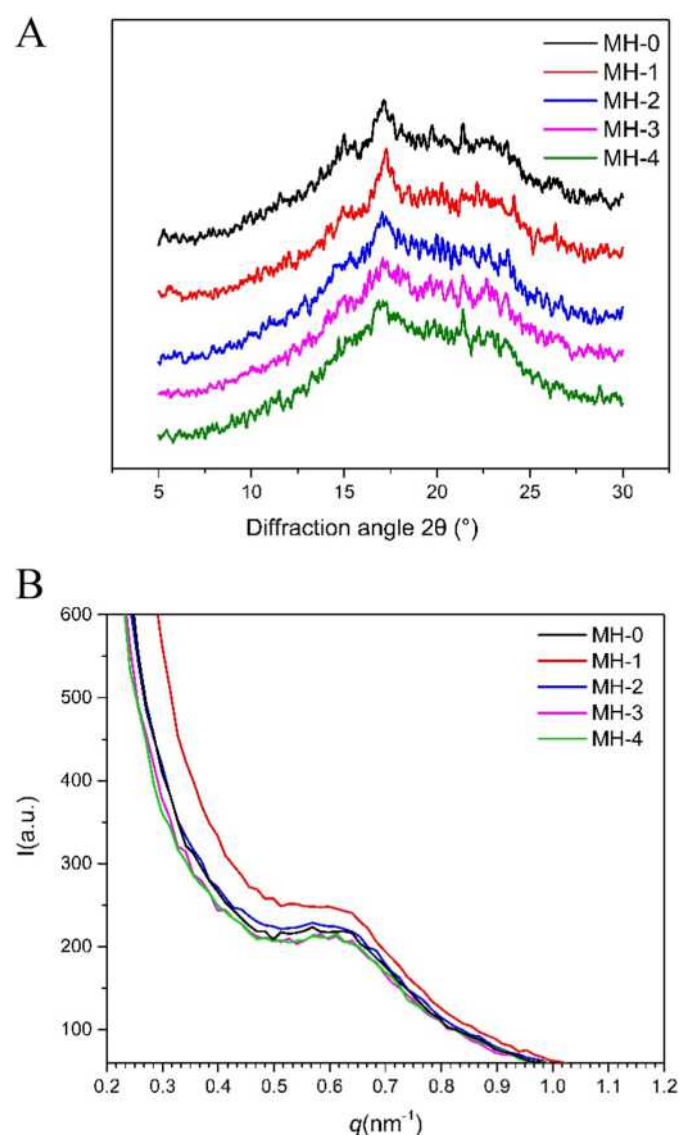
### 3.3. Granule morphology and internal microstructures

The microwave-induced time-course progress of HAMS granule morphological and internal structures was monitored by SEM and CLSM (Fig. 3). SEM images show that native high-amylose starch (MH-0) had a fraction of compound, elongated and irregular granules. Following short-time microwave treatment, starch granules were not disrupted and morphology was not significantly affected (Fig. 3A). It implied HAMS granules remained the integrity after microwave treatment, even for the MH-4, supporting the stability we found for the WAXS and SAXS data. CLSM images (see Fig. 3B) demonstrate that native HAMS granules displayed strong fluorescence intensity attributed to its relatively high molar ratio of reducing ends per anhydrous glucose residue present in the amylose [29]. Strong fluorescence intensity was also found in MH-1 (Fig. 3B), suggesting that more reducing ends were produced as an effect of cleaved amylopectin and amylose chains labelled by the APTS reagent. However, the fluorescence intensity for MH-2, MH-3, and MH-4 became gradually weaker, supporting the presence of very compact and inaccessible structures in these starches [14].

**Table 3**

Crystallinity and digestion properties of native and microwave-treated HAMS.

Samples	WAXS	Digestibility	
	Relative crystallinity (%)	DS (%)	RS (%)
MH-0	20.9 ± 0.8 <sup>b</sup>	59.3 ± 1.1 <sup>c</sup>	40.7 ± 1.1 <sup>b</sup>
MH-1	25.1 ± 0.4 <sup>a</sup>	45.2 ± 0.1 <sup>d</sup>	54.8 ± 0.1 <sup>a</sup>
MH-2	18.1 ± 1.0 <sup>c</sup>	65.1 ± 1.2 <sup>b</sup>	34.1 ± 1.2 <sup>c</sup>
MH-3	18.2 ± 0.8 <sup>c</sup>	69.8 ± 0.5 <sup>a</sup>	30.2 ± 0.5 <sup>d</sup>
MH-4	17.3 ± 0.7 <sup>c</sup>	70.5 ± 0.2 <sup>a</sup>	29.5 ± 0.2 <sup>d</sup>

All data are means ± SD of two trials. Values with different letters in the same column are significantly different at  $p < 0.05$ . DS (%) is the content of starch hydrolyzed for 120 min.

**Fig. 2.** Aggregation structural parameters of debranched HAMS after microwave treatment. A) WAXS diffraction spectra; B) Small-angle X-ray scattering patterns.



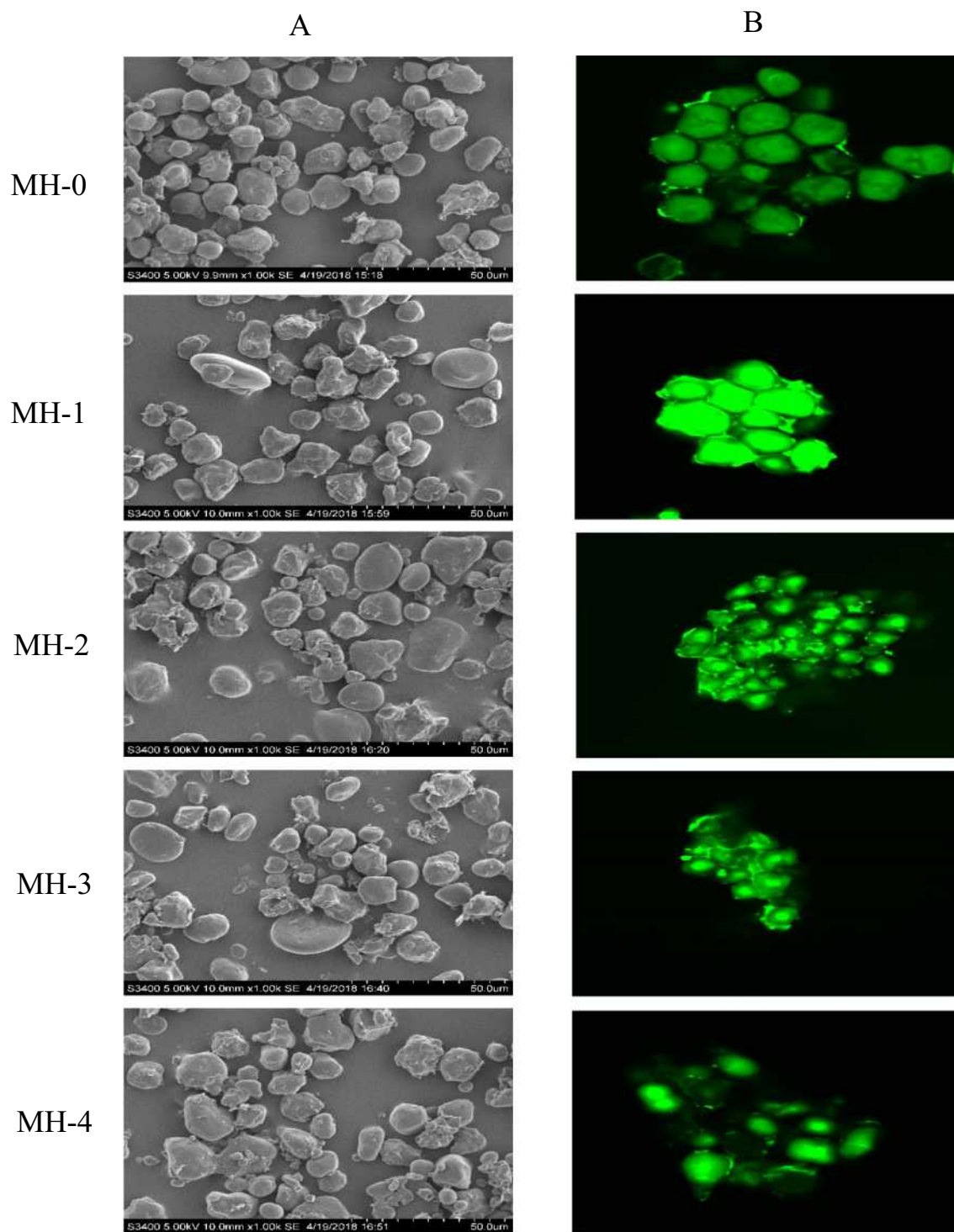


Fig. 3. Surface and inner structures of native and microwave-treated HAMS starches as analyzed by A) SEM and B) CLSM.

### 3.4. Pasting properties

Generally, high-amylose starch cannot be fully gelatinized at 100 °C [40], so we would not expect to find any major viscosity development for the native HAMS from conventional RVA. However, the partial rearrangements and breakdown in the chains in microwave-treated samples are expected to have increased swelling properties. MH-3 and MH-4 showed higher peak viscosity than MH-0 (Fig. 4) substantiating the view that the structures formed in microwave-treated HAMS support thermal swelling, increasing viscosity. MH-1, having higher

crystallinity (Table 3), showed reduced gelatinization and viscosity. The viscosity development during the heating process is directly related to the degree of swelling and integrity and re-association of starch granules and chains, respectively during heating and cooling [41,42]. On the other hand, the changes in amylose content also potentially affected the viscosity of microwave-treated samples. At the initial stage of microwave treatment, we assume that some amylose chains were broken down and re-associated in the final dry starch restricting gelatinization. Hence, microwave-assisted amylose leakage increased the possibility for diverse interactions between amylose–amylose or amylose

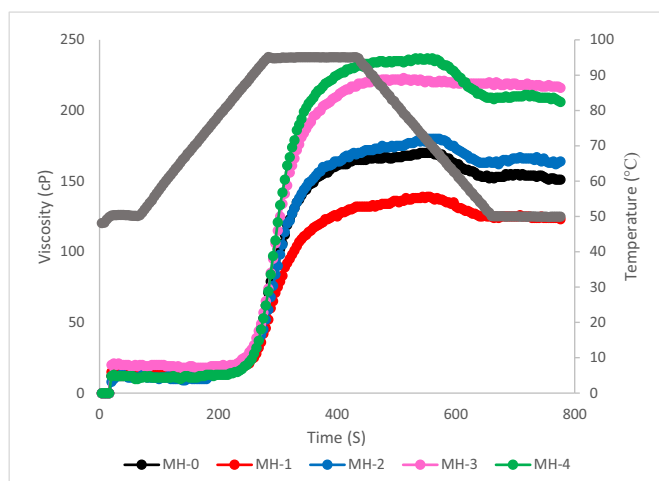


Fig. 4. Pasting properties of native and treated high-amylose maize starches. Values with different letters in figures denote significant difference at  $p < 0.05$ .

— amylopectin, and enhance the viscosity. Peak viscosity reflects the degree of swelling of starch granules during heating, trough is the viscosity after the disruption the paste network, and breakdown represents the ease of disrupting swollen starch granules [41,42]. After 3–4 min microwave treatment, HAMS displayed higher peak viscosity, trough and breakdown (Fig. S3), suggesting the degree of gelatinization of HAMS was possibly increased by microwave treatment. Final viscosity indicates the propensity of starch to gelation and retrogradation [41,42]. The increase of final viscosity in MH-3 and MH-4 implies more amylose chains may leached out and aggregated [43]. Setback is the retrogradation of starch and mainly affected by amylose [43]. Setback was not affected by microwave treatment, and thus the data was not shown.

### 3.5. *In vitro* digestibility

Typical starch digestion profiles of cooked native and microwave treated HAMS (Fig. 5) showed that all starches were digested rapidly during the initial 20 min and reached a plateau at about 80 min. However, MH-1 displayed a lower degree of hydrolysis than the native sample, MH-0, while MH-2, MH-3, and MH-4 exhibited a higher degree of hydrolysis. The observed difference in digestion is possibly a complex combination of the molecular and physical properties induced by the

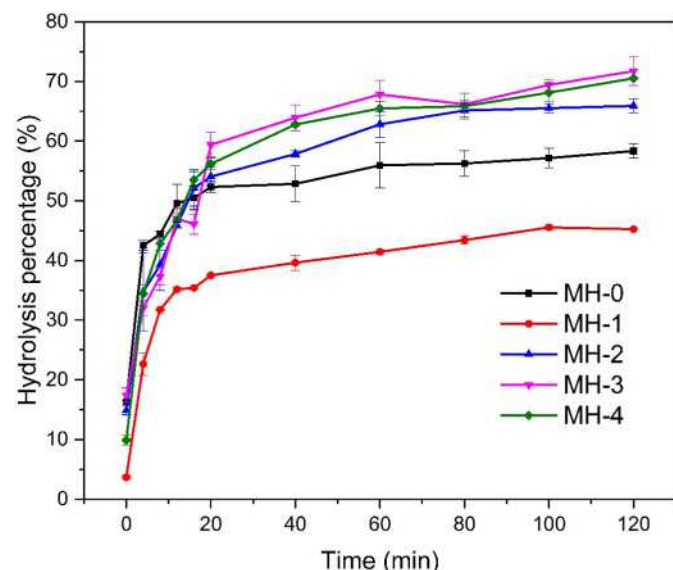


Fig. 5. Digestion properties of native and microwave-treated HAMS.

microwave energy. HAMS largely resists normal cooking processing as a consequence of stable double-helical short and long range interactions in this starch [44]. As an effect, MH-1, having the highest crystallinity, displayed the lowest digestion rate. MH-2, MH-3 and MH-4, that were more affected by microwave treatment, thereby showing lower gelatinization temperatures, were digested at higher rates. An increase in digestibility was also observed in high-amylose barley starch (amylose content: 46.5%) after long-time microwave heating [11].

### 3.6. Mechanistics of microwave irradiation of HAMS

Microwave treatment in food processing attracts much attention mainly due to that microwave energy is more efficient than the conventional heating and ensures more homogenous effects in complex matrices and greater penetrating depth. Being the major component in most cereal-based foods, starch must be functionally controlled at multiple scales. Structural and dynamic re-organization occurring upon microwave treatment, as based on the recently suggested “building block backbone model” [45], displays some important effects. The model for native normal starch suggests long flexible backbone chains from which branched building blocks extend. These are featured as “internal”, and are outspread along the backbone and form an integrated part. Short amylopectin chains extend from the building blocks and form double helices, which align to form crystalline lamellae [45]. It is widely accepted that in normal starch, amylose can distribute in granules as individual, radially, as well tangentially, oriented chains. These chains affect granule integrity and stability and could disrupt the structural order within the amylopectin crystallites [46]. However, also pure amylose starch granules have molecular and crystalline features resembling those of amylopectin [47].

Based on this information, a backbone model of HAMS can be established, from which structural dynamics of microwave-assisted re-structuring can be extended (Fig. 6). At the first stage, microwave irradiation energy causes specific, but partial, breakdown of fa, fb<sub>1</sub> and AM2 chains as demonstrated by the decrease of fa, fb<sub>1</sub> and AM2 content. The initial cleavage of amylose chains is supposedly occurring at sensitive, exposed and amorphous “hot spots” with molecular strain causing cleavage due to molecular vibration. Following this process, tangentially oriented cleaved chains can aggregate, resulting in increased crystallinity and lamellar re-ordering (Fig. 6). An alternative explanation has also been suggested where amylopectin crystalline defects are broken down [38]. The resulting structure can be described as a more relaxed and stable matrix. As an effect, longer treatment does not result in a further significant breakdown of starch molecules. However, the relative crystallinity and the lamellar ordering of the amylopectin chains decreased, suggesting disordering of double helical segments. Such effects can be related to the higher mobility of moistened HAMS molecules as demonstrated for starch subjected to rapid heating [39], causing the rearrangement of double helical segments. It is speculated that loosened double helices after microwave heating could also result in the lower crystallinity of samples [5]. In support of this effect, we found increased pasting and digestibility for these treatments.

The short microwave treatment times used in this work (1 min – 4 min) provide starch with only minor cleavage of amylose and amylopectin, and the rearrangement of both amylose and amylopectin generating a starch with retained, and improved, pasting and degradative properties.

### 4. Conclusion

HAMS was treated at a moisture content of 30% by short-time microwave irradiation for 1–4 min and the multi-scale structures and its pasting and digestibility properties were characterized by GPC, FACE, WAXS, SAXS, SEM, CLSM, RVA and *in vitro* digestion. Molecular profiling using GPC and FACE show that microwave treatment induced the minor breakdown of fa, fb<sub>1</sub> and AM2 chains. WAXS and SAXS data show that



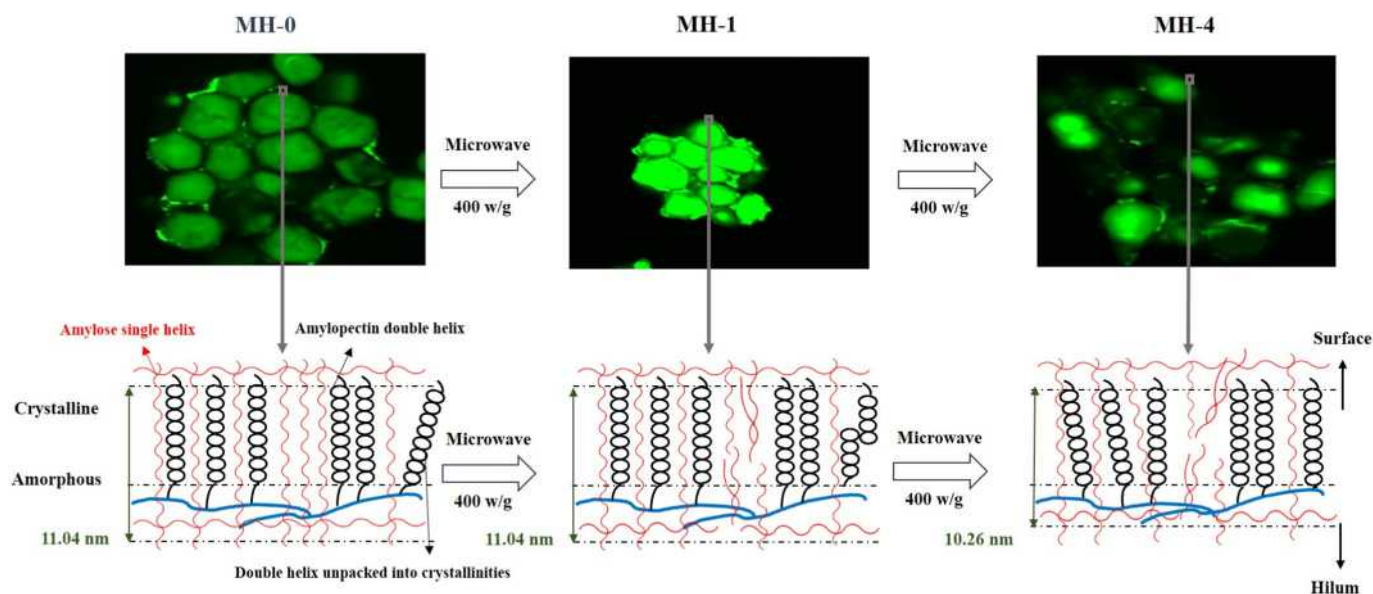


Fig. 6. Schematic mechanism of microwave treatment of HAMS.

the relative crystallinity and intensity of lamellar peak increased initially and then decreased with microwave treatment. These structural changes contributed to the decrease of viscosity and digestibility in 1 min microwave treatment. Further microwave treatment induced the increase of viscosity and digestive hydrolysis. Hence, 1 min microwave treatment can generate a more resistant and stable structure, for e.g. starch-based materials and resistant starch purposes. Our data provide a further understanding of the mechanisms of microwave processing, of value for processing of starch-based foods.

#### Declaration of Competing Interest

The authors declare that there is no conflict of interests regarding the publication of this paper.

#### Acknowledgements

This work was supported by Elite Scientists Sponsorship Program by CAST (YESS Program), Shaanxi Province Comprehensive Project (2015KTZDNY01-01-01), Yangling District technical Plan Project (2014NY-01), Zhongyin Tang Breeding Special Funding, and National Natural Science Foundation of China (31771930).

#### Appendix A. Supplementary data

Supplementary data to this article can be found online at <https://doi.org/10.1016/j.ijbiomac.2019.07.025>.

#### References

- [1] C. Salazar-González, M.F. San Martín-González, A. López-Malo, et al., Recent studies related to microwave processing of fluid foods, *Food Bioproc. Tech.* 5 (1) (2012) 31–46.
- [2] D. Fan, W. Ma, L. Wang, J. Huang, F. Zhang, J. Zhao, H. Zhang, W. Chen, Determining the effects of microwave heating on the ordered structures of rice starch by NMR, *Carbohydr. Polym.* 92 (2) (2013) 1395–1401.
- [3] R. Edgar, in: A.K. Datta, R.C. Anantheswaran (Eds.), *Handbook of Microwave Technology for Food Applications*, Marcel Dekker, Inc, New York, 2001.
- [4] S.A. Galema, Microwave chemistry, *Chem. Soc. Rev.* 26 (3) (1997) 233–238.
- [5] D. Fan, L. Wang, W. Chen, S. Ma, W. Ma, X. Liu, J. Zhao, H. Zhang, Effect of microwave on lamellar parameters of rice starch through small-angle X-ray scattering, *Food Hydrocoll.* 35 (2014) 620–626.
- [6] Q. Kuang, J. Xu, Y. Liang, F. Xie, F. Tian, S. Zhou, X. Liu, Lamellar structure change of waxy corn starch during gelatinization by time-resolved synchrotron SAXS, *Food Hydrocoll.* 62 (2017) 43–48.
- [7] Z. Li, X. Kong, X. Zhou, K. Zhong, S. Zhou, X. Liu, Characterization of multi-scale structure and thermal properties of Indica rice starch with different amylose contents, *RSC Adv.* 6 (109) (2016) 107491–107497.
- [8] H. Shen, D. Fan, L. Huang, Y. Gao, H. Lian, J. Zhao, H. Zhang, Effects of microwaves on molecular arrangements in potato starch, *RSC Adv.* 7 (24) (2017) 14348–14353.
- [9] G. Lewandowicz, T. Jankowski, J. Fornal, Effect of microwave radiation on physico-chemical properties and structure of cereal starches, *Carbohydr. Polym.* 42 (2) (2000) 193–199.
- [10] S. Zeng, B. Chen, H. Zeng, Z. Guo, X. Lu, Y. Zhang, B. Zheng, Effect of microwave irradiation on the physicochemical and digestive properties of lotus seed starch, *J. Agric. Food Chem.* 64 (12) (2016) 2442.
- [11] S. Emami, A. Perera, V. Meda, R.T. Tyler, Effect of microwave treatment on starch digestibility and physico-chemical properties of three barley types, *Food Bioprocess Technol.* 5 (6) (2012) 2266–2274.
- [12] M. Braşoveanu, M.R. Nemţanu, Behaviour of starch exposed to microwave radiation treatment, *Starch-Stärke* 66 (1–2) (2014) 3–14.
- [13] S. Chandrasekaran, S. Ramanathan, T. Basak, Microwave food processing—a review, *Food Res. Int.* 52 (1) (2013) 243–261.
- [14] Q. Yang, L. Qi, Z. Luo, X. Kong, Z. Xiao, P. Wang, X. Peng, Effect of microwave irradiation on internal molecular structure and physical properties of waxy maize starch, *Food Hydrocoll.* 69 (2017) 473–482.
- [15] Z. Luo, X. He, F. Xiong, F. Luo, Q.J.S.-S. Gao, Effect of microwave radiation on the physicochemical properties of normal maize, Waxy Maize and Amylomaize V Starches, 58(9) (2010) 468–474.
- [16] Y. Xie, M. Yan, S. Yuan, S. Sun, Q. Huo, Effect of microwave treatment on the physicochemical properties of potato starch granules, *Chem. Cent. J.* 7 (1) (2013) 113.
- [17] S.A. Oyeyinka, E. Umaru, S.J. Olatunde, J.K. Joseph, Effect of short microwave heating time on physicochemical and functional properties of Bambara groundnut starch, *Food Biosci.* 28 (2019) 36–41.
- [18] S. Guan, P. Wang, H. Liu, G. Liu, Y. Ma, L. Zhao, Production of high-amylose maize lines using RNA interference in *sbe2a*, *Afr. J. Biotechnol.* 10 (68) (2011) 15229–15237.
- [19] Y. Zhong, H. Zhu, W. Liang, X. Li, L. Liu, X. Zhang, H. Yue, J. Xue, X. Liu, D. Guo, High-amylose starch as a new ingredient to balance nutrition and texture of food, *J. Cereal Sci.* 8 (2018) 8–14.
- [20] Z. Luo, X. He, X. Fu, F. Luo, Q. Gao, Effect of microwave radiation on the physico-chemical properties of normal maize, waxy maize and amylo maize V starches, *Starch-Stärke* 58 (9) (2006) 468–474.
- [21] O. Paredes-López, L.A. Bello-Pérez, M.G. López, Amylopectin: structural, gelatinisation and retrogradation studies, *Food Chem.* 50 (4) (1994) 411–417.
- [22] E. Li, J. Hasjim, S. Dhital, I.D. Godwin, R.G. Gilbert, Effect of a gibberellin-biosynthesis inhibitor treatment on the physicochemical properties of sorghum starch, *J. Cereal Sci.* 53 (3) (2011) 328–334.
- [23] H. Li, S. Prakash, T.M. Nicholson, M.A. Fitzgerald, R.G. Gilbert, The importance of amylose and amylopectin fine structure for textural properties of cooked rice grains, *Food Chem.* 196 (2016) 702.
- [24] J. Hasjim, G.C. Lavau, M.J. Gidley, R.G. Gilbert, In vivo and in vitro starch digestion: are current in vitro techniques adequate? *Biomacromolecules* 11 (12) (2010) 3600–3608.
- [25] A.C. Wu, M.K. Morell, R.G. Gilbert, A parameterized model of amylopectin synthesis provides key insights into the synthesis of granular starch, *PLoS One* 8 (6) (2013) e65768.
- [26] K. Frost, D. Kaminski, G. Kirwan, E. Lascaris, R. Shanks, Crystallinity and structure of starch using wide angle X-ray scattering, *Carbohydr. Polym.* 78 (3) (2009) 543–548.

- [27] L. Lin, D. Guo, L. Zhao, X. Zhang, J. Wang, F. Zhang, C. Wei, Comparative structure of starches from high-amylose maize inbred lines and their hybrids, *Food Hydrocoll.* 52 (2016) 19–28.
- [28] J. Yang, F. Xie, W. Wen, L. Chen, X. Shang, P. Liu, Understanding the structural features of high-amylose maize starch through hydrothermal treatment, *Int. J. Biol. Macromol.* 84 (2016) 268–274.
- [29] A. Blennow, M. Hansen, A. Schulz, K. Jørgensen, A.M. Donald, J. Sanderson, The molecular deposition of transgenically modified starch in the starch granule as imaged by functional microscopy, *J. Struct. Biol.* 143 (3) (2003) 229–241.
- [30] A.A.o.C.C.A.M. Committee, Approved Methods of the American Association of Cereal Chemists, American Association of Cereal Chemists, 2000.
- [31] B. Zhang, Q. Huang, F.X. Luo, X. Fu, H. Jiang, J.L. Jane, Effects of octenylsuccinylation on the structure and properties of high-amylose maize starch, *Carbohydr. Polym.* 84 (4) (2011) 1276–1281.
- [32] H.N. Englyst, S. Kingman, J. Cummings, Classification and measurement of nutritionally important starch fractions, *Eur. J. Clin. Nutr.* 46 (1992) S33–S50.
- [33] J. Gayin, E.-S.M. Abdel-Aal, J. Manful, E. Bertoft, Unit and internal chain profile of African rice (*Oryza glaberrima*) amylopectin, *Carbohydr. Polym.* 137 (2016) 466–472.
- [34] L. Lin, D. Guo, J. Huang, X. Zhang, L. Zhang, C. Wei, Molecular structure and enzymatic hydrolysis properties of starches from high-amylose maize inbred lines and their hybrids, *Food Hydrocoll.* 58 (2016) 246–254.
- [35] M. Villanueva, B. De Lamo, J. Harasym, F. Ronda, Microwave radiation and protein addition modulate hydration, pasting and gel rheological characteristics of rice and potato starches, *Carbohydr. Polym.* 201 (2018) 374–381.
- [36] F. Corzana, M.S. Motawia, C. Hervé du Penhoat, F. van den Berg, A. Blennow, S. Perez, S.B. Engelsens, Hydration of the amylopectin branch point. Evidence of restricted conformational diversity of the  $\alpha$ -(1 $\rightarrow$ 6) linkage, *J. Am. Chem. Soc.* 126 (40) (2004) 13144–13155.
- [37] J. Yang, F. Xie, W. Wen, L. Chen, X. Shang, P. Liu, Understanding the structural features of high-amylose maize starch through hydrothermal treatment, *Int. J. Biol. Macromol.* 84 (2016) 268–274.
- [38] D.A. Koroteeva, V.I. Kiseleva, A.V. Krivandin, O.V. Shatalova, W. Błaszczak, E. Bertoft, K. Piyachomkwan, V.P. Yuryev, Structural and thermodynamic properties of rice starches with different genetic background: part 2. Defectiveness of different supramolecular structures in starch granules, *Int. J. Biol. Macromol.* 41 (5) (2007) 534–547.
- [39] M. Villanueva, J. Harasym, J.M. Muñoz, F. Ronda, Microwave absorption capacity of rice flour. Impact of the radiation on rice flour microstructure, thermal and viscometric properties, *J. Food Eng.* 224 (2018) 156–164.
- [40] H. Liu, L. Yu, F. Xie, L. Chen, Gelatinization of cornstarch with different amylose/amylopectin content, *Carbohydr. Polym.* 65 (3) (2006) 357–363.
- [41] S. Hedayati, M. Niakousari, Microstructure, pasting and textural properties of wheat starch-corn starch citrate composites, *Food Hydrocoll.* 8 (2018) 1–5.
- [42] Y. Huo, B. Zhang, M. Niu, C. Jia, S. Zhao, Q. Huang, H. Du, An insight into the multi-scale structures and pasting behaviors of starch following citric acid treatment, *Int. J. Biol. Macromol.* 116 (2018) 793–800.
- [43] A.A. Wani, P. Singh, M.A. Shah, U. Schweiggert-Weisz, K. Gul, I.A. Wani, Rice starch diversity: effects on structural, morphological, thermal, and physicochemical properties—a review, *Compr. Rev. Food Sci. Food Saf.* 11 (5) (2012) 417–436.
- [44] H.X. Jiang, M. Campbell, M. Blanco, J.L. Jane, Characterization of maize amylose-extender (ae) mutant starches: part II. Structures and properties of starch residues remaining after enzymatic hydrolysis at boiling-water temperature, *Carbohydr. Polym.* 80 (1) (2010) 1–12.
- [45] E. Bertoft, Understanding starch structure: recent progress, *Agronomy*. 7 (3) (2017) 56.
- [46] S. Pérez, E. Bertoft, The molecular structures of starch components and their contribution to the architecture of starch granules: a comprehensive review, *Starch-Stärke*. 62 (8) (2010) 389–420.
- [47] A. Goldstein, G. Annor, J.-L. Putaux, K.H. Hebelstrup, A. Blennow, E. Bertoft, Impact of full range of amylose contents on the architecture of starch granules, *Int. J. Biol. Macromol.* 89 (2016) 305–318.





# *ZmSMR4*, a novel cyclin-dependent kinase inhibitor (CKI) gene in maize (*Zea mays* L.), functions as a key player in plant growth, development and tolerance to abiotic stress

Feifei Li<sup>a,b,1</sup>, Licheng Wang<sup>a,b,1</sup>, Zhengquan Zhang<sup>a,b,1</sup>, Ting Li<sup>a,b</sup>, Jiaojiao Feng<sup>a,b</sup>, Shutu Xu<sup>a,b</sup>, Renhe Zhang<sup>a,b</sup>, Dongwei Guo<sup>a,b,\*</sup>, Jiquan Xue<sup>a,b,\*</sup>

<sup>a</sup> Key Laboratory of the Biology and Genetic Improvement of Maize in Arid Areas of the Northwest Region, Ministry of Agriculture, College of Agronomy, Northwest A&F University, China

<sup>b</sup> Maize Engineering and Technology Research Centre of Shaanxi Province, Yangling, Shaanxi, 712100, China

## ARTICLE INFO

### Keywords:

Maize  
Endoreduplication  
*ZmSMR*  
Precocious flowering  
Abortion

## ABSTRACT

Endoreduplication is a key cell cycle variant in the developing maize endosperm and has been associated with cell enlargement and dry matter accumulation. Therefore, identification of the key genes associated with endosperm development and endoreduplication would not only lay the groundwork for understanding the biological process of endoreduplication but also be important for maize breeding. Here, we identified 12 putative endoreduplication-related candidate genes as members of the *Zea mays* L. SIAMESE-RELATED (*ZmSMR*) gene family and denoted them *ZmSMR1*–*ZmSMR12*. Sequence analysis indicated that all the *ZmSMR* protein sequences exhibited modest sequence similarity to the *SIAMESE* gene from *Arabidopsis*. Further analyses suggested that most *ZmSMR* genes might be associated with the transition from mitosis to endoreduplication because the expression levels of most *ZmSMR* genes were upregulated in endosperm cells during the phase of switching to an endoreduplication cell cycle. Additionally, the *ZmSMRs* responded to various abiotic stresses at the transcriptional level. One member of the *ZmSMR* gene family, the *ZmSMR4* (KY946768) gene, was isolated as the first maize endoreduplication-related gene and has been used to develop transgenic *Arabidopsis* plants. *ZmSMR4* was localized to the nucleus and could interact with *ZmCDKA* and *ZmCDKB*. Moreover, *ZmSMR4* was able to rescue the multicellular trichome phenotype of *Arabidopsis* sim mutants and enhanced the endoreduplication levels of transgenic *Arabidopsis* plants. *Arabidopsis* plants overexpressing *ZmSMR4* not only displayed enhanced leaf margin serrations but also showed several interesting breeding phenotypes, such as early blossoming and fuller seeds. Taken together, our data suggest that the *ZmSMR4* gene is plant-specific and functions as a key player in the signalling network that controls plant growth, development and responses to abiotic stress by regulating the transition between the mitotic cycle and endoreduplication.

## 1. Introduction

Multicellular eukaryote development is a complex process that requires the coordinated integration of cell division, growth, and differentiation [1]. Unlike animals, plants are sessile and can respond to biotic and abiotic stresses only by regulating their growth and development. Thus, proper cell cycle regulation is crucial for plant survival and development and should be a tightly regulated, yet flexible and accurately coordinated, process in a multi-metabolic system. In such a system, to meet the growth and developmental demands of different

habitats, plants have developed various cell cycle types, such as asymmetric cell division, acytokinetic mitosis, normal mitosis and endoreduplication, and these division processes frequently occur in a sequential yet overlapping manner during organ and tissue development.

Endoreduplication involves one or several rounds of nuclear DNA synthesis without chromosomal and cellular division, which leads to cell polyploidization. This process is thought to be a result of evolution because it allows better functional adaptation to environmental challenges; however, the role of endoreduplication remains unclear. Many studies have confirmed that endoreduplication allows cells to increase

\* Corresponding authors at: Key Laboratory of the Biology and Genetic Improvement of Maize in Arid Areas of the Northwest Region, Ministry of Agriculture, College of Agronomy, Northwest A&F University, China

E-mail addresses: [gdwei1973@126.com](mailto:gdwei1973@126.com) (D. Guo), [xjq2934@163.com](mailto:xjq2934@163.com) (J. Xue).

<sup>1</sup> These authors contributed equally to this work.

<https://doi.org/10.1016/j.plantsci.2018.03.007>

Received 31 October 2017; Received in revised form 6 March 2018; Accepted 8 March 2018

Available online 13 March 2018

0168-9452/ © 2018 Elsevier B.V. All rights reserved.

gene expression and metabolic output, which might be advantageous for some cells or organisms. Additionally, previous studies have indicated that endoreduplication could support plant or organ growth under biotic and abiotic stress conditions by improving plant resistance. For example, endoreduplication levels have been enhanced in tobacco cells in response to fungi [2] or pathogens [3]. Under water deficit conditions, DNA content and epidermal cell size rapidly decrease in wild-type (WT) *Arabidopsis*, but transgenic *Arabidopsis* plants with a high endoreduplication level are less affected due to an increased leaf expansion rate and a larger cell size. Grime et al. (1982) revealed that the evolution of increased DNA contents is closely associated with enhanced plant growth capacity at low temperatures [4]. Endoreduplication might also be related to the adaptive response to salinity [5]. The advantages of increased endoreduplication in response to low temperatures, water deficits [6] and high salt levels might be associated with increased gene expression and protein synthesis, which suggests that endoreduplication might maintain the basic metabolic functions of plants under energy-limited conditions. However, notably, the correct timing of initiation, extent of endoreduplication, and appropriate gene expression can affect plant or animal growth and development. In plants, many tissues, including trichomes, leaf epidermal cells, root tip cells, and hypocotyl cells, exhibit endoreduplication [7,8]. Endoreplication typically occurs in cells that are specialized via differentiation, in highly metabolically active cells and in certain economically important organs and tissues, such as the maize endosperm [9], tomato fruits [10], cotton fibres [11], and root nodules [12].

There are many regulators of endoreduplication. However, most studies have demonstrated that cyclin-dependent kinase (CDK) inhibitors (CKIs) are some of the most important regulators of endoreduplication. CKIs can control the cell cycle by inhibiting the activity of CDKs in yeast and mammals [13]. In plants, two CKI families have been identified. One of these families is the Kip-related protein (KRP) family, whose sequences are similar to those of the mammalian Cip/Kip family. Seven *KRP* genes have been isolated from *Arabidopsis* [14]. A KRP-like CKI has also been isolated from tobacco, and the overexpression of this gene inhibits CDK activity in plants [15]. The other plant CKI family is the *SIAMESE-RELATED* (*SMR*) gene family [16]. The members of the *SMR* gene family can interact with several different CDK/CYC complexes [17]. For example, the *EL2* gene identified in rice can inhibit the activity of CDKA;1 and links cell cycle progression with biotic and abiotic stress responses [18]. Both *SIM* and the related *SMR* genes play key roles in promoting endoreplication [19].

The seed endosperm is the most important plant product, accounting for 80% of energy and carbohydrate consumption by humans worldwide. Maize endosperm development occurs in three overlapping phases: cell proliferation characterized by mitosis, cell enlargement characterized by endoreduplication, and programmed cell death [20]. Although crop performance and yields can be enhanced by manipulating the transitions between different stages, and previous studies have demonstrated that appropriate alteration of the cell cycle substantially affects yield [21], the regulation of these stages is not currently well understood. Therefore, the identification of the key genes involved in endosperm development and endoreduplication lays the groundwork for understanding the biological process of endoreplication, and the key genes associated with endoreduplication must also have potential value for maize breeding due to the importance of endoreduplication in maize endosperm development and its involvement in the responses to biotic and abiotic stress.

The accumulation of a CKI in the maize endosperm has been shown to correspond to endoreduplication, but neither the nature of the CKI nor its target genes have been identified [22]. Larkins et al. identified two maize CKIs, Zeama;KRP;1 and Zeama;KRP;2, and found that only Zeama;KRP;1 accounts for a portion of the CKI activity observed during endosperm development [23]. This result indicates the existence of other CKIs in addition to Zeama;KRP;1. Hence, the objective of this study was to identify the other types of CKIs present in the maize

endosperm and explore their roles in endoreduplication. First, we identified 12 putative endoreduplication-related candidate genes as members of the *ZmSMR* gene family by screening GDB maize and designated them *ZmSMR1-ZmSMR12*. Next, one endoreduplication-related gene from the *ZmSMR* gene family (*ZmSMR4*) was cloned and identified as a plant-specific CKI gene. This gene is a maize homologue of the *Arabidopsis thaliana* *SIAMESE* gene and has been shown to complement the trichome phenotype of *sim* mutants. The results showed that this gene localizes to the nucleus and interacts with CDKA and CDKB. Finally, plants overexpressing *ZmSMR4* not only displayed serrated leaves due to restricted cell proliferation but also exhibited phenotypes that might be relevant to breeding, such as early flowering and fuller seeds. These results will provide valuable information for facilitating maize improvements in the future.

## 2. Materials and methods

### 2.1. Plant materials and growth conditions

The maize (*Zea mays* L.) inbred line B73 was provided by the Key Laboratory of the Biology and Genetic Improvement of Maize in Arid Areas of the Northwest Region, College of Agronomy, Northwest A&F University and was grown in the field. Ears were self-pollinated on the same day. The endosperm was isolated via manual dissection at different developmental stages, rapidly frozen in liquid nitrogen and stored at  $-80^{\circ}\text{C}$ . *Arabidopsis thaliana* Col-0 was employed as the WT control and transgenic acceptor. The *sim* mutant (CS23884) was purchased from the Arabidopsis Biological Resource Center (ABRC), and homozygous *sim* mutants were identified by sequencing. WT, mutant and transgenic *Arabidopsis thaliana* seedlings were germinated on plates containing Murashige and Skoog (MS) medium with 0.7% agar and 3% sucrose and incubated at  $4^{\circ}\text{C}$  for 3 d. Two-week-old seedlings were then transferred to a pot with a mixture of forest soil and vermiculite (3:1). These seedlings, which were used to determine the rosette leaf number and tissue architecture, were planted in soil at a uniform density and grown in a greenhouse at  $22^{\circ}\text{C}$  under 70% relative humidity (RH) with a 16-h light/8-h dark photoperiod.

### 2.2. Sequence retrieval and analysis of the maize *ZmSMR* gene family

Most of the reference sequence information regarding the *ZmSMR* gene family in maize was kindly provided by Professor John C. Larkin (Department of Biological Sciences, Louisiana State University), and further retrieval and consolidation were performed. To identify members of the *ZmSMR* gene family, the amino acid sequences of the provided *ZmSMR* proteins were used as a query loci to screen the Maize GDB (<https://www.maizegdb.org/>) and Phytozome (<https://phytozome.jgi.doe.gov/pz/portal.html>) websites, and the conserved AtSMR domains were employed for comparative analysis. Highly repetitive sequences were considered to represent a gene. The *Arabidopsis* *SIAMESE* gene sequences were obtained using the accession numbers provided in the Supplemental Data 2 file from a previously published paper [24]. Multiple sequence alignment was performed using Clustal Omega [25]. The exact chromosomal position of each *ZmSMR* gene in the *Zea mays* genome was predicted with Phytozome (<http://phytozome.jgi.doe.gov/pz/portal.html>). *ZmSMR* gene family members were mapped onto *Zea mays* chromosomes using Map Chart software [26].

### 2.3. Cloning of *ZmSMR4* and generation of transgenic plants

The *ZmSMR4* gene sequence was obtained from the National Center for Biotechnology Information (NCBI) (<https://www.ncbi.nlm.nih.gov/>) through homology alignment. RNA from the endosperm at 15 days after pollination (DAP) was isolated using a Plant RNA Kit (Tiangen, China) following the manufacturer's instructions and was then



employed for cDNA synthesis using the Transcript First-Strand cDNA Synthesis SuperMix (Transgene Biotech, China). The *ZmSMR4* cDNA was amplified with the F-CTCTCCTCTTCTCTCTCTCG and R-CTAGA TGCTCTTCTTGTGGG primers. The high-fidelity PCR mixture (50 µL) contained 50 ng of single-stranded cDNA as the template, 1 unit of PrimeSTAR DNA Polymerase (Takara, Japan), 0.2 mM dNTP mix and 25 µL of 2 × GC Buffer. PCR amplification was performed under the following conditions: a 5-min initial denaturation at 94 °C; followed by 35 cycles of 45 s of denaturation at 94 °C, 45 s of annealing at 58 °C, and 45 s of elongation at 72 °C; and a 10-min final extension at 72 °C. The amplified PCR products were gel-purified and inserted into the pCambia1302 and HY107 vectors. The reconstructed vector was transfected into *Agrobacterium tumefaciens* strain GV3101, which was used to transform *Arabidopsis* via the floral dip method [27]. Transgenic plants were selected on kanamycin-containing plates and then transferred to soil. The T3-generation lines were employed for the complementation experiments and phenotypic analysis.

#### 2.4. Quantitative real-time PCR (qRT-PCR)

Maize seedlings were exposed to various stresses, including 100 µmol L<sup>-1</sup> abscisic acid (ABA), 20% polyethylene glycol (PEG), 200 mmol L<sup>-1</sup> NaCl, low temperature (4 °C) and high temperature (42 °C). All the treated and untreated maize materials were harvested at different time points and stored at -80 °C. We obtained maize endosperm samples for qRT-PCR as described above. Total RNA and cDNA were then extracted and synthesized, respectively, as described above. The expression pattern of the *ZmSMR* genes was analysed via qRT-PCR. All the genes were assayed in three independent biological replicates, and the relative expression values were determined using the 2<sup>-ΔΔCt</sup> method [28]. The relative expression values were log<sub>2</sub> transformed, and heat maps were prepared with the R package pheatmap.

#### 2.5. Subcellular localization

For subcellular location analysis of the *ZmSMR4* protein, the fusion expression vector pGFP-*ZmSMR4* was first constructed using homologous recombination, and leaf protoplasts were then prepared according to a previously described method [29]. The fusion expression vector pGFP-*ZmSMR4* and the control empty vector p16318:GFP were transferred into acceptor strains using a PEG-induced transformation method. Finally, the transformed protoplasts were placed in a dark environment for 16–24 h and observed under a confocal laser scanning microscope (FLV1200, Olympus Japan).

#### 2.6. Yeast two-hybrid assay

For the yeast two-hybrid assays, cDNA sequences were cloned into the pGADT7 or PGBKT7 vector, and the fusion and control vectors were then co-transformed into yeast strain AH109 cells via the lithium acetate (PEG/LiAc) method, according to the protocol handbook provided by the manufacturer (Clontech, USA). Three days later, the yeast strains were spread on selective Synthetic Dropout-Trp-Leu medium (SD-T-L) and Synthetic Dropout-Trp/Leu/His/Ade (SD-T-L-H-A) plates for the interaction test. The expression activity of the reporter gene *LacZ* was identified using the β-galactosidase assay, as described previously [30].

#### 2.7. Complementation experiment

The complementation phenotype was examined through scanning electron microscopy [31]. The first leaves of 2-week-old *Arabidopsis sim* mutants and *sim* mutants transformed with the HY107-*ZmSMR4* expression vector were mounted on specimen stubs and observed, and the number of *Arabidopsis* trichome branches on the adaxial side of selected leaves was counted. The cell number per *Arabidopsis* trichome site

(TIS) was determined using a fluorescence microscope [32].

#### 2.8. Plant flow cytometry analysis

The sixth leaf from the transgenic and control plants was sliced into pieces with a razor blade in 500 µL of nuclear isolation buffer (10 mmol L<sup>-1</sup> MgSO<sub>4</sub>·7H<sub>2</sub>O, 50 mmol L<sup>-1</sup> KCl, 5 mmol L<sup>-1</sup> HEPES, 3 mmol L<sup>-1</sup> DTT, and 0.2% Triton X-100), and the suspension was then filtered through a 50-µm filter. Next, 200 µL of recovery solution was added, and the nuclei were stained with DAPI (at a final concentration of 2 µg/ml) on ice for 30 min. The nuclear suspension was analysed with a flow cytometer (Aria SORP, BD, USA). The endoreduplication level was represented by the endoreduplication factor (EF), which was calculated according to the percentage of cells with different ploidy levels as follows: EF = (0 × 2C) + (1 × 4C) + (2 × 8C) + (3 × 16C) + (4 × 32C).

### 3. Results

#### 3.1. The members of the *ZmSMR* gene family exhibit modest sequence similarity to the *Arabidopsis SIAMESE* gene and are distributed across most of the maize chromosomes

In the present study, 12 genes were predicted to be members of the *ZmSMR* gene family and were designated *ZmSMR1*-*ZmSMR12*. The protein sequences of all 12 genes shared modest sequence identity with the *Arabidopsis SIAMESE* gene and presented at least two conservative domains. A multiple sequence alignment showed that although the sequence similarity between the different members of the *ZmSMR* gene family was limited to several shorter motifs, designated motif 1-motif 5 (Fig. 1), the motif order was consistent with that in the *SMRs* from *Arabidopsis* and other species. Motif 1 was highly conserved at two amino acid residues (threonine and proline), constituting the minimal CDK phosphorylation site, which might be crucial for *SMR* function [24]. Motif 2 was rich in proline residues and consisted of a typical PXXP structure followed by one or several residues. This motif is a functional protein interaction domain, which allows the protein to interact with certain partners by forming a PPII helix [33]. Motif 3 was a cyclin-binding domain similar to a Cy or zRxL domain; this motif is the binding site for several CKIs, E2F and RB cyclins, and CDK complexes [34,35]. Motif 4 was similar to motif 3 from the KRP proteins [14]. Motif 5 contained a short stretch that included a nuclear localization signal. A chromosome location map was generated using software (Map Chart V4.0) to visualize the gene distribution of the *ZmSMR* gene family across the maize chromosomes. *ZmSMR* family members were located on most of the maize chromosomes, except for the seventh, eighth and tenth chromosomes. As shown in Fig. 2, the ninth chromosome possessed the highest *ZmSMR* gene density, and the distance between the *ZmSMR* genes was shortest on this chromosome. An uneven gene distribution was observed, which might be a result of tandem duplication of *ZmSMR* genes.

#### 3.2. Cloning the *ZmSMR4* gene and generating transgenic plants

We isolated one gene from the *ZmSMR* gene family, which was designated *ZmSMR4*; we then submitted the gene to NCBI and obtained the accession number KY946768. *ZmSMR4* was located on the ninth chromosome (Fig. 2), encoded a 126-amino-acid protein and contained no introns. Similar to most CKIs, *ZmSMR4* is a low-molecular-weight protein with a molecular weight of only 13.7 kDa and an isoelectric point of 10.21. To determine whether *ZmSMR4* is a maize homologue of the *Arabidopsis SIAMESE* gene, we expressed the *ZmSMR4* gene in *sim* mutant plants (CS23884) under the control of a trichome-specific promoter (*GL3*). We also ectopically expressed the *ZmSMR4* gene in WT *Arabidopsis* plants under the control of the cauliflower mosaic virus 35S promoter to investigate the function of the *ZmSMR4* gene. The

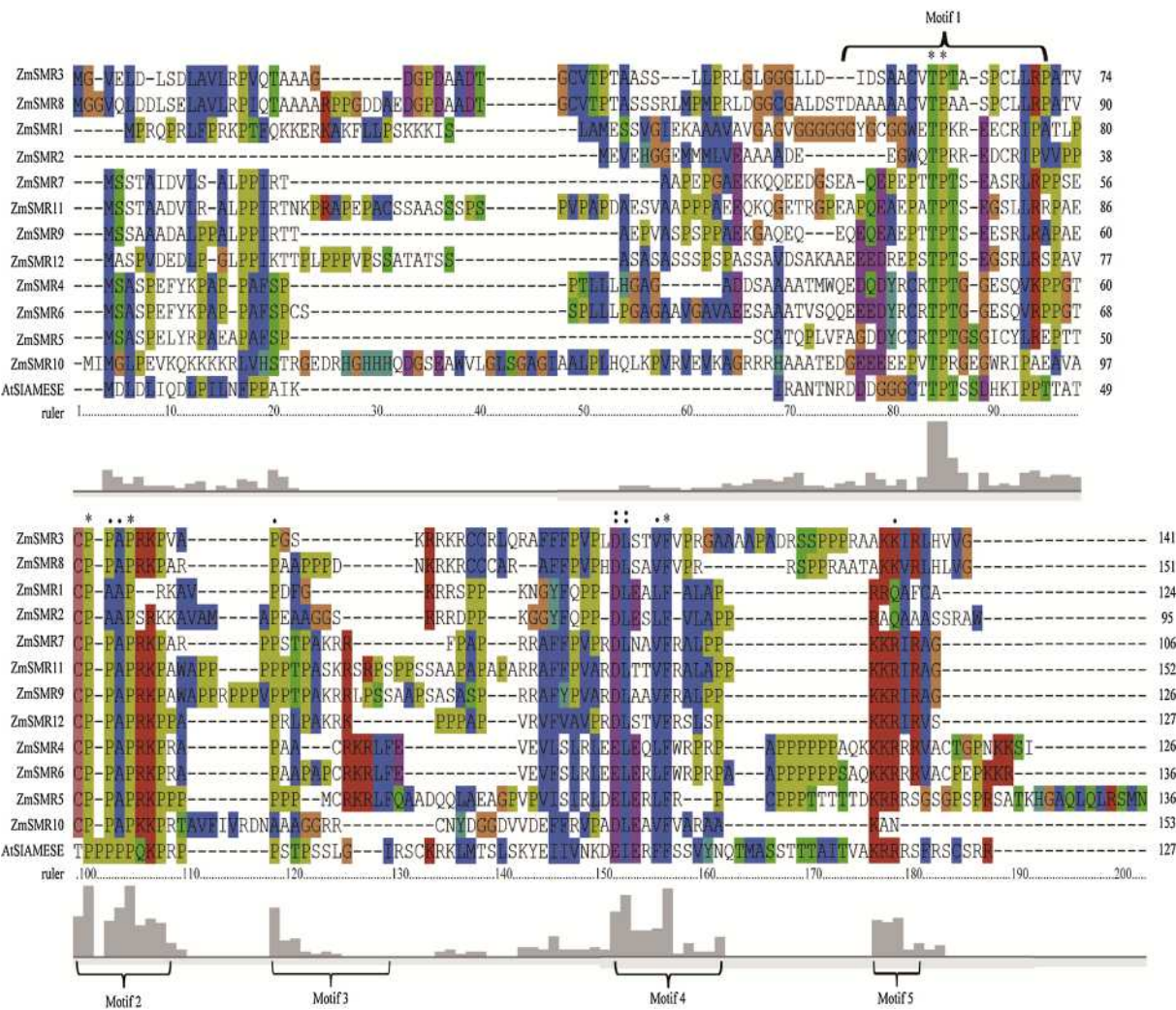


**Fig. 1.** Conservation of ZmSMR family protein sequences. Motifs 1–5 were identified by determining the domains conserved across all the ZmSMR protein sequences. A line above the alignment is used to mark strongly conserved positions. The following three characters ("\*", ":", and ".") are used: "." indicates that one of the following 'weaker' groups is fully conserved; "\*" indicates positions that have a single, fully conserved residue; and ":" indicates that one of the following 'strong' groups is fully conserved.

transgenic plants were selected through genotyping analysis using hygromycin until T3 homozygous transgenic plants were generated. Thirty T1 transgenic plants were successfully obtained through selection. Five independently selected lines (*sim* GL3:ZmSMR4 and 35S:ZmSMR4 T3) were confirmed to be positive plants via PCR

amplification of the *ZmSMR4* gene (Fig. 3A, B). The expression level of the *ZmSMR4* gene in these transgenic plants was measured through qRT-PCR. The results indicated that the *ZmSMR4* gene had been successfully expressed in the *sim* mutant and WT *Arabidopsis* plants and that the expression level of *ZmSMR4* was different in different

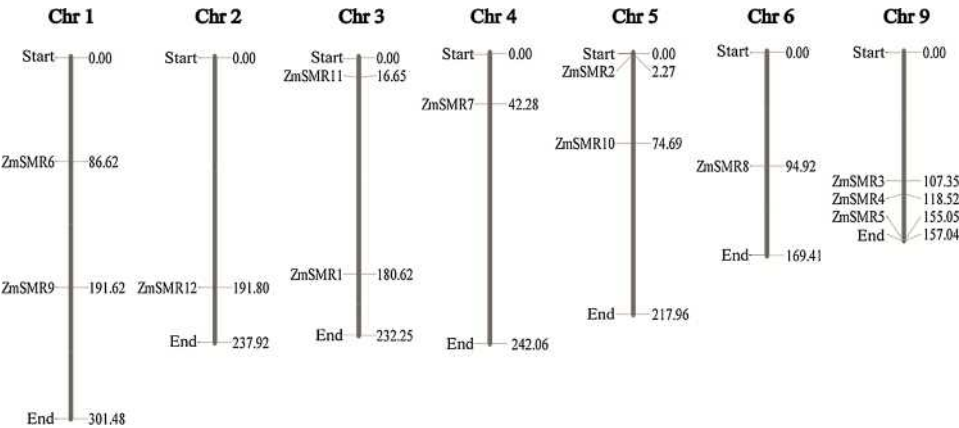


**Fig. 2.** Distribution of the 12 *ZmSMR* genes on the seven *Zea mays* L. chromosomes.



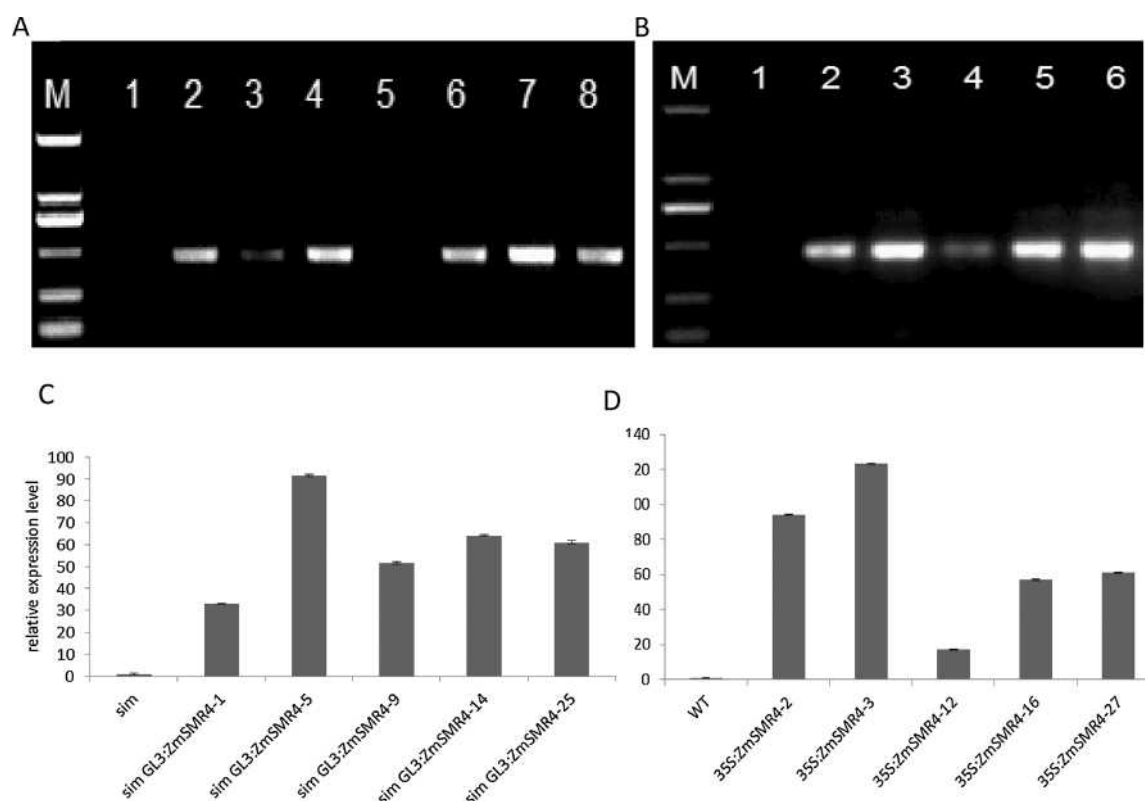


**Fig. 3.** Identification of *sim GL3:ZmSMR4* and *35S:ZmSMR4* transgenic plants. (A) PCR detection of *sim GL3:ZmSMR4* transgenic plants. M: DL2000 DNA marker; 1: *sim* mutant control plant; and 2–6: *sim GL3:ZmSMR4* transformants. (B) PCR detection of *35S:ZmSMR4* transgenic plants. M: DL2000 DNA marker; 1: WT control plant; and 2–8: *35S:ZmSMR4* transformants. (C) Comparative analysis of *ZmSMR4* expression by qRT-PCR in the *sim* mutant and *sim GL3:ZmSMR4* transgenic plants. (D) Comparative analysis of *ZmSMR4* expression by qRT-PCR in WT and *35S:ZmSMR4* transgenic plants.

transgenic plants (Fig. 3C, D).

### 3.3. Characteristics of *ZmSMR* gene expression

To investigate the temporal-spatial characteristics of *ZmSMR* gene expression during maize endosperm development and elucidate the role of the *ZmSMRs* in the response to abiotic stress, qRT-PCR was performed to determine the relative expression levels of the *ZmSMR* genes at different stages of maize endosperm development and under various treatment conditions. As shown in Fig. 4A, the expression levels of most *ZmSMR* genes, except for *ZmSMR2*, *ZmSMR3*, and *ZmSMR8*, were up-regulated 10 DAP and gradually declined thereafter. This result was expected because mitotic activity is known to reach a peak at approximately 8–10 DAP and to decline sharply thereafter. Additionally, maize endosperm cells switch from a mitotic to an endoreduplication cell cycle at approximately 8–10 DAP [9], and the accumulation of storage compounds begins at approximately 10 DAP. This finding suggested that most *ZmSMR* genes might be associated with the transition from mitosis to endoreduplication. Cell elongation due to endoreduplication could provide a site for the accumulation of storage compounds. The increase in gene copy numbers through endoreduplication might also promote high levels of zein gene expression and metabolic output. The expression levels of the *ZmSMR* genes gradually declined after 10 DAP, which indicated that these *ZmSMRs* might play a key role in the endoreduplication start-up phase rather than in endoreduplication progression. Interestingly, almost all the *ZmSMR* genes exhibited high expression levels at 35 DAP, which suggested that the *ZmSMR* genes might participate in the programmed cell death regulatory network. Additionally, the *ZmSMR* genes may also play a role in the activation of biological processes involved in dormancy and dehydration. The expression levels of *ZmSMR2*, *ZmSMR3*, and *ZmSMR8* were downregulated at 10 DAP, suggesting that these genes might only

play a role in preparing for the transition from mitosis to endoreduplication.

As shown in Fig. 4B, every member of the *ZmSMR* gene family responded to various abiotic stresses, suggesting that *ZmSMR* genes play a key role in the responses to abiotic stresses. The members of the *ZmSMR* gene family were divided into two large groups according to the hierarchical clustering results. Group I had seven members, including *ZmSMR4-ZmSMR7*, *ZmSMR9*, *ZmSMR11* and *ZmSMR12*, whereas the other members of the *ZmSMR* gene family were assigned to group II. As shown in Fig. 4, all the genes from group I were upregulated under various treatment conditions, whereas most of the genes from group II were downregulated. This result suggested that the *ZmSMR* genes from different groups might participate in different signalling networks in the response to abiotic stresses. The relative expression levels of the members of group I varied; therefore, we subdivided the genes from group I into two subgroups, designated subgroups A and B, based on their expression levels. Subgroup A included *ZmSMR7*, *ZmSMR9* and *ZmSMR12*, and the expression levels of the subgroup A members were lower than those of the subgroup B members. These findings suggested that *ZmSMR4-ZmSMR6* and *ZmSMR11* were more sensitive to abiotic stress than the other *ZmSMR* genes.

The members of group II showed inconsistent responses to different treatment conditions; therefore, we subdivided the genes from group II into two subgroups, which were designated subgroups C and D. Subgroup C included *ZmSMR2* and *ZmSMR8*, which were both upregulated and downregulated under most treatment conditions. For example, under low-temperature treatment, *ZmSMR2* expression levels were upregulated at 2 h and 4 h and then downregulated at 12 h and 24 h. In contrast, *ZmSMR8* expression levels were downregulated at 12 h after low-temperature treatment and then upregulated from 24 h to 72 h. These results indicated that the treatment time had a greater impact on *ZmSMR2* and *ZmSMR8* expression levels than on other

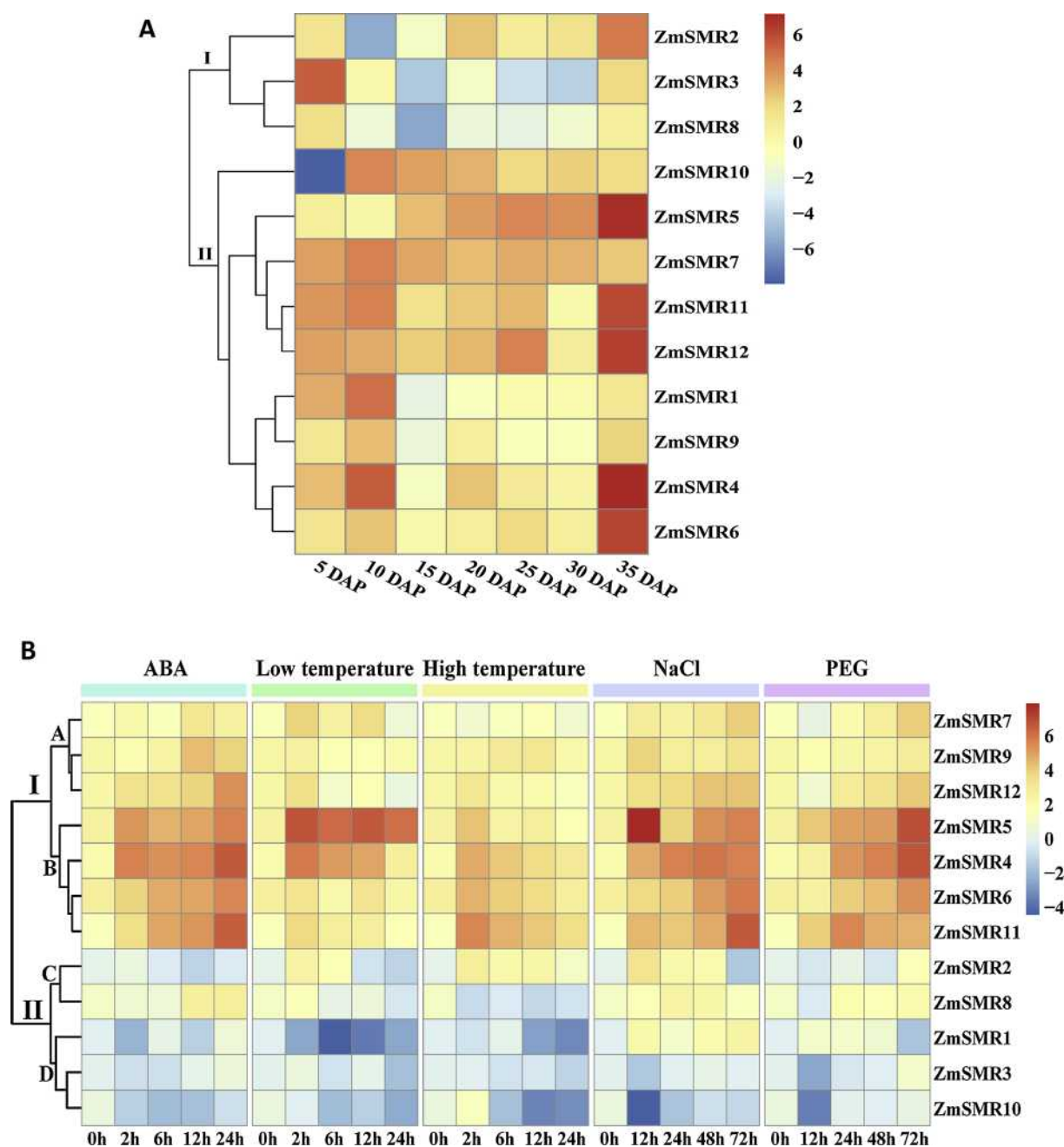


**Fig. 4.** Heat map representation and hierarchical clustering of *ZmSMR* genes during (A) different development stages in the maize endosperm and (B) in response to the abiotic stresses ABA, NaCl, drought (PEG), low temperature and high temperature for the indicated time periods. The expression levels of the *ZmSMR* genes at the different time points were calculated relative to its expression in the control sample (0 h). The expression of the *ZmSMR* genes and the maize actin gene was analysed in three independent biological replicates. The relative expression values were  $\log_2$ -transformed, and the heat maps were prepared with the R package pheatmap. The scale bar at the right-hand side of each heat map represents the  $\log_2$ -transformed values, with values -6 or -4, 0 or 1 and 6 representing low, intermediate and high expression, respectively.

*ZmSMR* genes. The relative expression levels of most of the genes from subgroup D were downregulated by most treatment conditions, except for *ZmSMR1* under NaCl and PEG stress conditions.

The relative expression level of the *ZmSMR4* gene was upregulated by all the treatment conditions, indicating that the *ZmSMR4* gene can respond to various abiotic stresses at the transcriptional level. After the plants were treated with ABA for 24 h, the expression level of the *ZmSMR4* gene was nearly 60-fold higher than in untreated maize, demonstrating that plant hormones can affect the expression level of the *ZmSMR4* gene. This result is similar to the reported expression of another CKI, KRP1, which is also induced by ABA [30]. When maize

seedlings were subjected to salt stress, *ZmSMR4* expression levels gradually increased with increases in the treatment time, peaking at 48 h after treatment and then gradually decreasing after 48 h, which suggests that the *ZmSMR4* gene can respond to salt stress. This result is in agreement with a report by Ceccarelli et al. [5]. Under drought treatment, the transcription of the *ZmSMR4* gene gradually increased with increases in the treatment time and peaked at 72 h (to a level that was 65-fold higher than the control). These results indicate that the *ZmSMR4* gene might be related to drought stress and that its expression might be dependent on ABA. The *ZmSMR4* gene is quite sensitive to temperature. The expression level of the *ZmSMR4* gene peaked at 2 h



after low- or high-temperature treatment. These results demonstrate that the *ZmSMR4* gene is sensitive to temperature. J.P. Grime and M.A. Mowforth suggested that low temperature can influence the rate of cell division, and a mechanism allowing plants to grow at low temperatures might involve the rapid inflation of large cells [36]. Our data show that the *ZmSMR4* gene can be induced by low temperature and can promote the transition between division and endoreduplication (Fig. 9A, B). Additionally, endoreduplication is associated with the rapid inflation of large cells. Therefore, we suggest that the *ZmSMR4* gene might respond to temperature stress by regulating the transition between mitosis and endoreduplication. These data indicate that *ZmSMR* genes positively regulate the responses to abiotic stresses via modulation of their expression at the transcription level and that these genes are involved in various signalling pathways.

### 3.4. *ZmSMR4* localizes to the nucleus and can interact with both CDKA and CDKB in yeast

The fusion expression vector pGFP-*ZmSMR4* and the control empty vector p16318:GFP were transferred into prepared protoplasts using the PEG-induced transformation method to identify the subcellular localization of the *ZmSMR4* protein and the position on the protein that interacts with CDK complexes. The pGFP-*ZmSMR4* fusion protein was expressed in the nucleus, whereas the GFP control was present throughout the cell (Fig. 5). This result implied that the *ZmSMR4* gene functions in the cell nucleus. To confirm the target proteins interacting with the *ZmSMR4* protein, we performed a yeast two-hybrid assay. Only the cells containing the *ZmSMR4* and CDKA or CDKB fusion vectors were capable of growth on Synthetic Dropout-Trp/Leu/His/Ade (SD-T-L-H-A) plates, and the colonies were blue, indicating that interactions between maize CDKs and *ZmSMR4* activated the expression of the *LacZ* reporter gene. The control cells only grew on Synthetic Dropout-Trp-Leu medium (SD-T-L) plates, and the colonies were white (Fig. 6). The detailed results are shown in Table 1.

### 3.5. *ZmSMR4* is a maize homologue of *Arabidopsis* SIAMESE and can complement the trichome phenotype of *sim* mutants

Based on sequence similarity, *ZmSMR4* was predicted to be a maize homologue of *Arabidopsis* SIAMESE. To test this hypothesis, the *ZmSMR4* gene was expressed in *sim* mutant plants under the control of the *GL3* promoter, which is a trichome-specific promoter. On *sim* mutant leaves, many trichomes were clustered and superficially appeared as 'twins' with neighbouring trichomes (Fig. 7A), indicating the absence of intervening cells between two or more adjacent trichomes. However, transgenic plant trichomes were similar to WT plant trichomes

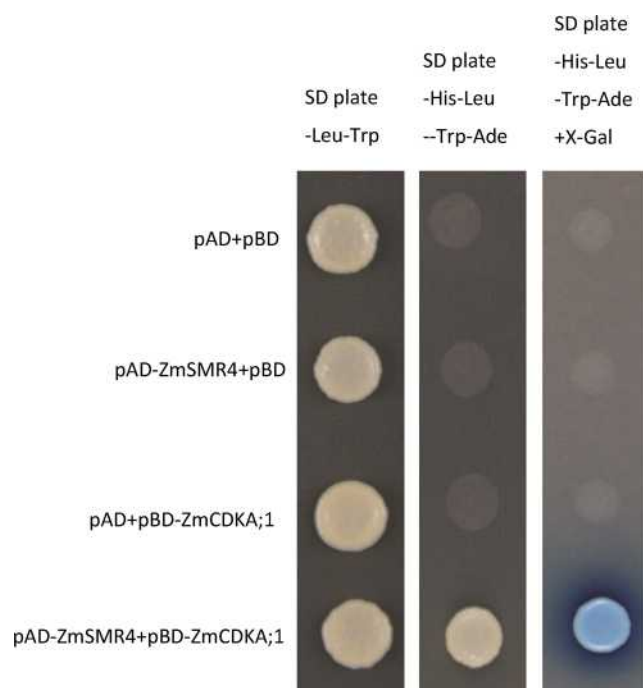


**Fig. 6.** Yeast two-hybrid analysis of the interaction between *ZmSMR4* and *ZmCDK*.

Yeast strain AH109 cells co-expressing bait and prey plasmids were allowed to grow on SD (-Leu/-Trp), SD (-His/-Leu/-Trp/-Ade) and SD (-His/-Leu/-Trp/-Ade/ + X-gal) plates to test for protein–protein interactions.

(Fig. 7B), and all the trichomes appeared as single cells. The detailed statistical results for the trichome phenotype parameters in *Arabidopsis* plants with different genotypes are shown in Table 2. Our results indicated that the *ZmSMR4* gene could complement the trichome phenotype of *sim* mutants (Fig. 7). *ZmSMR4* is therefore functionally equivalent to *SIAMESE* and might play a key role in the transition from mitosis to endoreduplication.

### 3.6. Heterologous expression of *ZmSMR4* affects the growth and development of *Arabidopsis*

To further confirm the biological role of the *ZmSMR4* gene, we analysed five T3-generation transgenic lines (35S:*ZmSMR4*). All the *ZmSMR4*-overexpressing transgenic lines (35S:*ZmSMR4*) displayed very different phenotypes from WT *Arabidopsis*. The transgenic *Arabidopsis*

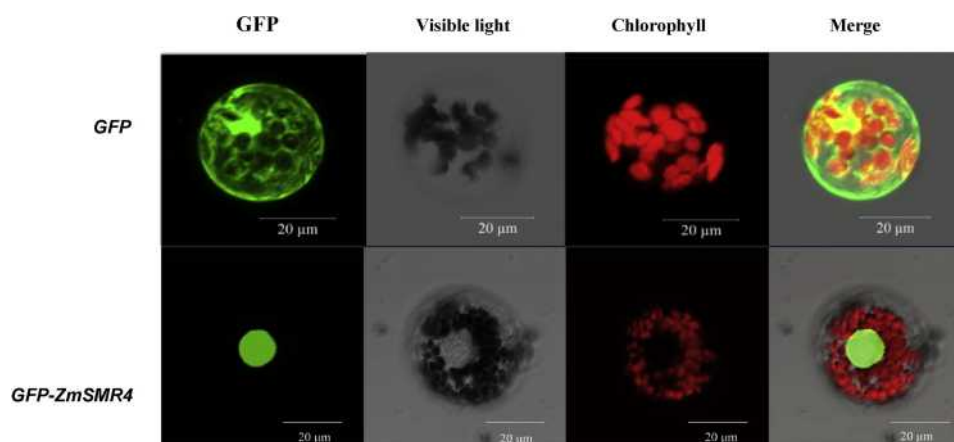


**Fig. 5.** Subcellular localization of the *ZmSMR4*-GFP fusion protein (35S:*ZmSMR4*-GFP) in maize protoplasts. Merge, merged image of the GFP, visible light, and chlorophyll images.

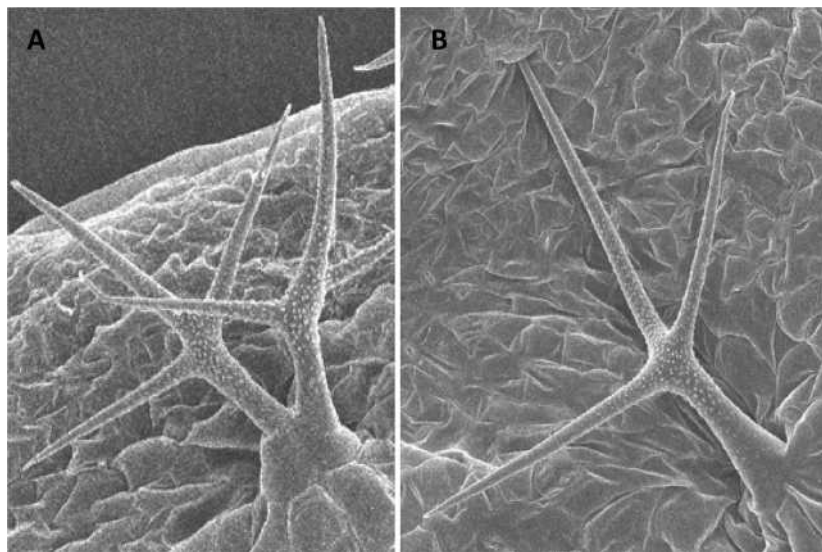


**Fig. 7.** The maize *ZmSMR4* gene can complement the phenotype of *Arabidopsis thaliana sim* mutants. (A) Trichomes from an *Arabidopsis thaliana sim* mutant. (B) A trichome from a transgenic *Arabidopsis thaliana sim GL3:ZmSMR4* plant.

plants overexpressing *ZmSMR4* were much shorter than the WT plants (Fig. 8A), and some transgenic *Arabidopsis* lines overexpressing *ZmSMR4* displayed early death. The degree of serration in the WT *Arabidopsis* leaves varied according to the developmental stage; juvenile leaves were smooth, whereas later-produced rosette leaves exhibited more serration. However, in the present study, all the leaves (including juvenile leaves) from the transgenic *Arabidopsis* plants overexpressing *ZmSMR4* displayed enhanced leaf margin serration (Fig. 8A, B), and the serrations in transgenic *Arabidopsis* lines were increased through both deepening of the sinuses and an increased number of serrations. Moreover, the different lines displayed varying degrees of serration, possibly due to their different expression levels of the *ZmSMR4* transcript. Both the rosette diameter and the leaf size of the transgenic *Arabidopsis* lines overexpressing *ZmSMR4* were decreased compared with those of WT plants (Fig. 8A, B). The transgenic *Arabidopsis* lines overexpressing *ZmSMR4* produced fewer leaves and bloomed at least one week early (Fig. 8C, D) compared with WT *Arabidopsis*. The transgenic *Arabidopsis* lines overexpressing *ZmSMR4* exhibited abnormally shaped siliques with the appearance of sugar-coated haws on a stick, possibly because the seeds of these plants were larger and rounder than those of WT plants (Fig. 8E, F). The results from the statistical analyses of the seed-related indicators agreed with our speculation. In many transgenic *Arabidopsis* lines overexpressing *ZmSMR4*, plant fertility declined (Fig. 8G, H) at the adult plant stage. The abnormal phenotypes from transgenic *Arabidopsis* plants overexpressing *ZmSMR4* clearly suggested that the heterologous expression of the *ZmSMR4* gene affected not only *Arabidopsis* growth but also *Arabidopsis* development.

### 3.7. Transgenic plants overexpressing the *ZmSMR4* gene exhibit increased endoreduplication levels

We analysed the endoreduplication levels in transgenic *Arabidopsis* lines overexpressing *ZmSMR4* and WT plants via flow cytometry to explain the serrated leaf phenotype observed in the transgenic plants overexpressing the *ZmSMR4* gene. Compared with the WT plants, the number of 2C and 4C cells was decreased in the transgenic plants, but the number of 8C and 16C cells was increased (Fig. 9A). The EF of the transgenic plants was higher than that of WT plants (Fig. 9B). The levels of endoreduplication in the WT and transgenic plants were assessed based on the EF, which indicated that the transgenic plants overexpressing the *ZmSMR4* gene exhibited increased endoreduplication levels compared with the WT plants. This result is in agreement with

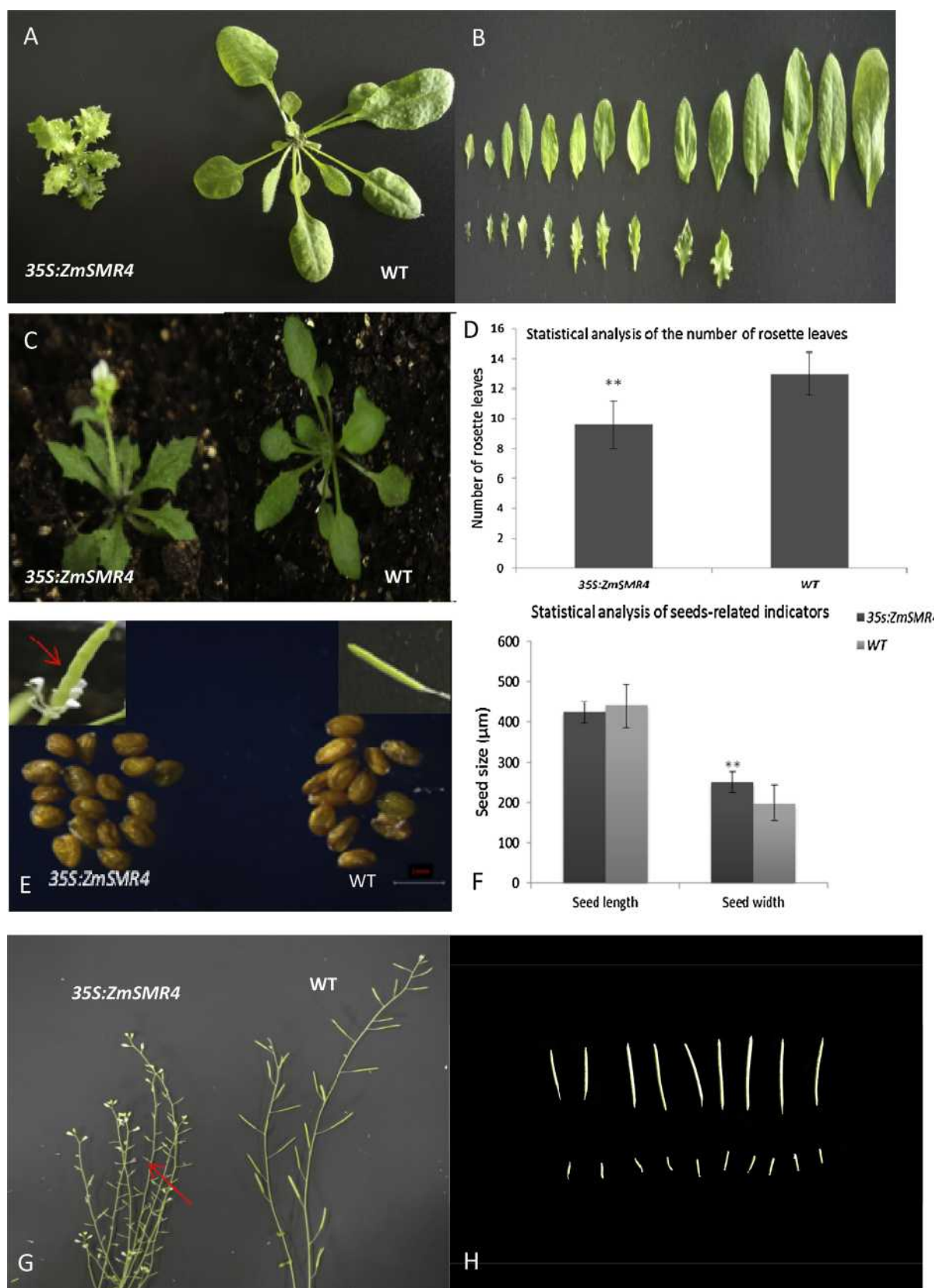
previous findings [16], suggesting that the *ZmSMR4* gene, similar to the *SIAMESE* gene in *Arabidopsis*, can promote the transition from mitosis to endoreduplication. The serrated leaf phenotype might be caused by cells that exhibit an increased endoreplication level but have experienced mitosis arrest. Our results also showed that the endoreduplication level increased during plant development, demonstrating that the cell cycle constantly adjusts as the plant grows. This result agrees with the results from a study conducted by Galbraith et al.

## 4. Discussion

Endoreduplication is a variation of the cell cycle that occurs in maize endosperm cells. Grafi and Larkins proposed that a CKI might affect endoreduplication levels in the developing maize endosperm [22], but the nature of the CKI and its target genes are not fully understood. Larkins et al. identified two maize CKIs, Zeama;KRP;1 and Zeama;KRP;2 but found that only Zeama;KRP;1 accounts for a portion of the CKI activity observed during endosperm development; thus, it is not possible to conclude whether or not Zeama;KRP;1 and Zeama;KRP;2 are functionally involved in endoreduplication [23]. According to previous reports, members of the plant-specific SMR family function as CKIs, regulating the transition between cell mitosis and endoreduplication by interacting with CDKs to inhibit their activity [24]. The first member of the SMR gene family, the *SIAMESE* (*SIM*) gene, was identified in 2006; *SIM* is a nuclear-localized, low-molecular-weight protein that can interact with D-type cyclins and CDKA;1. Plants overexpressing *SIM* are slow-growing and exhibit narrow leaves with an increased DNA content [16]. In this study, we identified 12 candidate *ZmSMR* family genes and successfully isolated the *ZmSMR4* gene. Based on a complementarity test, we further demonstrated that *ZmSMR4* is a maize homologue of the *Arabidopsis SIAMESE* gene. Our results showed that the *ZmSMR4* gene not only affected transgenic *Arabidopsis* growth and development by altering endoreduplication levels but also was involved in responses to abiotic stresses. Therefore, this study might contribute to maize molecular breeding.

Sequence analysis results showed that the members of this family exhibited modest sequence similarity to the *SIAMESE* gene from *Arabidopsis* and shared some key representative motifs. However, we observed that although the motifs occur in a certain order, their spacing might be variable, and there are additional significant discrepancies between the members of this family apart from the motif domain. These findings are not surprising because they appear to reflect the common





(caption on next page)

characteristics of plant CKI families, including the *Arabidopsis* SIAMESE-related family [24] and the KRP family from *Arabidopsis* [14] and rice. It is no accident that different members of the same gene

family have arisen in plants. Each member not only exhibits common basic biochemical activity but also likely plays a unique role in plant development or the response to stresses from the external environment

**Fig. 8.** Phenotypic analysis of *ZmSMR4*-overexpressing transgenic lines. (A) The leaves from *ZmSMR4*-overexpressing 35S:*ZmSMR4* transgenic plants are altered in size and morphology compared with WT plants. (B) The leaves from Fig. 8A were arranged from oldest (left) to youngest (right). (C) Three-week-old WT (right) and *ZmSMR4*-overexpressing 35S:*ZmSMR4* transgenic plants (left). The 35S:*ZmSMR4* plants exhibited a precocious flowering phenotype. (D) Quantitative comparison of the rosette leaf number between WT and 35S:*ZmSMR4* transgenic plants grown under long-day conditions. Leaves were counted on 10 plants of each genotype. (E) The transgenic *Arabidopsis* lines overexpressing *ZmSMR4* had abnormally shaped siliques that looked like sugar-coated haws on a stick (indicated by the red arrow). Microscopic observation of randomly selected mature seeds from WT (right) and *ZmSMR4*-overexpressing 35S:*ZmSMR4* transgenic plants (left). (F) Comparison of seed-related indicators between WT and 35S:*ZmSMR4* transgenic plants. (G) Two-month-old WT (right) and *ZmSMR4*-overexpressing 35S:*ZmSMR4* transgenic plants (left). The 35S:*ZmSMR4* plants exhibited an abortion phenotype; aborted siliques are indicated by the arrow. (H) The siliques from Fig. 8G were arranged in size order. Asterisks indicate significant differences compared with WT ( $P < 0.01$ ). Error bars indicate the standard deviation. (For interpretation of the references to colour in this figure legend, the reader is referred to the web version of this article.)

according to our expression data. The different roles of each family member are mainly due to transcriptional and post-transcriptional regulation, rather than their basic biochemical activity [24].

We isolated the *ZmSMR4* gene via homologous cloning and generated transgenic plants overexpressing this gene. Although there were significant discrepancies between the *ZmSMR4* and *AtSIAMESE* sequences, our experimental results demonstrated that *ZmSMR4* is a maize homologue of *Arabidopsis SIAMESE*. First, the functional domain of the *ZmSMR* gene is similar to that of *AtSIAMESE*, even though the domain sequence is quite short; additionally, neither gene contains introns and both proteins have a low molecular weight. Second, the complementarity test showed that *ZmSMR4* is functionally equivalent to *AtSIAMESE*. Additionally, the interaction targets of *ZmSMR4* and *SIAMESE* are the same. Finally, the phenotype of most of the transgenic plants overexpressing the *ZmSMR4* gene was similar to that of transgenic plants overexpressing the *SIAMESE* gene; these plants were short and exhibited enlarged cells and serrated leaves. Of course, the *ZmSMR4* transgenic plants also exhibited some specific phenotypes that might be useful for maize breeding, such as early blossoming and fuller seeds. Although the molecular mechanism regulating early blossoming in transgenic plants overexpressing the *ZmSMR4* gene remains unclear, a *SIAMESE* homologue in tomato has been shown to be associated with inflorescence development [37]. Transgenic *Arabidopsis* plants overexpressing the *KRP* gene have been found to exhibit early blossoming [38]. Additionally, some transgenic plants overexpressing the *ZmSMR4* gene show an abortion phenotype, which is in agreement with previous results obtained in transgenic *Brassica* plants overexpressing the *KRP* gene [39]. Transgenic plants overexpressing *ICK1* under the control of the *Bgp1* promoter exhibit a poor seed production ability due to poor pollen quality and low pollen numbers [40]. These results demonstrate that the *ZmSMR4* gene not only affects plant growth, but also is involved in plant organ development. The *ZmSMR4* gene is a maize homologue of the *Arabidopsis SIAMESE* gene, which means that this

**Table 1**  
Analysis of the interactions between maize CDKs and *ZmSMR4* in yeast two-hybrid assays.

pGBKT7-hybrid	pGADT7-hybrid	Growth <sup>a</sup>	Growth <sup>b</sup>	Colour <sup>c</sup>
pGBKT7-	pGADT7- <i>ZmSMR4</i>	+	–	White
pGBKT7- <i>ZmCDKA;1</i>	pGADT7- <i>ZmSMR4</i>	+	+	Blue
pGBKT7- <i>ZmCDKA;1</i>	pGADT7-	+	–	White
pGBKT7- <i>ZmCDKA;3</i>	pGADT7- <i>ZmSMR4</i>	+	+	Blue
pGBKT7- <i>ZmCDKA;3</i>	pGADT7-	+	–	White
pGBKT7- <i>ZmCDKB1;1</i>	pGADT7- <i>ZmSMR4</i>	+	+	Blue
pGBKT7- <i>ZmCDKB1;1</i>	pGADT7-	+	–	White
pGBKT7-53	pGADT7-T	+	+	Blue
pGBKT7-lam	pGADT7-T	+	–	White

gene also plays a key role in the transition from mitosis to endoreduplication. During seed filling, endoreduplication is directly associated with cell enlargement and the accumulation of dry weight, and the transition from mitosis to endoreduplication is therefore critical for seed development and directly influences the final yield [41,42]. Seed filling is markedly limited in rice overexpressing *KRP1* [43]. However, our results showed that transgenic *Arabidopsis* plants overexpressing the *ZmSMR4* gene produced fuller seeds, which suggested that the *ZmSMR4* gene is different from the *KRP* gene and that these two genes play different roles in the cell cycle, even though both the *KRP* and *SIAMESE* genes encode plant CKIs and exhibit similar gene structure characteristics. Notably, the effect of *KRP* on endoreduplication is dose-dependent, i.e., the endoreduplication level is reduced when *KRP* gene expression is high, whereas moderate expression of the *KRP* gene increases cell ploidy. In contrast, our larger seed could simply be due to the compensation effect resulting from a notably reduced seed number per silique. Our results showed that the endoreduplication level was elevated in transgenic *Arabidopsis* plants overexpressing the *ZmSMR4* gene (Fig. 8), and the expression level of the *SIAMESE* gene was

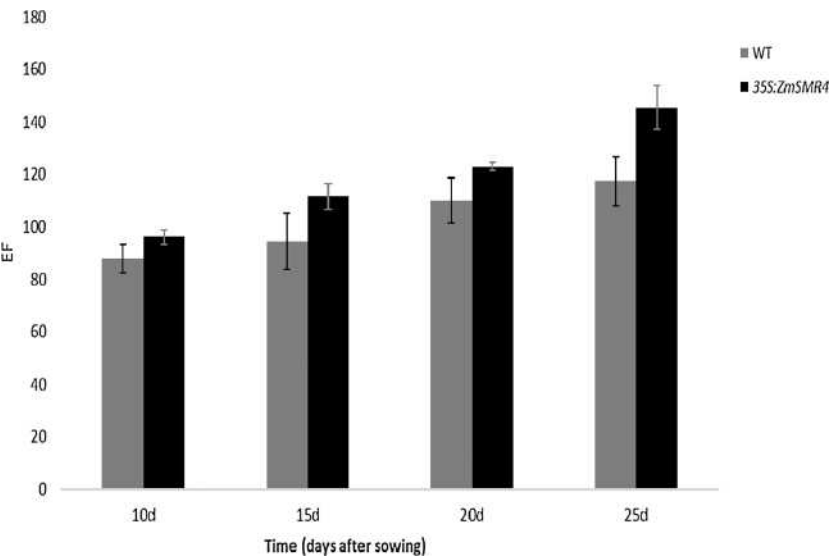


**Fig. 9.** The endoreduplication level is enhanced in transgenic plants overexpressing the *ZmSMR4* gene. (A) The nuclear DNA ploidy from cells from WT and 35S:*ZmSMR4* plants were assessed by flow cytometry. (B) The endoreduplication factor (EF) was determined at the indicated time points after sowing for WT and transgenic plants overexpressing *ZmSMR4*.  $n = 3$ ; error bars represent the SD.



**Table 2**Statistical analysis of the trichome phenotype parameters in *Arabidopsis* plants with different genotypes.

Genotype	Trichomes per leaf (mean $\pm$ s.d.)	TIS per leaf (mean $\pm$ s.d.)	% in clusters	Number of nuclei per TIS
Col	26.8 $\pm$ 1.48	26.9 $\pm$ 1.52	0.7	1 $\pm$ 0
<i>sim</i>	46.4 $\pm$ 1.35	31.2 $\pm$ 1.40	28.7	2.02 $\pm$ 0.02
<i>35S::ZmSMR4</i>	25.8 $\pm$ 1.14	25.9 $\pm$ 1.60	0.4	1.01 $\pm$ 0.02

positively correlated with the endoreduplication level. Moreover, the *SIAMESE* gene has only been identified in plants thus far, whereas the *KPP* gene has been identified in both plants and animals.

Localization to particular cellular regions is required for cell cycle regulators to exert their functions [44]. If cell cycle regulators are mis-localized, the cell cycle might be disrupted. *p27Kip1* is a CKI found in mammalian cells that plays an important role in inhibiting CDK2 and cell growth, and its function depends on its nuclear localization [45,46]. A popular view is that the mis-localization of *p27Kip1* is associated with cancer because *p27Kip1* is located in the cytoplasm rather than in the nucleus in tumour cell lines [47–49], and increased cytoplasmic localization of *p27Kip1* is observed in various cancers [50,51]. In this study, the *ZmSMR4* protein was localized to the nucleus, indicating that *ZmSMR4* functions in the cell nucleus. This result agrees with those of previous studies that demonstrated that both *SIAMESE* and *KRP*, two types of CKIs, localize to the nucleus, even though some of these CKIs have no obvious nuclear localization signal. Hence, these CKIs might use different nuclear localization mechanisms [52].

In summary, many studies have confirmed that plants exhibit more cell cycle regulators than do mammals because of their sessile lifestyle. These regulators not only participate in plant growth and development but also are involved in the responses to biotic and abiotic stresses. This study provides the first report of *SMR* genes in maize. We identified 12 members of the *ZmSMR* gene family and generated transgenic plants overexpressing the *ZmSMR4* gene. Our preliminary results demonstrated that the *ZmSMR4* gene not only affects plant growth but also regulates plant development. *ZmSMR4* is therefore a key cell cycle regulator gene.

## Conflicts of interest

The authors declare that there are no conflicts of interest regarding the publication of this paper.

## Author contributions

Jiquan Xue, Dongwei Guo, and Feifei Li conceived and designed the experiments. Feifei Li, Licheng Wang, Ting Li, Zhengquan Zhang, and Jiaojiao Feng performed the experiments. Feifei Li, Licheng Wang, Shutu Xu, and Renhe Zhang analysed the data. Feifei Li wrote the paper.

## Acknowledgements

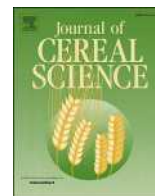
The authors are grateful to Professor John C. Larkin (Department of Biological Sciences, Louisiana State University) for his kind guidance and help with this study. We are also grateful to Professor Mingxun Chen, Zhonghua Wang and Shengbao Xu (Northwest A&F University) for their kind guidance regarding this paper and for providing the vectors. This work was supported by the Shaanxi Province Research and Development Project [grant number: 2017ZDCXL-NY-02-04], the Shaanxi Province Comprehensive Project [grant number: 2015KTZDNY01-01-01], the Yangling District Technical Plan Project [grant number: 2014NY-01], and the APAARI- Dryland Cereals Scholarship Program.

## References

- [1] R. Kasili, J.D. Walker, L.A. Simmons, J. Zhou, V.L. De, J.C. Larkin, *SIAMESE* co-operates with the CDH1-like protein CCS52A1 to establish endoreplication in *Arabidopsis thaliana* trichomes, *Genetics* 185 (2010) 257–268.
- [2] Y. Kadota, T. Watanabe, S. Fujii, K. Higashi, T. Sano, T. Nagata, S. Hasezawa, K. Kuchitsu, Crosstalk between elicitor-induced cell death and cell cycle regulation in tobacco BY-2 cells, *Plant J.* 40 (2004) 131–142.
- [3] S. Wang, Y. Gu, S.G. Zebell, L.K. Anderson, W. Wang, R. Mohan, X. Dong, A non-canonical role for the CKI-RB-E2F cell-cycle signaling pathway in plant effector-triggered immunity, *Cell Host Microbe* 16 (2014) 787–794.
- [4] J.P. Grime, M.A. Mowforth, Variation in genome size—an ecological interpretation, *Nature* 299 (1982) 151–153.
- [5] M. Ceccarelli, E. Santantonio, F. Marmottini, G.N. Amzallag, P.G. Cionini, Chromosome endoreplication as a factor of salt adaptation in *Sorghum bicolor*, *Protoplasma* 227 (2006) 113–118.
- [6] K. Vlieghe, V. Boudolf, G.T.S. Beemster, S. Maes, Z. Magyar, A. Atanassova, J.D.A. Engler, R.D. Groodt, D. Inzé, L.D. Veylder, The DP-E2F-like gene *DEL1* controls the endocycle in *Arabidopsis thaliana*, *Curr. Biol.* 15 (2005) 59–63.
- [7] D.W. Galbraith, K.R. Harkins, S. Knapp, Systemic endopolyploidy in *Arabidopsis thaliana*, *Plant Physiol.* 96 (1991) 985–989.
- [8] J.E. Melaragno, B. Mehrotra, A.W. Coleman, Relationship between endopolyploidy and cell size in epidermal tissue of *Arabidopsis*, *Plant Cell* 5 (1993) 1661–1668.
- [9] P.A. Sabelli, B.A. Larkins, The contribution of cell cycle regulation to endosperm development, *Sex. Plant Reprod.* 22 (2009) 207–219.
- [10] C. Chevalier, M. Nafati, E. Mathieuvivier, M. Bourdon, N. Frangne, C. Cheniclet, J.P. Renaudin, M. Hernould, Elucidating the functional role of endoreduplication in tomato fruit development, *Ann. Bot.* 107 (2011) 1159–1169.
- [11] T.A. Wilkins, K. Rajasekaran, D.M. Anderson, Cotton biotechnology, *Crit. Rev. Plant Sci.* 19 (6) (2000) 511–550.
- [12] E. Kondorosi, A. Kondorosi, Endoreduplication and activation of the anaphase-promoting complex during symbiotic cell development, *FEBS Lett.* 567 (2004) 152–157.
- [13] D.O. Morgan, Cyclin dependent kinases, clocks, and microprocessors, *Annu. Rev. Cell Dev. Biol.* 13 (1997) 261–291.
- [14] L.D. Veylder, T. Beeckman, G.T.S. Beemster, L. Krols, F. Terras, I. Landrieu, E.V.D. Schueren, S. Maes, M. Naudts, D. Inzé, Functional analysis of cyclin-dependent kinase inhibitors of *Arabidopsis*, *The Plant Cell* 13 (2001) 1653.
- [15] S. Jasinski, C. Riou-Khamlichi, O. Roche, C. Perennes, C. Bergounioux, N. Glab, The CDK inhibitor NtKIS1a is involved in plant development, endoreduplication and restores normal development of cyclin D3; 1-overexpressing plants, *J. Cell Sci.* 115 (2002) 973–982.
- [16] M. Churchman, M. Brown, N. Kato, V. Kirik, M. Hulskamp, D. Inzé, L. De Veylder, J.D. Walker, Z. Zheng, D. Oppenheimer, *SIAMESE*, a plant-specific cell cycle regulator, controls endoreplication onset in *Arabidopsis thaliana*, *Plant Cell* 18 (2006) 3145–3157.
- [17] J.V. Leene, J. Hollunder, D. Eeckhout, G. Persiau, E.V.D. Slijke, H. Stals, G.V. Isterdael, A. Verkest, S. Neirynck, Y. Buffel, Targeted interactomics reveals a complex core cell cycle machinery in *Arabidopsis thaliana*, *Mol. Syst. Biol.* 6 (2010) 397.
- [18] A. Peres, M.L. Churchman, S. Hariharan, K. Himanen, A. Verkest, K. Vandepoele, Z. Magyar, Y. Hatzfeld, D.S.E. Van, G.T. Beemster, Novel plant-specific cyclin-dependent kinase inhibitors induced by biotic and abiotic stresses, *J. Biol. Chem.* 282 (2007) 25588–25596.
- [19] A.H. Roeder, V. Chickarmane, A. Cunha, B. Obara, B.S. Manjunath, E.M. Meyerowitz, Variability in the control of cell division underlies sepal epidermal patterning in *Arabidopsis thaliana*, *PLoS Biol.* 8 (2010) e1000367.
- [20] R.A. Dante, B.A. Larkins, P.A. Sabelli, Cell cycle control and seed development, *Front. Plant Sci.* 5 (2013) 493.
- [21] X. Sun, J. Cahill, T.V. Hautegeem, K. Feys, C. Whipple, O. Novák, S. Delbare, C. Verstele, K. Demuynck, J.D. Block, Altered expression of maize *PLASTOCHRON1* enhances biomass and seed yield by extending cell division duration, *Nat. Commun.* 8 (2017) 14752.
- [22] G. Grafi, B.A. Larkins, Endoreduplication in maize endosperm: involvement of M phase-promoting factor inhibition and induction of S phase-related kinases, *Science* 269 (1995) 1262–1264.
- [23] C.M. Coelho, R.A. Dante, P.A. Sabelli, Y. Sun, B.P. Dilkes, W.J. Gordonkamm, B.A. Larkins, Cyclin-dependent kinase inhibitors in maize endosperm and their potential role in endoreduplication, *Plant Physiol.* 138 (2005) 2323–2336.
- [24] N. Kumar, H. Harashima, S. Kalve, J. Bramsiepe, K. Wang, B.L. Sizani, L.L. Bertrand, M.C. Johnson, C. Faulk, R. Dale, Functional conservation in the *SIAMESE*-RELATED family of cyclin-dependent kinase inhibitors in land plants, *Plant Cell* 27 (2015).
- [25] F. Sievers, A. Wilm, D. Dineen, T.J. Gibson, K. Karplus, W. Li, R. Lopez, H. McWilliam, M. Remmert, J. Söding, Fast, scalable generation of high-quality

- protein multiple sequence alignments using Clustal Omega, *Mol. Syst. Biol.* 7 (2011) 1429–1432.
- [26] R.E. Voorrips, MapChart: software for the graphical presentation of linkage maps and QTLs, *J. Hered.* 93 (2002) 77–78.
- [27] J.F. Topping, W. Wei, M.C. Clarke, P. Muskett, K. Lindsey, Agrobacterium-mediated transformation of *Arabidopsis thaliana*. Application in T-DNA tagging, *Methods Mol. Biol.* 49 (1995) 63.
- [28] K.J. Livak, T.D. Schmittgen, Analysis of relative gene expression data using real-time quantitative PCR and the 2(-Delta Delta C(T)) Method, *Methods* 25 (2001) 402–408.
- [29] S.D. Yoo, Y.H. Cho, J. Sheen, *Arabidopsis* mesophyll protoplasts: a versatile cell system for transient gene expression analysis, *Nat. Protoc.* 2 (2007) 1565.
- [30] H. Wang, Q. Qi, P. Schorr, A.J. Cutler, W.L. Crosby, L.C. Fowke, ICK1, a cyclin-dependent protein kinase inhibitor from *Arabidopsis thaliana* interacts with both Cdc2a and CycD3, and its expression is induced by abscisic acid, *Plant J. Cell Mol. Biology*. 15 (1998) 501–510.
- [31] J.C. Larkin, J.D. Walker, A.C. Bolognesiwinfield, J.C. Gray, A.R. Walker, Allele-specific interactions between ttg and gl1 during trichome development in *Arabidopsis thaliana*, *Genetics* 151 (1999) 1591–1604.
- [32] J.D. Walker, D.G. Oppenheimer, J. Concienne, J.C. Larkin, SIAMESE. a gene controlling the endoreduplication cell cycle in *Arabidopsis thaliana* trichomes, *Development* 127 (2000) 3931–3940.
- [33] B.K. Kay, M.P. Williamson, M. Sudol, The importance of being proline: the interaction of proline-rich motifs in signaling proteins with their cognate domains, *FASEB J.* 14 (2000) 231–241.
- [34] J.A. Wohlschlegel, B.T. Dwyer, D.Y. Takeda, A. Dutta, Mutational analysis of the Cy motif from p21 reveals sequence degeneracy and specificity for different cyclin-dependent kinases, *Mol. Cell. Biol.* 21 (2001) 4868–4874.
- [35] P.D. Adams, W.R. Sellers, S.K. Sharma, A.D. Wu, C.M. Nalin, K.W. Jr, Identification of a cyclin-cdk2 recognition motif present in substrates and p21-like cyclin-dependent kinase inhibitors, *Mol. Cell. Biol.* 16 (1996) 6623–6633.
- [36] J.P. Grime, M.A. Mowforth, Variation in genome size—an ecological interpretation, *Nature* 299 (1982) 151–153.
- [37] L. Pnueli, T. Gutfinger, D. Hareven, O. Benaïm, N. Ron, N. Adir, E. Lifschitz, Tomato SP-interacting proteins define a conserved signaling system that regulates shoot architecture and flowering, *Plant Cell*. 13 (2002) 2687–2702.
- [38] H. Wang, Y. Zhou, S. Gilmer, S. Whitwill, L.C. Fowke, Expression of the plant cyclin-dependent kinase inhibitor ICK1 affects cell division, plant growth and morphology, *Plant J.* 24 (2000) 613–623.
- [39] Y. Zhou, L. Fowke, H. Wang, Plant CDK inhibitors: studies of interactions with cell cycle regulators in the yeast two-hybrid system and functional comparisons in transgenic *Arabidopsis* plants, *Plant Cell Rep.* 20 (2002) 967–975.
- [40] Y. Zhou, L.C. Fowke, Control of petal and pollen development by the plant cyclin-dependent kinase inhibitor ICK1 in transgenic Brassica plants, *Planta* 215 (2002) 248.
- [41] R.A. Dante, B.A. Larkins, P.A. Sabelli, Cell cycle control and seed development, *Front. Plant Sci.* 5 (2014) 493.
- [42] R.S. Sekhon, C.N. Hirsch, K.L. Childs, M.W. Breitman, P. Kell, S. Duvick, E.P. Spalding, C.R. Buell, L.N. De, S.M. Kaeppler, Phenotypic and transcriptional analysis of divergently selected maize populations reveals the role of developmental timing in seed size determination, *Plant Physiol.* 165 (2014) 658.
- [43] R.M. Barrôco, A. Peres, A.M. Droual, L.D. Veylder, S.L.N. Le, J.D. Wolf, V. Mironov, R. Peerbolte, G.T.S. Beemster, D. Inzé, The cyclin-Dependent kinase inhibitor Orysa;KRP1 plays an important role in seed development of rice, *Plant Physiol.* 142 (2006) 1053.
- [44] J. Pines, Four-dimensional control of the cell cycle, *Nat. Cell Biol.* 1 (1999) E73–79.
- [45] Y. Jiang, R.C. Zhao, C.M. Verfaillie, Abnormal integrin-mediated regulation of chronic myelogenous leukemia CD34+ cell proliferation: BCR/ABL up-regulates the cyclin-dependent kinase inhibitor, p27Kip, which is relocated to the cell cytoplasm and incapable of regulating cdk2 activity, *Proc. Natl. Acad. Sci.* 97 (2000) 10538–10543.
- [46] C. Delong, The *Arabidopsis* Cdc2a-interacting protein ICK2 is structurally related to ICK1 and is a potent inhibitor of cyclin-dependent kinase activity in vitro, *Plant J.* 21 (2000) 379–385.
- [47] I. Shin, F.M. Yakes, F. Rojo, N.Y. Shin, A.V. Bakin, J. Baselga, C.L. Arteaga, PKB/Akt mediates cell-cycle progression by phosphorylation of p27(Kip1) at threonine 157 and modulation of its cellular localization, *Nat. Med.* 8 (2002) 1145–1152.
- [48] J. Slingerland, M. Pagano, Regulation of the cdk inhibitor p27 and its deregulation in cancer, *J. Cell. Physiol.* 183 (2000) 10.
- [49] G. Viglietto, M.L. Motti, L. Cito, A. Fusco, M. Santoro, Cytoplasmic re-localization and inhibition of the cyclin-dependent kinase inhibitor p27Kip1 by Akt-mediated phosphorylation in breast cancer, *Eur. J. Cancer*. 38 (2002) S48.
- [50] Y.H. Min, J.W. Cheong, J.Y. Kim, J.I. Eom, S.T. Lee, J.S. Hahn, Y.W. Ko, M.H. Lee, Cytoplasmic mislocalization of p27Kip1 protein is associated with constitutive phosphorylation of Akt or protein kinase B and poor prognosis in acute myelogenous leukemia, *Cancer Res.* 64 (2004) 5225.
- [51] D.G. Rosen, G. Yang, K.Q. Cai, R.C. Bast Jr, D.M. Gershenson, E.G. Silva, J. Liu, Subcellular localization of p27kip1 expression predicts poor prognosis in human ovarian cancer, *Clin. Cancer Res.* 11 (2005) 632–637.
- [52] Y. Zhou, H. Niu, F. Brandizzi, L.C. Fowke, H. Wang, Molecular control of nuclear and subnuclear targeting of the plant CDK inhibitor ICK1 and ICK1-Mediated nuclear transport of CDKA, *Plant Mol. Biol.* 62 (2006) 261–278.





# High-amylose starch as a new ingredient to balance nutrition and texture of food

Yuyue Zhong<sup>a</sup>, Heyuan Zhu<sup>a</sup>, Wenxin Liang<sup>b</sup>, Xu Li<sup>b</sup>, Linsan Liu<sup>a</sup>, Xudong Zhang<sup>a</sup>,  
Huifen Yue<sup>b</sup>, Jiquan Xue<sup>a</sup>, Xingxun Liu<sup>c,\*</sup>, Dongwei Guo<sup>a,\*\*</sup>

<sup>a</sup> Maize Biology and Genetic Laboratory in Northwest Arid Area in China, Ministry of Agriculture, Northwest A&F University, Yangling District, Shaan Xi Province, 712100, China

<sup>b</sup> College of Agronomy, Northwest A&F University, Yangling District, Shaan Xi Province, 712100, China

<sup>c</sup> Institute of Food Science and Technology (IFST), Chinese Academy of Agricultural Sciences (CAAS), Beijing, 100193, China

## ARTICLE INFO

### Article history:

Received 26 October 2017

Received in revised form

8 February 2018

Accepted 21 February 2018

Available online 26 February 2018

### Keywords:

High amylose maize starch

Resistant starch

Texture

## ABSTRACT

Starch can provide food (such as cake) with a good texture. However, starch also causes the postprandial glycaemic response, which leads to Type-2 diabetes and cardiovascular diseases. In this study, we developed high-amylose starch as a new ingredient. The molecular structure of high-amylose maize starch (HAMS) was also studied to explore the effects of HAMS on the physicochemical, digestion and texture properties of high-amylose maize flour cakes (HAMFCs). The results showed the small molecular size, low amounts of short amylopectin chains, and high amounts of long amylopectin chains and amylose chains of HAMS are helpful to understand the texture (the increase in hardness, cohesiveness, chewiness and resilience and the decrease in springiness) and digestion (the increase in SDS and RS and the decrease in RDS) properties, and the formation of V-type crystalline structure in HAMFCs. Special molecule structure of HAMS and V-type crystalline are the main reason for the improvement of RS in HAMFCs. Sensory evaluation showed that HAMFCs would be accepted by customers and 20% HAMF addition is the best scheme. In sum, the molecular structure of HAMS helps understand the quality of HAMFCs; and HAMFCs could be developed as novel food with a higher RS and acceptable sensory attributes.

© 2018 Elsevier Ltd. All rights reserved.

## 1. Introduction

The bakery foods such as bread, cake and biscuit, are palatable, easy-cooking and portable; thus, they are popular daily foods in the world. Bakery foods are starch-rich which provide a good texture for consumers, and it also contains a large amount of rapidly digestible starch (RDS) and a low amount of slowly digestible starch (SDS) and resistant starch (RS) (Giuberti et al., 2016). RDS is the starch that can be digested rapidly throughout the gastrointestinal tract and related to the post-meal glycaemia level in the human body. High amounts of RDS in the cake has great potential to induce an excessive postprandial glycaemic response and obesity. SDS is the starch that is digested slowly but completely and maintains plasma glucose levels over time. RS is the starch that cannot be

digested by the human digestive system but can be fermented by caecal and colonic microbial communities (Giuberti et al., 2016). In other words, RS is beneficial to reduce the glycaemia level in the human body. Moreover, RS has the ability to prevent colorectal cancers, decrease plasma cholesterol and triglyceride concentrations, and is a prebiotic to promote the growth of beneficial microflora (Birt et al., 2013). Therefore, current dietary guidelines suggest to reduce the consumption of RDS and to improve the consumption of RS in starchy food aiming to provide human health benefits (Nutrition and Allergies, 2012).

High amylose maize starch (HAMS), defining as the starch with more than 50% amylose, is commonly regarded as one important source of foodstuff with higher RS standards. Lin studied the molecular structure and enzymatic hydrolysis properties of starches from high amylose maize inbred lines and their hybrids, and found more than 43.6% RS in native starch and 6.8% RS in gelatinized starch (Lin et al., 2016). Mutlu treated the high amylose maize starch (about 70% amylose) by microwave irradiation and they

\* Corresponding author.

\*\* Corresponding author.

E-mail addresses: [ytbody652@163.com](mailto:ytbody652@163.com) (X. Liu), [gdwei1973@126.com](mailto:gdwei1973@126.com) (D. Guo).

obtained the starch with 43.4% RS content (Mutlu et al., 2017). Zhang found that the native high-amylose maize starch (about 50% amylose) has the RS content of 11.57% and RS content of starch reached 25.13% after de-branched combination with high temperature/pressure treatment (Zhang et al., 2013). In our previous study, the *in vitro* digestion of high amylose maize flour (HAMF) (about 54% amylose) was studied and a 20.52% RS content of the flour was measured while normal maize flour had only 4.52% RS content (Zhang et al., 2016). As a comparison, RS in wheat starch and flour from Luwang Company in China were only 2.27% and 1.09% respectively (Chen et al., 2015).

Therefore, high amylose starch could be acted as a new material for the preparation of novel starch-based food to improve the resistant starch content, which can then decrease the postprandial glycaemic response. High amylose starch has been added to cookies through using high amylose flour to substitute wheat flour (WF) in different levels. The RS content in cookies was 1.6% in pure WF cookie while 10.07% RS obtained with 50% high amylose flour substitution (Giuberti et al., 2016). Additionally, high amylose flour was also used to replace WF in bread-making and the results showed 50% substitution of high amylose flour can make bread with an improvement in RS content from 1.5% to 3.1% (Hung et al., 2005).

Cakes have an ever-increasing global market demand. Whole-grain cakes are developed for people who have Type-2 diabetes and cardiovascular diseases. However, the texture is not so good. Therefore, in this study, 0, 10%, 20%, 30% and 40% HAMF was added to cake to explore the effects of HAMS on the morphology, volume, specific volume and texture properties, *in vitro* digestion and crystallinity of the cake, with the purpose of developing one functional high amylose maize starch-based cakes (HAMSCs) with a higher RS content and acceptable sensory properties. Considering the high correlation between the molecular structure and the physicochemical, texture, digestion and crystal properties of starch (You et al., 2015; Zhao et al., 2016; Lee et al., 2017; Xu et al., 2017), the molecular structure of HAMS was also studied by Gel-permeation chromatography (GPC) since it is useful to understand the effects of high amylose maize starch on the high amylose maize starch based cake properties. The information obtained from this study is helpful for the development of high amylose maize starch and the understanding of effects of high amylose maize starch on the cake properties.

## 2. Materials and methods

### 2.1. Materials

High amylose maize (amylose content: 55.85%) and normal maize starch (NMS) (amylose content: 29%) were provided by the Maize Biology and Genetic Laboratory in Northwest Arid Area in China, Ministry of Agriculture, Northwest A&F University. Normal wheat flour was purchased from Luwang Company (Shandong, China). All other raw ingredients (food grade) were acquired in local supermarkets. Amyloglucosidase (Sigma A-7095, Sigma–Aldrich® Co., Milan, Italy), invertase (Sigma I-4504, Sigma–Aldrich® Co., Milan, Italy),  $\alpha$ -amylase from porcine pancreas (Merck 7130, Merck KGaA, Darmstadt, Germany) and glucose oxidase kit (GODPOD 4058, Giese Diagnostic snc, Rome, Italy) were purchased.

### 2.2. Gel-permeation chromatography (GPC)

Normal maize starch and high amylose maize starch were isolated according to the method of Xu (Xu et al., 2017). The molecular size distributions of branched and debranched normal maize starch

and high amylose maize starch were characterized using GPC (Agilent 1260 series, Agilent Technologies, USA) equipped with a refractive index detector (Optilab T-REX, WYATT Corp., USA), and a differential pressure detector (Viscostar-II, WYATT Corp., USA). Debranched starch was obtained following the method of Kuang (Syahariza et al., 2013): about 6 mg native starch were dissolved in DMSO/LiBr solution and then debranched using isoamylase in acetate buffer (PH ~3.5). The separation of molecules in GPC was based on the hydrodynamic volume ( $V_h$ ) of molecules or corresponding hydrodynamic radius ( $R_h$ ) according to the equation of  $V_h = 4/3 \pi R_h^3$ . The weight distributions,  $W(\log R_h)$ , of branched and debranched starch are denoted by  $W_{br}(\log R_h)$  and  $W_{de}(\log R_h)$ , respectively. The degree of polymerization (DP) of debranched starch was calculated following the method described elsewhere (You et al., 2015).

### 2.3. Preparation of cake

Cake preparation was modified from the method of Sirisoontaralak (Sirisoontaralak et al., 2017). Firstly, mixed flour (600 g), egg (600 g), sugar (400 g), salt (1 g), water (250 g), baking powder (4 g) and vegetable oil (15 g) were prepared. Then creaming mixed flour, baking powder and vegetable oil together. Eggs, salt and sugar were whipped together until semi-firm foam, followed by mixing the blend of sugar-egg foam, deionized water and creamed flour. Cake butter (20 g) was poured into different paper models and then put the model into a cake pan to bake at 200 °C for 1 h. Cakes were cooled at room temperature for 2 h before analysis. 0%, 10%, 20%, 30% and 40% (w/w) of HAMF were added to the mixed flour respectively, assigned as Control, HM10, HM20, HM30 and HM40. HAMF preparation procedure was using Zhang's method (Zhang et al., 2016).

### 2.4. Chemical composition and digestion properties of cake

Moisture content was calculated by the weight difference of  $2.0 \pm 0.1$  g of cake crumbs before and after drying in an oven (100 °C) for 24 h. Protein, total starch and RS were measured by the method of AACC (AACC, 2000). RDS and SDS were determined by the method of Giuberti (Giuberti et al., 2016).

### 2.5. Morphology, volume and specific volume of cake

Morphology of samples was observed by a digital camera, a stereo microscope (C-DSS230, Nikon, Japan) and a scanning electron microscope (Jane et al., 1999; Chen et al., 2011, 2015) (SN3500, Hitachi limited company, Japan). Surface appearance was observed by the digital camera and cross-section was observed by the digital camera and the stereomicroscope (2X magnification). Microstructure was observed by SEM at 800x magnification and 5.0 kV emission after sputtering gold.

Volume and specific volume were measured by a rapeseed displacement method. Rapeseed was used to fill the empty beaker and the volume of this rapeseed was calculated by a graduated cylinder. The volume of rapeseed was the volume of the empty beaker ( $V_1$ ). After baking, the cake was put into a beaker which full of rapeseed and part of rapeseed were expelled from the beaker until the cake was completely entered in the beaker. The volume of the rest of rapeseed ( $V_2$ ) was calculated by the graduated cylinder again. The mass of the cake (M) was measured by an analytical balance. The cake volume and specific volume were calculated as  $V_1 - V_2$  and  $(V_1 - V_2)/M$  respectively.



## 2.6. X-ray diffraction (XRD) analysis of cake

Wide-angle X-ray scattering patterns of cakes were performed on an X-ray diffractometer (model D/max-2200, Rigaku, Japan) on the first day. The diffractograms were collected under the conditions of 40 kV, 40 mA, with the scanning angle ( $2\theta$ ) from  $5^\circ$  to  $35^\circ$  at a scanning rate of  $4^\circ/\text{min}$ .

## 2.7. Texture properties of cake

Texture properties of cakes were analyzed by the texture profile analyzer (TPA, TVT 6700, Perten Swiss). The crust of cake was removed and the cake was prepared as  $3\text{ cm} \times 3\text{ cm} \times 3\text{ cm}$  for determination. The diameter of cylinder probe was 25 mm and the compression degree was 25%. Two cycles were required at a trigger load of 5 g and the test rate of 1 mm/s. The interval between two compressions was 15 s. After the test, hardness, springiness, cohesiveness, chewiness and resilience were calculated following Pons's method (Pons and Fiszman, 2010).

## 2.8. Sensory evaluation of cake

30 untrained customers were recruited to evaluate the sensory attributes of HAMFCs. These customers were volunteers from the students, staff and faculty at Northwest A&F University. All customers were received 5 different samples (Control, HM10, HM20, HM30, HM40) on the first day of baking and required to evaluate cake from five aspects (odor, aspect, tenderness, crumb color and taste).

Customers used a 10-point hedonic scale (1–2 = dislike extremely, 3–4 = dislike, 5–6 = neither dislike nor like, 7–8 = liked, and 9–10 = like extremely). The evaluation was based on the paper ballots containing the hedonic scales and instructions. Customers were instructed to rate each cake individually and asked to rinse their mouth with water between samples.

## 2.9. Statistical analyses

All data were conducted at least in triplicate, expressed as mean value and analyzed by analysis of variance (ANOVA) using the SPSS software (SPSS Inc., Chicago, IL, USA). Significance differences were examined by Duncan's test ( $P \leq 0.05$ ). The figures were processed by OriginPro 2016.

# 3. Results and discussion

## 3.1. Molecular structure of starch

Typical GPC weight distributions,  $W_{br}(\log R_h)$ , of fully branched NMS and HAMS are shown in Fig. 1A, normalized to the peak maximum of Ap. Two whole branched starch distribution in NMS and HAMS displayed two populations of  $\alpha$ -glucans: Am ( $R_h$  up to  $\sim 100\text{ nm}$ ) and Ap ( $R_h$  between  $100\text{ nm}$  and  $4000\text{ nm}$ ) (Zhao et al., 2016). The Am component of the whole-molecule distributions and the corresponding for the Ap are expressed as the value of  $R_h$  at the Am peak maximum and Ap peak maximum respectively, and  $H_{Am}/H_{Ap}$  is the height ratio of Am and Ap peak maximums (Zhao et al., 2016). The figure shows that NMS has a lower peak of Am than the peak in Ap, the lower area under the curve (AUC) in the amylose region than in the amylopectin region. Compared to NMS, the higher amylose content of HAMS contributed to its higher peak in Am than in Ap and higher AUC in the amylose region than in the amylopectin region. However, the molecular size in the  $R_h$  at the Am peak maximum of HAMS is smaller than NMS, while HAMS has the similar molecular size in  $R_h$  at the Ap peak maximum to NMS

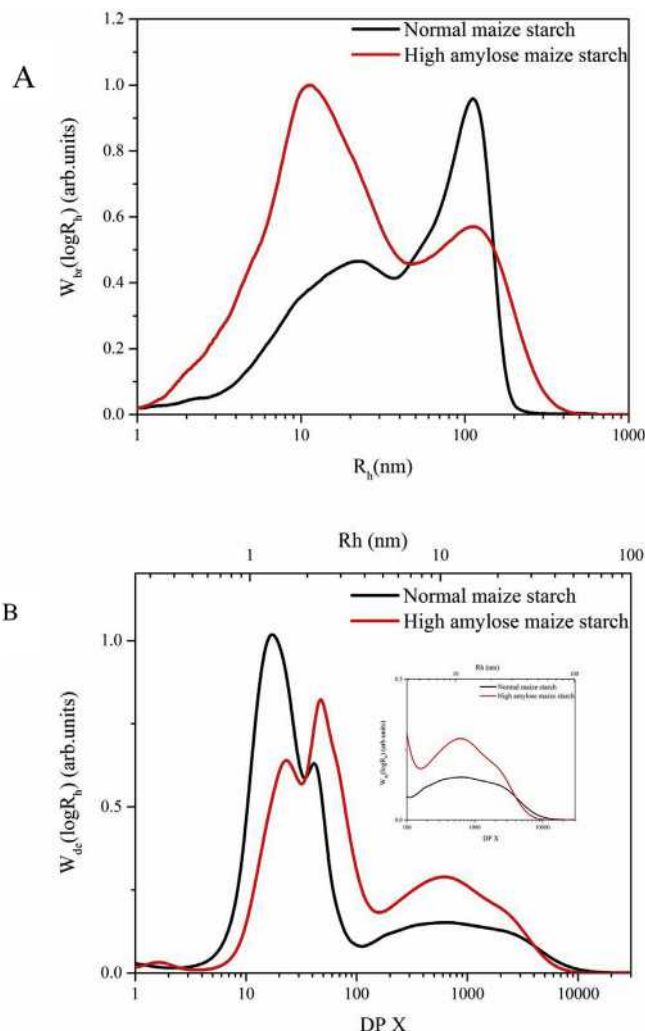


**Fig. 1.** (A) GPC weight chain-length distributions (CLDs) of branched normal maize starch and high amylose maize starch,  $W_{br}(\log R_h)$  as a function of molecular sizes of  $R_h$ , nm; (B) GPC weight CLDs of debranched normal maize starch and high amylose maize starch and an enlargement of the amylose region,  $W_{de}(\log R_h)$  as a function of  $R_h$ , nm and DP X.

(Table S1).

Typical GPC weight distributions,  $W_{de}(\log R_h)$ , of debranched normal maize starch (NMS) and high amylose maize starch (HAMS) are presented in Fig. 1B, normalized to the highest Ap peak maximum. The components with DP X < 100 (about  $R_h$  0.5–6 nm) are defined as amylopectin chains, while those with DP X > 100 ( $R_h$  > 6 nm) are defined as amylose chains (Zhao et al., 2016). The GPC weight distributions of debranched NMS and HAMS show the usual features: two large peaks for amylopectin chains (Ap<sub>1</sub> and Ap<sub>2</sub>) and several small peaks for amylose chains (Zhao et al., 2016). Ap<sub>1</sub> is comprised of the shorter amylopectin branches with lengths up to a DP of 30 ( $R_h$  0.5–2 nm); these are confined to one amorphous/crystalline lamella. Ap<sub>2</sub> is comprised of the longer amylopectin branches with DPs ranging from 30 to 99 ( $R_h$  2–4 nm); these span more than one crystalline lamella (Zhao et al., 2016). DPs from 100 to 20,000 ( $R_h$  from 4 to 300 nm) are the chain-length distributions (CLDs) of amylose (denoted Am). As observed in Fig. 1B, the global maximum in NMS is Ap<sub>1</sub> while the highest peak in HAMS is Ap<sub>2</sub>. AUC of Ap<sub>1</sub> in HAMS is much lower than that in NMS while AUC of Ap<sub>2</sub> in HAMS is higher. The Am and AUC in the amylose region in HAMS are significantly higher than those in NMS. There

are also significant differences in Am peaks between NMS and HAMS, arising from potentially discrete enzymatic starch biosynthetic processes. It may be related to the different isoforms of GBSS (the main enzyme synthesizing amylose) which synthesize different Am peaks (Wang et al., 2014).

To compare the fine structure of NMS and HAMS, a set of empirical parameters used as defined previously were obtained from GPC results (Xu et al., 2017).  $X_{Ap1}$ ,  $X_{Ap2}$  and  $X_{Am}$  indicate the DPs at the maximum of each peak.  $H_{Ap1}$ ,  $H_{Ap2}$  and  $H_{Am}$  are the heights at each peak maximum and the ratios of the peak height of Ap2 and Am to that of Ap1 are denoted  $H_{Ap2}/H_{Ap1}$  and  $H_{Am}/H_{Ap1}$ , respectively.  $X_{Ap1}$ ,  $X_{Ap2}$  and  $X_{Am}$  reflect the relative size of chains in each group of branches, while  $H_{Ap2}/H_{Ap1}$  and  $H_{Am}/H_{Ap1}$  represent the relative amount of chains in each group of branches (Wang et al., 2014). These parameters are displayed in Table S1. The  $X_{Ap1}$ ,  $X_{Ap2}$ ,  $X_{Am}$ ,  $H_{Ap2}/H_{Ap1}$  and  $H_{Am}/H_{Ap1}$  of HAMS are all higher than those of NMS. These results indicate that the CLDs of short amylopectin chains, long amylopectin chains and amylose chains in NMS and HAMS have significant differences.

### 3.2. Chemical composition of cake

The chemical composition of cake is presented in Table 1. Moisture content decreased significantly from 27.6% to 25.42%, 23.81%, 23.43%, 21.9% with increasing HAMF levels. It can be attributed to the reduction of hydroxyl groups on the starch chains participating in the formation of hydrogen bonds in HAMFCs as amylose has less hydroxyl groups than amylopectin. Besides, the higher retrogradation rate of amylose promoted the combination of amylose with long branch chains of amylopectin and lipid (Birt et al., 2013), and contributed to the loss of their water bonding capacity. HAMF addition gave rise to a reduction in the protein content from 16.75% to 16.54%, 16.14%, 15.88% and 15.41%, because the protein content (7.05%) of HAMF is lower than that of WF (10%) (Hung et al., 2005; Zhang et al., 2016). Although the protein content of HAMFCs decreased, it still meets the demand of human and can provide special nutrition. Zein, the main composition of maize protein, is particularly rich in glutamic acid (21–26%), leucine (20%), proline (10%) and alanine (10%) and has anti-oxidative activity (Shukla and Cheryan, 2001). The increasing HAMF levels led to a decrease in total starch content of the cake from 39.08% to 38.19%, 38.18%, 37.73% and 37.02%, which may relate to a higher starch content in maize than that in wheat.

### 3.3. Morphology, volume and specific volume of cake

The surface appearance and cross section of HAMFCs are presented in Fig. 2 and the microstructure is presented in Fig. 3. No significant difference can be observed in the appearance of HAMFCs except the decline in the height of cake (Fig. 2A). Gas cells of HAMFCs are smaller with the increment of HAMF levels, with the decreasing diameter of gas cell from about 50  $\mu\text{m}$  in Control to below 25  $\mu\text{m}$  in HM40 (Fig. 2B–C). Microstructure is presented in Fig. 3. Fig. 3A shows a loose protein matrix of Control which

covering all the starch granules with a big gas cell. With the increment of HAMF levels, tighter protein network structure, smaller gas cells and more exposed starch granules on the protein network were observed (Fig. 3B–E).

The volume of cake is an indicator of the cake size and reflects the amount of air initially entrapped during mixing, and the air, moisture, and CO<sub>2</sub> entrapped and expanded during baking. The over-high and over-low volume of the cake both does not indicate a desirable cake. The specific volume has direct relationship with the texture of the cake (Kamel and Rasper, 2010). Changes of volume and specific volume of HAMFCs are shown in Table 2. Volume and specific volume significantly decreased from Control to HM10; however, differences among HM10, HM20, HM30 and HM40 were less significant.

The reason that WF is the common raw material for making highly aerated and more defined cakes can be attributed to its sufficient viscosity and gluten content. The former is required for a good cake batter to prevent the incorporated air bubbles from rising to the surface and being lost during initial heating (Paton et al., 1982), while the latter is essential for forming foams during baking since it has the ability to provide cohesiveness and promote the retention of the CO<sub>2</sub> produced. However, HAMF is gluten-free and has low viscosity, weakening the ability of cake to maintain highly aerated and decreasing the volume. The low viscosity of HAMF is related to the inhibition of amylose on swelling of starch granules (Tester and Morrison, 1990). This is the reason for the decline of pore size after adding HAMF and the significant change of volume from Control to HM10. On the other hand, the final cake volume of baked cake did not only depend on the initial air incorporated into the cake batter, but also on its capacity to retain air during baking. Adding HAMF improves the abilities of cake to retain air during baking, because more amylose molecules leach out from starch granules, and form amylose-lipid complexes which help retain air. Therefore, with the increment of HAMF levels, although characters of low viscosity and gluten-free of HAMC batter further strengthened, amylose content accordingly increased and improved the ability to retain air and thus retarded the decrease in cake volume.

### 3.4. XRD analysis of cake

The XRD patterns of HAMFCs are shown in Fig. S1. The pure wheat flour cake (Control) showed an unstructured state with the dramatic loss in crystallinity and the relative increment in the amorphous region. All HAMFCs display peaks at around 7.5°, 13° and 20° (2 $\theta$ ), which are typical peaks of V-type crystalline (Zobel, 2010). The crystalline is the complexes of amylose/long amylopectin chains and lipid, with the structure of double helices and the resistance to enzyme hydrolysis (Birt et al., 2013). The existence of the crystalline is related to the special fine structure of HAMS. The presence of short chains (DP < 10) in amylopectin structure results in a decrease in the stability of the double helix, whereas a higher proportion of longer chains might result in a more perfect crystalline structure (Chung et al., 2011).

**Table 1**  
Chemical composition and digestion properties of control, HM10, HM20, HM30 and HM40.

Treatment	Moisture (%)	Protein (%)	Total starch (%)	Rapidly digestible starch (%)	Slowly digestible starch (%)	Resistant starch (%)
Control	27.63 $\pm$ 1.32a	16.75 $\pm$ 0.12a	39.08 $\pm$ 0.28e	34.90 $\pm$ 0.19a	3.02 $\pm$ 0.13e	0.58 $\pm$ 0.02e
HM10	25.42 $\pm$ 0.34b	16.54 $\pm$ 0.14b	39.24 $\pm$ 0.17d	32.91 $\pm$ 0.12b	4.23 $\pm$ 0.07d	1.05 $\pm$ 0.06d
HM20	23.81 $\pm$ 1.82c	16.14 $\pm$ 0.15c	39.46 $\pm$ 0.19c	31.95 $\pm$ 0.13b	4.95 $\pm$ 0.05c	1.28 $\pm$ 0.09c
HM30	23.43 $\pm$ 0.49c	15.88 $\pm$ 0.12d	39.69 $\pm$ 0.14b	29.75 $\pm$ 0.22c	6.02 $\pm$ 0.011b	1.96 $\pm$ 0.04b
HM40	21.90 $\pm$ 0.37d	15.41 $\pm$ 0.09e	39.88 $\pm$ 0.24a	27.06 $\pm$ 0.08d	7.11 $\pm$ 0.10a	2.86 $\pm$ 0.07a

Each value is expressed as mean  $\pm$  SD (n = 3). Different lowercase (a, b, c, d and e) indicate significant differences (p < 0.05) between different levels.



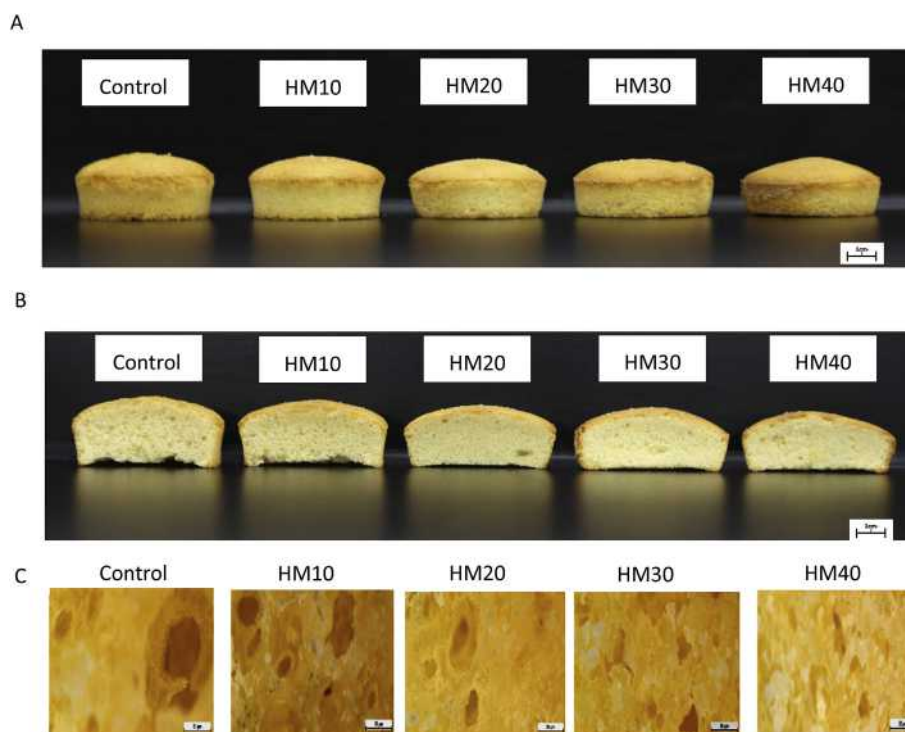


**Fig. 2.** Surface appearance and cross section of Control, HM10, HM20, HM30 and HM40. **Fig. 2A:** the surface appearance, **Fig. 2B:** the cross section from digital camera and **Fig. 2C:** the cross section from stereomicroscope.

### 3.5. Textural properties of cake

Texture analysis is one of the most effective analytical methods of cake as it is applicable to quantify the physical properties (hardness, springiness, cohesiveness, chewiness and resilience) of cake by exerting a controlled force to generate a deformation curve of its response. The increment of hardness and chewiness stands for the lower softness and the worse taste of cake, while the decline of springiness, cohesiveness and resilience implies that cake is more soft and non-stick teeth (Kocer et al., 2007). The results of these parameters are shown in Table 2. Hardness, the force necessary to attain a given deformation, increased from 48.67 N in Control to 53.00 N in HM10, 53.97 N in HM20, 55.63 N in HM30 and 56.33 N in HM40. The high amounts of amylose chains and long amylopectin chains, and the low amounts of short amylopectin chains in HAMS are the main reason for the change of hardness of cakes. Hardness is positively correlated with amounts of amylose chains and long amylopectin chains, while has negative correlations with short amylopectin chains and amylose molecular size. (Zhao et al., 2016). Besides, springiness, defining as the rate of a deformed material goes back to its un-deformed condition after removing the deforming force, decreased from 0.846 to 0.721, 0.719, 0.701 and 0.686 with increasing HAMS levels. The decline of springiness can attributed to the high amounts of long amylopectin chains in HAMS, since there is the significant negative correlation between springiness and the amounts of long amylopectin chains. Cohesiveness represents the internal resistance of cake structure and the ability of cake to stick to itself. After adding HAMS, it increased from 0.579 to 0.599, 0.612, 0.629 and 0.632. Chewiness is the energy required to disintegrate the cake for swallowing and it improved from 21.05 to 22.75, 23.68, 24.06 and 24.24. Resilience is the ratio of recoverable energy for deformation and adding HAMS improved the ratio from 0.225 to 0.235, 0.257, 0.270 and 0.275. Overall, adding HAMS increased the hardness, cohesiveness, chewiness and

resilience, and decreased the springiness.

### 3.6. Sensory evaluation of cake

Sensory evaluation is an evaluation method of cake quality largely based on personal judgment and subjective qualitative evaluation. It cannot be absolute but reflects the customer preferences. The sensory analysis of samples is shown in Fig. 4. After adding HAMS, scores of odor, taste and crumb color of cakes were improved and scores of tenderness and aspect declined. In overall acceptability, HM20 had the highest score of 8.63 while HM10 and HM30 was behind it (8.30 and 7.74, respectively). The overall acceptability of HM40 and Control was lowest with the score of 7.56 and 7.60, respectively. The results indicate that the sensory attributes of HAMSFCs were acceptable by customers, and this may be related to the bright color, special taste, fragrance and less sticky feeling of maize. The similar result can be found in the comparison of sensory analysis of noodles with maize starch and without maize starch (Yousif et al., 2012).

### 3.7. Digestion properties of cake

With the addition of HAMS, RDS in samples decreased from 34.90% to 32.91%, 31.95%, 29.75% and 27.06%, corresponding to the markedly improvement of SDS from 3.02% to 4.23%, 4.95%, 6.02% and 7.11% and RS from 0.58% to 1.05%, 1.28%, 1.96% and 2.86% (Table 1). It can be seen that the changes of RDS, SDS and RS should be related to the special molecule structure of HAMS in cake. It has been reported that RDS is positively correlated with short amylopectin branches of DP 6–12 and negatively correlated with amylose branches, while SDS and RS are positively correlated with amylose content and long chains of amylopectin (You et al., 2015). This is because that long amylopectin chains and amylose chains have limited substrate availability for digestive enzyme, and short

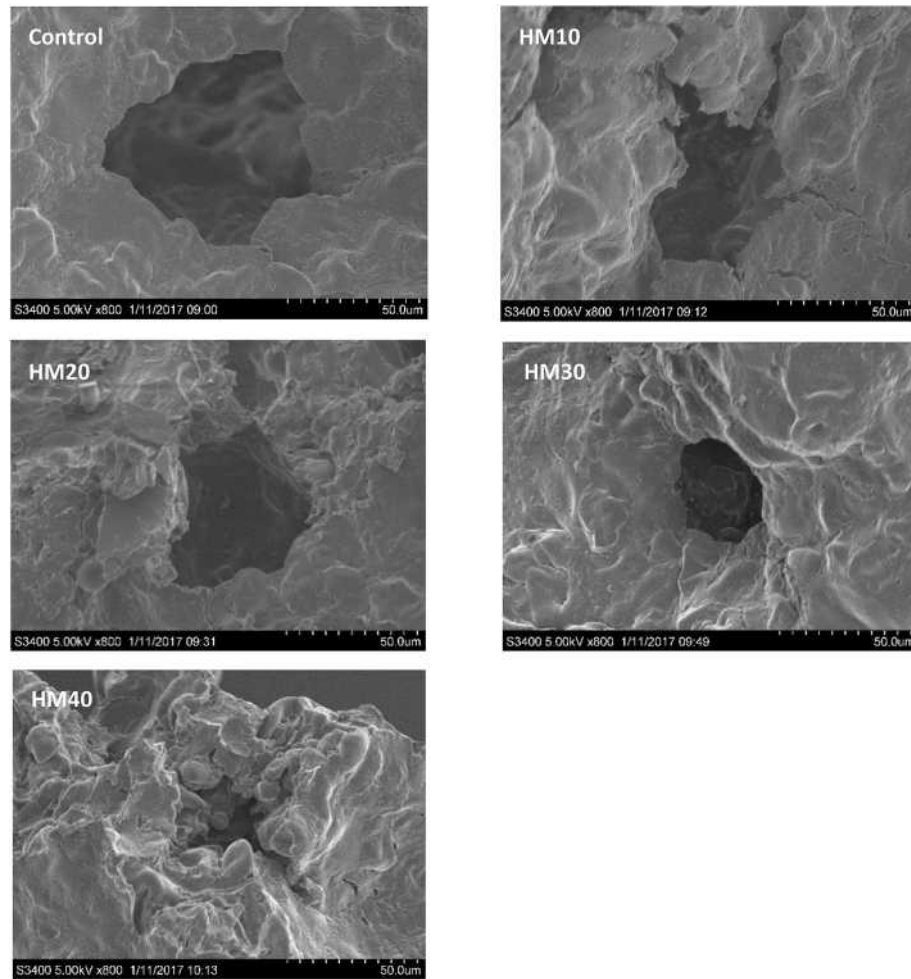


Fig. 3. SEM images (800 X) of Control, HM10, HM20, HM30 and HM40.

Table 2

vol, specific volume and texture properties of control, HM10, HM20, HM30 and HM40.

Treatment	Control	HM10	HM20	HM30	HM40
Volume (cm <sup>3</sup> )	52.21 ± 0.44a	41.62 ± 0.56b	40.79 ± 0.21c	40.21 ± 0.32c	38.05 ± 0.78d
Specific volume (cm <sup>3</sup> /g)	3.21 ± 0.11a	2.55 ± 0.04b	2.50 ± 0.06b	2.47 ± 0.02b	2.40 ± 0.03b
Hardness (N)	48.67 ± 2.08e	53.00 ± 3.57d	53.93 ± 2.51c	55.67 ± 3.09b	56.33 ± 4.72a
Springiness	0.8463 ± 0.0420a	0.7218 ± 0.0250b	0.7178 ± 0.0549b	0.7010 ± 0.0430c	0.6857 ± 0.0679d
Cohesiveness	0.5794 ± 0.0139e	0.5987 ± 0.0632d	0.6123 ± 0.0480c	0.6292 ± 0.0366b	0.6324 ± 0.0547a
Chewiness	21.05 ± 2.27e	22.75 ± 1.41d	23.68 ± 5.84c	24.06 ± 5.98b	24.24 ± 5.14a
Resilience	0.2254 ± 0.3353e	0.2346 ± 0.2346d	0.2566 ± 0.2566c	0.2697 ± 0.2797b	0.2753 ± 0.2703a

Each value is expressed as mean ± SD (n = 3). Different lowercase (a, b, c, d and e) indicate significant differences (p < 0.05) between different levels.

amylopectin chains have high substrate availability for digestive enzyme. The digestion rate of starch is positively correlated with amylose chains but negatively correlated with the ratios of long amylopectin and long amylose chains to short amylopectin chains (Syahariza et al., 2013). Here, compared with the high amounts of short amylopectin chains, low amounts of long amylopectin chains and amylose chains and a large amylose size in NMS, the feature molecule structure of HAMS also gives higher SDS and RS content, and lower RDS content of HAMFCs. In addition, the gelatinization temperature of maize starch increases with the improvement of amylose content (Chen et al., 2011). During baking of HAMFCs, the starch crystalline structure is disrupted and become susceptible to amylolytic degradation, however, HAMFCs have more amylose molecules with high compactness, which limit the degree of starch

swelling and the succeeding accessibility of starch to hydrolyzing enzymes during gelatinization. In the following cooling process, the formation of V-type crystalline structure in HAMFCs is another important reason for the increment of RS (Birt et al., 2013). As mentioned above, after adding HAME, the size of gas cell decreased (see Fig. 3), which may further retards the access of hydrolyzing enzymes. Unfortunately, the RS content of cake is still below 3%, although the RS content already has increased markedly after adding HAME. This is maybe related to the low total flour (<50%) and HAME content (<20%) in the recipe of cake-making in this study. Another reason for the undesirable RS content of HAMFCs is attributed to the decrement of gluten in these cakes. It has been reported that gluten network formed and entrapped starch granules after cooking, which acted as a barrier to inhibit the



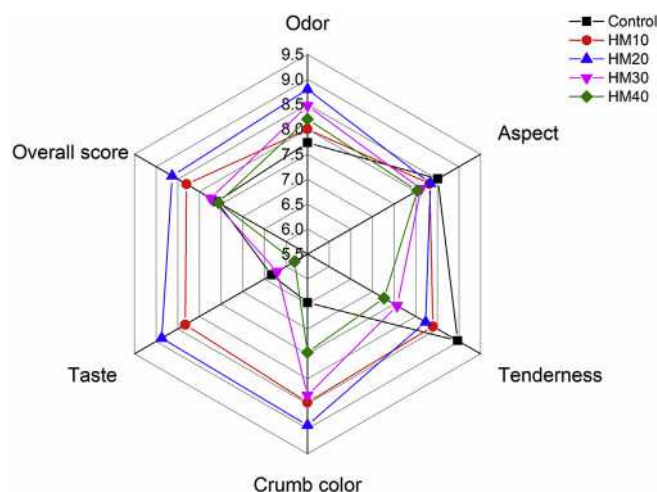


Fig. 4. Sensory analysis of Control, HM10, HM20, HM30 and HM40.

accessibility of enzymes and slowing enzyme digestion rate (Zou et al., 2015). In the future, adding more gluten to recover the ability of gluten network or other non-starch polysaccharides to improve RS content in HAMFCs will be studied.

#### 4. Conclusion

In this paper, the molecular structure of HAMS was studied and a novel formulation of functional cake production with HAMF was developed. HAMS displayed low short amylopectin chains, small molecular size, and high long amylopectin chains and amylose chains. The molecular structure is highly related to the physical properties of HAMS and the quality of HAMFCs, since the relations between the molecular structure and some properties such as physicochemical, texture, digestion and crystal properties of starch have been found by previous studies (You et al., 2015; Zhao et al., 2016; Lee et al., 2017; Xu et al., 2017). The molecular structure of HAMS and the reduction of gluten can be used to explain the morphology, volume, texture, digestion and crystal properties of HAMFCs. Overall, the molecular structure of HAMS has a significant influence on the quality of cake, and HAMFCs could be incorporated into cake and provide cake with acceptable sensory attributes, high resistant starch and without obvious negative effects on other physicochemical properties of cake.

#### Conflicts of interest

The authors declare that there is no conflict of interests regarding the publication of this paper.

#### Acknowledgements

This work was supported by the Young Elite Scientists Sponsorship Program by CAST (YESS Program), Shaanxi Province Comprehensive Project (grant number: 2015KTZDNY01-01-01), Yangling District technical Plan Project (grant number: 2014NY-01) and Zhongyin Tang Breeding Special Funding.

#### Appendix A. Supplementary data

Supplementary data related to this article can be found at <https://doi.org/10.1016/j.jcs.2018.02.009>.

#### References

- AACC, 2000. International Approved Methods of the American Association of Cereal Chemists, tenth ed. AACC, St. Paul, MN, USA. (2000).
- Birt, D.F., Boylston, T., Hendrich, S., Jane, J.L., Hollis, J., Li, L., McClelland, J., Moore, S., Phillips, G.J., Rowling, M., 2013. Resistant starch: promise for improving human health. *Adv. Nutr.* 4 (6), 587.
- Chen, P., Yu, L., Simon, G.P., Liu, X., Dean, K., Chen, L., 2011. Internal structures and phase-transitions of starch granules during gelatinization. *Carbohydr. Polym.* 83 (4), 1975–1983.
- Chen, X., He, X., Fu, X., Huang, Q., 2015. In vitro digestion and physicochemical properties of wheat starch/flour modified by heat-moisture treatment. *J. Cereal. Sci.* 63, 109–115.
- Chung, H.J., Liu, Q., Lee, L., Wei, D., 2011. Relationship between the structure, physicochemical properties and in vitro digestibility of rice starches with different amylose contents. *Food Hydrocolloids* 25 (5), 968–975.
- Giuberti, G., Gallo, A., Fortunati, P., Rossi, F., 2016. Influence of high-amylose maize starch addition on in vitro starch digestibility and sensory characteristics of cookies. *Starch - Stärke* 68 (5–6), 469–475.
- Hung, P.V., Yamamori, M., Morita, N., 2005. Formation of enzyme-resistant starch in bread as affected by high-amylose wheat flour substitutions. *Cereal Chem.* 82 (6), 690–694.
- Jane, J., Chen, Y.Y., Lee, L.F., McPherson, A.E., Wong, K.S., Radosavljevic, M., Kasemsuwan, T., 1999. Effects of amylopectin branch chain length and amylose content on the gelatinization and pasting properties of starch. *Cereal Chem.* 76 (5), 629–637.
- Kamel, B.S., Rasper, V.F., 2010. Effects of emulsifiers, sorbitol, polydextrose, and crystalline cellulose on the texture of reduced-calorie cakes. *J. Texture Stud.* 19 (3), 307–320.
- Kocer, D., Hicasmaz, Z., Bayindirli, A., Katnas, S., 2007. Bubble and pore formation of the high-ratio cake formulation with polydextrose as a sugar- and fat-replacer. *J. Food Eng.* 78 (3), 953–964.
- Lee, S., Lee, J.H., Chung, H.J., 2017. Impact of diverse cultivars on molecular and crystalline structures of rice starch for food processing. *Carbohydr. Polym.* 169, 33.
- Lin, L., Guo, D., Huang, J., Zhang, X., Zhang, L., Wei, C., 2016. Molecular structure and enzymatic hydrolysis properties of starches from high-amylose maize inbred lines and their hybrids. *Food Hydrocolloids* 58, 246–254.
- Mutlu, S., Kahraman, K., Öztürk, S., 2017. Optimization of resistant starch formation from high amylose corn starch by microwave irradiation treatments and characterization of starch preparations. *Int. J. Biol. Macromol.* 95, 635–642.
- Nutrition and Allergies, 2012. Scientific Opinion on the substantiation of a health claim related to *Rhodiola rosea* L. extract and reduction of mental fatigue pursuant to Article 13(5) of Regulation (EC) No 1924/2006. *Efsa J.* 10 (7) n/a-n/a).
- Paton, D., Larocque, G.M., Holme, J., 1982. Development of cake structure: influence of ingredients on the measurement of cohesive force during baking. *Cereal Chem.* 58 (6), 527–529.
- Pons, M., Fiszman, S.M., 2010. Instrumental texture profile analysis with particular reference to gelled systems. *J. Texture Stud.* 27 (6), 597–624.
- Shukla, R., Cheryan, M., 2001. Zein: the industrial protein from corn. *Ind. Crop. Prod.* 13 (3), 171–192.
- Sirisoontaralak, P., Suthirak, P., Papaka, K., Vongsawasdi, P., 2017. Development of shelf stable chiffon cake using gamma irradiation. *LWT - Food Sci. Technol. (Lebensmittel-Wissenschaft -Technol.)* 75, 78–84.
- Syahriza, Z.A., Sar, S., Hasjim, J., Tizzotti, M.J., Gilbert, R.G., 2013. The importance of amylose and amylopectin fine structures for starch digestibility in cooked rice grains. *Food Chem.* 136 (2), 742.
- Tester, R.F., Morrison, W.R., 1990. Swelling and gelatinization of cereal starches. I. Effects of amylopectin, amylose, and lipids. *Cereal Chem.* 67, 551–557.
- Wang, K., Hasjim, J., Wu, A.C., Henry, R.J., Gilbert, R.G., 2014. Variation in amylose fine structure of starches from different botanical sources. *J. Agric. Food Chem.* 62 (19), 4443–4453.
- Xu, J., Kuang, Q., Wang, K., Zhou, S., Wang, S., Liu, X., Wang, S., 2017. Insights into molecular structure and digestion rate of oat starch. *Food Chem.* 220, 25–30.
- You, S.Y., Oh, S.K., Kim, H.S., Chung, H.J., 2015. Influence of molecular structure on physicochemical properties and digestibility of normal rice starches. *Int. J. Biol. Macromol.* 77 (3), 375.
- Yousif, E.I., Gadallah, M.G.E., Sorour, A.M., 2012. Physico-chemical and rheological properties of modified corn starches and its effect on noodle quality. *Ann. Agric. Sci. (Cairo)* 57 (1), 19–27.
- Zhang, B., Chen, L., Zhao, Y., Li, X., 2013. Structure and enzymatic resistivity of debranched high temperature-pressure treated high-amylose corn starch. *J. Cereal. Sci.* 57 (3), 348–355.
- Zhang, X., Chen, Y., Zhang, R., Zhong, Y., Luo, Y., Xu, S., Liu, J., Xue, J., Guo, D., 2016. Effects of extrusion treatment on physicochemical properties and in vitro digestion of pregelatinized high amylose maize flour. *J. Cereal. Sci.* 68, 108–115.
- Zhao, L., Liu, X., Hu, Z., Li, L., Li, B., 2016. Molecular structure evaluation of wheat gluten during frozen storage. *Food Biophys.* 1–9.
- Zobel, H.F., 2010. Starch crystal transformations and their industrial importance. *Starch - Stärke* 40 (1), 1–7.
- Zou, W., Sissons, M., Gidley, M.J., Gilbert, R.G., Warren, F.J., 2015. Combined techniques for characterising pasta structure reveals how the gluten network slows enzymic digestion rate. *Food Chem.* 188, 559–568.

# Bivariate Flow Cytometric Analysis and Sorting of Different Types of Maize Starch Grains

Xudong Zhang,<sup>1,2†</sup> Jiaojiao Feng,<sup>1†</sup> Heng Wang,<sup>1†</sup> Jianchu Zhu,<sup>1</sup> Yuyue Zhong,<sup>1</sup> Linsan Liu,<sup>1</sup> Shutu Xu,<sup>1</sup> Renhe Zhang,<sup>1</sup> Xinghua Zhang,<sup>1</sup> Jiquan Xue,<sup>1</sup> Dongwei Guo<sup>1\*</sup>

<sup>1</sup>Key Laboratory of Biology and Genetic Improvement of Maize in Arid Area of Northwest Region, Ministry of Agriculture, College of Agronomy, Northwest A&F University, Yangling, Shaanxi, China

<sup>2</sup>Institute of Crop Science, Quality of Plant Products, University Hohenheim, Stuttgart, Germany

Received 12 June 2017; Revised 17 July 2017; Accepted 8 September 2017

Grant sponsor: Scie-tech Project of Yangling City, Grant number: 2014NY-01

Grant sponsor: Tang Foundation, Grant number: A212021205

Grant sponsor: Shaanxi Science & Technology Co-ordination & Innovation Project, Grant number: 2015KTZDNY01-01-01

Additional Supporting Information may be found in the online version of this article.

\*Correspondence to: Dongwei Guo, Key Laboratory of Biology and Genetic Improvement of Maize in Arid Area of Northwest Region, Ministry of Agriculture, College of Agronomy, Northwest A & F University, Yangling, 712100, Shaanxi, China. E-mail: gdwei@nwsuaf.edu.cn

†Equal contribution to the work.

Published online 4 October 2017 in Wiley Online Library (wileyonlinelibrary.com)

DOI: 10.1002/cyto.a.23261

© 2017 International Society for Advancement of Cytometry

## • Abstract

Particle-size distribution, granular structure, and composition significantly affect the physicochemical properties, rheological properties, and nutritional function of starch. Flow cytometry and flow sorting are widely considered convenient and efficient ways of classifying and separating natural biological particles or other substances into subpopulations, respectively, based on the differential response of each component to stimulation by a light beam; the results allow for the correlation analysis of parameters. In this study, different types of starches isolated from waxy maize, sweet maize, high-amylose maize, pop maize, and normal maize were initially classified into various subgroups by flow cytometer and then collected through flow sorting to observe their morphology and particle-size distribution. The results showed that a 0.25% Gelzan solution served as an optimal reagent for keeping individual starch particles homogeneously dispersed in suspension for a relatively long time. The bivariate flow cytometric population distributions indicated that the starches of normal maize, sweet maize, and pop maize were divided into two subgroups, whereas high-amylose maize starch had only one subgroup. Waxy maize starch, conversely, showed three subpopulations. The subgroups sorted by flow cytometer were determined and verified in terms of morphology and granule size by scanning electron microscopy and laser particle distribution analyzer. Results showed that flow cytometry can be regarded as a novel method for classifying and sorting starch granules. © 2017 International Society for Advancement of Cytometry

## • Key terms

maize starch; flow cytometry; granule sorting; starch morphology; particle-size distribution

**GRANULE** size and distribution strongly influence the composition, physicochemical properties, swelling power, solubility and enzymatic digestibility of starch. Other factors such as the amylose and amylopectin concentration, molecular weight and fine structure of individual starch granules are also likely to have an effect (1). Different plant sources exhibit variations in starch granule size (1–100  $\mu\text{m}$ ), complexity, shape, and distribution pattern (2). Specifically, wheat, as a typical bimodal crop in which starch grains that generate optical properties with bimodal distributions, features starch granules with lenticular (A-type) and spherical (B-type) shapes, with a large fraction of granules ranging from 15 to 35  $\mu\text{m}$  in size and a small fraction measuring approximately 2–10  $\mu\text{m}$  (2,3), respectively. Unimodal distribution patterns are observed for maize and potato starches, with a wide variety of particle sizes ranging from approximately 2–30  $\mu\text{m}$  and from 5 to 100  $\mu\text{m}$ , respectively, some of which can be classified into large, medium and small size subpopulations (2,4). Other plant species have also been explored, including barley (lenticular and spherical, bimodal, 2–30  $\mu\text{m}$ ), pea (reniform, unimodal, 5–10  $\mu\text{m}$ ), rice (polyhedral, unimodal, single



3–8  $\mu\text{m}$ , compound 150  $\mu\text{m}$ ), and sorghum (spherical, unimodal, 5–20  $\mu\text{m}$ ) (2).

Studying the structural traits and functional properties of different-sized granules can provide insight into the role that particle size plays in the application of starches (4). Bimodal crop starches such as wheat and barley are usually composed of two types of starch fractions: large (A-type) and small (B-type) (5). In practice, starches with a higher proportion of B-type granules are commonly employed as fat replacements, article coatings, or transporter materials in cosmetics, whereas starches predominantly composed of A-type granules are suited for use in manufacturing biodegradable plastic bags or films, producing copy article with a low carbon concentration and fermenting beer (1). By contrast, with respect to unimodal plant starches found in potato and maize, the pasting viscosity and amylose concentration increase whereas the extent of hydrolysis and the gelatinization temperature decrease with increasing granule size. The amount of amylose strongly affects the physicochemical traits and functionality of starch. Amylose is considered the source of resistant starch (RS), which is resistant to digestion and provides numerous health benefits (6). Moreover, the relationship between the molecular structure of amylopectin and functionality has been analyzed in different-sized subpopulations of high-amylose and normal maize starch (7).

Determining how to separate starch granules into different fractions with a narrow size range and collect starch components to explore the structural and quality properties of starch subpopulations has been studied extensively in recent decades. Although many methods have been developed, a great proportion of them are dependent on density or gravity gradients to distinguish between various starch granules, such as those based on sieving, sedimentation, centrifugation, and electrical resistance (1,8). However, current methods suffer from certain shortcomings. Common obstacles include the limitations associated with detecting small starch granules, the inability to obtain homogeneous granule groups and the lack of accuracy in separating granules into well-defined fractions (1,8).

To overcome these difficulties, an innovative approach to classifying starch granules has been proposed using a flow cytometer, which is a multidimensional particle counter. A flow cytometer can be used to characterize specific particle properties through light scattering and fluorescence principles. Thus, flow cytometry (FC) has become a powerful method for characterizing micron-sized objects. Although FC is mainly known for its utility in cell analysis, it can be extended to other micron-sized objects such as starch granules once the appropriate calibration is performed (9). In fact, any suspended granule or cell measuring 0.2–150  $\mu\text{m}$  is suitable for analysis, but cells from solid substances must be disaggregated before measurement (10). Light scattering occurs when a particle deflects incident laser light. The scatter measurements can reveal granular features in the suspensions in relation with particle size, particle shape, particle orientation, refractive index, surface topography, and its structure. Therefore, they can empirically distinguish populations in terms of

general characteristics such as multimodal scatter distributions, which may or may not directly relate to the physical properties of the particles (11). However, few studies have explored the use of FC to analyze starch granules. Specifically, Cl  dat et al. (2004) showed that FC-sedimentation field–flow fractionation (SdFFF) could be used as an alternative to Coulter counting to obtain a number versus size histogram of rice starch particles after calibrating the forward angle signal (FS) with respect to size (9). FC was introduced as a rapid method for evaluating chloroplastic starch granules. The method could generate information pertaining to the mean number of starch granules in chloroplasts within a few minutes (12).

In our work, we firstly attempted to separate native starch suspensions rather than pretreated starch under FC-SdFFF and ultimately collected starch fractions by flow sorting. Five different types of maize starch were used in our experiment. The aim was to select an optimal starch suspension reagent to meet the requirements of flow sorting and explore the morphology and granule distribution of starch subpopulations obtained by flow sorting through scanning electron microscopy (SEM) and laser particle distribution analyser (LPDA). The starch fractions acquired are expected to be useful in studying the physicochemical properties, rheological properties, and functional characteristics of starches.

## MATERIALS AND METHODS

### Plant Material

Normal maize (Shaandan 609), waxy maize (Huangnuo 1), sweet maize (Chaotian 2000), high-amylose maize H1 (BS14201\*AS1415-6, AC = 58.60%) and pop maize (Baolie 1) were provided by the Key Laboratory of Biology and Genetic Improvement of Maize in Arid Area of Northwest Region, Ministry of Agriculture, Northwest A&F University. These hybrids were planted at the Xibo Maize Research Station of NAFU, Yangling, Shaanxi, China from May 2, 2015 to October 5, 2015. The biological materials were gathered from the testing field in triplicate for each sample.

### Chemicals

Starch suspension reagents: Polyethylene glycol 6000 and mannitol were obtained from Kemiou (Tianjin, China) and Biotopped (Beijing, China), respectively. Ficoll 400 and Gelzan were obtained from Sigma-Aldrich (St. Louis, MO).

FACSAria reagents: Reagents included a PBS solution (sheath fluid), autoclaved distilled water gathered through a 0.22  $\mu\text{m}$  filter membrane, 75% ethanol, FACSClean solution, FACSDiva CST Research Beads and Accudrop beads (Becton Dickinson; [BD Biosciences], San Jose, CA, USA). The PBS solution was made by dissolving 8.0 g NaCl, 0.2 g KCl, 1.44 g  $\text{Na}_2\text{HPO}_4$ , and 0.24 g  $\text{KH}_2\text{PO}_4$  in 800 ml distilled water, adjusting the pH to 7.2–7.4 and then adding distilled water to a constant volume of 1 l. The solution was stored at room temperature after being filtered through a 0.22  $\mu\text{m}$  filter membrane.

Starch granules staining reagents: 15% acetic acid: 30  $\mu\text{l}$  acetic acid was dissolved in 1.7 ml double-distilled

water (ddH<sub>2</sub>O). 1-Aminopyrene-3,6,8-trisulfonic acid (APTS) (Sigma-Aldrich, St. Louis, MO): APTS powder was mixed with 100  $\mu$ l 15% acetic acid to make a 200 mM mother solution; 5  $\mu$ l of the mother solution was dissolved in 45  $\mu$ l 15% acetic acid each time for starch dissolution. 1 M NaBH<sub>3</sub>CN: 0.1256 g NaBH<sub>3</sub>CN powder was dissolved in 2 ml ddH<sub>2</sub>O. Agar-glycerol mixture: 2 mg agar was mixed with 85  $\mu$ l glycerol and 15  $\mu$ l ddH<sub>2</sub>O in a boiled water bath for 5 min and then cooled and stored at room temperature.

### Starch Isolation

Starch isolation was carried out using a previously published method (13) with a small modification. Ten maize seeds in the middle of the ear were saturated in 40 ml of a 0.25% H<sub>2</sub>SO<sub>4</sub> solution for 16 h and then peeled. The embryo was then removed before being ground into a starch mixture paste and was subsequently filtered through a 200  $\mu$ m mesh sieve three times. The acquired starch paste was brought to a volume of 45 ml with ddH<sub>2</sub>O and then centrifuged at 1,000 r/min for 8 min. After decanting the supernatant, the sediment was dissolved in 40 ml 0.2% NaOH and kept in solution for 4 h. The sediment was regained by removing the supernatant and then mixed with ddH<sub>2</sub>O. The mixture was centrifuged at 1,000 r/min for 4 min three times to rinse the sediment. The sediment was then mixed with 15 ml acetone and centrifuged at 4,000 r/min for 17 min. The final starch pellets acquired were dried in a fume hood.

### Starch Staining

Starch granules were stained according to a modified method (14). First, 2 mg starch was homogeneously mixed with 3  $\mu$ l of 20 mM APTS solution and 3  $\mu$ l of 1 M NaBH<sub>3</sub>CN and then stained without exposure to light for 15 h at 30°C. After staining, starch particles were rinsed with ddH<sub>2</sub>O five times and subsequently suspended in 50% glycerol. Then, 1  $\mu$ l of a starch-glycerol suspension was homogenized with 4  $\mu$ l of an agar-glycerol mixture for analysis and sorting by flow cytometer (BD FACSAria III). An inverted fluorescence microscope (TE2000-U, Nikon, Japan) was utilized to examine the starch staining efficiency at an excitation wavelength of 488 nm (blue light) and an emission wavelength of 500–535 nm (green light).

### Selection of Starch Suspension Reagent

To improve the efficiency of flow sorting, the suspension stabilities of six suspension reagents were evaluated and compared. The specific suspension concentrations (Table 1) were set with the aim of screening. Each reagent was mixed at 45°C at 2,000 r/min by a magnetic stirrer and diluted to 100 ml using ddH<sub>2</sub>O. An aliquot (10 ml) of each reagent was prepared to resuspend 50 mg starch in tubes. The suspended sample (10  $\mu$ l) was gathered from the middle of the tubes in 15 min intervals. A TE2000-S microscope (Nikon, Japan) with 200 $\times$  magnification was used to observe the number of starch particles in each starch suspension; three replicates were obtained for each sample.

### Sample Preparation and Flow Cytometry Sorting

Following the APTS staining treatment, the starch samples were washed five times with ddH<sub>2</sub>O and suspended in 0.25% Gelzan solution. The suspension was filtered through a 45  $\mu$ m sieve for flow sorting analysis. An Aria SORP sorter (BD Bioscience) equipped with a 1.0 optical filter was used. The device is a six-laser system (355, 405, 457, 488, 561, and 640 nm) with a maximum of 17 simultaneous fluorescence detectors. BD FACSDiva<sup>TM</sup> software (BD Bioscience) was utilized to provide new features to analyze the sorting characteristics of starch particles. FSC and SSC signals were excited by a laser with a power of 20 mw and wavelength of 488 nm and then transmitted through FSC/SSC-specific channels. The APTS signal was activated by the same laser and detected in the APTS channel. Bivariate flow histograms of different types of maize starch were acquired by adjusting the FSC value, SSC value and voltage of the APTS channel. Therefore, two different levels of voltages were set to prove that the polydispersity detected in flow analysis was a real property of the subpopulations rather than an optical artifact. The voltages were FSC (79–143), SSC (201–223), and APTS channel (257–425) for the first group and FSC (129–255), SSC (192–237), and APTS channel (267–417) for the second group. The flow analysis performed to classify the starch into subgroups was conducted with six replicates for each sample.

The bivariate flow histograms were graphed as log-log plots, and the different subgroups of each starch sample were gated at the zones of highest dot concentration according to the contour lines. The gated fractions were subsequently sorted and collected by a 85  $\mu$ m nozzle under a pressure of 20 psi in the sheath fluid bucket. Other parameters were established as follows: Drop Delay: 27.03, Ampl: approximately 10, Freq: 30–40, 2nd Drop: approximately 11, 3rd Drop: approximately 6, and 4th Drop: 1. As each starch sample was detected, the above mentioned parameters were slightly adjusted to reach the optimal sorting efficiency.

The stained starch suspension (20 ml) was evenly mixed with 3–4 ml 0.25% Gelzan solution and filtered through a 75  $\mu$ m mesh sieve. The filtered starch granule suspension was completely dispersed by ultrasonic vibration for 10 s. Flow sorting (BD FACSAriaIII) was employed to sort starch granules. The various subgroups of the starch suspension were transferred into 2 ml centrifuge tubes and then centrifuged at 13,000 r/min for 5 min. The sediment was dried at 40°C in an oven for 12 h. Data were collected in four replicates.

### Starch Morphology

Following a previously published method (6), the morphology of sorted starch granules was observed at 1,000 $\times$  magnification under a 3400 N scanning electron microscope (Hitachi SN3400, Tokyo, Japan) with digital image acquisition software (Quartz PCI, Vancouver, Canada).

### Granule Size Analysis

The granule size of the starch samples was measured by a laser particle size analyzer (Microtrac 3500) according to a previously reported method (15). The analyzer can measure particles measuring 0.02–2,800  $\mu$ m, which greatly exceeds the



**Table 1.** Number of suspended starch particles in each suspension reagent\*

PEG	20%	30%	40%	50%	60%	
0 min	35.33 ± 2.52 <sup>a</sup>	43.67 ± 3.21 <sup>a</sup>	43.33 ± 4.93 <sup>a</sup>	35.67 ± 7.23 <sup>a</sup>	34.67 ± 0.58 <sup>a</sup>	
15 min	33.67 ± 3.21 <sup>ab</sup>	27.33 ± 4.93 <sup>b</sup>	42.67 ± 7.51 <sup>a</sup>	35.00 ± 11.79 <sup>a</sup>	29.33 ± 5.13 <sup>ab</sup>	
30 min	25.33 ± 5.03 <sup>c</sup>	30.67 ± 10.79 <sup>b</sup>	28.67 ± 2.89 <sup>b</sup>	40.67 ± 15.95 <sup>a</sup>	28.33 ± 5.69 <sup>ab</sup>	
45 min	29.00 ± 1.00 <sup>bc</sup>	23.67 ± 1.53 <sup>b</sup>	24.00 ± 6.24 <sup>b</sup>	31.33 ± 8.50 <sup>a</sup>	25.00 ± 2.00 <sup>b</sup>	
60 min	25.00 ± 2.65 <sup>c</sup>	33.67 ± 8.50 <sup>ab</sup>	33.00 ± 1.00 <sup>b</sup>	24.67 ± 4.04 <sup>a</sup>	27.33 ± 2.31 <sup>b</sup>	
Sucrose	10%	20%	30%	40%	50%	60%
0 min	35.33 ± 5.51 <sup>a</sup>	36.33 ± 8.51 <sup>a</sup>	29.00 ± 11.34 <sup>b</sup>	25.67 ± 3.06 <sup>bc</sup>	32.00 ± 7.94 <sup>a</sup>	30.00 ± 4.58 <sup>bc</sup>
15 min	32.00 ± 6.56 <sup>a</sup>	39.67 ± 4.51 <sup>a</sup>	43.67 ± 4.73 <sup>a</sup>	25.00 ± 5.57 <sup>bc</sup>	29.33 ± 13.28 <sup>a</sup>	56.00 ± 3.61 <sup>a</sup>
30 min	9.00 ± 2.00 <sup>bc</sup>	20.67 ± 3.51 <sup>b</sup>	20.33 ± 1.53 <sup>bc</sup>	62.33 ± 13.58 <sup>a</sup>	27.67 ± 3.06 <sup>a</sup>	37.00 ± 5.20 <sup>bc</sup>
45 min	15.67 ± 3.22 <sup>b</sup>	11.67 ± 1.16 <sup>b</sup>	11.00 ± 5.57 <sup>c</sup>	13.33 ± 2.89 <sup>c</sup>	28.00 ± 6.25 <sup>a</sup>	28.33 ± 5.03 <sup>c</sup>
60 min	5.67 ± 2.52 <sup>c</sup>	13.00 ± 5.57 <sup>b</sup>	19.67 ± 3.22 <sup>bc</sup>	28.67 ± 4.73 <sup>b</sup>	18.33 ± 0.58 <sup>a</sup>	38.33 ± 4.72 <sup>b</sup>
Ficoll 400	2.5%	5%	10%	20%	30%	40%
0 min	35.00 ± 4.36 <sup>a</sup>	35.00 ± 5.29 <sup>a</sup>	33.67 ± 4.93 <sup>a</sup>	35.67 ± 7.37 <sup>a</sup>	23.33 ± 3.21 <sup>b</sup>	49.00 ± 4.36 <sup>b</sup>
15 min	36.67 ± 2.08 <sup>a</sup>	35.67 ± 4.51 <sup>a</sup>	37.67 ± 4.04 <sup>a</sup>	33.33 ± 5.03 <sup>a</sup>	31.33 ± 5.03 <sup>a</sup>	39.00 ± 2.00 <sup>c</sup>
30 min	14.67 ± 1.15 <sup>b</sup>	14.00 ± 3.61 <sup>b</sup>	35.67 ± 5.03 <sup>a</sup>	37.33 ± 3.79 <sup>a</sup>	14.33 ± 2.08 <sup>c</sup>	20.67 ± 1.53 <sup>c</sup>
45 min	4.33 ± 2.31 <sup>c</sup>	8.00 ± 3.61 <sup>bc</sup>	24.33 ± 1.15 <sup>b</sup>	15.67 ± 0.58 <sup>b</sup>	29.33 ± 1.53 <sup>ab</sup>	30.33 ± 0.58 <sup>d</sup>
60 min	2.33 ± 1.15 <sup>c</sup>	5.67 ± 1.53 <sup>c</sup>	19.67 ± 6.11 <sup>b</sup>	30.67 ± 2.52 <sup>a</sup>	25.00 ± 2.65 <sup>ab</sup>	64.67 ± 7.02 <sup>a</sup>
Mannitol	5%	10%	15%	20%		
0 min	53.67 ± 8.08 <sup>a</sup>	50.33 ± 2.31 <sup>a</sup>	33.67 ± 4.93 <sup>a</sup>	37.00 ± 8.19 <sup>a</sup>		
15 min	22.00 ± 7.55 <sup>b</sup>	20.67 ± 4.51 <sup>b</sup>	15.33 ± 2.52 <sup>b</sup>	40.67 ± 13.87 <sup>a</sup>		
30 min	7.67 ± 2.08 <sup>c</sup>	6.33 ± 2.08 <sup>c</sup>	13.00 ± 2.00 <sup>b</sup>	11.33 ± 3.79 <sup>b</sup>		
45 min	11.67 ± 3.21 <sup>bc</sup>	9.33 ± 1.15 <sup>c</sup>	12.00 ± 3.00 <sup>bc</sup>	22.33 ± 3.79 <sup>b</sup>		
60 min	7.33 ± 6.66 <sup>c</sup>	8.00 ± 6.00 <sup>c</sup>	6.33 ± 2.52 <sup>c</sup>	10.00 ± 1.00 <sup>b</sup>		
Gelzan	0.05%	0.10%	0.15%	0.20%	0.25%	0.30%
0 min	32.33 ± 8.33 <sup>a</sup>	26.00 ± 5.57 <sup>b</sup>	33.67 ± 4.04 <sup>a</sup>	21.67 ± 4.51 <sup>ab</sup>	29.33 ± 8.74 <sup>a</sup>	29.67 ± 5.69 <sup>ab</sup>
15 min	30.67 ± 4.04 <sup>a</sup>	37.00 ± 2.00 <sup>a</sup>	24.33 ± 2.52 <sup>b</sup>	30.67 ± 7.23 <sup>a</sup>	23.67 ± 3.06 <sup>a</sup>	17.00 ± 1.00 <sup>c</sup>
30 min	10.33 ± 3.21 <sup>b</sup>	17.33 ± 1.15 <sup>c</sup>	24.33 ± 6.66 <sup>b</sup>	28.67 ± 7.51 <sup>ab</sup>	29.67 ± 4.04 <sup>a</sup>	36.67 ± 0.58 <sup>a</sup>
45 min	15.67 ± 4.93 <sup>b</sup>	16.67 ± 5.03 <sup>cd</sup>	19.33 ± 0.58 <sup>bc</sup>	17.67 ± 5.03 <sup>b</sup>	32.00 ± 8.72 <sup>a</sup>	17.67 ± 3.51 <sup>c</sup>
60 min	9.00 ± 1.00 <sup>b</sup>	9.67 ± 4.04 <sup>d</sup>	13.67 ± 3.21 <sup>c</sup>	24.00 ± 7.21 <sup>ab</sup>	23.00 ± 2.00 <sup>a</sup>	23.00 ± 6.08 <sup>bc</sup>
Glycerol	20%	30%	40%	50%	60%	
0 min	26.67 ± 6.66 <sup>b</sup>	33.67 ± 6.03 <sup>a</sup>	44.67 ± 4.04 <sup>a</sup>	36.33 ± 3.51 <sup>a</sup>	24.67 ± 3.06 <sup>c</sup>	
15 min	34.33 ± 3.51 <sup>a</sup>	37.00 ± 6.93 <sup>a</sup>	36.00 ± 4.36 <sup>b</sup>	26.33 ± 5.69 <sup>ab</sup>	37.67 ± 7.37 <sup>ab</sup>	
30 min	15.00 ± 2.65 <sup>c</sup>	11.33 ± 2.52 <sup>b</sup>	17.33 ± 2.52 <sup>cd</sup>	24.33 ± 8.14 <sup>b</sup>	29.00 ± 3.61 <sup>bc</sup>	
45 min	9.33 ± 2.52 <sup>c</sup>	5.67 ± 0.58 <sup>bc</sup>	20.00 ± 1.73 <sup>c</sup>	31.33 ± 5.13 <sup>ab</sup>	41.33 ± 7.09 <sup>a</sup>	
60 min	13.33 ± 3.06 <sup>c</sup>	0.00 ± 0.00 <sup>c</sup>	12.33 ± 1.53 <sup>d</sup>	27.00 ± 4.58 <sup>ab</sup>	19.67 ± 2.31 <sup>c</sup>	

\*The superscript letters refer to significant difference in the number of suspended starch particles among each type of suspending reagent at different time points.

typical scope of maize starch particles, that is, approximately 2–50  $\mu\text{m}$ . The PartanDP-GC software (Anatec) was utilized to analyze the size data in three replicates.

## RESULTS

### Evaluation of Different Starch Suspension Reagents

To investigate the suspension stability of various reagents, the number of suspended starch particles among six suspension reagents was measured using a microscope at each time point. As shown in Table 1, there were no significant differences between 50% polyethylene glycol, 50% sucrose, and 0.25% Gelzan over time, which demonstrates their high suspension stability. Furthermore, Figure 1 clearly shows that 0.25% Gelzan tended to disperse particles better than the other two suspension reagents because some starch granules

in the 50% polyethylene glycol and 50% sucrose solutions adhered to each other and even led to aggregation. Furthermore, another issue that must be considered is the suspension reagent concentration. Because the starch suspensions had to pass through the tubing of the flow cytometer, the concentration of the suspension reagents should be controlled to within the narrowest range possible. Otherwise, the dense suspension stream might clog the capillaries and nozzle of the flow cytometry and make them difficult to clean. To summarize, 0.25% Gelzan was regarded as the optimal suspension reagent for dispersing starch granules for flow sorting.

### Bivariate Flow Cytometric Analysis

The maize starch granule suspensions were analyzed biparametrically, and plots of side-scattered light (SSC) versus forward-scattered light (FSC) and side-scattered light (SSC)

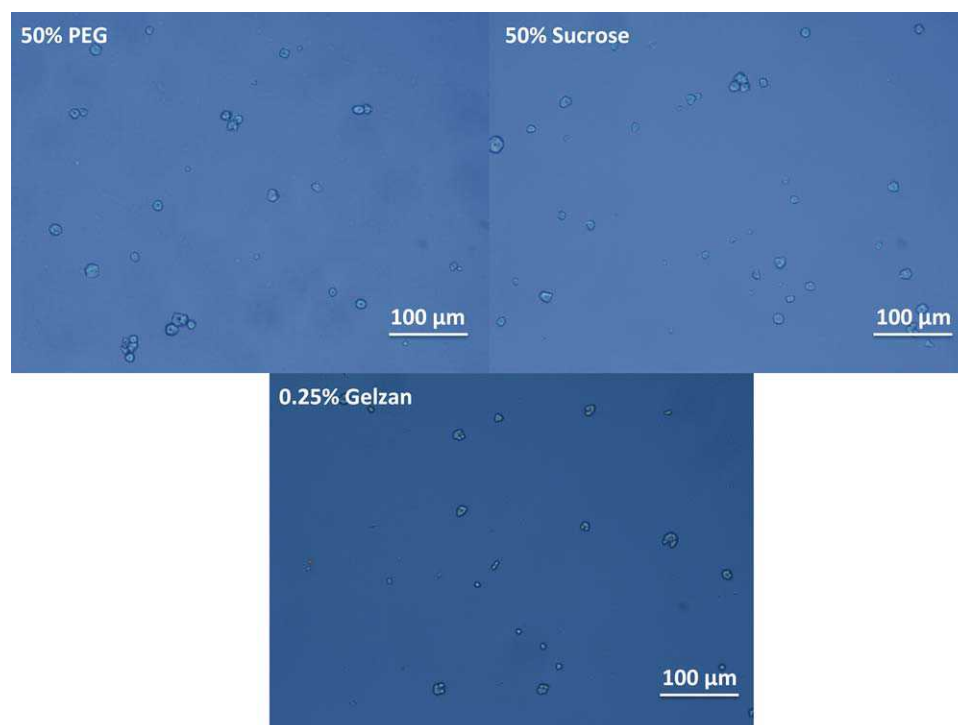


**Figure 1.** Microscopy images of suspended starch granules at 60 min for three different suspension reagents. [Color figure can be viewed at [wileyonlinelibrary.com](http://wileyonlinelibrary.com)]

versus 1-Aminopyrene-3,6,8- trisulfonic acid (APTS) were created to reflect the characteristics of the starch granules. Specifically, SSC versus FSC histograms represent the classification of starch granules considering granule size and integral structure complexity. FSC versus APTS refers to the particle features of granule size and internal structure. The amount of green fluorescence produced by the APTS-stained particles provides another empirical means to characterize the population, although it will be a complex function of different factors, including granule size, starch content, opacity, and stain penetration. In general, both of them can complementarily reflect the general characteristics of particles from different aspects. Therefore, to prove that the polydispersity detected by flow analysis was a real property of the subpopulations rather than an optical artifact, two groups with different FSC, SSC and APTS voltages were tested with all other instrument parameters held constant. According to the SSC-FSC plots shown in Figure 2, the subpopulations in the starch samples were labeled  $P_1$ ,  $P_2$ , and  $P_3$  in decreasing order of granule size (FSC value).

Figure 2 clearly demonstrates that each type of maize starch showed the same size fraction pattern between the first and second groups. This finding proved that the polydispersity observed could reflect the real properties of the subgroups and was not an optical artifact. As shown in Figure 2A<sub>1</sub>, normal maize starch was composed of three subgroups,  $P_1$ ,  $P_2$ , and  $P_3$ , where a large number of the particles in the  $P_3$  subgroup were likely debris. These findings appear to be supported by fluorescence imaging (Figure 2A<sub>1'</sub>), which showed that the  $P_1$  and  $P_2$  subgroups could be stained by APTS

whereas the impurity group  $P_3$  could not be stained by the starch-specific dye. Moreover, there was no impurity group in the normal maize starch fractions, as shown in Figure 2A<sub>2</sub> and 2A<sub>2'</sub>. Thus, normal maize starch was actually classified into two subgroups. The reason for this finding might be that the threshold value in our experiment was too low. Normally, a large proportion of maize starch granules measure 2–30  $\mu\text{m}$  (16), whereas the minimum size the cytometer could recognize was 0.5  $\mu\text{m}$ . It is possible that a minority proportion of the smallest starch granules could have been expelled together with any impurities if a higher threshold value had been applied. Therefore, foreign substances may appear in the dual-parameter flow graph. Waxy maize starch (Figure 2B<sub>1</sub> and B<sub>2</sub>) could also be separated into three subgroups, where  $P_1$  consisted of starch granules with maximum size and complexity,  $P_2$  consisted mainly of starch granules with medium size and complexity and  $P_3$  consisted of the smallest and least complex starch particles. Sweet maize starch was composed of three fractions (Figure 2C<sub>1</sub> and C<sub>2</sub>), where the granule size and complexity of  $P_1$  appeared to be greater than that of  $P_2$ , although there was only a small intersection in the forward scattering angle between these two fractions. However,  $P_3$  was indeed a complicated group involving both small starch particles and debris. This finding was supported by fluorescence imaging (Figure 2C<sub>1'</sub> and C<sub>2'</sub>), which showed that a slight proportion of starch particles in  $P_3$  were stained by APTS whereas the fluorescence intensity of the rest of the starch granules was quite low, in some cases reaching zero intensity. Interestingly, high-amylose maize starch only displayed a single subgroup, as indicated in Figure 2D<sub>1</sub> and D<sub>2</sub>. This results suggests that



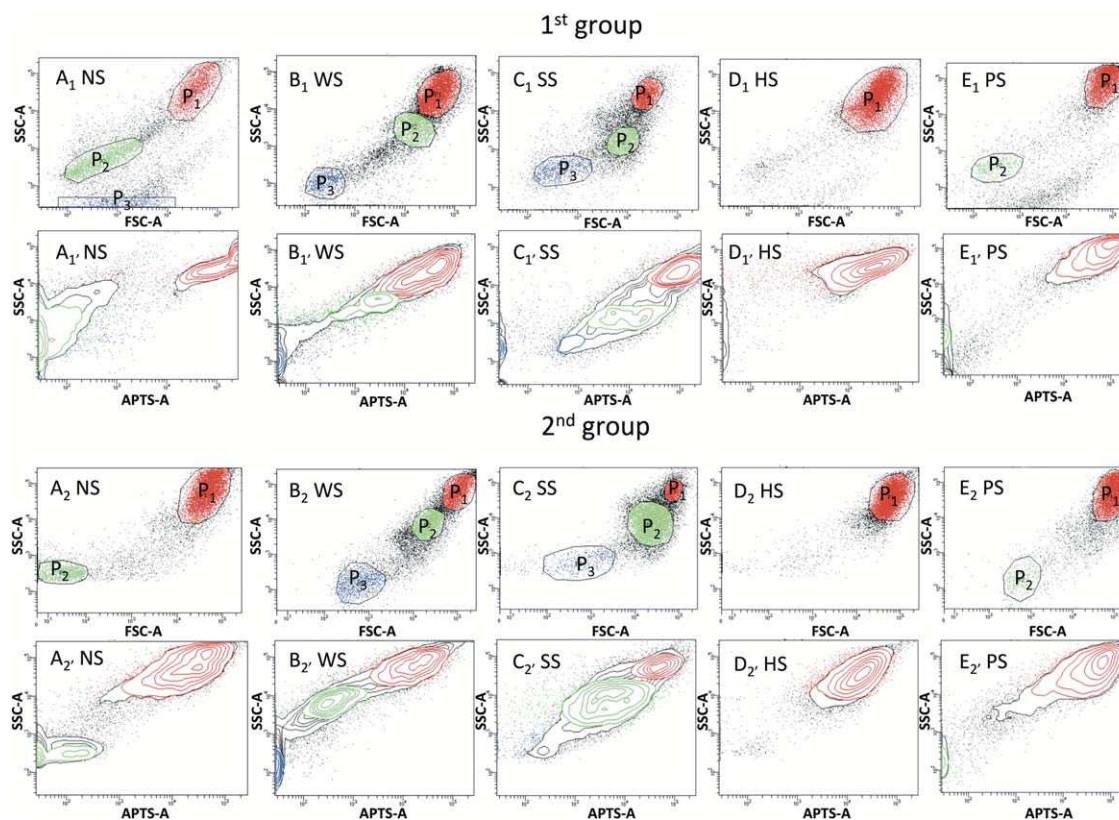


**Figure 2.** Bivariate flow cytometric histograms of five different types of maize starch: 1st group: FSC voltage (79–143), SSC voltage (201–223), and APTS channel voltage (257–425); 2nd group: FSC voltage (129–255), SSC voltage (192–237), and APTS channel voltage (267–417); NS, normal maize starch; WS, waxy maize starch; SS, sweet maize starch; HS, high-amylose maize starch; and PS, pop maize starch. [Color figure can be viewed at [wileyonlinelibrary.com](http://wileyonlinelibrary.com)]

there were no significant differences in particle size or fine structure in the high-amylose maize starch such that flow cytometry could not classify starch granules into different subgroups based on the new classification principle. Moreover, the scattered distribution in Figure 2D<sub>1'</sub> and 2D<sub>2'</sub> demonstrates that the starch granule size of high-amylose maize appeared to vary internally in a continuous fashion despite these starch granules belonging to one subgroup. By contrast, pop maize (Figure 2E<sub>1</sub> and 2E<sub>2</sub>) showed two fractions P<sub>1</sub> and P<sub>2</sub> with a large granule size and complexity and with a small granule size and little complexity, respectively.

#### Determination of Sorted Starch Subgroups by Morphology and Particle-Size Distribution

The granule fractions obtained for the different types of maize starch were collected by flow sorting and then observed by scanning electron microscopy to further determine the implications of the unique populations. From a general perspective, Figure 3 shows that the starch subpopulations observed among the different types of maize starch exhibited the same pattern in terms of granule size as that in the bivariate flow histograms shown in Figure 2. As shown in Figure 3A<sub>2</sub> and B<sub>3</sub>, the small starch granules of normal maize and waxy maize were round and spherical with a smooth surface. The morphology of the large starch granules in normal maize

and waxy maize (Figure 3A<sub>1</sub> and B<sub>1</sub>) were polygonal, where the surface of the large starch granules in normal maize appeared coarser than that of the large granules in waxy maize. The medium-sized starch fraction of waxy maize showed both spherical and polygonal starch granules (Figure 3B<sub>2</sub>). As shown in Figure 3C<sub>1</sub> and C<sub>2</sub>, a vast number of large starch granules displayed oval and spherical shapes, whereas small particles were polygonal in shape in sweet maize. Surprisingly, a variety of shapes ranging from spherical to polygonal to irregular occur in Figure 3C<sub>3</sub>, likely due to the combination of foreign matter with the smallest starch particles. This finding is in accord with the fluorescence images shown in Figure 2C<sub>1'</sub> and C<sub>2'</sub>. However, high-amylose maize starch (Figure 3D<sub>1</sub>) mainly showed elongated and spherical particles concurrently with slightly irregular particles, among which the different sizes of starch were randomly dispersed. This finding further proves that the starch granule size of high-amylose maize underwent a successive variation internally in the sorted fraction comprising a mixture of various sized and shaped starch granules, as demonstrated by the bivariate flow graphs in Figure 2D<sub>1'</sub> and D<sub>2'</sub>. Pop maize contained a considerable proportion of polygonal starch granules with coarse surfaces and laminar crack bulges, whereas a minority of spherical starch particles occurred in the small starch fraction (Figure 3E<sub>2</sub>).

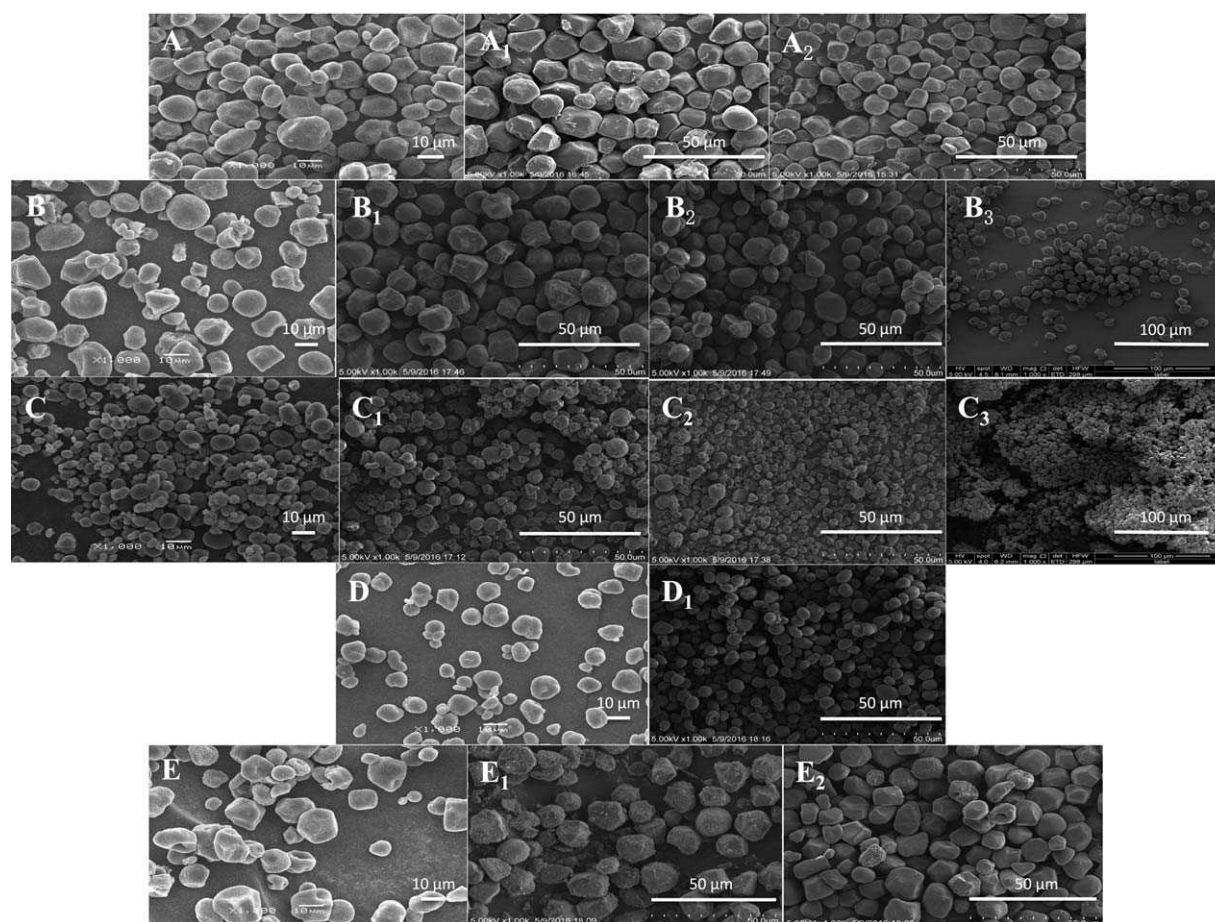


**Figure 3.** SEM images of different types of native starch and sorted starch fractions: (A) native normal maize starch, (B) native waxy maize starch, (C) native sweet maize starch, (D) native high-amylose maize starch, and (E) Native pop maize starch. (A1) P1 fraction of sorted normal maize starch. (A2) P2 fraction of sorted normal maize starch. (B1) P1 fraction of sorted waxy maize starch. (B2) P2 fraction of sorted waxy maize starch. (B3) P3 fraction of sorted waxy maize starch. (C1) P1 fraction of sorted sweet maize starch. (C2) P2 fraction of sorted sweet maize starch. (C3) P3 fraction of sorted sweet maize starch. (D1) P1 fraction of sorted high-amylose maize starch. (E1) P1 fraction of sorted pop maize starch. (E2) P2 fraction of sorted pop maize starch.

With respect to particle-size distribution, a slight contradiction with the bivariate flow histograms (Figure 2) was observed because the particle-size distribution of certain subgroups could not be recognized by LPDA. Specifically, the P<sub>3</sub> subgroups of normal starch and sweet starch were believed to be impurity groups, whereas the P<sub>3</sub> subgroup of waxy starch and the P<sub>2</sub> subgroup of both pop starch and high-amylose maize starch could not be detected, likely because the granule size was too small ( $< 2 \mu\text{m}$ ) to reach the minimum detectable level. Figure 4 shows that all starch samples were normally distributed, despite a significant difference among various types of native and sorted maize starch. In the normal maize starch and waxy maize starch fractions, the volumetric proportion of starch particles with an average diameter in P<sub>2</sub> was greater than that in P<sub>1</sub>, indicating that the size distribution of P<sub>2</sub> was more concentrated than that of P<sub>1</sub>. In contrast, sweet maize starch fractions demonstrated the opposite trend. The volumetric percentage in the P<sub>1</sub> subgroup of pop maize starch tended to be significantly higher than that in the same subgroup of high-amylose maize starch. According to the size

data in Table 2, for native maize starch, the particle size of pop maize starch was largest ( $19.09 \mu\text{m}$ ), followed by that of waxy maize starch ( $16.91 \mu\text{m}$ ), normal maize starch ( $15.58 \mu\text{m}$ ), and sweet starch ( $12.45 \mu\text{m}$ ) in. This trend was also observed by SEM (Figure 2A–E). The average size of the small starch fraction (P<sub>2</sub>) tended to be similar between normal maize starch and waxy maize starch, whose granules were clearly larger than those of sweet maize starch; this finding is supported by SEM (Figure 2A<sub>2</sub>, B<sub>2</sub>, and C<sub>2</sub>). Similarly, with respect to the large-size starch subgroups (P<sub>1</sub>), normal maize starch had the largest granule size; the granules of waxy maize starch were smaller, and those of pop maize were the smallest. The corresponding SEM images show the same pattern from Figure 2A<sub>1</sub> to E<sub>1</sub>.

## DISCUSSION

Previously developed methods for separating starch primarily include screening, sedimentation and centrifugation. Wheat starch is typically separated into two fractions, that is, A-type and B-type, through a  $10 \mu\text{m}$  mesh sieve (17).



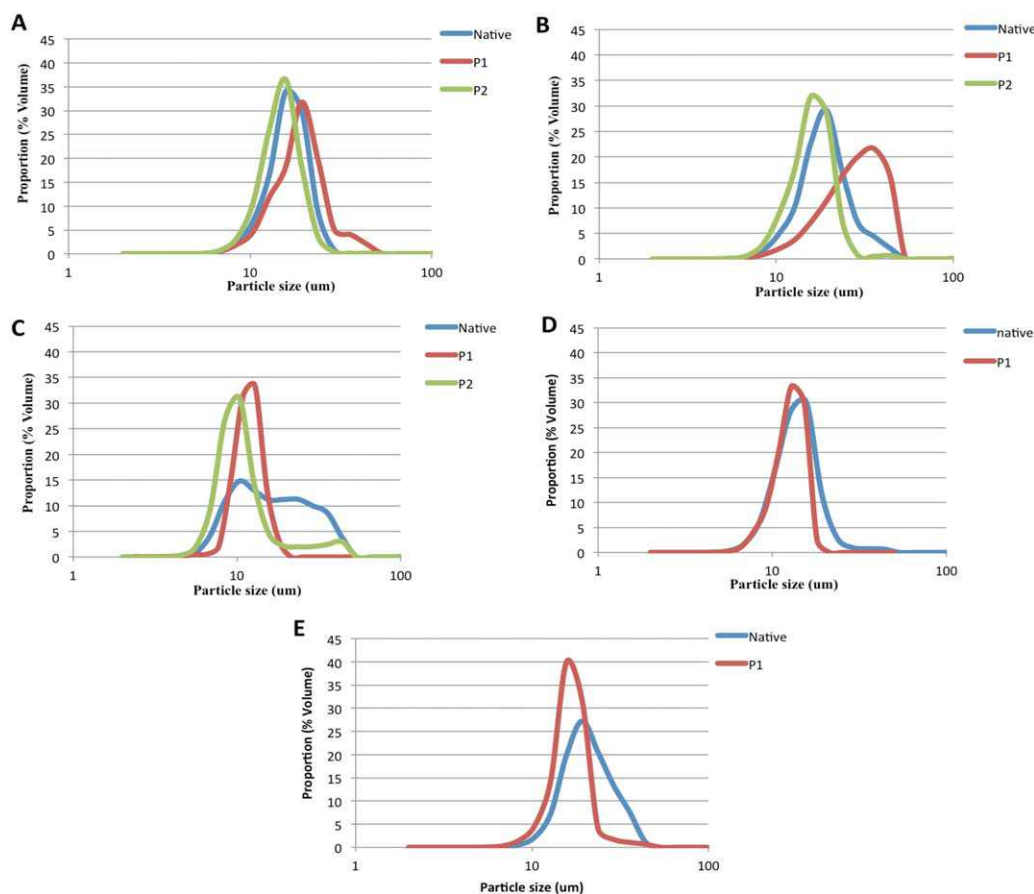


**Figure 4.** Particle-size distributions of different types of native and sorted maize starch: (A) normal maize starch, (B) waxy maize starch, (C) sweet maize starch, (D) high-amylose maize starch, and (E) pop maize starch. [Color figure can be viewed at [wileyonlinelibrary.com](http://wileyonlinelibrary.com)]

However, the above mentioned methods have shown low screening efficiency and purity because large starch granules tend to be easily underestimated due to their ellipsoidal shape and because some medium-sized and small granules remain among the large starch granules. Sedimentation using water has been utilized to segregate starch granules. For example, barley starch was fractionated into three subgroups: large, medium, and small starch granules with average diameters of 20, 7.5, and 2.3  $\mu\text{m}$ , respectively. However, the sedimentation method was still not able to distinguish between A-type and

B-type starch, clearly due to the mutual mixture between large and small starch granules, even though its efficiency was somewhat improved compared with that of the screening remedy (18). Furthermore, the centrifugation method has been exploited by comparing the separation efficiency and product purity of different starch suspension reagents containing maltose, sucrose, and cell extract (Percoll). The results demonstrated that centrifugation with Percoll was the optimal method for separating starch granules, exhibiting high fractionation efficiency and purity (17). Moreover, glycerol

**Table 2.** Particle number and size of different native maize starch and subgroups

	NATIVE STARCH		P <sub>1</sub>		P <sub>2</sub>	
	PARTICLE NUMBER	MEAN DIAMETER(M)	PARTICLE NUMBER	MEAN DIAMETER (M)	PARTICLE NUMBER	MEAN DIAMETER (M)
Normal starch	145,002	15.58	20,376	16.82	17,861	13.26
Waxy starch	21,694	16.91	3,117	21.74	37,035	15.03
Sweet starch	39,823	12.45	835	11.14	51,822	9.91
High amylose starch	196,174	13.12	20,253	12.32	/	/
Pop starch	10,556	19.09	20,249	16.10	/	/

The number of particles in each sample represents the value for all three replicates. Entries with "/" indicate no data.

centrifugation has also been proposed, in which starch granules are separated by size more effectively due to the more significant variation in sedimentation rates between different-sized starch particles because of the higher density of glycerol versus that of water (7). However, this method relies solely on starch granule size to separate starch granules, which appears too one-dimensional to study the characteristics of starch comprehensively.

The shapes of starch granules of different maize types appear to be quite different and include ellipsoidal, round, spherical, polygonal, and even irregular shapes (16), largely depending on the amylose/amylopectin ratio. Normal maize starch presents spherical and polygonal granules; however, the granule shape of high-amylose maize varies greatly, from ovals to irregular polygons (6). Other researchers have also indicated that the ranges of starch granule size and morphology of high-amylose maize are wider than those of normal maize starch, particularly native starch (8). This finding was confirmed by morphological images (Figure 3) in this study. The same phenomenon has been reported in other studies, namely that a large number of high-amylose crop starches are composed of morphologically diverse particles, including elongated particles in maize (19), hollow granules in wheat (20), and aggregate forms in rice (21). Previous studies have indicated that pop maize starch granules are arranged more tightly because their endosperm exhibits a vitreous texture (22), whereas sweet maize starch appears less compact due to its higher soluble sugar content (23). In another study, the arrangement of starch particles in normal maize and that in waxy maize appeared similar although the particle shapes varied greatly (24). This finding was mirrored in this study, particularly the arrangement of the large- and medium-size fractions (Figure 3A<sub>1</sub>, A<sub>2</sub>, B<sub>1</sub>, B<sub>2</sub>).

The starch granule sizes of different maize cultivars mainly vary from 2 to 30  $\mu\text{m}$ , where the mean diameter is approximately 15  $\mu\text{m}$  (16,25). In previous work, large starch granules tended to contain a greater amount of amylose in bimodal crops (17,26,27), whereas other researchers have demonstrated that small and large starch granules could contain the identical amount of amylose (28,29). Similarly, as shown in Figure 3, the large-size fraction in normal maize was larger than its counterpart in waxy maize, whereas there appeared to be no significant difference in the small starch subgroups between normal maize starch and waxy maize starch.

In conclusion, unlike other methods based solely on density or weight gradients, flow cytometry can be employed to comprehensively classify and analyze starch fractions. The method appears quite convenient, allowing the user to choose the target group freely and separate and collect starch fractions according to their particle size and internal complexity. Therefore, further investigation would be valuable in exploring how the method described in this article benefits starch synthesis and determining the relationship between the amylose/amylopectin ratio and starch fractions and the corresponding physicochemical properties.

## ACKNOWLEDGMENT

The authors declare that no conflict of interest exists.

## LITERATURE CITED

1. Lindeboom N, Chang PR, Tyler RT. Analytical, biochemical and physicochemical aspects of starch granule size, with emphasis on small granule starches: A review. *Starch/Stärke* 2004;56:89–99.
2. Tester RF, Karkalas J, Qi X. Starch—composition, fine structure and architecture. *J Cereal Sci* 2004;39:151–165.
3. Ao Z, Jane J. I. Characterization and modeling of the A- and B-granule starches of wheat, triticale, and barley. *Carbohydr Polym* 2007;67:46–55.
4. Dhital S, Shrestha AK, Hasjim J, Gidley MJ. Physicochemical and structural properties of maize and potato starches as a function of granule size. *J Agric Food Chem* 2011;59:10151–10161.
5. Li W, Shan Y, Xiao X, Luo Q, Zheng J, Ouyang S, Zhang G. Physicochemical properties of A- and B-starch granules isolated from hard red and soft red winter wheat. *J Agric Food Chem* 2013;61:6477–6484.
6. Zhang X, Chen Y, Zhang R, Zhong Y, Luo Y, Xu S, Liu J, Xue J, Guo D. Effects of extrusion treatment on physicochemical properties and in vitro digestion of pregelatinized high amylose maize flour. *J Cereal Sci* 2016;68:108–115.
7. Lin L, Cai C, Gilbert RG, Li E, Wang J, Wei C. Relationships between amylopectin molecular structures and functional properties of different-sized fractions of normal and high-amylose maize starches. *Food Hydrocolloids* 2016;52:359–368.
8. Cai C, Lin L, Man J, Zhao L, Wang Z, Wei C. Different structural properties of high-amylose maize starch fractions varying in granule size. *J Agric Food Chem* 2014;62:11711–11721.
9. Clédat D, Battu S, Mokriani R, Cardot PJP. Rice starch granule characterization by flow cytometry scattering techniques hyphenated with sedimentation field–flow fractionation. *J Chromatogr A* 2004;1049:131–138.
10. Biosciences BD. Introduction to Flow Cytometry: A Learning Guide. Manual Part. 2000. p. 1. <https://www.bu.edu/flow-cytometry/files/2010/10/BD-Flow-Cytom-Learning-Guide.pdf>
11. Margossian T, Reppel L, Makdissy N, Stoltz J-F, Bensoussan D, Huselstein C. Mesenchymal stem cells derived from Wharton's jelly: comparative phenotype analysis between tissue and in vitro expansion. *Bio-Med Mater Eng* 2012;22:243–254.
12. Yang Y-P, Juang Y-S, Hsu B-D. A quick method for assessing chloroplastic starch granules by flow cytometry. *J Plant Physiol* 2002;159:103–106.
13. Sui Z, Huber KC, BeMiller JN. Effects of the order of addition of reagents and catalyst on modification of maize starches. *Carbohydr Polym* 2013;96:118–130.
14. Chung Y-L, Lai H-M. Molecular and granular characteristics of corn starch modified by HCl-methanol at different temperatures. *Carbohydr Polym* 2006;63:527–534.
15. Sawut M, Ghulam A, Tiyyip T, Zhang Y-J, Ding J-L, Zhang F, Maimaitiyiming M. Estimating soil sand content using thermal infrared spectra in arid lands. *Int J Appl Earth Obs Geoinf* 2014;33:203–210.
16. Hoover R. Composition, molecular structure, and physicochemical properties of tuber and root starches: A review. *Carbohydr Polym* 2001;45:253–267.
17. Peng M, Gao M, Abdel-Aal ES, Hucl P, Chibbar RN. Separation and characterization of A- and B-type starch granules in wheat endosperm. *Cereal Chem* 1999;76:375–379.
18. Morrison WR, Gadan H. The amylose and lipid contents of starch granules in developing wheat endosperm. *J Cereal Sci* 1987;5:263–275.
19. Jiang H, Campbell M, Blanco M, Jane J-L. Characterization of maize amylose-extender (ae) mutant starches: Part II. Structures and properties of starch residues remaining after enzymatic hydrolysis at boiling-water temperature. *Carbohydr Polym* 2010;80:1–12.
20. Slade AJ, McGuire C, Loeffler D, Mullenberg J, Skinner W, Fazio G, Holm A, Brandt KM, Steine MN, Goodstal JF. Development of high amylose wheat through TILLING. *BMC Plant Biol* 2012;12:69.
21. Wei C, Qin F, Zhu L, Zhou W, Chen Y, Wang Y, Gu M, Liu Q. Microstructure and ultrastructure of high-amylose rice resistant starch granules modified by antisense RNA inhibition of starch branching enzyme. *J Agric Food Chem* 2009;58:1224–1232.
22. Li YL. Effect of normal corn pollen burst of maize grain and burst characteristics. *Chin Agric Sci Bull* 1999;15:24–26.
23. Liu P, Hu C-H, Dong S-T, Wang K-J, Zhang J-W, Zhang BR. Comparison of enzymes activity associated with sucrose metabolism in the developing grains between sweet corn and normal corn. *Sci Agric Sin* 2005;1:009.
24. Cui L, Dong S, Zhang J, Liu P. Starch granule size distribution and morphogenesis in maize (*Zea mays* L.) grains with different endosperm types. *Aust J Crop Sci* 2014;8:1560.
25. Olkku J, Rha C. Gelatinisation of starch and wheat flour starch—a review. *Food Chem* 1978;3:293–317.
26. Takeda Y, Takeda C, Mizukami H, Hanashiro I. Structures of large, medium and small starch granules of barley grain. *Carbohydr Polym* 1999;38:109–114.
27. Li JH, Vasanthan T, Rosnagel B, Hoover R. Starch from hull-less barley: I. Granule morphology, composition and amylopectin structure. *Food Chem* 2001;74:395–405.
28. Evers AD, Greenwood CT, Muir DD, Venables C. Studies on the biosynthesis of starch granules. Part 8. A comparison of the properties of the small and the large granules in mature cereal starches. *Starch Stärke* 1974;26:42–46.
29. Myllrinen P, Autio K, Schulman AH, Poutanen K. Heat-induced structural changes of small and large barley starch granules. *J Inst Brewing* 1998;104:343–349.



# SCIENTIFIC REPORTS

OPEN

## Evolutionary, structural and expression analysis of core genes involved in starch synthesis

Jianzhou Qu<sup>1,2</sup>, Shutu Xu<sup>1,2</sup>, Zhengquan Zhang<sup>1,2</sup>, Guangzhou Chen<sup>1,2</sup>, Yuyue Zhong<sup>1,2</sup>, Linsan Liu<sup>1,2</sup>, Renhe Zhang<sup>1,2</sup>, Jiquan Xue<sup>1,2</sup> & Dongwei Guo<sup>1,2</sup>

Received: 26 March 2018

Accepted: 30 July 2018

Published online: 24 August 2018

**Starch is the main storage carbohydrate in plants and an important natural resource for food, feed and industrial raw materials. However, the details regarding the pathway for starch biosynthesis and the diversity of biosynthetic enzymes involved in this process are poorly understood. This study uses a comprehensive phylogenetic analysis of 74 sequenced plant genomes to revisit the evolutionary history of the genes encoding ADP-glucose pyrophosphorylase (AGPase), starch synthase (SS), starch branching enzyme (SBE) and starch de-branching enzyme (DBE). Additionally, the protein structures and expression patterns of these four core genes in starch biosynthesis were studied to determine their functional differences. The results showed that AGPase, SS, SBE and DBE have undergone complicated evolutionary processes in plants and that gene/genome duplications are responsible for the observed differences in isoform numbers. A structure analysis of these proteins suggested that the deletion/mutation of amino acids in some active sites resulted in not only structural variation but also sub-functionalization or neo-functionalization. Expression profiling indicated that AGPase-, SS-, SBE- and DBE-encoding genes exhibit spatio-temporally divergent expression patterns related to the composition of functional complexes in starch biosynthesis. This study provides a comprehensive atlas of the starch biosynthetic pathway, and these data should support future studies aimed at increasing understanding of starch biosynthesis and the functional evolutionary divergence of AGPase, SS, SBE, and DBE in plants.**

Starch is the predominant reserve form of carbohydrate and energy in plants and can be divided into two types, transitory starch and storage starch, based on biological function. In photosynthetic tissues, transient starches accumulate in chloroplasts during the day. During the night, they are then transported and degraded to provide energy and nutritional substances for growth and metabolism. In non-photosynthetic tissues, such as seed endosperm, tubers and storage roots, storage starches are kept for long periods of time in specialized plastids termed amyloplasts, from which they can be remobilized in preparation for germination, sprouting or regrowth<sup>1</sup>. Additionally, starch is an important resource for agriculture, human consumption and industry. For example, it is a major contributor to the harvestable starch-storing organs of crop plants, which include cereal seeds (e.g., maize), tubers (e.g., *Solanum*) and storage roots (e.g., *Ipomoea*). Moreover, starch provides abundant calories for human diet and animal feed and is an economical, biodegradable and renewable industrial raw material<sup>2</sup>.

Starch consists of two types of polysaccharides: amylose and amylopectin. Amylose is a linear polymer composed of  $\alpha$ -1,4-linked glucan chains and has very few branches connected by  $\alpha$ -1,6-glycosidic bonds. The amylopectin molecule is larger than the amylose molecule and contains abundant  $\alpha$ -1,6-branches that connect  $\alpha$ -1,4-linked glucan chains and make up a structural framework of repeated amorphous and crystalline lamellae<sup>3</sup>. Linear amylose adjacent parallel side chains are distributed in the semi-crystalline matrix formed by amylopectin, and this organization underlies the semi-crystalline structure of starch<sup>1</sup>. Thus, the amylose:amylopectin ratio has a major influence on the appearance and structure of starch granules and also affects the quality of crop storage organs, food production and industrial applications.

Starch biosynthesis is a complex and highly regulated process that requires coordinated activities among multiple enzymes, including ADP-glucose pyrophosphorylase (AGPase), starch synthase (SS), starch branching

<sup>1</sup>The key Laboratory of Biology and Genetics Improvement of Maize in Arid Area of Northwest Region, Ministry of Agriculture, College of Agronomy, Northwest A&F University, Yangling, 712100, Shaanxi, China. <sup>2</sup>Maize Engineering Technology Research Centre of Shaanxi Province, Yangling, 712100, Shaanxi, China. Correspondence and requests for materials should be addressed to J.X. (email: [xjq2934@163.com](mailto:xjq2934@163.com)) or D.G. (email: [gdwei1973@126.com](mailto:gdwei1973@126.com))

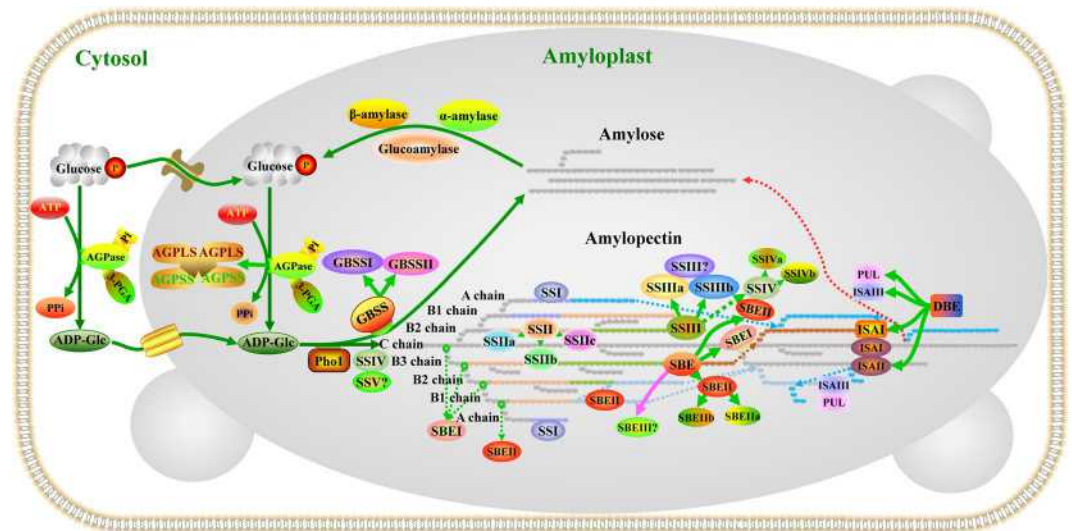


**Figure 1.** The starch biosynthesis pathway. AGPase synthesizes ADP-glucose from Glc1P and ATP and as a heterotetramer ( $L_2S_2$ ) consisting of two large and two small subunits; AGPSS plays a catalytic function, while AGPLS is mainly responsible for modulating the allosteric regulatory properties of AGPase<sup>4,68</sup>. Amylose is mainly produced via the activity of GBSS. Amylopectin synthesis depends on coordinated interactions among at least 17 different genes encoding isoforms of SS, SBE, ISA, PUL and PHO1. Of these, SSI plays an important role in elongating short chains from a degree of polymerization (DP) of 6–7 chains at the branch point to DP 8–12 in the A or B1-chains of amylopectin<sup>56,69</sup>. SSII plays a distinct role in catalysing the formation of intermediate chains (usually DP 13–25) of amylopectin<sup>70</sup>. SSIII mainly catalyses the synthesis of amylopectin B2 to B4 chains, and some of its functions overlap with those of SSII in amylopectin biosynthesis<sup>71,72</sup>. SSIV plays an essential role in the priming of starch granule formation, the morphology of starch granules and the degree of starch accumulation; moreover, its functions can be partially supported by SSIII depending on the plant species<sup>57,58</sup>. SBEI preferentially produces longer chains (B1 to B3), while SBEIIa and SBEIIb preferentially promote the production of short amylopectin chains (DP 6–12) and further impact the structure and phenotype of amylopectin during starch biosynthesis<sup>73,74</sup>. The ISAI homomultimer and/or ISAI/ISAI heteromultimer have a higher affinity for relatively long external branches and a greater impact on amylopectin structure, while ISAI may be indirectly involved in de-branching because it recognizes special branch points and facilitates the ability of ISAI to remove nearby branches<sup>15,34,75</sup>. Additionally, ISAI partially compensates for the function of the ISAI/ISAI heteromultimer and plays a major role in starch breakdown by de-branching short external chains of glucans as well as influencing the activity of  $\alpha$ -amylase and  $\beta$ -amylase<sup>76,77</sup>. PUL has partially overlapping functions with ISA and is involved in cleaving short branched chains during starch biosynthesis<sup>60,78</sup>. Here, different colours represent different enzymes involved in starch synthesis. The dotted line represents the shift in the direction of the chain. The question mark indicates that the specific function of the enzyme in starch synthesis is unknown.

enzyme (SBE) and starch de-branching enzyme (DBE) (Fig. 1). AGPase, as the first enzyme in the starch biosynthesis pathway, catalyses the limiting reaction by converting glucose 1-phosphate (Glc-1-P) and ATP to ADP-Glc and inorganic pyrophosphate (PPi) in amyloplasts. The enzyme's catalytic activity is stimulated by 3-phosphoglyceric acid (3-PGA) and inhibited by inorganic phosphate (Pi). The activity of AGPase is also limited by the oxidation-mediated formation of disulfide bridges between adjacent AGPSSs, which can lead to re-activation by reduced thioredoxin (or dithiothreitol *in vitro*)<sup>4,5</sup>. SS can be further divided into granule-bound starch synthase (GBSS), which is responsible for the synthesis of amylose and the extra-long-chain fraction of amylopectin, and soluble starch synthase (SSS), which is mainly responsible for the synthesis of amylopectin<sup>6,7</sup>. SBEs belong to the  $\alpha$ -amylase family, the branching activity of which is regulated by Q-enzyme, which introduces a branched structure by cleaving the  $\alpha$ -1,4-glucan chain in polyglucans and then reattaching the cleaved chain onto an acceptor chain via an  $\alpha$ -1,6-glucan linkage, thereby creating a branch in the same or another chain<sup>8</sup>. DBEs are another glucan-modifying enzyme that occurs in two forms, namely, isoamylase-type DBE (ISA) and pullulanase-type DBE (PUL). The most important functional difference between these forms is that ISA generally acts upon phytyloglycogen and amylopectin by hydrolysing the  $\alpha$ -1,6-linkages of polyglucans, which play important roles in the modification of excessively branched chains or the removal of improper branches of amylopectin formed by branching enzymes to maintain the cluster structure of amylopectin. Moreover, ISA likely provides branched chains for amylose. PUL usually cleaves the  $\alpha$ -1,6-linkages of polyglucans in pullulan and, to a lesser degree, amylopectin, and exerts little or no activity towards glycogen<sup>9</sup>. Recent studies have suggested that the plastidial pathway of starch synthesis exists in all extant higher plants and green algae and that the starch biosynthetic enzymes of higher plants underwent a complex sequence of changes during evolution<sup>10</sup>. Moreover, the isoform types and functionality of starch biosynthetic enzymes are remarkably similar to those found in green algae<sup>10</sup>. This similarity indicates that in starch biosynthetic enzyme genes, the functional regions or sites that control starch synthesis are relatively well-conserved because these lineages diverged from a common ancestor.



In plants, AGPase subunits share a common nucleoside triphosphate (NTP) transferase domain, which allows AGPase to transfer nucleotides from one compound to another, providing substrates for starch biosynthesis. Ss share a highly conserved core region located in the C-terminus that generally consists of conserved starch catalytic glucosyl transferase family 5 (GT5) and GT1 domains, which mediate an inverting mode of glucosyl transfer during glucosyl transferase<sup>11</sup>. Both the GT5 and GT1 domains belong to the GT-B superfamily according to the CAZy database (<http://www.cazy.org/>), and they possess conserved amino acid residues that can bind the glucosyl donor (ADP-Glc). These enzymes usually merge into the base catalytic region of starch synthases. All SBEs and DBEs belong to glycoside hydrolase family 13 (GH13), an important member of clan GH-H, which is also known as the  $\alpha$ -amylase family (Amy). These enzymes not only share an Amy domain but also possess conserved carbohydrate-binding module family 48 domains in the N-terminal sequence. Moreover, SBEs have retained a C-terminal  $\beta$ -sheet catalytic domain (Amy\_C), while pullulanase (PUL) has a DUF3372 domain located in the N-terminal sequence, and this domain may play important roles in recognition and/or interaction with certain substrates or be involved in modulating PUL activity and interacting with other starch biosynthetic enzymes in specific environmental conditions<sup>12,13</sup>.

Many previous studies have reported enzymes that are directly involved in starch biosynthesis in algae<sup>14</sup>, potato<sup>15</sup>, *Arabidopsis thaliana*<sup>16</sup>, barley<sup>17</sup>, wheat<sup>18,19</sup>, and rice<sup>20,21</sup>. However, far less research has been devoted to the core regulatory network involved in starch metabolism. This paucity of research means that limited information is available to assist breeders and biotechnologists in improving and increasing starch content in a predictable manner. In the present study, we present and discuss the starch synthesis network, which is regulated by multiple starch biosynthetic enzymes, and evolutionary patterns in starch biosynthetic enzymes in 74 plant genomes. By combining data related to the structures, functions and expression patterns of maize starch biosynthetic enzyme genes, we reveal previously undetected information about starch biosynthetic enzymes and the starch synthesis network. It is anticipated that these results will enhance our understanding of the starch synthesis process.

## Results

**Phylogenetic, structural and functional sites analysis of AGPase subunits.** All AGPase-encoding genes have been identified in many plant genomes (Fig. 2). The phylogenetic tree of AGPase subunits from 73 plant species showed that there is considerable evolutionary divergence in these plant species (Supplementary Table 1). In particular, we did not detect similar AGPase-encoding genes in the *Porphyrumbilicalis* genome (Fig. 2). This result echoed previous studies<sup>2,22,23</sup>. Additionally, the evolution of AGPLs was markedly different from that of AGPSSs in the studied plant species, and this difference may have arisen as a result of different duplication events and selection pressures between AGPLs and AGPSSs<sup>24,25</sup> (Fig. 3 and Supplementary Fig. 1).

Although there has been a divergence between AGPLs and AGPSSs during evolution, they share a core region of approximately 31 kDa that is indispensable for catalytic activity and is often designated the NTP\_transferase (nucleotidyl transferase) domain (Fig. 4A). An analysis of conserved motifs revealed that motif 6 was not detected in the NTP\_transferase domain of AGPSS4, while other AGPase subunits all contained motifs 1, 2, 3, 4, 6, 9, 10 and 11 (Fig. 4A and Supplementary Fig. 2). Additionally, a secondary structure analysis showed that there were more  $\alpha$  helices and  $\beta$  sheets in the catalytic domain of AGPSSs than in the catalytic domain of AGPLs (except for AGPSS4, Fig. 4A and Supplementary Fig. 3).

To further explore the active sites for AGPase subunits, we aligned the protein sequences of maize AGPase subunits with those of potato sequences (sequence similarity was greater than 46%)<sup>26</sup>. Sulfate is an inhibitor of the potato tuber ADP-Glc PPase  $\alpha$  subunit homotetramer under certain conditions<sup>26</sup>. Three areas were found that could interact with the sulfate in maize AGPase subunits. The first sulfate-binding area involved Arg107, Arg119, Asp469, Lys470 and Lys507; the Lys470 was replaced by Met in AGPLS1 and AGPLS2 and by His313 in AGPSS4 (Fig. 4B,C and Supplementary Fig. 4). In the second area, five residues participated in sulfate binding, including Arg149, His150, Gln380, and Arg382 and a double-active site at Arg119; Gln380 was substituted by Ala and Ser in AGPLS1 and AGPLS2-4, respectively (Fig. 4B,C and Supplementary Fig. 4). In the third sulfate-binding area, Lys135, Arg149, His200 and Asn201 participated in binding sulfate, His200 was substituted with a Lys in AGPLSs, while Asn201 was a highly variable site that was replaced by Ser, Ala, Cys or Asp in four AGPLs (Fig. 4B,C and Supplementary Fig. 4). Additionally, multiple ATP-binding sites in maize AGPSSs were consistent with those found in potato except for AGPSS4, and Arg84, Pro162, Ala176, Ser199 and Ser312 had changed in AGPLs (Fig. 4B and Supplementary Fig. 4). Glucose, a major substrate for starch synthase, binds with multiple residues of AGPase that are conserved among AGPase subunits, except for Asn248 of AGPLS1 and Tyr 250 of AGPLS2 (Fig. 4B and Supplementary Fig. 4). Compared to AGPSSs, the ADP-Glc binding site Lys94 was replaced by Thr in AGPLS1 and AGPLS2 (Fig. 4B and Supplementary Fig. 4). In agreement with a previous study on potato AGPase, we found that multiple amino acid residues on the active sites of maize AGPase subunits were consistent with those found in potato AGPSS and that the interactive residues of AGPSSs were more conserved than were those of AGPLs<sup>26</sup> (Supplementary Fig. 4).

**Phylogenetic, structural and functional divergence of starch synthesis genes.** To explore the evolutionary relationships of Ss, a phylogenetic tree was constructed using SS-encoding protein sequences collected from 74 plant species (Fig. 2). The phylogeny was classified into six different clades, of which clades I, II, III, IV, V and VI typically represent SSII, SSI, SSIV, SSIII, SSV and GBSS, respectively, according to the maize SS isoforms (Supplementary Fig. 5). The phylogenetic analysis showed that in most species, SS isoforms have undergone gene duplication to different degrees, and SSV demonstrated a close evolutionary relationship with SSIV (Supplementary Fig. 5 and Fig. 5).

The domain analysis of SS isoforms found that GT5 and GT1 domains were detected in almost all SS isoforms except SSV. The SSIII, SSIV and SSV isoforms contained one or two coiled-coil domains in the N

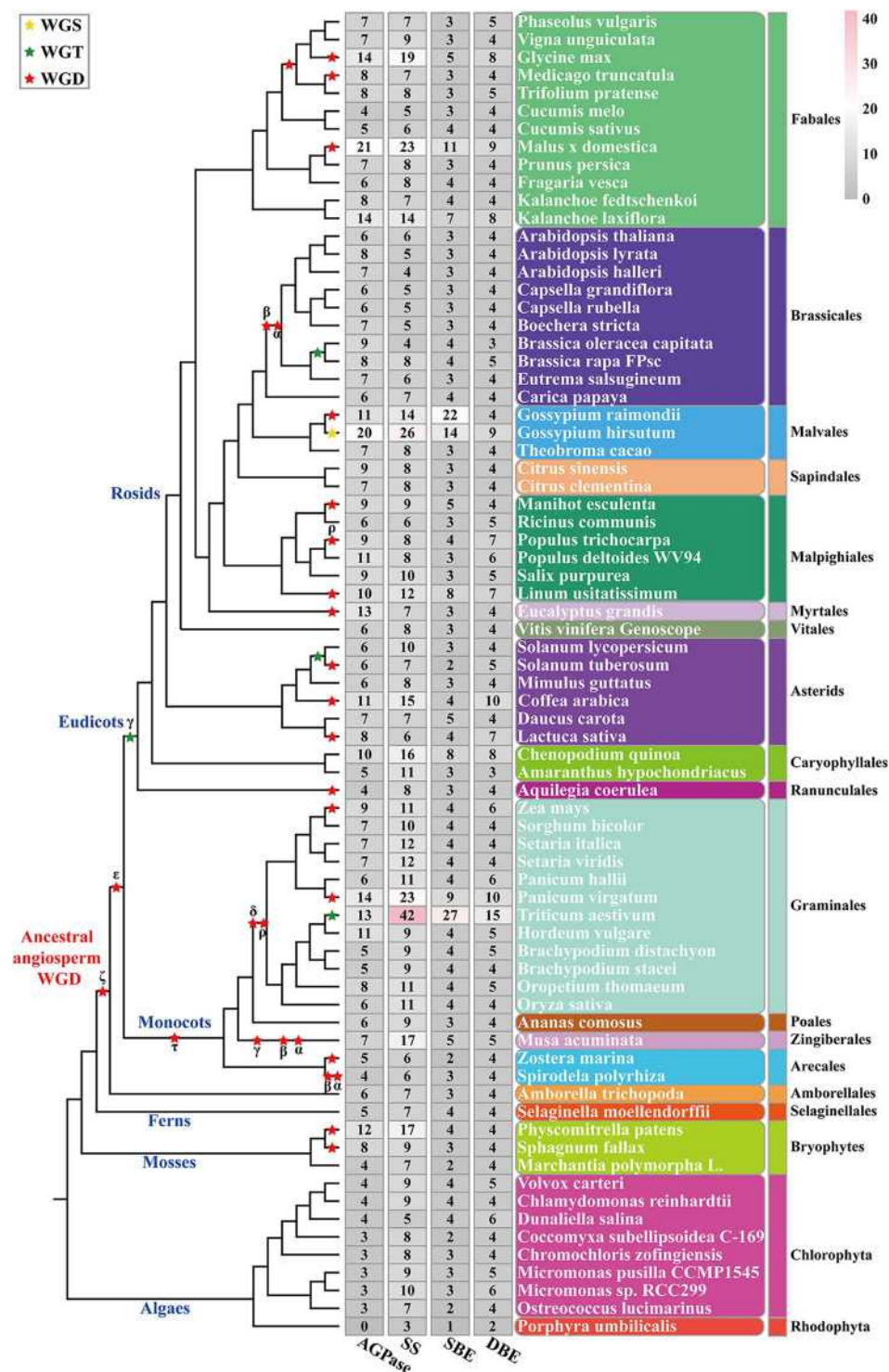


**Figure 2.** Branch-specific expansion of AGPase, SS, SBE and DBE genes in every sub-group on every branch of the phylogenetic tree. The tree on the left displays all polyploidy events (marked with stars). Red stars represent whole-genome duplication events, green stars represent whole-genome triplication events, and yellow stars represent whole-genome sextuplication events. The total number of protein isoforms of the four core enzymes and the number in each group identified in each plant genome are indicated on the right. Species names are shown on the right side.

terminus that are involved in regulating protein-protein interactions<sup>27</sup> (Fig. 6A). Additionally, three conserved carbohydrate-binding modules (CBM53 domain) were detected in the N-terminal regions of SSIII isoforms that play important roles in substrate binding<sup>28</sup> (Fig. 6A).



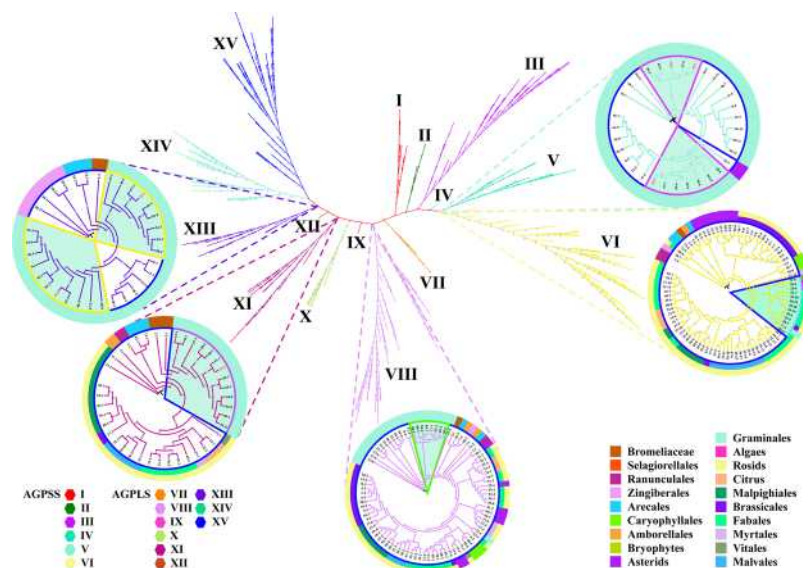


**Figure 3.** Phylogenetic analysis of the amino acid sequences of AGPase of 74 plant species. Sequences classified into subfamilies I–XV are shown in colour. Of these, I–VI and VII–XV represent the AGPSSs and AGPLSs, respectively, found in the 73 plant species. The branches of protein sequences in maize are highlighted in red with a light blue background. As an example, we have illustrated the internal divergence between AGPLS and AGPSS. For detailed species ID and protein sequences, please refer to Supplementary Table 1.

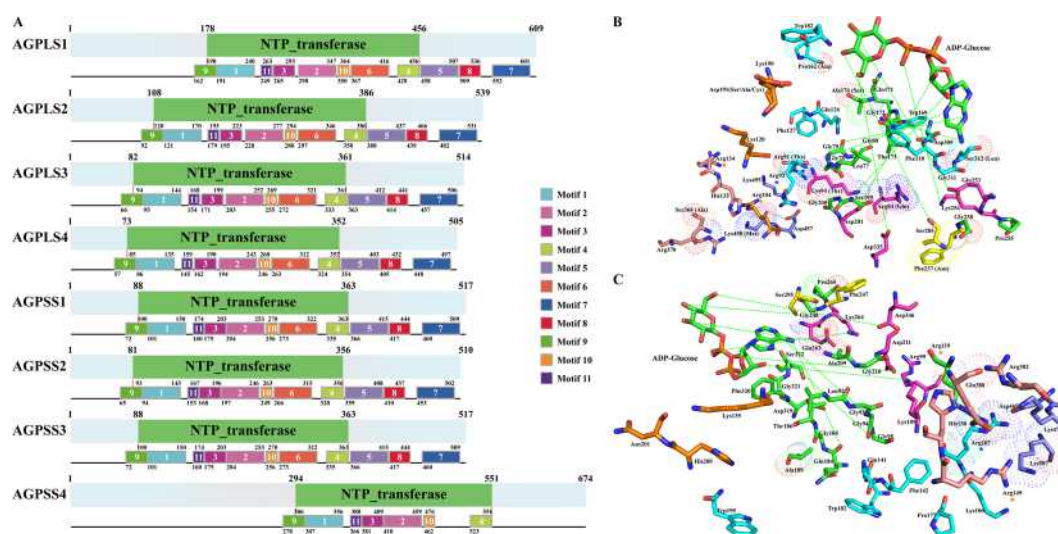


**Figure 4.** Structure and active site analysis of AGPase subunits. Maize is shown as an example. (A) The composition and distribution of domain structures and conserved motifs in AGPase proteins are marked and annotated in different colours. Based on the conservation of functional sites, we selected representative subunits for analysis. (B) Stereo view of the active sites of AGPLSs based on the sequence of AGPLS4 and (C) of AGPSSs based on the sequence of AGPSS1. Interaction sites between AGPSSs/AGPLSs and ADP-glucose are linked by broken green lines. Different colour stars and amino acids represent different functional sites. The same site with different amino acids is marked with dots in AGPase subunits.

The secondary structures of maize SS isoforms were constructed based on the reference models of wheat SSI (83% identity with maize SSI) and rice GBSSI (62–83% identity, A2Y8X2.2)<sup>17,29</sup>. Comparative studies revealed that the main divergence in secondary structure between the SSI and SSII isoforms was in the GT5 domain, both of which were quite different from that of the SSIII isoforms with regard for the positions and compositions of  $\alpha$  helices and  $\beta$  sheets (Fig. 6A and Supplementary Fig. 6). The main divergence between SSIV and SSV occurred in the GT1 domain, in which one  $\alpha$  helix was absent in SSIV. The differences between GBSSI and GBSSII were that in the GT5 domain, one  $\beta$  sheet was absent in GBSSI and one  $\alpha$  helix was absent in GBSSII, and in the GT1 domain, one  $\beta$  sheet was absent in GBSSII (Fig. 6A). Furthermore, an analysis of conserved motifs revealed that motif 24 was only detected in SSII isoforms, and the motif compositions were similar between SSS and GBSS

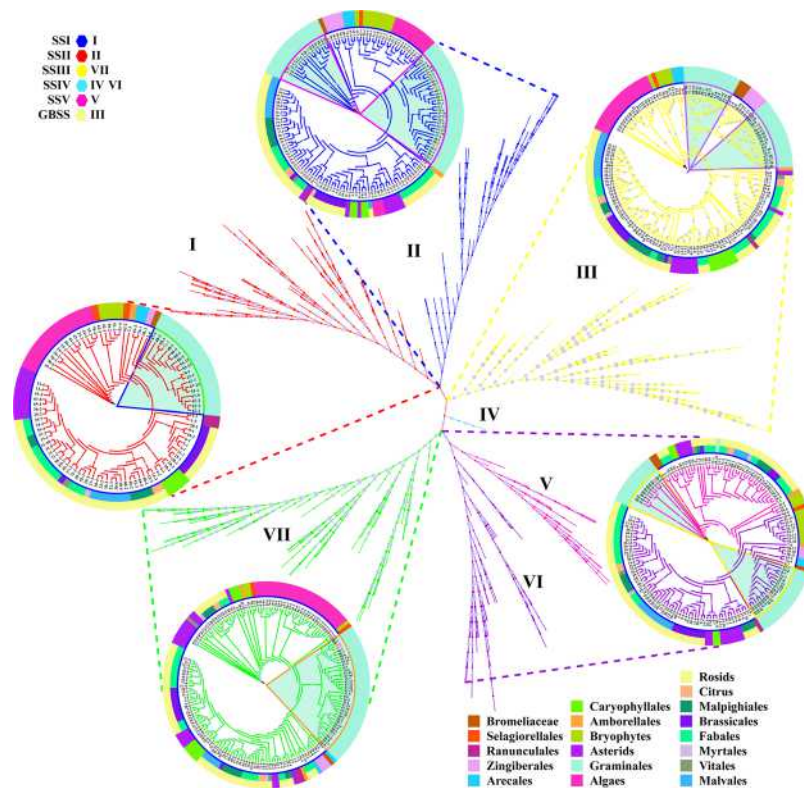


**Figure 5.** Phylogenetic analysis of the amino acid sequences of SS in 74 plant species. Sequences classified into subfamilies I-VI are shown in colour. Clades I, II, III, IV and VI/V/VII represent SSI, SSII, GBSS, SSIV and SSV, respectively, of 74 plant species. The branches of protein sequences found in maize are highlighted in red with a light blue background. For detailed species IDs, please refer to Supplementary Table 1.

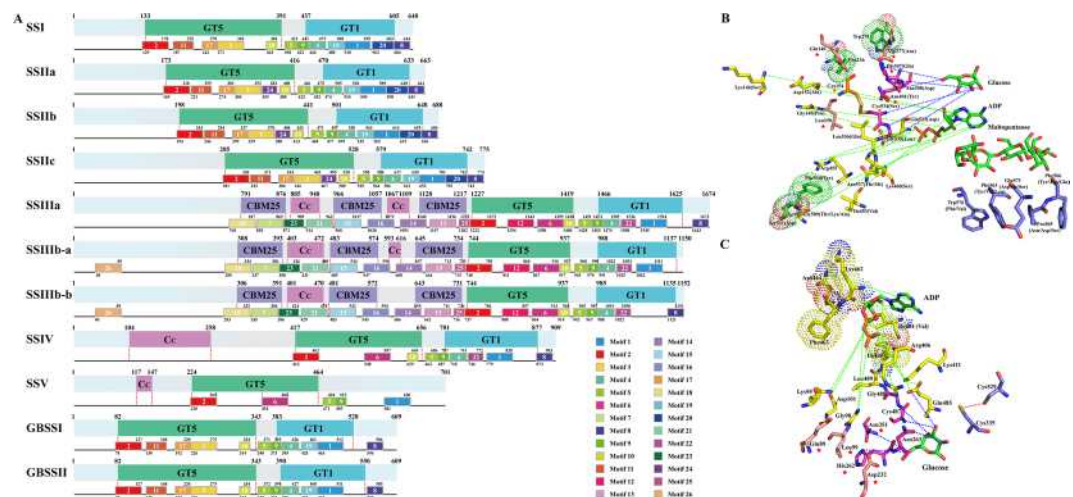


**Figure 6.** Structural features and active site analysis of SS isoforms. Maize is shown as an example. (A) Compositions and distributions of domain structures and conserved motifs of SS proteins are marked and annotated in different colours. (B) Stereo view of the active sites of SS isoforms based on the sequence of SSI and (C) GBSS isoforms based on the sequence of GBSSI. The same site with different amino acids is marked with dots in SS isoforms. Interaction sites between SSs and ADP are shown as linked broken green lines. Interaction sites between SSSs and glucose are marked in pink. Red stars and lines shown in light pink represent catalytic sites. Amino acid sites that interact with maltopentaose are marked in blue, and these active sites are not conserved in SSIII, SSIV and SSV. Additionally, disulfide bonds were found only in SSI and GBSSI and are marked with orange stars in SSSs and as blue amino acids in GBSSI.



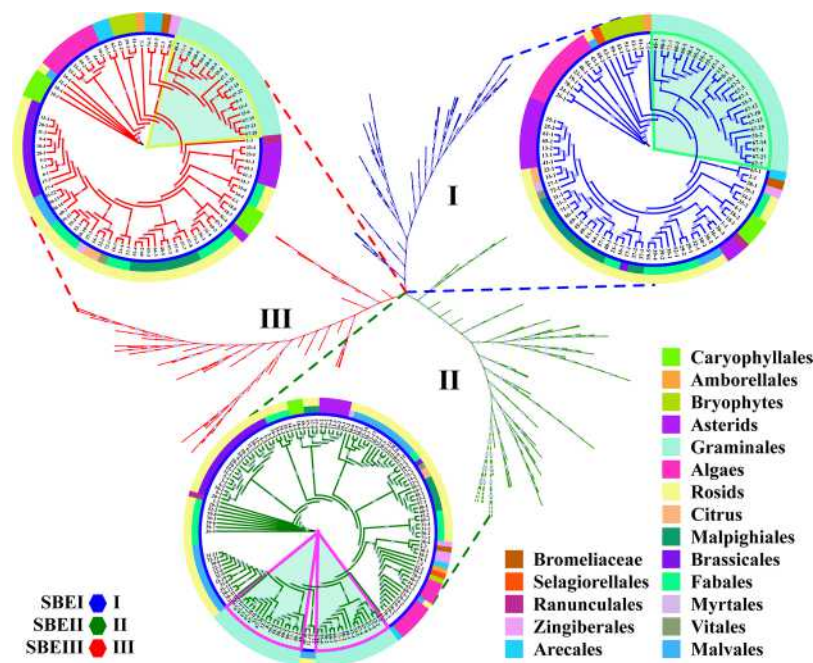


**Figure 7.** Phylogenetic analysis of the amino acid sequences of SBE in 74 plant species. Sequences classified into subfamilies I–III are shown in colour. Clade I, clade II and clade III represent SBEI, SBEII and SBEIII, respectively, in 74 plant species. The branches of protein sequences in maize are highlighted in red with a light blue background. For detailed species IDs, please refer to Supplementary Table 1.

isoforms except for motifs 24 and 20 (Fig. 6A and Supplementary Fig. 7). Although special motif compositions were found among SSIII isoforms (e.g., motif 1 and motif 26), they were different from the motifs found in other SS isoforms in the GT1 and GT5 domains (Fig. 6A). The distribution of motifs in the GT5 domain was similar between SSIV and SSV, but there was a significant divergence between the motifs found in the GT1 domain of these two isoforms.

To further explore the more subtle differences among SS isoforms, we aligned the maize SSS protein sequences with the reported *Escherichia coli* glycogen synthase (EcGS) and barley SSI protein sequences (Supplementary Fig. 8). The results indicated that multiple active sites were conserved in most of these sites and that the amino acid residues at these sites were involved in the combination of glucose, ADP and maltopentaose (Fig. 6B,C and Supplementary Fig. 8). In particular, the active sites of SSV were less conserved than those of other SS isoforms, and portions of the active sites were conserved and found to be similar to those of SSIII and SSIV (Fig. 6B and Supplementary Fig. 8). Moreover, variations in the amino acid residues located in active sites also caused the associative and catalytic activities of SSV to be different from those of other SSS isoforms, especially during interactions with glucose. This result indicated that SSV may not be directly involved in the extension of glucan but may instead coordinate with other SSSs to regulate the extension of glucan. Additionally, disulfide bonds were detected only in active sites in SSI and not in other SSS isoforms (Fig. 6B). These results suggest that gene duplications likely resulted in SSS isoforms accumulating higher numbers of mutations, which resulted in their sub-functionalization or neo-functionalization. Furthermore, when we compared maize GBSS isoforms with rice GBSSI, *Agrobacterium tumefaciens* glycogen synthase (AtGS) and EcGS, we found that the binding sites for ADP and glucose were conserved in maize GBSS isoforms except for residues Lys462, Phe463, Asn464 and Ile490 (Fig. 6C and Supplementary Fig. 9)<sup>29–31</sup>. Furthermore, the only identified inter-domain disulfide bridge was found in GBSSI, and this bridge was not present in GBSSII because the amino acid residue Ile was replaced by Val (Fig. 6C and Supplementary Fig. 9). This result suggested that a nonsynonymous substitution of amino acid residues between GBSSI and GBSSII might have caused them to diverge in spatial structure and function.

**Expansion of starch branch proteins in evolution, structure and active sites.** A phylogenetic analysis of the protein sequences of SBE in 74 plant species indicated that SBE sequences could be clustered into three clades, clade I, clade II and clade III, which were designated SBEI, SBEII and SBEIII, respectively, according to the annotation for maize (Supplementary Fig. 10). In particular, almost all plant species that possessed multiple SBE isoforms were in clade II rather than clade I and clade III (Figs 2 and 7). This result indicated that the genes retained in the duplicated SBE gene pairs likely accumulated more beneficial variations than did the genes lost during evolutionary history, and this probably contributed to the diversified functions observed in the retained genes in starch metabolism (Supplementary Fig. 10 and Fig. 7).

To further explore the differential features of SBE isoforms, we analysed the domain structures of the maize SBE isoforms. The domains of these SBEs were characterized by a modular architecture composed of an N-terminal domain containing a carbohydrate-binding module family 48 (CBM48) domain, a central catalytic

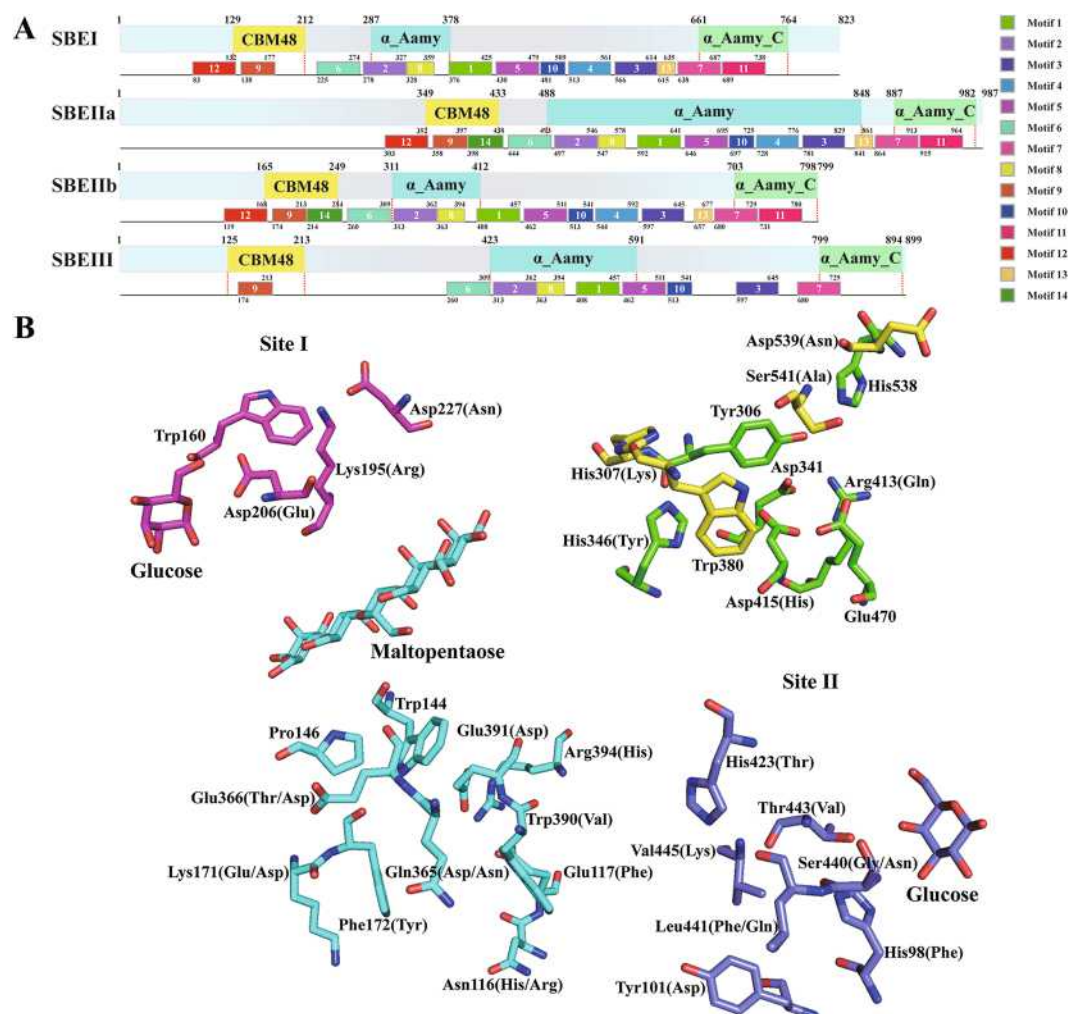


**Figure 8.** Structural and functional site analysis of maize SBE proteins. Maize is shown as an example. (A) Compositions and distributions of domain structures and conserved motifs of SBE proteins are marked and annotated in different colours. (B) Interaction site I between SBEs and glucose is shown as a magenta line. Interaction site II between SBEs and glucose are shown as light blue line, while interaction sites between SBEs and maltopentaose are shown as blue lines. The catalytic site of SBEs is shown as a green line. A yellow line indicates other active sites. Additionally, the amino acids shown in brackets represent variable sites in other SBE isoforms.

domain ( $\alpha$ -amylase) characterized by a  $(\beta/\alpha)_8$ -barrel, as well as an  $\alpha$ -amylase C-terminal domain (Fig. 8A). Moreover, an overall structure model analysis demonstrated that while the secondary structures of SBEI, SBEIIa and SBEIIb were highly similar, some  $\alpha$  helix and  $\beta$  sheets were absent in the CBM48 and  $\alpha$ -amylase domains of SBEIII (Supplementary Fig. 11). Additionally, a conserved motif analysis showed that motif 14 was only present in SBEIIa and SBEIIb, and multiple motifs were not found in SBEIII (Fig. 8A and Supplementary Fig. 12).

The differences in functional regions or sites among the SBE isoforms were investigated by aligning maize SBE protein sequences with those reported for rice BEI (approximately 84% identity)<sup>32,33</sup>. The results indicated that some of the binding sites for maltopentaose and glucose were not conserved among SBE isoforms, and the alternative residues were mainly found in SBEIII (Fig. 8B and Supplementary Fig. 13). The catalytic sites of the maize SBE isoforms were relatively more conserved than those of rice BEI and branching enzyme (EcGBE) of *Escherichia coli*, except for Y495, Q559 and H561 in SBEIII (Fig. 8B and Supplementary Fig. 13). These phenomena indicate that SBEIII may perform different biological functions during starch metabolism than other SBE isoforms. Additionally, a comparative analysis of cyclodextrin (CD)-binding sites between EcGBE and maize SBE isoforms revealed that CD-binding sites I and V in SBEI, CD-binding sites VI and VII in SBEIIa and SBEIIb, and CD-binding sites III and IV in SBEIII were relatively conserved and that CD-binding site II was more conserved in SBEIIa, SBEIIb and SBEIII than in SBEI (Fig. 8B and Supplementary Fig. 13).

**Evolutionary, structural and functional features of starch de-branching proteins.** DBE protein sequences from ancestral lineages of algae, mosses, ferns, monocots and eudicots were used to construct a phylogenetic tree. The analysis showed that DBEs could be clustered into four clades, clade I, clade II, clade III and



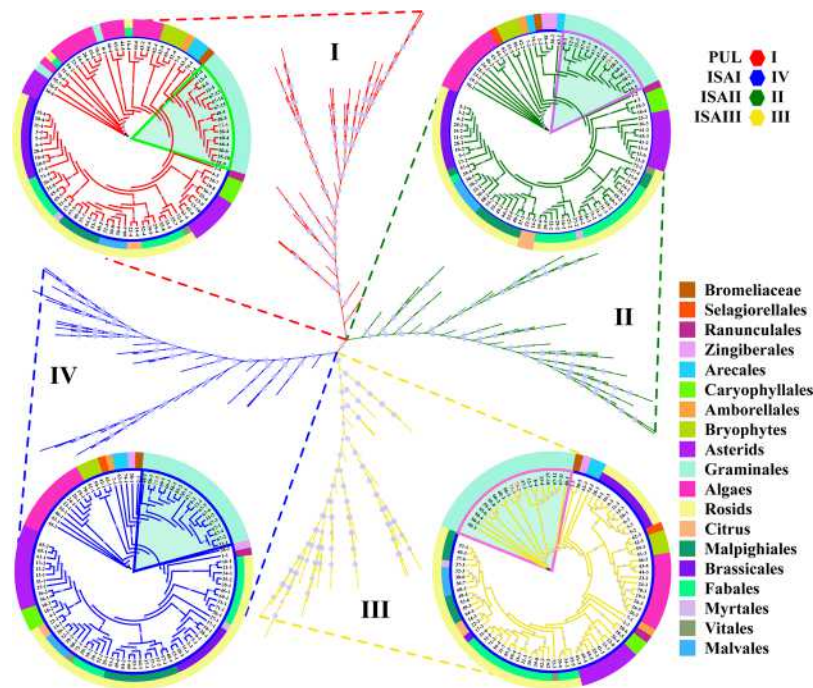


**Figure 9.** Phylogenetic analysis of the amino acid sequences of DBE in 74 plant species. Sequences classified into subfamilies I–IV are shown in colour. Clade I, clade II, clade III and clade IV represent PUL, ISAI, ISAI and ISAI, respectively, in 74 plant species. The branches of protein sequences in maize are highlighted in red with a light blue background. For detailed species IDs, please refer to Supplementary Table 1.

clade IV, which corresponded to ISAI, ISAI and PUL of maize, respectively (Supplementary Fig. 14). Notably, not all species have the same number of DBE isoforms. This variation in the number of DBE isoforms was closely associated with the number of AGPase, SS and SBE isoforms (Fig. 2). This result suggested that the differential inheritance of DBE genes and lineage-specific expansions was a major component of DBE gene evolution and that the expansion of DBE genes was likely regulated by gene-function balance in starch metabolism (Fig. 9 and Supplementary Fig. 14).

DBE and SBE share a common modular architecture, but the greatest difference between them is that SBEs usually have an  $\alpha$ -amylase C-domain, while isoamylase-type DBE has only a long extension area with a DUF3372 domain in pullulanase-type DBE (Fig. 10A). Further secondary structure analysis of DBE isoforms revealed that the Amy domain was more enriched in  $\alpha$  helices and  $\beta$  sheets in PUL than in ISA isoforms. As a special PUL domain, the DUF3372 domain contains six  $\alpha$  helices and seven  $\beta$  sheets (Supplementary Fig. 15). Furthermore, the divergence in secondary structures among ISA isoforms is relatively small except for motif 5 and motif 9, which are special motifs in ISAI, and motif 7, which is shared by both ISAI and su1 (also named ISAI) (Fig. 10A and Supplementary Fig. 16). These results are consistent with the DBE gene phylogeny and suggest that divergences among ISA isoforms have had little effect on their structures. Remarkably, both ISAs and PUL have unique functional regions and specific structures, indicating that they likely play unique roles in regulating the crystallization and degradation of starch.

To identify subtle differences in DBE isoforms, we aligned the protein sequences of DBE isoforms with those reported for the *Chlamydomonas* ISAI protein (52% identity with maize ISAI) and wheat PUL (74% identity with maize PUL)<sup>34–36</sup>. The analysis showed that the binding and catalytic sites of maltotriose and maltopentaose were not conserved in ISAI and that partial residues were changed in ISAI (Fig. 10B and Supplementary Fig. 17). Notably, these altered residues may not only change the configuration but may also constrain interactions between active sites and specific substrates. Additionally, five binding sites for calcium ions were found in PUL, and of these, the first to fourth were near the active cleft and the fifth was in the C terminus. These calcium ion binding sites were near the sugar moiety binding sites and catalytic sites, suggesting that calcium ions may, to some extent, affect the interactions between PUL and specific substrates (Fig. 10C).

**Temporal and spatial expression patterns of core genes for starch metabolism.** RNA-seq data obtained from multiple materials and organizations and at different developmental stages were used to explore the dynamic expression patterns of core genes related to starch synthesis in maize<sup>37</sup> (Supplementary Table 2). In embryos of the maize inbred line B73, twenty-seven key genes for starch biosynthesis could be divided into two clusters according to their expression levels, as follows: ten genes with relatively high expression and sixteen with relatively low expression (Fig. 11A). Of these, the high expression genes, including two AGPLs and two AGPSs, formed an optimal heterotetramer that could initiate starch biosynthesis in the embryo. The other six genes were

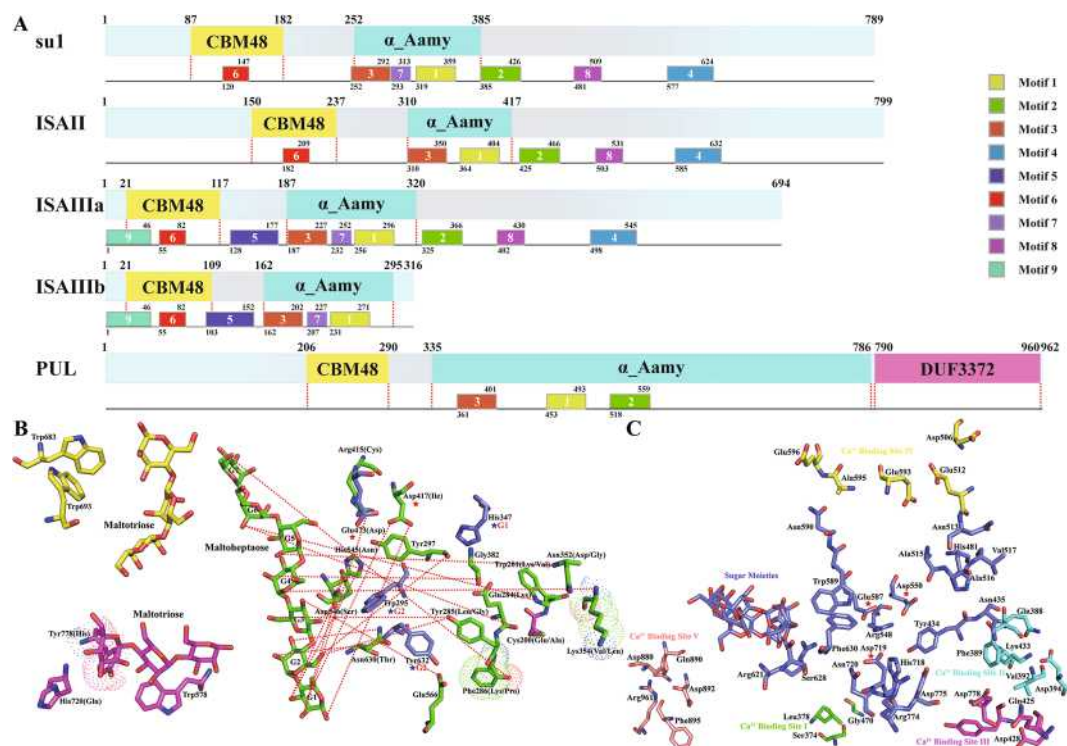


**Figure 10.** Structural and functional site analysis of maize SBE proteins. Maize is shown as an example. (A) Compositions and distributions of domain structures and conserved motifs of DBE proteins are marked and annotated in different colours. (B) Stereo view of the active sites of DBE isoforms based on the sequence of su1 and (C) PUL. In SBE isoforms, the same site with different amino acids is marked with dots. Different coloured stars and amino acids indicate different functional sites. For the detailed functions of the amino acid sites in SBE and DBE isoforms, please refer to Supplementary Figs 13 and 17.

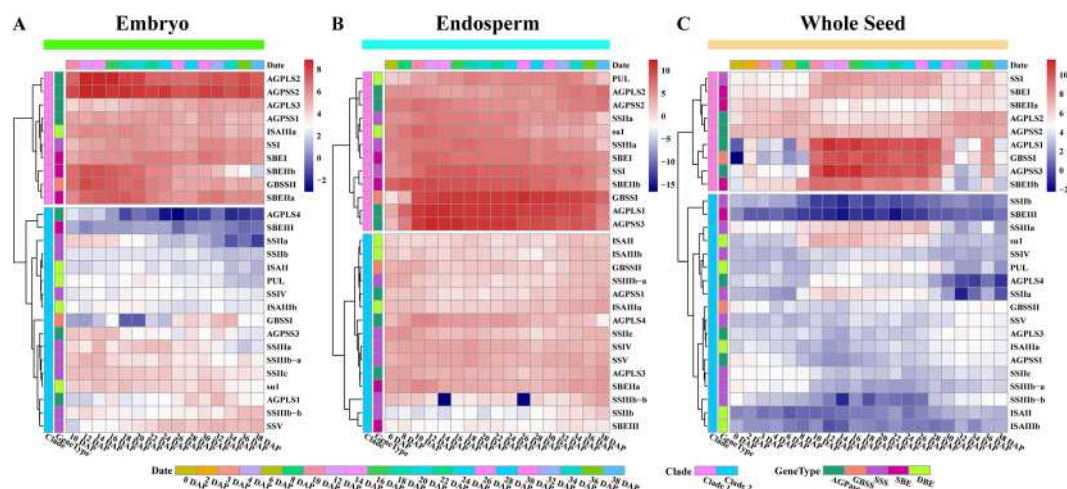


**Figure 11.** Expression patterns of starch synthesis-related genes during maize embryogenesis and endosperm and kernel development. The embryonic module includes sixteen developmental stages, the endosperm module includes eighteen developmental stages, and the whole seed module includes twenty-one developmental stages. Coloured bars represent the date, cluster and gene symbol. The scale bar shows the normalized RPKM values.

mainly responsible for the synthesis and modification of amylose and short amylopectin. These results suggested that amylose and short amylopectin were likely the main products during embryo development.

In the endosperm of maize inbred line B73, seventeen developmental stages were selected to analyse the expression patterns of key regulatory genes in starch synthesis. The results showed that twenty-seven of the expressed genes could be further divided into a cluster of fifteen relatively low-expressing genes and a cluster of twelve relatively high-expressing genes (Fig. 11B). Unlike what was observed in embryos, AGPLS1 and AGPSS3 were expressed at high levels in endosperm, in which they replaced AGPLS3 and AGPSS1 to form an optimal



heterotetramer that could initiate starch biosynthesis (Fig. 11B). In addition, GBSSI rather than GBSSII was expressed at high levels in endosperm (Fig. 11B). This observation is consistent with previous studies of the early stages of endosperm development<sup>38</sup> (Supplementary Fig. 18 and Supplementary Table S2). Notably, while AGPLS4, GBSSII, SSV and SBEIIa were expressed at high levels in the endosperm of maize hybrid SD609, they were expressed at low levels in the endosperm of maize inbred line B73 (Fig. 11 and Supplementary Fig. 18). Therefore, differences in starch synthesis in different materials is likely caused by changes in the expression levels of specific genes involved in the process of starch synthesis.

Twenty-seven core genes evaluated at twenty-one developmental stages in whole seeds of maize inbred line B73 were also divided into two clusters based on gene expression levels (Fig. 11C). In particular, we found that the expression patterns of these genes were different from those observed in embryos and endosperm in co-expression modules and an evaluation of fluctuations in the characteristics of specific gene expression patterns during seed growth. For example, AGPLS1, AGPSS3, GBSSI, SSI, SSIIa, SSIIb, SBEI, SBEIIb and SU1 were expressed at higher levels from approximately 10 days after pollination (DAP) to 30 DAP than during the early and late phases of whole-seed development. Additionally, they displayed two transition points resulting in an up-down expression pattern. This feature may be closely related to the process of seed cell development. The period from 0–10 DAP is the crucial time for cell proliferation and differentiation; while approximately 10–30 DAP, a period of rapid embryo and endosperm growth, is the crucial time for grain filling and yield formation<sup>38–42</sup>. Subsequently, the starch synthesis rate decreases and switches to a drying-out period, during which genes such as SBEIIa, AGPSS1 exhibit a down-up expression pattern throughout the process of seed development (Fig. 11C). These fluctuating expression patterns indicate that the core genes for starch synthesis likely regulate the dominant functions of starch metabolism via these expression transitions.

## Discussion

Starch biosynthesis is a highly regulated metabolic process that requires the coordinated activities of multiple enzymes, and most of the enzymes involved in these catalytic reactions are the same between amyloplasts and chloroplasts, as shown in Fig. 1. In green plants, the starch biosynthesis pathway involves a complex network of genes, most of which are members of large multigene families with multiple isoforms. However, the starch synthesis-related enzyme isoforms have not yet been identified and classified in some plants. To date, homology hybridization and PCR screening are two main strategies for screening starch biosynthesis-related genes, but because these screening processes are based on conserved known gene sequences in addition to protein isolation, purification and sequencing, they may fail to identify novel isoforms of starch biosynthesis-related enzymes that have low sequence similarities with other known genes involved in starch biosynthesis or they may fail to purify all isozymes because they may have extremely similar activities and molecular weights across green plants. Recently, the development of next-generation high-throughput sequencing technologies has provided a robust tool for using full-length cDNAs to map and quantify the genome in many plant species. This has provided unique opportunities to use genome-wide screening to study starch synthesis-related enzyme families. Moreover, combining DNA/protein sequence information from sequenced genomes with molecular biology experiments is a good strategy for isolating and verifying new genes in different plant species.

Initial starch biosynthesis can be traced back to plastid endosymbiosis in photosynthetic eukaryotes. A primary endosymbiotic event occurred in a heterotrophic eukaryotic cell that internalized a cyanobacterial cell, bringing plastids into eukaryotes, thereby rendering them able to perform oxygenic photosynthesis during the continuous evolution of cyanobacterial endosymbionts (cyanobionts)<sup>43,44</sup>. Moreover, protein-targeting machinery in the cytosol of this evolving plastid appeared and retargeted the organelle for transshipment of the remaining genes and their products. Additionally, subsequent to the endosymbiosis of the plastid, the cyanobiont polysaccharide storage metabolism was reconstructed to perform starch metabolism. Additionally, monophyletic Archaeplastida emerged and spawned three Archaeplastida lineages: Glaucophyta (glaucophytes), Rhodophyceae (red algae) and Chloroplastidae (green algae and all land plants)<sup>14,45</sup>. In particular, glaucophytes and red algae produce and store starch in the cytoplasm, whereas green algae and all land plants perform starch biosynthesis and then store starches in the plastid compartment<sup>46</sup>.

In this paper, a phylogenetic analysis suggested that the first duplication in the AGPLS family occurred earlier than the duplication in the AGPSS family, and there were more gene duplications in AGPLS than in AGPSS (Fig. 2 and Supplementary Fig. 1). In particular, AGPase is involved in the synthesis of starch, during which it acts as a heterotetramer in angiosperms and green algae. Nevertheless, there is a mismatch in the numbers of AGPLS subunits in these combinations (Supplementary Fig. 1), suggesting that AGPLS and AGPSS may have been exposed to different selection pressures over time and that the composition of these heterotetramers during starch biosynthesis may differ among different species or be dynamic across different developmental stages in the same plant species. Importantly, the two AGPLSs or the two AGPSSs in the heterotetramer perform complementary rather than redundant functions<sup>24,47</sup>. Furthermore, the spatio-temporal expression profiles of AGPase gene subunits also indicate that the potential combinations of AGPLS and AGPSS are different in different locations during starch synthesis (Fig. 11). AGPase acts as a transporter of glucose during starch synthesis, and its constituent components are key factors that limit starch accumulation to specific locations<sup>5</sup>.

The phylogenetic relationships among Ss showed that there were more gene duplications in SSII and SSIII than in other SSSs and that SSIV and SSV are phylogenetically closest. Moreover, there are more structural similarities among SSI, SSII and GBSS than among SSIII, SSIV and SSV (Fig. 6). These divergences between SS isoforms are likely related to their genetic origin and the occurrence of gene duplications. Previous studies have supported the idea that GBSS was acquired through endosymbiotic gene transfer from a symbiont<sup>14</sup>. SSI and SSII, similar to GBSS, evolved from the symbiont, while the ancestor of SSIII–SSV was transmitted via lateral gene transfer from intracellular chlamydial pathogens, and two subsequent duplications resulted in three clades encoding SSIII, SSIV and SSV<sup>10,14,23</sup>. In addition, we infer that the deletion or insertion of nucleotide fragments

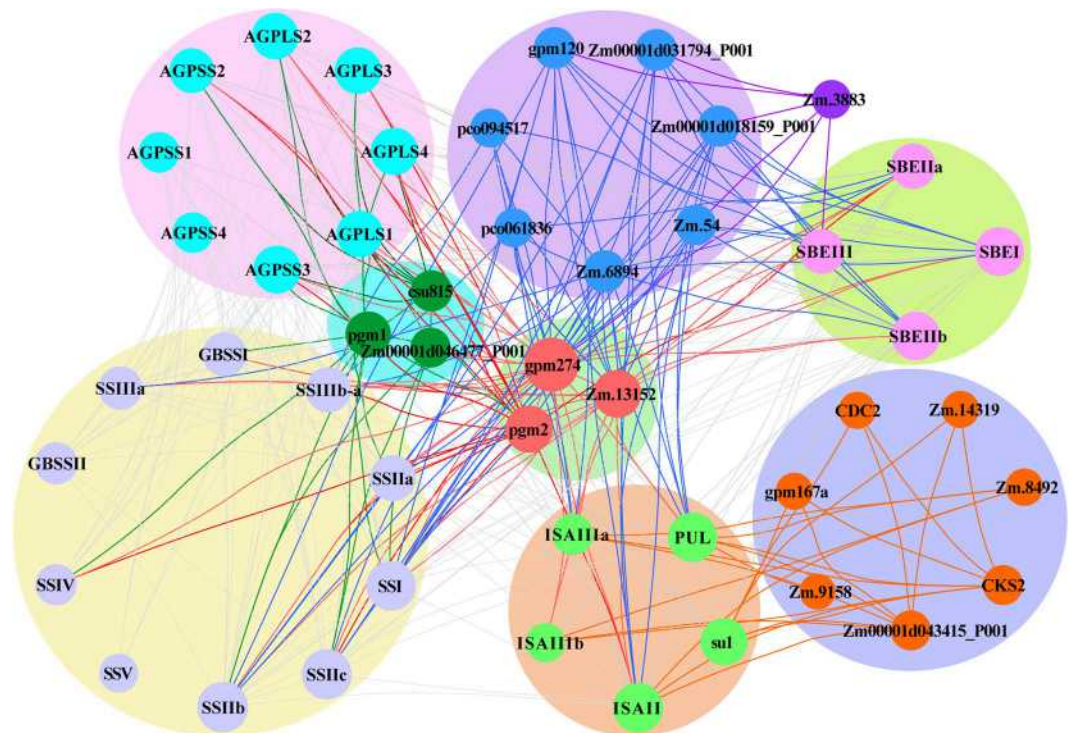


**Figure 12.** Interaction network of starch synthesis-related enzymes. Interactions among SS and AGPase subunits and SBE and DBE isoforms are shown as grey lines. Interactions between starch synthesis-related enzymes and other proteins are shown as specific coloured lines.

or sites could potentially cause functional differences in SS isoforms after gene duplication, leading to their sub-functionalization or neo-functionalization. Our phylogenetic analysis of SBEs showed that there is an obvious difference in isoform numbers among plant species and that the SBEII class is subdivided into two or more distinct gene clusters in some green plants (Supplementary Fig. 10). These results are likely related to the main types of starches present in some plant species. For example, SBEI has a preference for amylose as a substrate and transfers relatively longer glucan chains (up to DP 30, with the majority being DP 10–13), while SBEII isoforms transfer shorter chains (DP 6–14) and prefer amylopectin as a substrate.<sup>48–50</sup>

During starch metabolism, SSI and SSII isoforms and either SBEIIa or SBEIIb form a trimeric complex to regulate the starch metabolic rhythm. For example, in maize, this trimeric complex generally consists of SSI, SSIIa and SBEIIb<sup>51</sup>. Additionally, a new stromal complex involving SSI, SSIIa, SBEI, SBEIIa and phosphorylase (PHO1) was found in the amylose extender (ae1.1) mutant, and SBEIIb deficiencies have been shown to affect SSI and SBEI binding to starch granules<sup>52,53</sup>. Moreover, subsequent experiments showed that PHO1 interacts with SBEI or SBEIIb<sup>54</sup>. The outcome of the amylose extender (ae1.2) mutation experiment also showed that SSI, SSIIa, SBEI and SBEIIb form another multiple enzyme complex, and there were obvious differences in amylose content and granule size between two *ae* mutations from two near-isogenic maize lines<sup>55</sup>. Furthermore, a high molecular weight, multiple enzyme complex composed of SSIIa, SSIII, SBEIIa and SBEIIb was found in maize and was shown to further assemble into a 670-kD complex by interacting with pyruvate orthophosphate dikinase (PPDK) and the sucrose synthase isoform SUS-SH1<sup>33</sup>. A lack of SSIIIa function, as in the maize dull mutation, caused a decrease in the activity of SBEIIa and SSII. Researchers were also able to use SSIII to co-precipitate the small subunit of AGPase encoded by bt2, and the large subunit of AGPase encoded by sh2 was recovered from an SSIIIHD affinity column<sup>27,56</sup>. In particular, a temporal expression pattern analysis of genes in the 670-kD complex revealed that while the expression levels of SSIIa, SSI and SBEIIb were similar in maize endosperm, they were out of sync in embryos and whole seeds (Fig. 11). Thus, we propose that the forms this complex takes in different structures are likely to be closely related to the expression patterns of these genes. For instance, a compatible combination composed of AGPLs and AGPSs is selectively expressed at high levels in different tissues (Fig. 11).

A previous study demonstrated that SSIII isoforms and SSIV were involved in starch granule initiation, whereas SSIII and SSIV double-mutant plants could not accumulate starch<sup>57</sup>. Nevertheless, these proteins were not completely equivalent in regulating the synthesis of starch granules because SSIII but not SSIV was able to use ADP-glucose as a substrate to synthesize linear glucans without other primers<sup>57–59</sup>. The functional divergence between these isoforms was not only related to their active sites and gene expression patterns but may also have been affected by other interacting proteins. An analysis of potential interrelationships between proteins showed that core proteins involved in starch synthesis might interact directly or communicate with each other via other proteins (Fig. 12). Moreover, these starch synthases all have specific interaction proteins, except for certain proteins that form homopolymers.



A phylogenetic analysis of DBEs suggested that there is no significant difference in the numbers of ISAI, ISAI, ISAI and PUL in green plants except for the structural difference between PUL and ISAI-ISAII (Fig. 10 and Supplementary Fig. 14). Mutation experiments performed in ISAs (ISAI and ISAI) and SSIIa showed that SSIIa could compensate for a lack of ISAI in the ISAI/ISAI heteromer and coordinate the ability of the ISAI homomer to regulate normal starch crystallization and restrict phytylglycogen accumulation<sup>7</sup>. Moreover, a study of a double mutant for ISAI and PUL demonstrated that the function of PUL partially overlapped with that of ISAI and that the contribution of PUL to amylopectin trimming was much weaker than that of ISAI<sup>60</sup>. However, the details of the mechanisms underlying coordination between ISAI and PUL during the regulation of normal starch crystallization remains unclear. Nevertheless, our analysis of protein-protein interaction networks indicated that su1 remained in contact with PUL via two hub proteins, CKS2 and a protein encoded by the *Zm00001d043415* gene (Fig. 12). These results provide novel insight that increases our understanding of the detailed interrelationships between the core genes involved in starch synthesis.

## Methods

**Data collection.** In the present study, the sequenced genomes and corresponding proteomes of 74 plant species were used to establish an initial data set. These included twelve species from Fabales, ten from Brassicales, three from Malvales, two citrus species, six from Malpighiales, six aster species, two from Caryophyllales, twelve from Graminales, two from Arecales, three bryophytes, nine chlorophytes, and single genomes and proteomes from Myrtales (*Eucalyptus grandis*), Vitales (*Vitis vinifera* Genoscope), Ranunculales (*Aquilegia coerulea*), Bromeliaceae (*Ananas comosus*), Zingiberales (*Musa acuminata*), Amborellales (*Amborella trichopoda*) and Selaginellales (*Selaginella moellendorffii*). The phylogeny of these species is provided in Supplementary Table 1. Starch synthesis-related gene expression data were obtained from examined RNA-seq data for the maize (*Zea mays* L.) hybrid Shandan 609 and the inbred line B73, which were derived from our previously published (BioProject accession number PRJNA299361) and openly published papers (The National Center for Biotechnology Information Sequence Read Archive accession number SRP037559 and GenBank data library)<sup>37,38</sup>.

**Sequence retrieval.** Candidate AGPase, SS, SBE and DBE genes were initially identified using HMMER3.0 with default settings (domain signature NTP\_transferase for AGPase; GT1, GT5 and CBM25 for SS;  $\alpha$ -Amy,  $\alpha$ -Amy\_C and CBM48 for SBE; and  $\alpha$ -Amy, CBM48 and DUF3372) for each of the 74 proteome data sets<sup>61</sup>. To search for potential AGPase, SS, SBE and DBE genes, the corresponding amino acid sequences acquired in the previous step were used as queries to run a BLASTp search against the proteomes of 74 species in Phytozome with default settings (version 12.1; <http://www.phytozome.net/>). All hits obtained using the PFAM (<http://pfam.xfam.org/search>), CDD (<http://www.ncbi.nlm.nih.gov/Structure/cdd/wrpsb.cgi>), and SMART (<http://smart.embl-heidelberg.de/>) databases were further verified. Sequences that did not have a detectable domain or a threshold E-value of less than 1e-10 were excluded. Only the longest transcript was retained when two or more transcripts were identified from the alternative splicing of a gene. Finally, the genes verified by the above steps were used in this study.

**Phylogenetic analysis.** Amino acid sequences of all identified candidate AGPase, SS, SBE and DBE genes were aligned in ClustalW v2.1 with default settings<sup>62</sup>. The obtained alignments were then manually corrected in MEGA 7.0 software<sup>63</sup>. Phylogenetic trees were constructed using the maximum likelihood method with PhyML 3.0, the substitution model was assessed with the Akaike information criterion, and the reliability of internal nodes was evaluated by calculating Shimodaira-Hasegawa approximate likelihood ratio test (SH-aLRT) values<sup>64</sup>. This evaluation method has been shown to be an accurate, powerful and robust tool for processing large data sets<sup>65</sup>. Finally, the phylogenetic tree was annotated and visualized using iTOL v3<sup>66</sup>.

**Motif analysis.** All amino acid sequences of maize AGPase, SS, SBE and DBE genes were analysed with MEME (v4.11.4) to discover novel conserved patterns (<http://meme-suite.org/tools/meme>). The following parameters were used: repetitions per sequence = zero or one occurrence per sequence and the number of motifs selected was based on an E-value less than 10e-10 and other parameters as default settings.

**Structural model building.** The amino acid sequences of maize AGPase, SS, SBE and DBE isoforms were retrieved and submitted to the SWISS-MODEL (<https://swissmodel.expasy.org/>) and RCSB-PDB (<http://www.rcsb.org/pdb/home/home.do>) databases to search for the best reference model. Then, the PDB files corresponding to each starch-related enzyme isoform were analysed, visualized, and edited with PyMOL (0.99rc6) software (<http://www.pymol.org/>).

**Gene expression and protein interaction analysis.** RNA-seq data were obtained from an article that we previously published and from openly published papers and corresponding libraries that were produced using the methods described in these papers<sup>37,38</sup>. The expression levels of the four types of starch metabolism-related enzyme isoform-encoding genes were computed in RPKM (reads per kilobase of exon per million mapped reads) on maize gene models. Then, gene expression values were normalized (log2(expression value of genes)) for hierarchical clustering, and the complete linkage method as well as the Euclidean distance measure were used for hierarchical clustering of gene expression profiles with the R function hclust. Additionally, protein sequences of multiple enzyme isoforms were retrieved for protein-protein interaction analysis in string software (v10.5) (<https://string-db.org/>). The protein-protein interaction network was edited with Cytoscape software (version 3.4.0; <http://www.cytoscape.org/download.php>)<sup>67</sup>. All statistical analyses and drawings were performed using the R language (<http://www.r-project.org/>).

## References

- Pfister, B. & Zeeman, S. C. Formation of starch in plant cells. *Cell Mol Life Sci* **73**(14), 2781–807, <https://doi.org/10.1007/s00018-016-2250-x> (2016).
- Zeeman, S. C., Kossmann, J. & Smith, A. M. Starch: its metabolism, evolution, and biotechnological modification in plants. *Annu Rev Plant Biol* **61**, 209–234, <https://doi.org/10.1146/annurev-arplant-042809-112301> (2010).
- Jeon, J. S., Ryoo, N., Hahn, T. R., Walia, H. & Nakamura, Y. Starch biosynthesis in cereal endosperm. *Plant Physiol Biochem* **48**, 383–392, <https://doi.org/10.1016/j.plaphy.2010.03.006> (2010).
- Cross, J. M. *et al.* Both subunits of ADP-glucose pyrophosphorylase are regulatory. *Plant physiology* **135**, 137–144, <https://doi.org/10.1104/pp.103.036699> (2004).
- Ballicora, M. A., Iglesias, A. A. & Preiss, J. ADP-glucose pyrophosphorylase: a regulatory enzyme for plant starch synthesis. *Photosynth. Res.* **79**, 1–24, <https://doi.org/10.1023/B:PRES.0000011916.67519.58> (2004).
- Denyer, K., Waite, D., Motawia, S., Möller, B. L. & Smith, A. M. Granule-bound starch synthase I in isolated starch granules elongates malto-oligosaccharides processively. *Biochemical Journal* **340**, 183–191, <https://doi.org/10.1042/bj3400183> (1999).
- Lin, Q. *et al.* Functional interactions between starch synthase III and isoamylase-type starch-debranching enzyme in maize endosperm. *Plant physiology* **158**, 679–692, <https://doi.org/10.1104/pp.111.189704> (2012).
- Yamanouchi, H. & Nakamura, Y. Organ specificity of isoforms of starch branching enzyme (Q-enzyme) in rice. *Plant and Cell Physiology* **33**, 985–991, <https://doi.org/10.1093/oxfordjournals.pcp.a078351> (1992).
- Nakamura, Y. *et al.* Starch debranching enzyme (R-enzyme or pullulanase) from developing rice endosperm purification, cDNA and chromosomal localization of the gene. *Planta* **119**, 209–218, <https://doi.org/10.1007/bf00196561> (1996).
- Deschamps, P. *et al.* Metabolic symbiosis and the birth of the plant kingdom. *Mol Biol Evol* **25**, 536–548, <https://doi.org/10.1093/molbev/msm280> (2008).
- Ross, J., Li, Y., Lim, E. K. & Bowles, D. J. Higher plant glycosyltransferases. *Genome biology* **2**, 1–6, <https://doi.org/10.1186/gb-2001-2-2-reviews3004> (2001).
- Bateman, A., Coghill, P. & Finn, R. D. DUFs: families in search of function. *Acta Crystallogr Sect F Struct Biol Cryst Commun* **66**, 1148–1152, <https://doi.org/10.1107/S1744309110001685> (2010).
- Goodacre, N. F., Gerloff, D. L. & Uetz, P. Protein domains of unknown function are essential in bacteria. *MBio* **5**, e00744–00713, <https://doi.org/10.1128/mBio.00744-13> (2014).
- Ball, S., Colleoni, C., Cenci, U., Raj, J. N. & Tirtiaux, C. The evolution of glycogen and starch metabolism in eukaryotes gives molecular clues to understand the establishment of plastid endosymbiosis. *J Exp Bot* **62**, 1775–1801, <https://doi.org/10.1093/jxb/erq411> (2011).
- Hussain, H. Three Isoforms of Isoamylase Contribute Different Catalytic Properties for the Debranching of Potato Glucans. *Plant Cell* **15**, 133–149, <https://doi.org/10.1105/tpc.006635> (2003).
- Brust, H., Orzechowski, S., Fette, J. & Steup, M. Starch Synthesizing Reactions and Paths: *in vitro* and *in vivo* Studies. *Journal of Applied Glycoscience* **60**, 3–20, [https://doi.org/10.5458/jag.jag.JAG-2012\\_018](https://doi.org/10.5458/jag.jag.JAG-2012_018) (2013).
- Cuesta-Seijo, J. A. *et al.* Structure of starch synthase I from barley: insight into regulatory mechanisms of starch synthase activity. *Acta Crystallogr D Biol Crystallogr* **69**, 1013–1025, <https://doi.org/10.1107/S090744491300440X> (2013).
- Stamova, B. S., Laudencia-Chinguanco, D. & Beckles, D. M. Transcriptomic analysis of starch biosynthesis in the developing grain of hexaploid wheat. *Int J Plant Genomics* **2009**, 407–426, <https://doi.org/10.1155/2009/407426> (2009).
- Kang, G. *et al.* Molecular cloning and expression analysis of the starch-branching enzyme III gene from common wheat (*Triticum aestivum*). *Biochem Genet* **51**, 377–386, <https://doi.org/10.1007/s10528-013-9570-4> (2013).
- Lu, B., Guo, Z. & Liang, J. Effects of the activities of key enzymes involved in starch biosynthesis on the fine structure of amylopectin in developing rice (*Oryza sativa* L.) endosperms. *Sci China C Life Sci* **51**, 863–871, <https://doi.org/10.1007/s11427-008-0120-y> (2008).
- Nakamura, Y., Aihara, S., Crofts, N., Sawada, T. & Fujita, N. *In vitro* studies of enzymatic properties of starch synthases and interactions between starch synthase I and starch branching enzymes from rice. *Plant Sci* **224**, 1–8, <https://doi.org/10.1016/j.plantsci.2014.03.021> (2014).
- Deschamps, P., Haferkamp, I., D'hulst, C., Neuhaus, H. E. & Ball, S. G. The relocation of starch metabolism to chloroplasts: when, why and how. *Trends Plant Sci* **13**, 574–582, <https://doi.org/10.1016/j.tplants.2008.08.009> (2008).
- Patron, N. J. & Keeling, P. J. Common Evolutionary Origin of Starch Biosynthetic Enzymes in Green and Red Algae1. *Journal of Phycolgy* **41**, 1131–1141, <https://doi.org/10.1111/j.1529-8817.2005.00135.x> (2005).
- Georgelis, N., Braun, E. L., Shaw, J. R. & Hannah, L. C. The two AGPase subunits evolve at different rates in angiosperms, yet they are equally sensitive to activity-altering amino acid changes when expressed in bacteria. *Plant cell* **19**, 1458–1472, <https://doi.org/10.1105/tpc.106.049676> (2007).
- Georgelis, N., Shaw, J. R. & Hannah, L. C. Phylogenetic analysis of ADP-glucose pyrophosphorylase subunits reveals a role of subunit interfaces in the allosteric properties of the enzyme. *Plant physiology* **151**, 67–77, <https://doi.org/10.1104/pp.109.138933> (2009).
- Jin, X., Ballicora, M. A., Preiss, J. & Geiger, J. H. Crystal structure of potato tuber ADP-glucose pyrophosphorylase. *The EMBO Journal* **24**, 694–704, <https://doi.org/10.1038/sj.emboj.7600551> (2005).
- Hennen-Bierwagen, T. A. *et al.* Proteins from Multiple Metabolic Pathways Associate with Starch Biosynthetic Enzymes in High Molecular Weight Complexes: A Model for Regulation of Carbon Allocation in Maize Amyloplasts. *Plant Physiol* **149**(3), 1541–1559, <https://doi.org/10.1104/pp.109.135293> (2009).
- Valdez, H. A. *et al.* Role of the N-terminal starch-binding domains in the kinetic properties of starch synthase III from *Arabidopsis thaliana*. *Biochemistry* **47**(9), 3026–3032, <https://doi.org/10.1021/bi702418h> (2008).
- Momma, M. & Fujimoto, Z. Interdomain disulfide bridge in the rice granule bound starch synthase I catalytic domain as elucidated by X-ray structure analysis. *Biosci Biotechnol Biochem* **76**, 1591–1595, <https://doi.org/10.1271/bbb.120305> (2012).
- Sheng, F., Jia, X., Yep, A., Preiss, J. & Geiger, J. H. The crystal structures of the open and catalytically competent closed conformation of *Escherichia coli* glycogen synthase. *J Biol Chem* **284**, 17796–17807, <https://doi.org/10.1074/jbc.M809804200> (2009).
- Buschiazio, A. *et al.* Crystal structure of glycogen synthase: homologous enzymes catalyze glycogen synthesis and degradation. *The EMBO Journal* **23**, 3196, <https://doi.org/10.1038/sj.emboj.7600324> (2014).
- Noguchi, J. *et al.* Crystal structure of the branching enzyme I (BEI) from *Oryza sativa* L. with implications for catalysis and substrate binding. *Glycobiology* **21**, 1108–1116, <https://doi.org/10.1093/glycob/cwr049> (2011).
- Chaen, K., Noguchi, J., Omori, T., Kakuta, Y. & Kimura, M. Crystal structure of the rice branching enzyme I (BEI) in complex with maltopentaose. *Biochem Biophys Res Commun* **424**, 508–511, <https://doi.org/10.1016/j.bbrc.2012.06.145> (2012).
- Sim, L. *et al.* Crystal structure of the Chlamydomonas starch debranching enzyme isoamylase ISA1 reveals insights into the mechanism of branch trimming and complex assembly. *J Biol Chem* **289**, 22991–23003, <https://doi.org/10.1074/jbc.M114.565044> (2014).
- Mikami, B. *et al.* Crystal structure of pullulanase: evidence for parallel binding of oligosaccharides in the active site. *J Mol Biol* **359**, 690–707, <https://doi.org/10.1016/j.jmb.2006.03.058> (2006).
- Vester-Christensen, M. B., Abou Hachem, M., Svensson, B. & Henriksen, A. Crystal structure of an essential enzyme in seed starch degradation: barley limit dextrinase in complex with cyclodextrins. *J Mol Biol* **403**, 739–750, <https://doi.org/10.1016/j.jmb.2010.09.031> (2010).



37. Chen, J. *et al.* Dynamic transcriptome landscape of maize embryo and endosperm development. *Plant physiology* **166**, 252–264, <https://doi.org/10.1104/pp.114.240689> (2014).
38. Qu, J. Z. *et al.* Transcriptome Dynamics during Maize Endosperm Development. *PLoS One* **11**, e0163814, <https://doi.org/10.1371/journal.pone.0163814> (2016).
39. Lopes, A. M. & Larkins, B. A. Endosperm Origin, Development, and Function. *The Plant cell* **5**, 1383, <https://doi.org/10.1105/tpc.5.10.1383> (1993).
40. Olsen, O. A. ENDOSPERM DEVELOPMENT: Cellularization and Cell Fate Specification. *Annual review of plant physiology and plant molecular biology* **52**, 233–267, <https://doi.org/10.1146/annurev.arplant.52.1.233> (2001).
41. Olsen, O. A. Nuclear endosperm development in cereals and Arabidopsis thaliana. *Plant cell* **16**(Suppl), S214–227, <https://doi.org/10.1105/tpc.017111> (2004).
42. Leroux, B. M. *et al.* Maize early endosperm growth and development: from fertilization through cell type differentiation. *Am J Bot* **101**, 1259–1274, <https://doi.org/10.3732/ajb.1400083> (2014).
43. Moreira, D., Le Guyader, H. & Herve, P. The origin of red algae and the evolution of chloroplasts. *Nature* **405**, 69, <https://doi.org/10.1038/35011054> (2000).
44. Raven, J. A., Beardall, J., Flynn, K. J. & Maberly, S. C. Phagotrophy in the origins of photosynthesis in eukaryotes and as a complementary mode of nutrition in phototrophs: relation to Darwin's insectivorous plants. *J Exp Bot* **60**, 3975–3987, <https://doi.org/10.1093/jxb/erp282> (2009).
45. Adl, S. M. *et al.* The new higher level classification of eukaryotes with emphasis on the taxonomy of protists. *J Eukaryot Microbiol* **52**, 399–451, <https://doi.org/10.1111/j.1550-7408.2005.00053.x> (2005).
46. Ball, S. G. & Morell, M. K. From bacterial glycogen to starch: understanding the biogenesis of the plant starch granule. *Annu Rev Plant Biol* **54**, 207–233, <https://doi.org/10.1146/annurev.arplant.54.031902.134927> (2003).
47. Hannah, L. C. & Nelson, O. E. Jr. Characterization of ADP-glucose pyrophosphorylase from shrunken-2 and brittle-2 mutants of maize. *Biochem Genet* **14**, 547–560, <https://doi.org/10.1007/bf00485834> (1976).
48. Takeda, Y., Guan, H. P. & Preiss, J. Branching of amylose by the branching isoenzymes of maize endosperm. *Carbohydr Res* **240**, 253–263, [https://doi.org/10.1016/0008-6215\(93\)84188-C](https://doi.org/10.1016/0008-6215(93)84188-C) (1993).
49. Kuriki, T., Stewart, D. C. & Preiss, J. Construction of chimeric enzymes out of maize endosperm branching enzymes I and II: activity and properties. *J. Biol. Chem.* **272**, 28999–29004, <https://doi.org/10.1074/jbc.272.46.28999> (1997).
50. Guan, H. P. & Preiss, J. Differentiation of the properties of the branching isozymes from maize (*Zea mays*). *Plant Physiol* **102**, 1269–1273, <https://doi.org/10.1104/pp.102.4.1269> (1993).
51. Tetlow, I. J. *et al.* Analysis of protein complexes in wheat amyloplasts reveals functional interactions among starch biosynthetic enzymes. *Plant physiology* **146**, 1878–1891, <https://doi.org/10.1104/pp.108.116244> (2008).
52. Liu, F. *et al.* The amylose extender mutant of maize conditions novel protein-protein interactions between starch biosynthetic enzymes in amyloplasts. *J Exp Bot* **60**, 4423–4440, <https://doi.org/10.1093/jxb/erp297> (2009).
53. Abe, N. *et al.* Relationships between starch synthase I and branching enzyme isozymes determined using double mutant rice lines. *BMC plant biology* **14**, 80, <https://doi.org/10.1186/1471-2229-14-80> (2014).
54. Subasinghe, R. M. *et al.* Multimeric states of starch phosphorylase determine protein-protein interactions with starch biosynthetic enzymes in amyloplasts. *Plant Physiology and Biochemistry* **83**, 168–179, <https://doi.org/10.1016/j.plaphy.2014.07.016> (2014).
55. Liu, F. *et al.* Allelic variants of the amylose extender mutation of maize demonstrate phenotypic variation in starch structure resulting from modified protein-protein interactions. *J Exp Bot* **63**, 1167–1183, <https://doi.org/10.1093/jxb/err341> (2012).
56. Cao, H., James, M. G. & Myers, A. M. Purification and Characterization of Soluble Starch Synthases from Maize Endosperm. *Archives of Biochemistry and Biophysics* **373**, 135–146, <https://doi.org/10.1006/abbi.1999.1547> (2000).
57. Szydlowski, N. *et al.* Starch granule initiation in Arabidopsis requires the presence of either class IV or class III starch synthases. *The Plant cell* **21**, 2443–2457, <https://doi.org/10.1105/tpc.109.066522> (2009).
58. Roldan, I. *et al.* The phenotype of soluble starch synthase IV defective mutants of Arabidopsis thaliana suggests a novel function of elongation enzymes in the control of starch granule formation. *The Plant journal: for cell and molecular biology* **49**, 492–504, <https://doi.org/10.1111/j.1365-3113X.2006.02968.x> (2007).
59. Liu, H. *et al.* Identification and Phylogenetic Analysis of a Novel Starch Synthase in Maize. *Front Plant Sci* **6**, 1013, <https://doi.org/10.3389/fpls.2015.01013> (2015).
60. Fujita, N. *et al.* Characterization of pullulanase (PUL)-deficient mutants of rice (*Oryza sativa* L.) and the function of PUL on starch biosynthesis in the developing rice endosperm. *J Exp Bot* **60**, 1009–1023, <https://doi.org/10.1093/jxb/ern349> (2009).
61. Finn, R. D. *et al.* Pfam: the protein families database. *Nucleic acids research* **42**, D222–230, <https://doi.org/10.1093/nar/gkt1223> (2014).
62. Larkin, M. A. *et al.* Clustal W and Clustal X version 2.0. *Bioinformatics* **23**, 2947–2948, <https://doi.org/10.1093/bioinformatics/btm404> (2007).
63. Kumar, S., Stecher, G. & Tamura, K. MEGA7: Molecular Evolutionary Genetics Analysis Version 7.0 for Bigger Datasets. *Mol Biol Evol* **33**, 1870–1874, <https://doi.org/10.1093/molbev/msw054> (2016).
64. Guindon, S. *et al.* New algorithms and methods to estimate maximum-likelihood phylogenies: assessing the performance of PhyML 3.0. *Syst Biol* **59**, 307–321, <https://doi.org/10.1093/sysbio/syq010> (2010).
65. Anisimova, M., Gil, M., Dufayard, J. F., Dessimoz, C. & Gascuel, O. Survey of branch support methods demonstrates accuracy, power, and robustness of fast likelihood-based approximation schemes. *Syst Biol* **60**, 685–699, <https://doi.org/10.1093/sysbio/syr041> (2011).
66. Letunic, I. & Bork, P. Interactive tree of life (iTOL)v3: an online tool for the display and annotation of phylogenetic and other trees. *Nucleic acids research* **44**, W242–245, <https://doi.org/10.1093/nar/gkw290> (2016).
67. Shannon, P. *et al.* Cytoscape: a software environment for integrated models of biomolecular interaction networks. *Genome research* **13**, 2498–2504, <https://doi.org/10.1101/gr.1239303> (2003).
68. Crevillen, P., Ballicora, M. A., Merida, A., Preiss, J. & Romero, J. M. The different large subunit isoforms of Arabidopsis thaliana ADP-glucose pyrophosphorylase confer distinct kinetic and regulatory properties to the heterotetrameric enzyme. *J Biol Chem* **278**, 28508–28515, <https://doi.org/10.1074/jbc.M304280200> (2003).
69. Fujita, N. *et al.* Function and characterization of starch synthase I using mutants in rice. *Plant physiology* **140**, 1070–1084, <https://doi.org/10.1104/pp.105.071845> (2006).
70. Nakamura, Y. *et al.* Essential amino acids of starch synthase IIa differentiate amylopectin structure and starch quality between japonica and indica rice varieties. *Plant molecular biology* **58**, 213–227, <https://doi.org/10.1007/s11103-005-6507-2> (2005).
71. Fujita, N. *et al.* Characterization of SSIIa-deficient mutants of rice: the function of SSIIa and pleiotropic effects by SSIIa deficiency in the rice endosperm. *Plant physiology* **144**, 2009–2023, <https://doi.org/10.1104/pp.107.102533> (2007).
72. Zhang, X. *et al.* Overlapping functions of the starch synthases SSII and SSIII in amylopectin biosynthesis in Arabidopsis. *BMC plant biology* **8**, 96, <https://doi.org/10.1186/1471-2229-8-96> (2008).
73. Nishi, A., Nakamura, Y., Tanaka, N. & Satoh, H. Biochemical and Genetic Analysis of the Effects of Amylose-Extender Mutation in Rice Endosperm. *Plant physiology* **127**, 459–472, <https://doi.org/10.1104/pp.010127> (2001).
74. Satoh, H. *et al.* Starch-branching enzyme I-deficient mutation specifically affects the structure and properties of starch in rice endosperm. *Plant physiology* **133**, 1111–1121, <https://doi.org/10.1104/pp.103.021527> (2003).

75. Delatte, T., Trevisan, M., Parker, M. L. & Zeeman, S. C. Arabidopsis mutants Atisa1 and Atisa2 have identical phenotypes and lack the same multimeric isoamylase, which influences the branch point distribution of amylopectin during starch synthesis. *The Plant journal: for cell and molecular biology* **41**, 815–830, <https://doi.org/10.1111/j.1365-313X.2005.02348.x> (2005).
76. Streb, S. *et al.* Starch granule biosynthesis in Arabidopsis is abolished by removal of all debranching enzymes but restored by the subsequent removal of an endoamylase. *The Plant cell* **20**, 3448–3466, <https://doi.org/10.1105/tpc.108.063487> (2008).
77. Yun, M. S., Umemoto, T. & Kawagoe, Y. Rice debranching enzyme isoamylase3 facilitates starch metabolism and affects plastid morphogenesis. *Plant Cell Physiol* **52**, 1068–1082, <https://doi.org/10.1093/pcp/pcr058> (2011).
78. Takashima, Y. *et al.* Differential chain-length specificities of two isoamylase-type starch-debranching enzymes from developing seeds of kidney bean. *Bioscience, Biotechnology, and Biochemistry* **71**, 2308–2312, <https://doi.org/10.1271/bbb.70215> (2007).

## Acknowledgements

We would like to thank Chuang Ma and Xiaojun Nie for comments on the manuscript and discussions. This work was supported by National Natural Science Foundation of China (31371626), Shaanxi Province Science and Technology Innovation coordination Project (2015KTZDNY01-01-01), the Fund of Northwest A&F University (Z111021403 and Z109021514) and the Natural Key Research and Development Program of China (2017YFD0300304).

## Author Contributions

Jianzhou Qu, Jiquan Xue, and Dongwei Guo initially conceived the project. Jianzhou Qu designed, performed, and analyzed experiments. Jianzhou Qu wrote the original draft. Jianzhou Qu, Dongwei Guo, Shutu Xu, Zhengquan Zhang, Guangzhou Chen, Yuyue Zhong, Linsan Liu, Renhe Zhang, and Jiquan Xue reviewed and edited the manuscript.

## Additional Information

**Supplementary information** accompanies this paper at <https://doi.org/10.1038/s41598-018-30411-y>.

**Competing Interests:** The authors declare no competing interests.

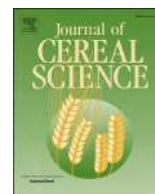
**Publisher's note:** Springer Nature remains neutral with regard to jurisdictional claims in published maps and institutional affiliations.



**Open Access** This article is licensed under a Creative Commons Attribution 4.0 International License, which permits use, sharing, adaptation, distribution and reproduction in any medium or format, as long as you give appropriate credit to the original author(s) and the source, provide a link to the Creative Commons license, and indicate if changes were made. The images or other third party material in this article are included in the article's Creative Commons license, unless indicated otherwise in a credit line to the material. If material is not included in the article's Creative Commons license and your intended use is not permitted by statutory regulation or exceeds the permitted use, you will need to obtain permission directly from the copyright holder. To view a copy of this license, visit <http://creativecommons.org/licenses/by/4.0/>.

© The Author(s) 2018





# Effects of extrusion treatment on physicochemical properties and *in vitro* digestion of pregelatinized high amylose maize flour

Xudong Zhang<sup>1</sup>, Yaofeng Chen<sup>\*\*</sup>, Renhe Zhang<sup>1</sup>, Yuyue Zhong, Yan Luo, Shutu Xu, Jianchao Liu, Jiquan Xue<sup>1</sup>, Dongwei Guo<sup>\*</sup>

The Key Laboratory of Biology and Genetics Improvement of Maize in Arid Area of Northwest Region, Ministry of Agriculture, College of Agronomy, Northwest A & F University, Yangling, 712100, Shaanxi, China

## ARTICLE INFO

### Article history:

Received 6 July 2015

Received in revised form

18 December 2015

Accepted 20 January 2016

Available online 22 January 2016

### Chemical compounds studied in this article:

Iodine (PubChem CID: 807)

Sodium chloride (PubChem CID: 5234)

Hydrochloric acid (PubChem CID: 313)

Copper(II) sulfide (PubChem CID: 14831)

Sulphuric acid (PubChem CID: 1118)

Potassium chloride (PubChem CID: 4873)

### Keywords:

Amylose

Extrusion

Digestion

Resistant starch

## ABSTRACT

High amylose maize flour (HAMF), normal maize flour (NMF), extruded normal maize flour (ENMF) and extruded high amylose maize flour (EHAMF) were employed to analyze the effects of the extrusion process on their physicochemical properties and *in vitro* digestion. The disruption degree of NMF and HAMF under extrusion followed the degree of gelatinization order. HAMF and EHAMF had higher onset temperature, peak temperature and conclusion temperature but lower melting enthalpies in comparison with NMF and ENMF. Extrusion treatment decreased viscosity and transformed A-type and B-type starch in NMF and HAMF into B + V-type. The solubility of all samples and swelling power of NMF and HAMF showed an increase, while swelling power of extruded maize flour decreased with increasing temperature. HAMF and EHAMF had a higher content of resistant starch but a lower content of slowly digestible starch and rapidly digestible starch than NMF and ENMF.

© 2016 Elsevier Ltd. All rights reserved.

## 1. Introduction

Maize is a rich nutritional source of vitamins, minerals and functional elements, which can meet high demands of the growing

**Abbreviations:** AACC, American Association of Cereal Chemistry; AOAC, Association of Official Analytical Chemists; DG, degree of gelatinization; DSC, differential scanning calorimeter; EHAMF-I, extruded high amylose maize flour with initial moisture content of 12.47%; EHAMF-II, extruded high amylose maize flour with initial moisture content of 19.00%; ENMF, extruded normal maize flour; HAMF, High amylose maize flour; NMF, normal maize flour; RDS, rapidly digestible starch; RS, resistant starch; RVA, rapid visco-analyser; SDS, slowly digestible starch; SEM, scanning electron microscope; SOL, solubility; SP, swelling power; T<sub>0</sub>, onset temperature; T<sub>p</sub>, peak temperature; T<sub>c</sub>, conclusion temperature; ΔH, enthalpy change; ΔT, the difference between conclusion temperature and onset temperature.

\* Corresponding author.

\*\* Corresponding author.

E-mail addresses: [chenyf3828@126.com](mailto:chenyf3828@126.com) (Y. Chen), [gdwei@nwsuaf.edu.cn](mailto:gdwei@nwsuaf.edu.cn) (D. Guo).

<sup>1</sup> Equal contribution to the work.

<http://dx.doi.org/10.1016/j.jcs.2016.01.005>

0733-5210/© 2016 Elsevier Ltd. All rights reserved.

society. Starch is the major component of maize accounting for about 70%. Normal maize starch is commonly composed of approximately 25% amylose and 75% amylopectin. The starch with more than 50% amylose is defined as high amylose starch. It is beneficial for industrial and food applications and it has been widely used as a bonding agent, setting agent, corrugated case, degradable plastic, food additive, packing material, and cream or gelatin substitution, etc. Some previous papers have reported extrusion parameters of high amylose maize starch and properties of extruded high amylose maize starch. Lai and Kokini (1992) estimated the viscous heat effects in slit flows of 98% amylopectin and 70% amylose corn starches under extrusion treatment. Shrestha et al. (2010) studied the enzymatic resistance and structural organization in extruded high amylose maize starch. However, high amylose flour is different from high amylose starch in application and processing due to their different components and properties. To investigate physicochemical properties, *in vitro* digestibility of extruded high amylose flour may provide much more

valuable information for processing of high amylose puffed food.

One way to overcome the stability of high amylose maize is using extrusion cooking. It has been widely used to produce expanded snack foods, ready-to-eat cereals and pet foods in recent years. The high temperature with short time extrusion cooking has a significant effect on modification of the physicochemical properties of starch-based raw material. The thermal energy released by viscous dissipation during extrusion quickly changes the quality of raw material including viscosity, internal structure, texture, digestibility, palatability, etc. Specifically, the quality of products considerably depends on material sources as well as on processing parameters such as extruder type, screw configuration, feed moisture, temperature profile in the barrel sections, screw speed and feed rate. In the case of extrusion treatment on biopolymers, raw materials have to experience a necessary phase transition, in which the sudden pressure decrease induces certain amount of water to vaporize which shapes an expanded porous structure (Padmanabhan and Bhattacharya, 1989).

However, starch structure becomes partially destroyed and changes into more easily digestible forms altering its enzymatic resistance as a result of the extrusion treatment. Many other factors could make contribution to enzymatic resistance such as high pressure cooking/extrusion, heating time, temperature, amylose content, moisture content, and the presence of additives including sugar, lipid, and dietary fiber (Escarpa et al., 1997). According to its sensitivity to enzymatic digestion, starch can be divided into three types: rapidly digestible starch (RDS), slowly digestible starch (SDS) and resistant starch (RS). RDS is known as rapidly and completely digested in the small intestine, while SDS is considered as slowly but completely digested in the small intestine. RS has been defined as the sum of starch and products of starch degradation not absorbed by small intestine of healthy individuals in the framework of EURESTA (Kendall et al., 2004). When digested, RS induces less starch being converted to glucose resulting in decreasing glycemic index. It potentially influences on diabetes and energy intake provides fermentable carbohydrates for colonic bacteria and makes short fatty chain fatty acid beneficial for the colon and physiology. However, major RS types, like native starch granules (RS2) and retrograded or recrystallized starch (RS3) may be partially or completely destroyed under processing treatment. It is beneficial that RS2 mainly originates from high amylose maize which could retain a higher RS level after processing. For this reason, it is commonly regarded as an essential source of foodstuff with higher RS standards (Htoon et al., 2009).

Here, we designed a study, for the first time, to combine high amylose maize flour with extrusion methodology and to explore the effect of extrusion treatment on physicochemical properties. In particular, extruded high amylose maize flour with different moisture content has been characterized in the context of significant gap of degree of gelatinization, and *in vitro* digestion. The main parameters studied included morphology, thermal properties, pasting characteristics, crystal structure, solubility and swelling power. In addition, digestibility was also determined to find out the quantitative change of RDS, SDS, RS. A comparison was made between normal and high amylose maize flour subjected to extrusion treatment. It provided statistical evidence to evaluate a possibility of using high amylose maize flour as a raw material to produce HAMF-based puffed foodstuff with nutritionally higher RS levels.

## 2. Materials and methods

### 2.1. Materials

High amylose maize and normal maize cultivars were provided by the Maize Biology and Genetic Breeding Laboratory in

Northwest Arid Areas, Ministry of Agriculture, Northwest A&F University. Maize kernels were subjected to peel and germ removal using an LG-36 peeling machine (Qufu Lin Gong Machinery Co, Shan dong Province, China), and were subsequently ground to flour using a DF-35 continuous milling machine (Wenling Linda Machinery Co, Zhejiang Province, China) and passed through a mesh with 100  $\mu$ m pores for analysis. High amylose maize flour with moisture content 12.47% was extruded to make extruded high amylose maize flour (EHAMF)-I and high amylose maize flour with moisture content 19.00% was treated under the same extrusion conditions to make extruded high amylose maize flour (EHAMF)-II. They were produced to ensure an adequate gap of degree of gelatinization (the ratio of the amount of gelatinized starch to the amount of total starch) with a co-rotating twin screw extruder (DS32-II, Saixin Machinery Co, Shan dong Province, China) using a feed rate of 225 g/min, temperature of 150 °C, and screw rotational speed of 225 rpm. Extruded normal maize flour (ENMF) was also attained at the same extrusion conditions.

Pancreatin from porcine pancreas (Cat. No. P-1625, activity  $3 \times$  USP/g) was purchased from Sigma–Aldrich Chemical Company (St. Louis, Mo, USA). Amyloglucosidase (EC 3.2.1.3, 3260 Units/mL) and glucose oxidase-peroxidase assay kit (Cat. No. K-GLUC) were acquired from Megazyme (Megazyme International Ireland Ltd., Bray, Ireland).

### 2.2. Chemical composition analysis

Moisture, ash, fiber and lipid content were determined according to the protocols (AOAC, 1995). Protein content was measured using an automatic protein analyzer (Kjeltec 8400, Foss Co, Germany) with nitrogen conversion factor of 6.25. Total starch content was calculated using the HCl hydrolysis using a 3,5-Dinitrosalicylic acid (DNS) colorimetric method (Guoquan and Xiuling, 2002). Amylose content was determined with a dual wavelength iodine binding technique (Zhu et al., 2008). Amylose–iodine complex formation was used to determine the degree of gelatinization (Juansang et al., 2012).

### 2.3. Granular morphology

The morphological features of maize flour were observed with a Hitachi S-3400N field emission scanning electron microscope (Hitachi Ltd, Tokyo, Japan) equipped with Quartz PCI digital image acquisition software (Quartz Imaging Corp., Vancouver, BC, Canada). The flour samples were loaded on a metal plate with double-sided adhesive tape, coating with gold: palladium (60:40) using a Polaron SC500 sputter coater (Quorum Technologies, East Sussex, UK), and examined at 15.0 kV accelerating voltage and 500–3000 times magnification.

### 2.4. Thermal properties

Gelatinization characteristics of maize flour were measured using a differential scanning calorimeter (Q2000 DSC, TA Instruments, New Castles, DE). Each flour sample (about 3 mg dry weight) with excess water (1:3) was heated from 30 °C to 150 °C at 10 °C/min rate in sealed aluminum pans, using an empty pan as the reference. The sample was analyzed in triplicate and the data were calculated by Universal Analysis 2000 (TA Instruments, New Castles, DE).

### 2.5. Pasting properties

The pasting properties of maize flours were measured with a Rapid Visco-Analyser (RVA-SUPER 3, Newport Scientific,



Warriewood, Australia). Flour slurry (2.5 g dry basis, 20 mL of deionized water) was placed in a disposable aluminium canister. The slurry was first held at 50 °C for 1 min, heated to 95 °C at 12 °C/min, held for 2.5 min at 95 °C, cooled to 50 °C at 12 °C/min, and finally held at 50 °C for 2 min. The temperature corresponding to the initial increase in viscosity was designated as pasting temperature. The paddle would rotate at 960 rpm for the first 10 s, then at 160 rpm for the remainder of the analysis. Parameters recorded were viscosity (peak, through, final, breakdown, and setback viscosity), expressed in centipoise (cP).

## 2.6. X-ray diffraction

X-ray diffraction patterns of five different groups of maize flour were observed using Rigaku D/max 2200 pc X-ray powder diffraction (Rigaku, Tokyo, Japan) with Nickel filtered Cu K $\alpha$  radiation ( $\lambda = 1.54056 \text{ \AA}$ ) at a voltage of 40 kV and current of 30 mA. The scattered radiation was detected in the angular range of 5°–35° (2 $\theta$ ), with a scanning speed of 8° (2 $\theta$ )/min and step size of 0.02° (2 $\theta$ ). The crystalline degree was calculated with Jade 5.0.

## 2.7. Solubility and swelling power

The solubility (SOL) and swelling power (SP) of maize flour when heating to 55–95 °C in excess of deionized water were analyzed according to the method (Liu et al., 1999). SOL was derived from the ratio in weight of the dried supernatant to the initial weight of the dry starch. SP was obtained from the ratio in weight of the wet sediment to the initial weight of the dry starch.

## 2.8. In vitro digestion

*In vitro* digestion of maize flour was determined with pancreatin from porcine pancreas and amyloglucosidase (AACC, 2009). The glucose content of supernatant was measured using a glucose oxidase-peroxidase kit.

Rapidly digestible starch (RDS) was the amount of complete digested starch after incubation 0.5 h and slowly digestible starch (SDS) was the amount of complete digested starch between incubation 0.5 h and 16 h. The resistant starch (RS) was the undigested starch remaining after 16 h of incubation.

## 2.9. Statistical analysis

All analyses were measured at least in duplicate. The data were analyzed using analysis of variance (ANOVA) and expressed as mean values, whereas significance differences were examined by Duncan's test ( $P \leq 0.05$ ), using the SPSS software (SPSS Inc., Chicago, IL, USA), version 19.0.

# 3. Results and discussion

## 3.1. Chemical composition

The chemical composition data is summarized in Table 1. Moisture content in EHAMF-I, EHAMF-II, ENMF, NMF, and HAMF amounted to 6.46%, 7.28%, 7.92%, 12.75% and 12.47%, respectively. HAMF seemed to have a higher protein content than normal maize flour and the same as treated flour. One possible reason is that amylose was compounded by granular bound starch synthesis, and combined with starch granules which constrained its mobility (Morita et al., 2007). Although total starch slightly decreased in HAMF from 76.35% to 76.03% and in NMF from 77.76% to 77.33%, there were no significant differences ( $p > 0.05$ ). This was because internal  $\alpha$ -1,4-glycosidic bond of starch structure was disrupted

under extrusion treatment resulting in separation of starch molecules into low molecular products such as glucose, maltose and maltodextrin. Amylose content of HAMF considerably decreased, while NMF increased amylose content during extrusion. This result is consistent with previous studies (Goodman and Rao, 1984). The decrease of amylose content in HAMF may be induced by the higher amylose and lipid contents, where excessive leaching of amylose components was bound with free lipids to form amylose–lipid complex during extrusion cooking. In the NMF group, crude fiber and ash content increased in total from 2.79% to 3.14% and from 0.46% to 0.51%, respectively. In the HAMF group, the observed increase in crude fiber and ash was from 3.48% to 5.82% and from 0.72% to 0.80%, respectively. This might be caused by the reduction in the moisture content after extrusion, which is consistent with other reports (Bhatnagar and Hanna, 1994). The degree of gelatinization of ENMF was considerably higher than that of EHAMF. In addition, EHAMF-I showed a greater gelatinization degree than EHAMF-II. Therefore, a lower amylose and moisture contents seem to achieve a higher degree of gelatinization at the same extrusion conditions, which concurs with the report (Bhattacharya and Hanna, 1987).

## 3.2. Morphological characteristics of the flour

The morphology of starch granules in five samples analyzed by scanning electron microscopy is shown in Fig. 1. The SEM images (Fig. 1, A and B) show that normal maize starch was concentrated in larger agglomerates as spherical and polygonal granules with smoother surface than those of high amylose maize starch. In HAMF, the starch granules showed different sizes, with different shapes from oval to irregular polygons with numerous emulsion bumps (Fig. 1, C and D). However, as observed previously in other high amylose maize starch (not shown), some granules can be elongated forming filaments in various directions, whose formation was suggested to result from the aberrant initiation of new granules (Glaring et al., 2006). Occasionally, there were apparent differences in shapes and sizes between normal and high amylose maize starch granules, which probably resulted from genetic mutation of maize cultivars (Matveev et al., 2001).

Starch structure in NMF and HAMF after extrusion treatment had been partially destroyed or lost, which was manifested by irregularly shaped or sized relatively larger and nearly amorphous particles (Fig. 1, E to J). The size distribution was rather broad, ranging from small particles with the diameter of approx. a few micrometers to aggregates larger than 100  $\mu\text{m}$ . The growing coarseness can be clearly observed at 3000  $\times$  magnification, when compared with the smoother surface of the normal maize starch granules. From a general perspective, the disruption degree of starch granules in treated group was in the order of ENMF > EHAMF-I > EHAMF-II, which followed the order of degree of gelatinization. It seems that the greater the DG value, the greater the disruption level of starch granules.

## 3.3. Thermal properties

The gelatinization temperatures ( $T_0$ ,  $T_p$  and  $T_c$ ) and enthalpy ( $\Delta H$ ) of five samples are displayed in Table 2. The DSC thermogram in total exhibited a single endothermic peak (Fig. 2, A), which was created by starch gelatinization, specifically by amylopectin partition. There were significant differences in gelatinization behavior among these samples. Untreated and treated HAMF had higher gelatinization temperature than the corresponding NMF. The remarkable difference of gelatinization temperature between NMF and HAMF could be subjected to differences in protein content and starch structure. The gelatinization temperature of EHAMF-I,

**Table 1**  
Chemical composition of EHAMF-I, EHAMF-II, ENMF, NMF and HAMF.<sup>a,b</sup>

Sample	Moisture (%)	Protein (%)	Lipid (%)	Fiber (%)	Ash (%)	Total starch (%)	Amylose (%)	Degree of gelatinization (%)
EHAMF-I	6.46 ± 0.17 <sup>d</sup>	7.12 ± 0.11 <sup>a</sup>	1.18 ± 0.02 <sup>b</sup>	5.82 ± 0.13 <sup>a</sup>	0.80 ± 0.02 <sup>a</sup>	76.14 ± 0.78 <sup>a</sup>	38.69 ± 0.97 <sup>b</sup>	72.96 ± 1.28 <sup>b</sup>
EHAMF-II	7.28 ± 0.18 <sup>c</sup>	7.16 ± 0.11 <sup>a</sup>	1.10 ± 0.04 <sup>c</sup>	5.75 ± 0.07 <sup>a</sup>	0.75 ± 0.03 <sup>ab</sup>	76.03 ± 0.15 <sup>a</sup>	37.53 ± 0.94 <sup>b</sup>	66.73 ± 0.42 <sup>c</sup>
ENMF	7.92 ± 0.16 <sup>b</sup>	4.78 ± 0.09 <sup>b</sup>	1.09 ± 0.06 <sup>c</sup>	3.14 ± 0.10 <sup>c</sup>	0.51 ± 0.02 <sup>c</sup>	77.33 ± 1.66 <sup>a</sup>	28.17 ± 0.61 <sup>c</sup>	83.23 ± 2.38 <sup>a</sup>
NMF	12.75 ± 0.20 <sup>a</sup>	4.32 ± 0.12 <sup>c</sup>	1.20 ± 0.02 <sup>b</sup>	2.79 ± 0.07 <sup>d</sup>	0.46 ± 0.04 <sup>c</sup>	77.76 ± 0.45 <sup>a</sup>	26.64 ± 0.68 <sup>c</sup>	20.58 ± 2.81 <sup>d</sup>
HAMF	12.47 ± 0.18 <sup>a</sup>	7.05 ± 0.03 <sup>a</sup>	1.65 ± 0.06 <sup>a</sup>	3.48 ± 0.10 <sup>b</sup>	0.72 ± 0.04 <sup>b</sup>	76.35 ± 0.59 <sup>a</sup>	55.85 ± 1.36 <sup>a</sup>	23.27 ± 1.80 <sup>d</sup>

<sup>a</sup> Mean of three replicates. Values followed by different letters in each column indicate significant differences ( $p \leq 0.05$ ).

<sup>b</sup> EHAMF-I, extruded high amylose maize flour with initial moisture content 12.47%; EHAMF-II, extruded high amylose maize flour with initial moisture content 19.00%; ENMF, extruded normal maize flour; NMF, normal maize flour; HAMF, high amylose maize flour.

EHAMF-II and ENMF showed negative correlation with the amylose content (shown earlier in Table 1). It may be related to genetic differences between cultivars, granule structure, crystallinity transformation, and formation of complexes under extrusion conditions. NMF and ENMF showed lower  $\Delta T$  values than HAMF and treated HAMF. Clearly, extruded NMF and HAMF exhibited significantly lower melting enthalpies of gelatinization than untreated flour characterized by approximately two order of magnitude higher  $\Delta H$  values. It could be induced by a complex effect of evaporating water and to some extent by formation of amylose-lipid complexes. Interestingly, NMF and ENMF had higher melting enthalpies than HAMF and treated HAMF. This can be explained by the single peak (Fig. 2, A) mainly from melting of amylopectin components, while the second peak of amylose-lipid complexes did not appear due to the lower temperature.

### 3.4. Pasting characteristics

The pasting characteristics of five samples are also summarized in Table 2. These data suggest that extrusion treatment decreased viscosity of NMF and HAMF, where the viscosity of NMF was the highest and EHAMF-II was the lowest one. Pasting properties can be affected by several factors involving amylose content, lipid content, and amylopectin branch chain length distribution. As shown in Table 1, in terms of amylose content, NMF contained slightly elevated level of 28.17% after extrusion while HAMF showed substantial drop to 38.69% and 37.53% in EHAMF-I and EHAMF-II, respectively. The pasting temperature of treated NMF and HAMF displayed a similar trend with amylose content change. NMF and HAMF had higher peak and final viscosity than the counterparts of extruded flour. Heat-moisture treatment such as extrusion could constrain the swelling capability of starch granules as well as few leached fractions, which led to a reduction in whole pasting viscosities. A shell surrounding partially gelatinized starch granules could be produced under autoclave heating treatment, which can serve as an obstacle for water to inhibit successive pasting and gelatinization (Liu et al., 2000). Breakdown viscosity is defined as the difference between peak viscosity and through viscosity (ie. minimum viscosity), which reflects the stability of hot starch pastes. The breakdown viscosity of ENMF, EHAMF-I and EHAMF-II significantly decreased ( $P \leq 0.05$ ), indicating that treated flour are likely steadier to shear than native flour (Jyothi et al., 2010). Setback viscosity is regarded as the difference between final viscosity and through viscosity (ie. minimum viscosity), which refers to the stability of starch pastes at room temperature. Setback viscosity of NMF was significantly ( $P \leq 0.05$ ) higher than ENMF, while HAMF displayed an opposite trend. Setback value was expected to have a close relationship with the structure of amylose and amylopectin, influencing retrogradation tendency. The decrease of setback value was probably caused by additional interactions between amylose–amylose and/or amylopectin–amylopectin chain under extrusion treatment (da Rosa Zavareze et al., 2010). The pasting temperature

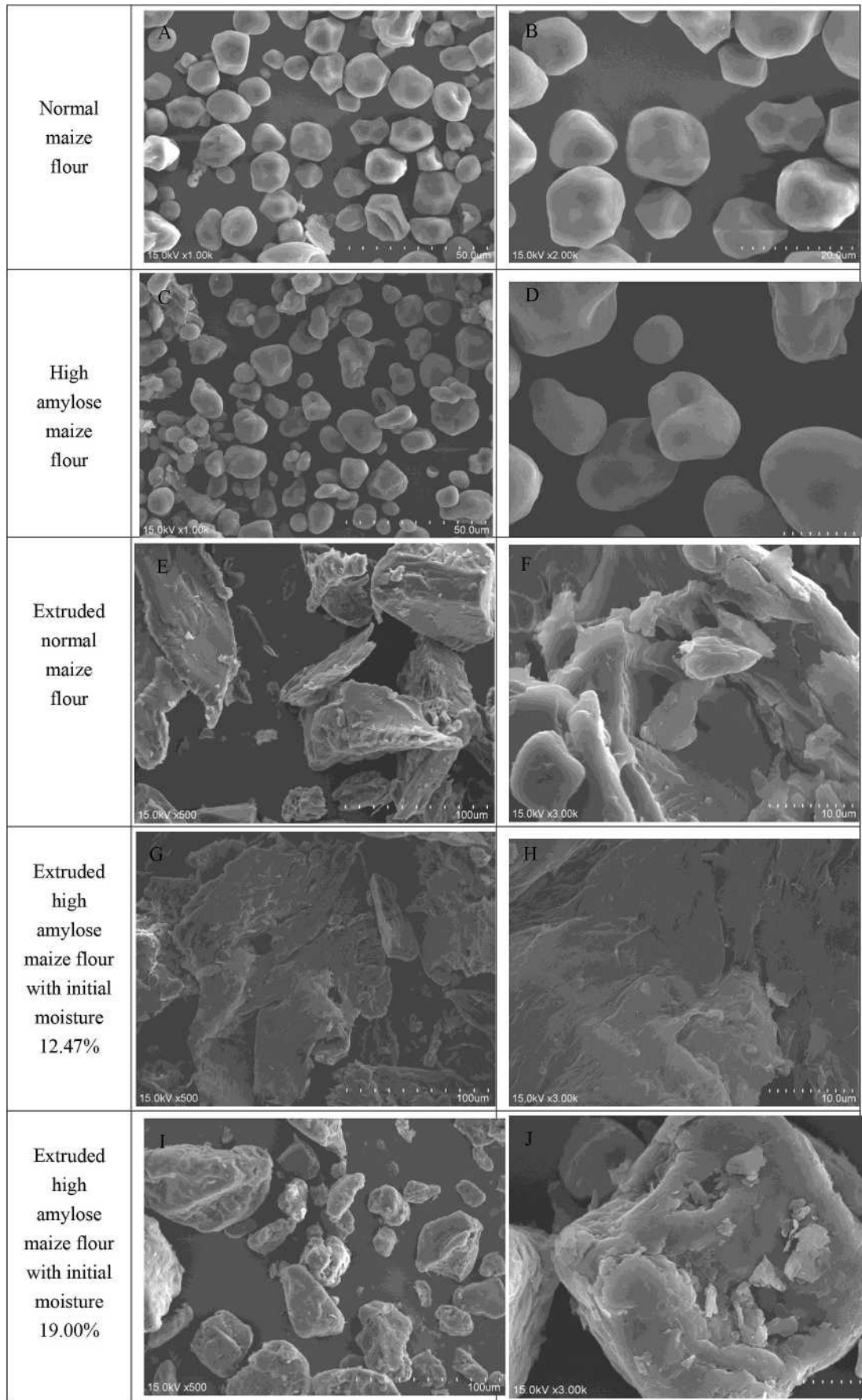
of HAMF was higher than NMF which was probably related to the formation of amylose-lipid complexes and higher protein content, where a large pool of protein probably strengthened the protein-starch bonding, lowering swelling power, and thus raising the pasting temperature (Liu et al., 2007). However, the higher viscosity of NMF may be attributed to its higher total starch content and lower protein content, in which the starch could promote swelling power of starch granules.

### 3.5. X-ray diffraction analysis

The X-ray diffraction patterns of the five samples are presented in Fig. 2, B. According to the X-ray diffraction pattern, starch structure is divided into A-type, B-type, C-type and V-type. A-type has one single peak roughly at  $2\theta$  values of  $15^\circ$ ,  $23^\circ$ , and a double peak at  $17^\circ$  and  $18^\circ$ . The specific peak of B-type occurs approximately at  $2\theta$  values of  $5.6^\circ$ ,  $17^\circ$  and  $20^\circ$  with a single peak at  $22^\circ$ ,  $24^\circ$  with a doublet. C-type is a combination of A-type and B-type. Finally, the  $2\theta$  values of V-type have peaks emerging at approximately  $7.2^\circ$ ,  $13.5^\circ$  and  $19.5^\circ$  (Buléon et al., 1998).

NMF clearly exhibited A-type with  $2\theta$  values of peak points at  $15.3^\circ$ ,  $17.24^\circ$ ,  $18^\circ$  and  $23.24^\circ$ , while HAMF was characterized by B-type with signal peaks at  $5.58^\circ$ ,  $15.08^\circ$ ,  $17.28^\circ$ ,  $20.1^\circ$ ,  $22.06^\circ$  and  $23.98^\circ$ . In general, nearly all starch granules changed their signature peaks to some extent in extrusion treatment, making it difficult to distinguish the accurate crystallinity formation (Eisenhaber and Schulz, 1992). The typical peak of B-type in HAMF may transform from around  $5.6^\circ$ – $7.0^\circ$  similarly as observed by Shrestha et al. (2010). The B-type and V-type patterns simultaneously existed in the EHAMF-I and EHAMF-II based on the  $2\theta$  values at  $7.34^\circ$ ,  $21.76^\circ$  and  $12.44^\circ$ ,  $20.18^\circ$  in EHAMF-I as well as  $6.92^\circ$ ,  $23.78^\circ$  and  $19.86^\circ$  in EHAMF-II. The A-type structure in NMF was completely degraded to the B + V-type pattern after extrusion. The formation of V-type can be attributed to closely aggregated single helices of amylose including lipid complexes which existed along with B-polymorphs in high amylose native starch (Kibar et al., 2010). NMF had the lower amylose content (26.64%) and the higher degree of crystallinity (24.99%) relative to HAMF with 55.85% amylose content and 15.48% crystallinity degree. It is worth noting that the proportion of starch crystallinity increased with decreasing amylose content among native starch groups. However, treated flour was consistent with this trend, as the crystallinity degree of EHAMF-I, EHAMF-II and ENMF were 16.72%, 28.65% and 14.38%, respectively. Previous reports showed that high amylose starch typically retains a significant level of crystallinity even under pressure cooking/extrusion whereas low amylose starch would lose the granular structure due to melting of crystallites and underlying helices, generating a more or less amorphous structure (Błaszczak et al., 2005). EHAMF-I also had a lower crystallinity degree than EHAMF-II probably due to its lower moisture content in accordance with report (Huang et al., 2004).

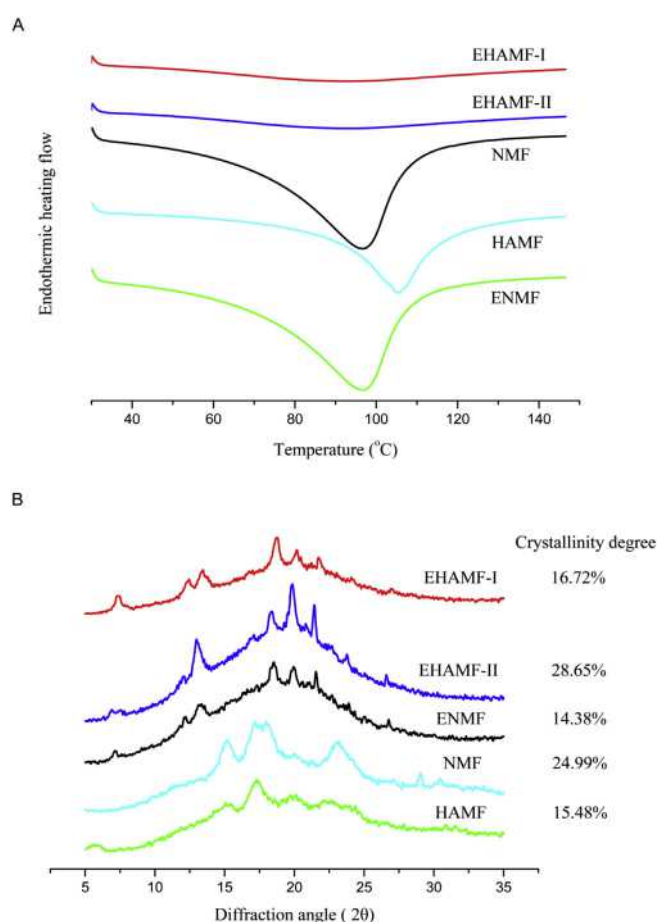




**Fig. 1.** Scanning electron micrographs of starch granules in five samples at different magnification. (A) Normal maize flour 1000 × ; (B) Normal maize flour 2000 × ; (C) High amylose maize flour 1000 × ; (D) High amylose maize flour 3000 × ; (E) Extruded normal maize flour 500 × ; (F) Extruded normal maize flour 3000 × ; (G) Extruded high amylose maize flour with initial moisture 12.47% 500 × ; (H) Extruded high amylose maize flour with initial moisture 12.47% 3000 × ; (I) Extruded high amylose maize flour with initial moisture 19.00% 500 × ; (J) Extruded high amylose maize flour with initial moisture 19.00% 3000 × .

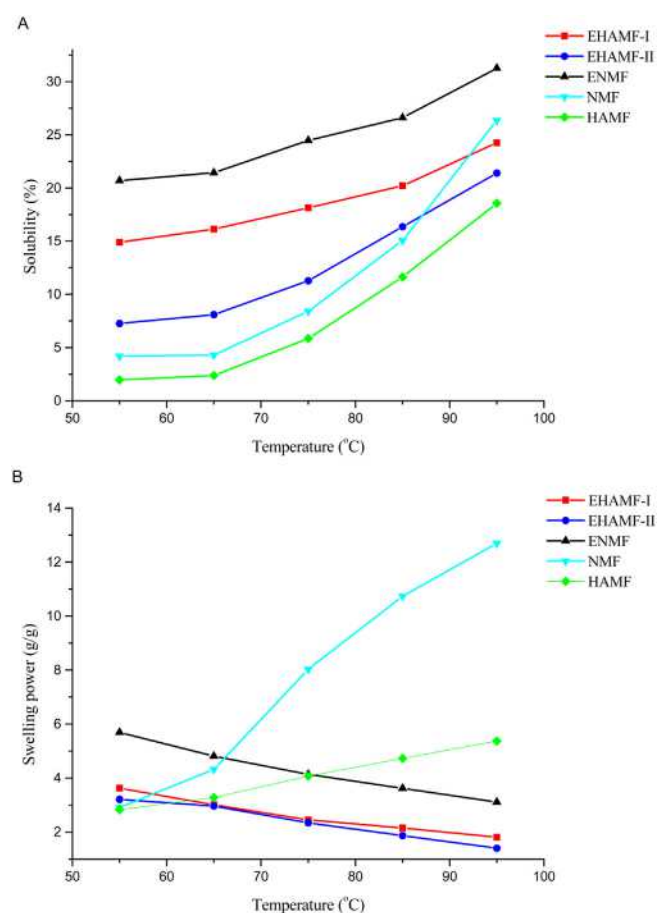
**Table 2**Gelatinization characteristics and pasting properties of EHAMF-I, EHAMF-II, ENMF, NMF and HAMF.<sup>a,b</sup>

Sample	T <sub>0</sub> (°C)	T <sub>p</sub> (°C)	T <sub>c</sub> (°C)	ΔH (J/g)	ΔT (°C)
EHAMF-I	118.4 ± 1.6 <sup>a</sup>	125.0 ± 1.7 <sup>a</sup>	136.2 ± 0.8 <sup>a</sup>	1.5 ± 0.3 <sup>c</sup>	17.9 ± 0.8 <sup>c</sup>
EHAMF-II	100.1 ± 0.5 <sup>b</sup>	117.3 ± 1.3 <sup>b</sup>	127.7 ± 0.6 <sup>b</sup>	2.6 ± 0.1 <sup>c</sup>	27.7 ± 0.2 <sup>a</sup>
ENMF	81.2 ± 0.7 <sup>d</sup>	93.4 ± 0.3 <sup>d</sup>	98.0 ± 1.9 <sup>e</sup>	3.6 ± 0.1 <sup>c</sup>	16.3 ± 0.3 <sup>c</sup>
NMF	82.9 ± 0.8 <sup>d</sup>	96.5 ± 1.0 <sup>d</sup>	105.6 ± 1.3 <sup>d</sup>	321.8 ± 2.3 <sup>a</sup>	22.8 ± 2.1 <sup>b</sup>
HAMF	90.8 ± 1.0 <sup>c</sup>	104.2 ± 1.4 <sup>c</sup>	116.6 ± 1.2 <sup>c</sup>	159.9 ± 2.1 <sup>b</sup>	25.9 ± 2.1 <sup>ab</sup>
Sample	Pasting temperature (°C)	Peak Viscosity (cP)	Breakdown (cP)	Setback (cP)	Final Viscosity (cP)
EHAMF-I	64.13 ± 2.31 <sup>a</sup>	126.33 ± 3.06 <sup>d</sup>	54.33 ± 5.03 <sup>d</sup>	23.67 ± 6.43 <sup>c</sup>	89.00 ± 5.29 <sup>c</sup>
EHAMF-II	63.70 ± 0.83 <sup>a</sup>	86.00 ± 17.09 <sup>d</sup>	27.67 ± 3.79 <sup>d</sup>	25.00 ± 4.36 <sup>c</sup>	82.33 ± 9.29 <sup>c</sup>
ENMF	64.55 ± 0.93 <sup>a</sup>	615.33 ± 27.30 <sup>b</sup>	218.67 ± 4.93 <sup>b</sup>	53.00 ± 10.58 <sup>b</sup>	315.00 ± 30.00 <sup>b</sup>
NMF	63.98 ± 0.49 <sup>a</sup>	2853.67 ± 50.96 <sup>a</sup>	1402.00 ± 34.00 <sup>a</sup>	2101.67 ± 19.04 <sup>a</sup>	3553.33 ± 40.38 <sup>a</sup>
HAMF	64.55 ± 0.93 <sup>a</sup>	406.33 ± 44.79 <sup>c</sup>	88.33 ± 2.52 <sup>c</sup>	20.00 ± 0.00 <sup>c</sup>	330.00 ± 52.46 <sup>b</sup>

<sup>a</sup> Mean of three replicates. Values followed by different letters in each column indicate significant differences ( $p \leq 0.05$ ).<sup>b</sup> EHAMF-I, extruded high amylose maize flour with initial moisture content 12.47%; EHAMF-II, extruded high amylose maize flour with initial moisture content 19.00%; ENMF, extruded normal maize flour; NMF, normal maize flour; HAMF, high amylose maize flour.**Fig. 2.** DSC thermogram and X-ray diffraction pattern of EHAMF-I, EHAMF-II, ENMF, NMF and HAMF. Data have been offset for clarity. EHAMF-I, extruded high amylose maize flour with initial moisture content 12.47%; EHAMF-II, extruded high amylose maize flour with initial moisture content 19.00%; ENMF, extruded normal maize flour; NMF, normal maize flour; HAMF, high amylose maize flour.

### 3.6. Solubility (SOL) and swelling power (SP)

The solubility and swelling power curves of five samples are shown in Fig. 3. Judging from Fig. 3, A, the solubility of all samples experienced an increase due to an accelerated dissolution of starch and non-starch components as temperature went up. ENMF had the highest solubility followed by EHAMF-I, and EHAMF-II, while

**Fig. 3.** Solubility and swelling power curves of EHAMF-I, EHAMF-II, ENMF, NMF and HAMF. EHAMF-I, extruded high amylose maize flour with initial moisture content 12.47%; EHAMF-II, extruded high amylose maize flour with initial moisture content 19.00%; ENMF, extruded normal maize flour; NMF, normal maize flour; HAMF, high amylose maize flour.

the solubility of NMF was slightly higher than that of HAMF. Thus, the extrusion treatment could increase the solubility of NMF and HAMF. All samples reached the maximum solubility at 95 °C with 31.26% in ENMF, 26.37% in NMF, 24.25% in EHAMF-I, 21.41% in EHAMF-II and 18.57% in HAMF. NMF increased the most steeply from 55 °C to 95 °C.

As shown in Fig. 3, B, the swelling power curves displayed an increase in NMF and HAMF with maximum values of 12.69%, and



5.37%, respectively, at 95 °C, where swelling power of NMF was considerably higher than that of HAMF. Presumably, swelling power might mainly reflect the amylopectin properties. A tight micelle network of internal starch granules in HAMF probably confined its swelling properties (Stone and Lorenz, 1984). Interestingly, an inverse trend occurred in treated group. ENMF had the higher SP than extruded HAMF, whereas the SP values of EHAMF-II were lower than those of EHAMF-I. This was probably because the starch granules in EHAMF-I were not completely destroyed and retained more starch particles under extrusion treatment due to the lower moisture content, higher amylose content and more steadier starch structure. In general, SP values of treated flour were greater than those of native flour at the initial temperature, while they showed an opposite trend after pasting temperature at about 65 °C. This result is consistent with Rapid Visco Analyzer data shown earlier in Table 2. This suggests that some starch granules have swollen and others were partially or completely destroyed during extrusion due to differences of starch sources, starch granule size, moisture content, etc. These swollen starch granules led to the higher swelling power of treated flour at initial temperature, and were subsequently destroyed completely to become more resistant to swelling with increasing temperature, resulting eventually in decreasing swelling power after pasting temperature.

### 3.7. *In vitro* digestion

The enzymatic *in vitro* digestion of five samples is presented in Table 3. RDS, SDS and RS content of these flour samples showed significant differences ( $p \leq 0.05$ ). The lowest RDS content existed in HAMF (19.32%) and the highest in ENMF (66.83%). SDS content ranged from 2.7% in EHAMF-I to 46.71% in NMF. RS kept the following order: HAMF (20.52%) > EHAMF-II (8.56%) > EHAMF-I (7.75%) > ENMF (5.38%) > NMF (4.52%).

Many factors could be attributed to starch digestibility such as starch source, granule morphology, granule surface and size, amylose-amylopectin ratio, the degree of molecular association among chemical components, crystallinity level, amylose chain length and amylose-lipid complexes (Vieira and Sarmiento, 2008). NMF appeared to be more susceptible to digestion than HAMF due to its higher RDS and SDS content as a result of higher amylopectin content. Although NMF and HAMF together became more vulnerable to digestion with more RDS and less SDS after extrusion treatment, EHAMF-I and EHAMF-II still had a higher level of RS content (indicating slow hydrolysis rate and low hydrolysis extent) than ENMF. The lower hydrolysis rate of EHAMF-I and EHAMF-II could be attributed to their higher amylose and protein content than in ENMF resulting from growing starch–protein combination to constrain enzyme function (Chung et al., 2008). The digestion of extruded HAMF with different moisture content showed slightly diverse tendency probably because of the starch crystallinity type and crystallinity degree transformation under extrusion treatment.

**Table 3**  
Starch fractions of digestion *in vitro* of EHAMF-I, EHAMF-II, ENMF, NMF and HAMF.<sup>a,b</sup>

Sample	RDS (%)	SDS (%)	RS (%)
EHAMF-I	65.69 ± 1.09 <sup>a</sup>	2.70 ± 0.48 <sup>d</sup>	7.75 ± 0.20 <sup>b</sup>
EHAMF-II	62.52 ± 1.05 <sup>b</sup>	4.95 ± 0.29 <sup>c</sup>	8.56 ± 0.90 <sup>b</sup>
ENMF	66.83 ± 0.45 <sup>a</sup>	5.55 ± 0.26 <sup>c</sup>	5.38 ± 0.26 <sup>c</sup>
NMF	26.10 ± 2.15 <sup>c</sup>	46.71 ± 1.57 <sup>a</sup>	4.52 ± 0.31 <sup>c</sup>
HAMF	19.32 ± 1.17 <sup>d</sup>	36.51 ± 1.60 <sup>b</sup>	20.52 ± 2.00 <sup>a</sup>

<sup>a</sup> Mean of three replicates. Values followed by different letters in each column indicate significant differences ( $p \leq 0.05$ ).

<sup>b</sup> EHAMF-I, extruded high amylose maize flour with initial moisture content 12.47%; EHAMF-II, extruded high amylose maize flour with initial moisture content 19.00%; ENMF, extruded normal maize flour; NMF, normal maize flour; HAMF, high amylose maize flour.

## 4. Conclusions

The effects of the extrusion process clearly influenced physico-chemical properties and *in vitro* digestion of the high amylose maize flours. Specifically, differences in physicochemical properties including chemical composition, morphology, thermal properties, viscosity, crystal structure, solubility, swelling power and *in vitro* digestion were characterized in native and extruded NMF and HAMF. Native and treated HAMF clearly showed the lower hydrolysis extent and slower hydrolysis rate than NMF and ENMF due to higher protein content, amylose content and melting temperature. The digestion in NMF and ENMF could be explained by their higher amylopectin content and reduced gelatinization temperature. The observed differences in digestion of treated HAMF and NMF could be regarded as an evidence for the close relationship between chemical composition and physicochemical profiles inherited by genetic differences. Our study suggests that modified HAMF via extrusion can be useful for the production of foodstuff with higher RS content, explores the change of its physicochemical properties and *in vitro* digestion and provides some available parameters for food processing. Future studies should focus on further refinement of the extrusion process to optimize the most desired parameters of the final flour products.

## Acknowledgment

The authors thank Vice Professor Guo Dongwei for his technical support and Professor Ioanna Mandala at Agricultural University of Athens. Financial support for this study is gratefully acknowledged from Scie-tech Project of Yangling City (grant number 2014NY-01), Scie-Tech Innovation, Achievement Transformation Found of Northwest A & F University (grant number Z222021317), and Tang Foundation (grant number A212021205).

## References

- AACC, 2009. Approved Methods of the American Association of Cereal Chemists (Method 32-40). American Association of Cereal Chemists, St. Paul, MN.
- AOAC, 1995. Official Methods of Analysis, sixteenth ed. AOAC International, Washington.
- Bhatnagar, S., Hanna, M.A., 1994. Amylose-lipid complex formation during single-screw extrusion of various corn starches. *Cereal Chem.* 71, 582–586.
- Bhattacharya, M., Hanna, M., 1987. Textural properties of extrusion-cooked corn starch. *Lebensmittel-Wissenschaft Technol.* 20, 195–201.
- Błaszczak, W., Fornal, J., Valverde, S., Garrido, L., 2005. Pressure-induced changes in the structure of corn starches with different amylose content. *Carbohydr. Polym.* 61, 132–140.
- Bulón, A., Colonna, P., Planchot, V., Ball, S., 1998. Starch granules: structure and biosynthesis. *Int. J. Of Biol. Macromol.* 23, 85–112.
- Chung, H.-J., Liu, Q., Hoover, R., Warkentin, T.D., Vandenberg, B., 2008. *In vitro* starch digestibility, expected glycemic index, and thermal and pasting properties of flours from pea, lentil and chickpea cultivars. *Food Chem.* 111, 316–321.
- da Rosa Zavareze, E., Storck, C.R., de Castro, L.A.S., Schirmer, M.A., Dias, A.R.G., 2010. Effect of heat-moisture treatment on rice starch of varying amylose content. *Food Chem.* 121, 358–365.
- Eisenhaber, F., Schulz, W., 1992. Monte carlo simulation of the hydration shell of double-helical amylose: a left-handed antiparallel double helix fits best into liquid water structure. *Biopolymers* 32, 1643–1664.
- Escarpa, A., Gonzalez, M., Morales, M., Saura-Calixto, F., 1997. An approach to the influence of nutrients and other food constituents on resistant starch formation. *Food Chem.* 60, 527–532.
- Glaring, M.A., Koch, C.B., Blennow, A., 2006. Genotype-specific spatial distribution of starch molecules in the starch granule: a combined CLSM and SEM approach. *Biomacromolecules* 7, 2310–2320.
- Goodman, D., Rao, R., 1984. Amylose content and puffed volume of gelatinized rice. *J. Food Sci.* 49, 1204–1205.
- Guoquan, L., Xiuling, L., 2002. Quick analysis of starch content of sweetpotato by HCl hydrolysis-DNS method. *Chin. Cereals Oils Assoc.* 17, 25–28 (in Chinese).
- Htoon, A., Shrestha, A., Flanagan, B., Lopez-Rubio, A., Bird, A., Gilbert, E., Gidley, M., 2009. Effects of processing high amylose maize starches under controlled conditions on structural organisation and amylase digestibility. *Carbohydr. Polym.* 75, 236–245.
- Huang, Q., Luo, F.-X., Yang, L.-S., 2004. Progress of research on the starch granules. *Polym. Mater. Sci. Eng.* 20, 19–23.

- Juansang, J., Puttanlek, C., Rungsardthong, V., Pancha-arnon, S., Uttapap, D., 2012. Effect of gelatinisation on slowly digestible starch and resistant starch of heat-moisture treated and chemically modified canna starches. *Food Chem.* 131, 500–507.
- Jyothi, A.N., Sajeev, M.S., Sreekumar, J.N., 2010. Hydrothermal modifications of tropical tuber starches. 1. effect of heat-moisture treatment on the physicochemical, rheological and gelatinization characteristics. *Starch-Stärke* 62, 28–40.
- Kendall, C.W., Emam, A., Augustin, L.S., Jenkins, D.J., 2004. Resistant starches and health. *J. AOAC Int.* 87, 769–774.
- Kibar, E.A.A., Gönenc, İ., Us, F., 2010. Gelatinization of waxy, normal and high amylose corn starches. *J. Food* 35, 237–244.
- Lai, L.S., Kokini, J.L., 1992. Estimation of viscous heat effects in slit flows of 98% Amylopectin (Amioca), 70% Amylose (Hylon 7) corn starches and corn meal during extrusion. *J. Food Eng.* 16, 309–318.
- Liu, H., Corke, H., Ramsden, L., 2000. The effect of autoclaving on the acetylation of ae, wx, and normal maize starches. *Starch-Stärke* 52, 353–360.
- Liu, H., Ramsden, L., Corke, H., 1999. Physical properties of cross-linked and acetylated normal and waxy rice starch. *Starch-Stärke* 51, 249–252.
- Liu, Q., Gu, Z., Donner, E., Tetlow, I., Emes, M., 2007. Investigation of digestibility in vitro and physicochemical properties of A- and B-type starch from soft and hard wheat flour. *Cereal Chem.* 84, 15–21.
- Matveev, Y.I., Van Soest, J., Nieman, C., Wasserman, L., Protserov, V., Ezernitskaja, M., Yuryev, V., 2001. The relationship between thermodynamic and structural properties of low and high amylose maize starches. *Carbohydr. Polym.* 44, 151–160.
- Morita, T., Ito, Y., Brown, I.L., Ando, R., Kiriya, S., 2007. In vitro and in vivo digestibility of native maize starch granules varying in amylose contents. *J. AOAC Int.* 90, 1628–1634.
- Padmanabhan, M., Bhattacharya, M., 1989. Extrudate expansion during extrusion cooking of foods. *Cereal Foods World (USA)* 34, 945–949.
- Shrestha, A.K., Ng, C.S., Lopez-Rubio, A., Blazek, J., Gilbert, E.P., Gidley, M.J., 2010. Enzyme resistance and structural organization in extruded high amylose maize starch. *Carbohydr. Polym.* 80, 699–710.
- Stone, L., Lorenz, K., 1984. The starch of amaranthus-physicochemical properties and functional characteristics. *Starch-Stärke* 36, 232–237.
- Vieira, F.C., Sarmiento, S., 2008. Heat-moisture treatment and enzymatic digestibility of peruvian carrot, sweet potato and ginger starches. *Starch-Stärke* 60, 223–232.
- Zhu, T., Jackson, D.S., Wehling, R.L., Geera, B., 2008. Comparison of amylose determination methods and the development of a dual wavelength iodine binding technique. *Cereal Chem.* 85, 51–58.



RESEARCH ARTICLE

# Transcriptome Dynamics during Maize Endosperm Development

Jianzhou Qu<sup>1</sup>\*, Chuang Ma<sup>2</sup>\*, Jiaojiao Feng<sup>1</sup>, Shutu Xu<sup>1</sup>, Lei Wang<sup>1</sup>, Feifei Li<sup>1</sup>, Yibo Li<sup>1</sup>, Renhe Zhang<sup>1</sup>, Xinghua Zhang<sup>1</sup>, Jiquan Xue<sup>1\*</sup>, Dongwei Guo<sup>1\*</sup>

**1** The Key Laboratory of Biology and Genetics Improvement of Maize in Arid Area of Northwest Region, Ministry of Agriculture, Northwest A&F University, Yangling, Shaanxi, China, **2** State Key Laboratory of Crop Stress Biology for Arid Areas, College of Life Sciences, Northwest A&F University, Yangling, Shaanxi, China

\* These authors contributed equally to this work.

\* [xjq2934@163.com](mailto:xjq2934@163.com) (JQX); [gdwei@nwsuaf.edu.cn](mailto:gdwei@nwsuaf.edu.cn) (DWG)



## OPEN ACCESS

**Citation:** Qu J, Ma C, Feng J, Xu S, Wang L, Li F, et al. (2016) Transcriptome Dynamics during Maize Endosperm Development. PLoS ONE 11(10): e0163814. doi:10.1371/journal.pone.0163814

**Editor:** Maoteng Li, Huazhong University of Science and Technology, CHINA

**Received:** June 23, 2016

**Accepted:** September 14, 2016

**Published:** October 3, 2016

**Copyright:** © 2016 Qu et al. This is an open access article distributed under the terms of the [Creative Commons Attribution License](https://creativecommons.org/licenses/by/4.0/), which permits unrestricted use, distribution, and reproduction in any medium, provided the original author and source are credited.

**Data Availability Statement:** The RNA-seq data has been deposited in NCBI's SRA database under the BioProject accession number PRJNA299361.

**Funding:** This work was supported by Tang Foundation (A212021207), National Natural Science Foundation of China (31371626), Shaanxi Province Science and Technology Innovation coordination Project 2015KTZDNY01-01-01 and the Fund of Northwest A&F University (Z111021403; Z109021514); grant holders: DWG.

**Competing Interests:** The authors have declared that no competing interests exist.

## Abstract

The endosperm is a major organ of the seed that plays vital roles in determining seed weight and quality. However, genome-wide transcriptome patterns throughout maize endosperm development have not been comprehensively investigated to date. Accordingly, we performed a high-throughput RNA sequencing (RNA-seq) analysis of the maize endosperm transcriptome at 5, 10, 15 and 20 days after pollination (DAP). We found that more than 11,000 protein-coding genes underwent alternative splicing (AS) events during the four developmental stages studied. These genes were mainly involved in intracellular protein transport, signal transmission, cellular carbohydrate metabolism, cellular lipid metabolism, lipid biosynthesis, protein modification, histone modification, cellular amino acid metabolism, and DNA repair. Additionally, 7,633 genes, including 473 transcription factors (TFs), were differentially expressed among the four developmental stages. The differentially expressed TFs were from 50 families, including the bZIP, WRKY, GeBP and ARF families. Further analysis of the stage-specific TFs showed that binding, nucleus and ligand-dependent nuclear receptor activities might be important at 5 DAP, that immune responses, signalling, binding and lumen development are involved at 10 DAP, that protein metabolic processes and the cytoplasm might be important at 15 DAP, and that the responses to various stimuli are different at 20 DAP compared with the other developmental stages. This RNA-seq analysis provides novel, comprehensive insights into the transcriptome dynamics during early endosperm development in maize.

## Introduction

Maize (*Zea mays*) is one of the world's most important crops and is used for food, animal feed and biofuel [1]. Development of the maize seed is initiated by double fertilization of a haploid egg cell and dikaryotic central cell to produce two filial structures: a diploid embryo and triploid endosperm. The endosperm occupies ~85% of the seed volume at maturity [2–4], providing nutrients and signals to the embryo throughout seed development and functioning as the

site of starch and protein synthesis [5–6]. Thus, understanding the gene regulatory mechanisms involved in maize endosperm development is vital to improving seed yield and quality.

Development of maize endosperm is a very complex process that takes much longer than development of *Arabidopsis thaliana* endosperm [7–9]. Maize endosperm is histologically simple yet developmentally complex, with nuclear-type development; the primary endosperm nucleus undergoes several rounds of division without cytokinesis, forming a symplasm at 0–3 DAP in which many free nuclei occupy the peripheral cytoplasm surrounding a large central vacuole [2,8]. At 4–5 DAP, the endosperm cellularization process is essentially complete, and endosperm cell differentiation and proliferation begins. A phase of mitotic cell division that occurs after cellularization is largely responsible for generating the final population of endosperm cells. The endosperm grows rapidly, from 8 to 12 DAP, filling the entire seed cavity, and the maize endosperm cells gradually and asynchronously switch from a mitotic to an endoreduplication cell cycle. Cell division continues until approximately 20 to 25 DAP in the external cell layer of the endosperm, which develops into the aleurone and subaleurone layers. During the late period of endosperm development, programmed cell death occurs in the endosperm, as manifested by nuclear deformation and cell death following amyloid enrichment [2–5,7–8,10–11]. Studies have revealed that many key physiological progresses and most vigorous metabolic activities related to endosperm development usually occur before 25 DAP. Valuable information obtained from further analyses of gene activities during the early developmental stages (before 25 DAP) will allow for a deeper understanding of the developmental mechanisms of maize endosperm.

AS results in the generation of multiple mRNA transcripts from a single gene, which increases transcriptome complexity in plants in response to physiological and environmental changes [12–14]. Furthermore, AS is a central mode of genetic regulation that controls the developmental progression of maize endosperm [15–16]. At present, AS events have been identified and documented in several tissues of maize, including the ear, embryo, endosperm, leaf, root, shoot and tassel [14,17–18]. However, most previous studies have focused on only one developmental stage, and little attention has been paid to the dynamic AS events occurring in the endosperm at different developmental stages.

High-throughput next-generation sequencing (NGS) technologies are robust tools used in transcriptome analyses that enable increased understanding of the transcriptional regulatory mechanisms involved in maize endosperm development [6,14,19–21]. However, the NGS-based transcriptome study of endosperm development is still far from complete. For instance, gene expression patterns have not been extensively analysed at 5, 10, 15 or 20 DAP [6,14,20,22–23]. In addition, most previous analyses of AS events have focused on a single time point, ignoring the dynamics of endosperm development [14,16]. Finally, the functions of differentially expressed transcription factors (DETFs) during endosperm development need to be examined [6,14].

In this study, to further understand the genome-wide transcriptional regulation of endosperm development in maize, we applied next-generation high-throughput RNA-seq to perform transcriptomic analysis of maize endosperm at 5, 10, 15 and 20 DAP and explored the dynamic AS events and gene expression patterns during maize endosperm development. We also identified stage-specific AS events, genes and TFs that may be involved in developmental pathways. Our results enabled generation of a map of the transcriptional network and revealed the dynamic patterns of AS events and TFs associated with endosperm development in maize.



## Materials and Methods

### Ethics statement

The study was approved by the Ethics Committee of Northwest A&F University, Shaanxi, China. The experimental land was provided by Northwest A&F University and this study was carried out in strict accordance with the all relevant regulations. In the process of experiment, the study did not involve endangered or protected species and all necessary permits were obtained for the described study.

### Plant materials and conditions

The maize (*Zea mays*. L) hybrid Shandan 609, derived from the hybridization of chang 7–2 (male) and 91227 (female), was grown under field conditions at approximately 67,500 plants ha<sup>-1</sup> in the summer of 2013 in Yangling, Shaanxi Province, China. The ears were bagged before silk emergence, followed by manual self-pollination. Three biological replicates of the ears were harvested at 5, 10, 15 and 20 days after self-pollination and then the endosperm tissues of the different biological replicates were separated by removing all tissues, from the pedicle up to the hilar region, after cutting open the pericarp along the edge of the hilar region using sterilised forceps and a surgical blade under a stereomicroscope (S1 Fig). To ensure for the integrity and specificity of the endosperm tissues and the absence of contamination by any other tissues, all slightly damaged endosperm tissues were discarded. Then, 60, 40, 15 and 15 complete endosperm tissues corresponding to 5, 10, 15 and 20 DAP were placed in three 2.0 mL RNase-free tubes and frozen immediately in liquid nitrogen. The tubes containing the samples were stored at -80°C prior to RNA extraction.

### RNA isolation, library construction and transcriptome sequencing

Total RNA of endosperm from three biological replicates was extracted separately from each sample using TRIzol-A+ Reagent (Invitrogen) following the manufacturer's instructions. The concentration of purified RNA was quantified using a Q5000 spectrophotometer (Quawell, San Jose, CA, USA), and RNA integrity was evaluated with an Agilent 2100 Bioanalyzer (Agilent Technologies, Santa Clara, CA, USA). An amount of 10µg RNA per sample was used for RNA sequencing. Maize endosperm mRNA sequencing libraries were constructed according to the standard Illumina protocol. RNA enrichment was achieved with an NEBNext Poly(A) mRNA Magnetic Isolation Module (NEB, E7490). RNA-seq libraries were prepared using an NEBNext mRNA Library Prep Master Mix Set for Illumina (NEB, E6110) and NEBNext Multiplex Oligos for Illumina (NEB, E7500). Fragments were size-selected by 1.8% agarose gel electrophoresis, followed by PCR amplification with a Library Quantification Kit-Illumina GA Universal (Kapa, KK4824). All established RNA-seq libraries were sequenced to generate 2×100-nucleotide paired-end reads with the Illumina HiSeq<sup>TM</sup> 2000 platform.

### Read cleaning and mapping

Clean RNA-seq reads from each sample were obtained using Trimmomatic software (<http://www.usadellab.org/cms/?page=trimmomatic>), which filters raw reads containing segments with low sequencing quality scores (quality score < 20) and/or containing two or more ambiguous nucleotides (Ns). The quality of the clean reads was examined using FASTQC software (<http://www.bioinformatics.babraham.ac.uk/projects/fastqc/>). The clean reads were aligned to the maize B73 reference genome (ZmB73\_RefGen\_v2; <http://www.maizesequence.org/>) with Tophat2 (v2.09; <http://ccb.jhu.edu/software/tophat/index.shtml>) program using Bowtie2 read alignment software [24,25], allowing for two mismatches and one insertion and/or deletion (indel).

## Detection of AS events

AS events supported by the RNA-seq data were detected and visualized using the SpliceGrapher software (v0.2.2; <http://splicegrapher.sourceforge.net>), which makes meaningful predictions even for genes with low read coverage, discriminates between real and spurious splice sites, and can improve the reliability of detection of AS [26]. Six major types of AS events were recognized: exon skipping (ES), intron retention (IR), alternative 3' splicing (A3SS), alternative 5' splicing (A5SS), alternative first exon (AFE) splicing and alternative last exon (ALE) splicing. To further verify the newly identified transcribed regions, the reads that mapped to the reference gene model were visualized using Integrative Genomics Viewer (IGV) software (v2.3.34; <https://www.broadinstitute.org/igv/>) [27]. Additionally, all alternative splice sequences of the genes were extracted and used to identify protein domains according to the Pfam database (v29.0; <http://pfam.xfam.org/>) [28].

## Estimation of gene expression abundance

The transcripts of the maize hybrid Shandan 609 were first assembled from the clean reads using Cufflinks software (v2.1.0; <http://cole-trapnell-lab.github.io/cufflinks>), and they were then used to update the annotated maize gene models (<http://www.maizesequence.org>) using Cuffmerge program (<http://cole-trapnell-lab.github.io/cufflinks/cuffmerge>). Transcripts with lengths of shorter than 200 bp were further filtered. The normalised expression level of each gene was estimated by calculating fragments per kilobase of transcript per million mapped reads (FPKM) values with Cufflinks software. The FPKM method eliminates the influences of genetic differences in length and sequence and can be used to compare gene expression between samples [29]. DEGs were identified by comparing two biological conditions using EBseq software [30], which estimates the variance of RNA-seq data without biological replicates. This program provides posterior probabilities (P-values) by adjusting for multiplicity using the Benjamini-Hochberg procedure [31], and utilizes corrected P-values to determine false discovery rates (FDRs). Detection of DEGs was based on an FDR was  $<0.01$  and no less than a two-fold change ( $\log_2$  ratio value of  $>1$  or  $<-1$ ) in FPKM between the two conditions.

## Statistical analysis

For a given gene set, enrichment analysis of Gene Ontology (GO) terms was performed using the online tool AgriGO (<http://bioinfo.cau.edu.cn/agriGO/analysis.php>) [32]. The significance levels ( $p$ -values) of the GO terms were determined with Fisher's exact test and adjusted with the Benjamini-Hochberg algorithm for multiple comparisons. A GO term was considered significantly enriched if the adjusted  $p$ -value was lower than 0.05. REVIGO (<http://revigo.irb.hr/>) was further used to summarize and visualize the enriched GO term sets in the non-redundant mode [33]. Gene expression patterns were identified by the K-mean clustering analysis with the squared Euclidean distance measure, this analysis was performed based on 15 clusters determined using the Calinski-Harabasz (CH) index [34]. Further, hierarchical clustering analysis was performed with the R package pheatmap (<https://cran.r-project.org/web/packages/pheatmap/index.html>) using Pearson's correlation coefficient as the distance measure.

## Real-time quantitative PCR

To verify the gene expression levels and AS events from determined by RNA-seq, quantitative real-time PCR was performed using SYBR green I (Bio-Rad) and a CFX96 Real-time PCR detection system (Bio-Rad, Hercules, USA). Three biological replicates were tested for each time point. Total RNA (10  $\mu$ g per sample) was reverse transcribed using a FastQuant RT Kit



(with gDNase) (TIANGEN, Beijing, CN) following the manufacturer's instructions (10  $\mu$ L of reaction mix, including 2  $\mu$ L of 10 $\times$ Fast RT Buffer, 1  $\mu$ L of RT Enzyme Mix, 2  $\mu$ L of FQ-RT Primer Mix and 5  $\mu$ L of RNase-Free ddH<sub>2</sub>O). Gene-specific primers were designed using the Primer Premier 5.0 software (Premier, CAN). To identify homologous sequences and to ensure for primer specificity, the target-specific gene sequences and primer pair sequences were blasted against the non-redundant (Nr) database and Primer-BLAST (GenBank, NCBI), respectively. The secondary structures of the gene sequences as well as the dimers and hairpin structures of the primer pair sequences, were analysed to further ensure for primer specificity. All primers were synthesised by Shenggong Corporation (Shenggong, CN). The gene-specific primer pair sequences are listed in [S1 Table](#). Quantitative real-time PCR was performed to determine transcript abundances in a total volume of 20  $\mu$ L (10  $\mu$ L of 2 $\times$ SuperReal PreMix Plus (SYBR Green) (TIANGEN, Beijing, CN), 0.6  $\mu$ L of forward primer, 0.6  $\mu$ L of reverse primer, 4.8  $\mu$ L of RNase-free ddH<sub>2</sub>O and 4  $\mu$ L of template). The thermal cycling conditions were as follows: 95°C for 15 min and 40 cycles of 95°C for 10 s, 60°C for 20 s and 72°C for 30 s, followed by a melting curve programme (95°C for 10 s, followed by an increase from 65°C to 95°C in 5 s increments of 0.5°C). Real-time PCR was performed for validation of alternatively spliced gene expression, then the products were resolved on a 1.5% agarose gel and stained with ethidium bromide to confirm the generation of specific products with the correct sizes. The house-keeping gene Actin (gene ID: *GRMZM2G082484*) was used as an endogenous reference and an internal control to normalise the C<sub>T</sub> values of the target genes in the same run [35]. The normalised C<sub>T</sub> values were manually filtered using a cut off of 35. The relative expression levels were calculated as previously described [36]. The C<sub>T</sub> values of the target genes are listed in [S2 Table](#).

## Results

### Transcriptome sequencing of endosperm at four developmental stages

To obtain an overview of the transcriptional profile during early endosperm development in maize, we utilized the Illumina HiSeq2000 platform to perform paired-end RNA-seq of the endosperm tissues at 5, 10, 15 and 20 DAP. After removing low-quality sequencing reads (reads with a quality score of smaller than 20 and/or reads containing two more ambiguous bases (Ns)), we obtained 49,371,842, 48,483,950, 50,254,726 and 44,555,238 clean reads from the endosperm tissues at 5, 10, 15 and 20 DAP, respectively ([Table 1](#)). We further mapped these clean reads to maize reference genome sequences (ZmB73\_RefGen\_v2; <http://www.maizesequence.org>) with Tophat2 (v2.09) software [24], allowing for two mismatches and one indel. The proportion of mapped reads aligned to the B73 genome sequences (70.66% ~ 75.26%) was comparable to those reported in other maize transcriptome studies [37]. The proportion of uniquely mapped reads was greater than 95% ([Table 1](#)). Furthermore, coverage of the reads mapped to the maize genome sequences varied across the four stages ([S2 Fig](#)), indicating that the transcriptome is dynamic during the early stage of maize endosperm development.

**Table 1. Statistical results for sequenced and mapped reads to the maize B73 genome.**

Stage	Clean reads	Mapped reads (%)	Unique mapped (%)	Multiple mapped (%)
<b>5 DAP</b>	49,371,842	75.18	95.95	4.05
<b>10 DAP</b>	48,483,950	70.66	95.27	4.73
<b>15 DAP</b>	50,254,726	75.26	96.02	3.98
<b>20 DAP</b>	44,555,238	74.92	95.29	4.71

doi:10.1371/journal.pone.0163814.t001

## Dynamics of alternative splicing during maize endosperm developmental stages

Using SpliceGrapher (v0.2.2) [26], we identified 44,973 AS events for 11,010 protein-coding genes at four developmental stages (S3 Table). These AS events could be grouped into the following six categories: A3SS (6,587, 14.65%), A5SS (3,715, 8.26%), AFE (5,570, 12.39%), ALE (2,933, 6.52%), IR (13,426, 29.85%) and ES (12,742, 28.33%) (Fig 1A). Among these categories, IR was the most prevalent AS event observed during maize endosperm development. This finding is in agreement with a previous study of embryo and endosperm tissues of early developing seeds at 9 DAP [14]. ES was also found to be a predominant AS event in our study (Fig 1A). This result is in contrast with previous studies of *A. thaliana*, which have reported low levels of ES (<5%) [38,39].

Further analysis revealed that dynamic AS events occurred during maize endosperm development at 5, 10, 15 and 20 DAP (Figs 1B–1C and 2). We found that the numbers of the six types of AS events differed among the four developmental stages (Fig 1B). For instance, 3,162, 3,597, 3,378 and 3,289 IR events occurred at 5, 10, 15 and 20 DAP, respectively (Fig 1B). Furthermore, a large number of maize genes exhibited stage-specific AS patterns (Fig 1C). For instance, 5,905 genes only exhibited one of the six types of AS events during one developmental stage (Fig 2A and S4 Table). These genes were belonged to several TF families, including the CAMTA (GRMZM2G447551), Dof (GRMZM2G456452 and GRMZM2G176063), GATA (GRMZM2G163200 and GRMZM2G104390), GRF (GRMZM2G096709), WOX (GRMZM2G031882 and GRMZM2G409881), and YABBY (GRMZM2G088309 and GRMZM2G529859) families, as well as the bHLH family. GRMZM2G050933 is an example of a newly identified transcribed gene with IR event (chromosome 7: 156667822–156668205). The mapped reads further verified this transcribed region (S3A Fig), and its developmentally regulated splicing event was only observed at 5 DAP (Fig 2B). We also extracted all of the exon sequences, including the retained intron sequence, and identified a novel protein domain (cyclin, C-terminal domain) using the Pfam database (S1 Table). GRMZM2G412075 is an example of a gene exhibiting the second most frequently observed type of AS event; this gene contained a novel junction, and this developmentally regulated splicing event was only observed at 15 DAP (S4 Fig). We next extracted the complete exon sequences, in addition to all of the complete, non-overlapping exon sequences, and Pfam analysis showed that the protein domain belonged to the RRM\_1 and poly-adenylate binding protein (PABP) families. Interestingly, the position of the protein domain formation (Poly-adenylate binding protein, PABP) moved forward to the 5' end in sequence and the length of annotation decreased when the overlapping exon sequences were removed (S1 Table). We also detected genes with A5SS or A3SS events (S5 and S6 Figs), and some genes with AS events were selected for validation by qRT-PCR (S7 Fig). Rigorous GO analysis revealed the functional enrichment of genes with single AS events in diverse biological processes, such as intracellular protein transport, signal transmission, cellular carbohydrate metabolism, cellular lipid metabolism, lipid biosynthesis, and protein modification (S5 Table and S8A Fig). Additionally, a comparable number of maize genes (5,116) showed multiple AS events during the four developmental stages (Fig 2C and S6 Table). A typical example is GRMZM2G310069, a gene encoding a hypothetical protein that may regulate secondary metabolism (the protein domain is Amidohydro\_3). This gene not only presented with multiple AS events at different stages but also provided a preliminary map of temporal AS events (Fig 2D and S3B Fig). Genes with multiple AS events were also significantly enriched in many key biological processes, including histone modification, tRNA processing, cellular amino acid metabolism, DNA repair and intracellular transport (S7 Table and S8B Fig). These results



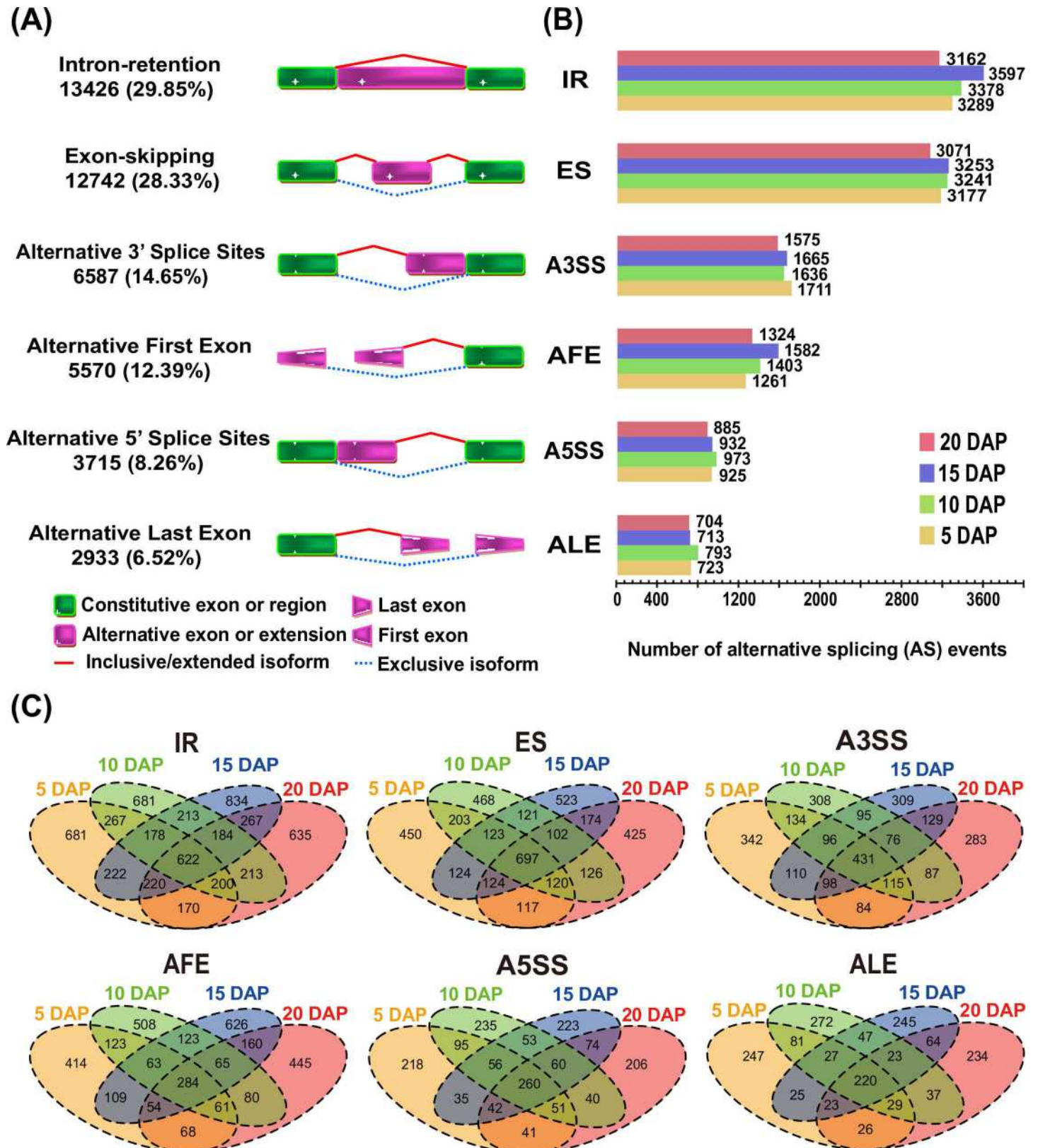


**Fig 1. Overview and identification of AS events during endosperm development.** (A) Alternative splicing (AS) events were categorized into the six most frequent types: alternative 3' splicing (A3SS), alternative 5' splicing (A5SS), alternative first exon (AFE) splicing, alternative last exon (ALE) splicing,

intron retention (IR) and exon skipping (ES). The total number of all types of AS events and their frequencies are shown; these numbers include newly identified and annotated AS events. (B) The bar chart presents the number of AS events detected at the four developmental stages. (C) The Venn diagrams depict shared and unique AS events among the four developmental stages of maize endosperm.

doi:10.1371/journal.pone.0163814.g001

indicate that AS is a vital event that generates proteins with diverse functions to regulate endosperm development in maize.

## Dynamic changes in maize endosperm gene expression at four developmental stages

The sequenced reads in this study were valuable for investigating gene expression in maize endosperm during the four developmental stages. By assembling transcripts with clean reads using Cufflinks software (v2.1.0) [29], the boundaries of 19,164 annotated maize genes could be further extended, and 2,504 putative new genes were found to be expressed at these four stages (S8 Table). Significant BLAST hits for a proportion of these putative new genes were obtained in the Nr (96.34%), SwissProt (52.08%), GO (70.13%), KEGG (16.25%) and COG (14.85%) databases (S9 Table). Among these genes, 59 appear to have roles in transcriptional regulation (S9 Table).

To gain a global overview of gene expression during the four examined developmental stages, gene expression abundance was estimated by calculating FPKM values (Fig 3A and S10 Table). Less than 7% of the genes were highly expressed (FPKM > 100), whereas more than 30% had FPKM values ranging from 10–100. An FPKM value of  $\geq 1$  was observed for 20,777, 21,923, 21,488 and 21,648 genes expressed at 5, 10, 15 and 20 DAP, respectively, and 18,072 genes were consistently expressed at all four developmental stages (Fig 3B). Further, 14703 (50.3%) and 19714 (68.6%) expressed genes reported by Chen *et al.* (2014) overlapped with our data at 10 and 20 DAP, respectively. However, 19714 (72.8%) expressed genes reported by Li *et al.* (2014) overlapped with our data at 10 DAP. These differences may have resulted from the use of different maize varieties. In our study, we used the maize hybrid Shandan 609, while Chen *et al.* (2014) and Li *et al.* (2014) examined the maize inbred line B73, and used two different methods to filter gene sets, which likely led to the differences in the numbers of expressed genes. We expected that our data would be enriched for the maize endosperm transcriptome. Furthermore, 405, 773, 766 and 643 genes with diverse biological processes, cellular components, and molecular function annotations were specifically expressed at 5, 10, 15 and 20 DAP (Fig 3B), respectively. For instance, genes specifically expressed at 5 DAP were mainly involved in transferase activity and the transferring of hexosyl groups (S11 Table). In contrast, significant enrichment for transcriptional regulation, the carbohydrate catabolic process, and the defence response was observed among the genes specifically expressed at 10 DAP (S11 Table). These results are in agreement with earlier reports showing that the active accumulation of storage compounds begins at approximately 10 DAP [6,20]. Additionally, the genes specifically expressed at 15 DAP were mainly involved in lipid and protein metabolism (S11 Table), and those specifically expressed at 20 DAP were closely related to transcriptional regulation and carbohydrate and lipid metabolic processes (S11 Table).

To further identify dynamic changes in gene expression during early maize endosperm development, we carried out hierarchical clustering analysis of genes that were differentially expressed among the different development stages. Genes with no less than a two-fold change ( $\log_2$  ratio value of  $>1$  or  $<-1$ ) and FDR of  $\leq 0.01$  were considered differentially expressed. We identified 7,633 DEGs among the different developmental stages using EBSeq [30] (Table 2 and S12 Table), and then grouped them into fifteen clusters (TL-1 –TL-15) based on the CH index [34] (Fig 4 and S13 Table). The DEGs in TL-2, TL-5, TL-6, TL-7, TL-9, TL-12 and TL-13



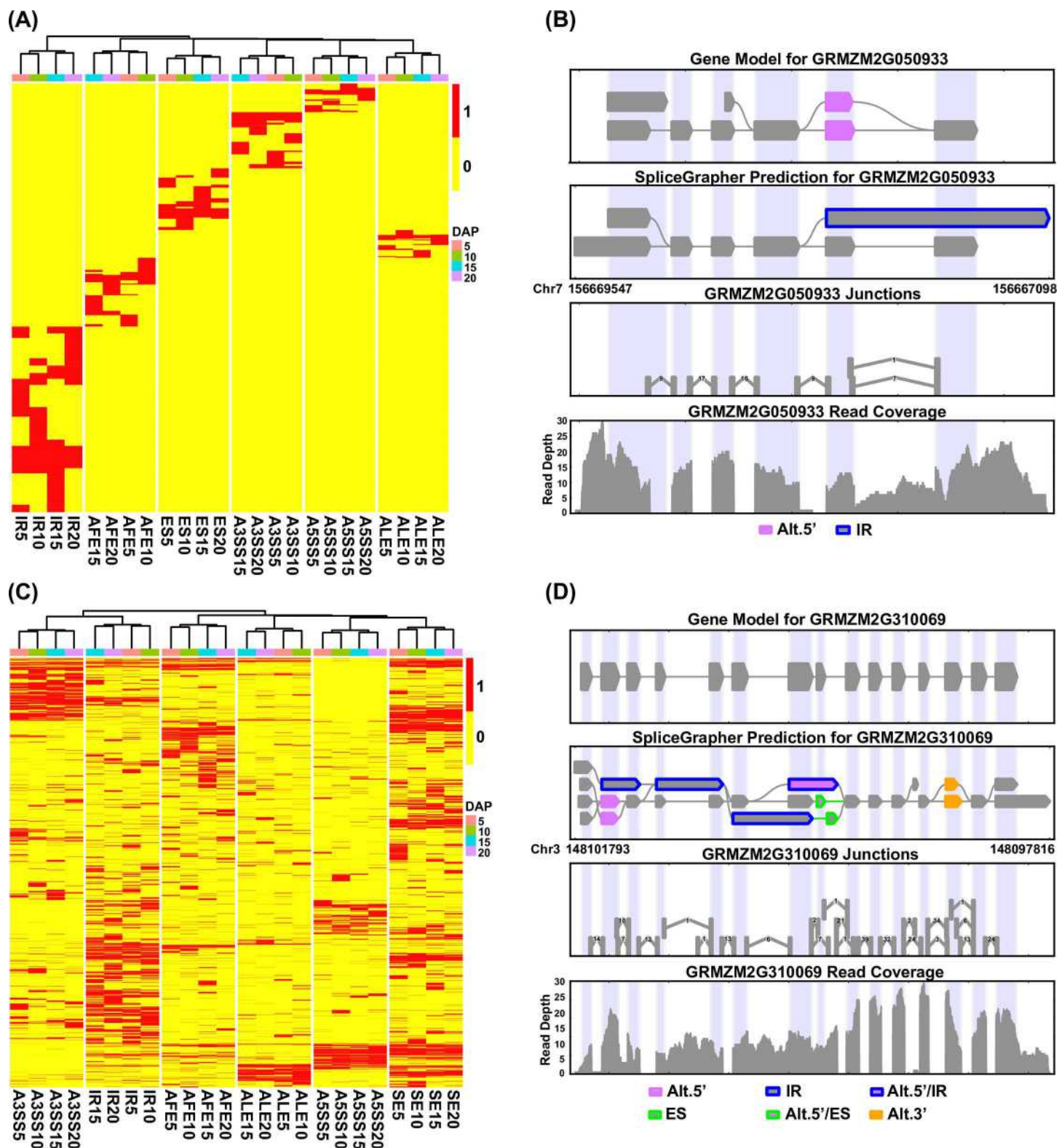


**Fig 2. Discovery of a single AS event or multiple AS events in maize endosperm genes.** (A) The heat map shows the dynamic changes in 5,905 genes with a single AS event during endosperm development, and the scale bar indicates whether an event occurred (red: event occurrence; yellow: no event occurrence). (B) An example of a single AS event occurring in a newly identified transcribed region (chromosome 7: 129960922–129965733); this developmentally regulated splicing event was only observed at 15 DAP. (C) Dynamic variation in multiple AS events in 5,116 genes is indicated at several

developmental stages (the scale bar is defined in A). (D) An example of multiple AS events in *GRMZM2G051866*, indicating the diversity of newly identified transcribed regions (chromosome 10: 130393296–130404103) and the various developmentally regulated splicing events that occur at this locus during different developmental stages.

doi:10.1371/journal.pone.0163814.g002

showed a single transition point at 10 or 15 DAP. In contrast, the DEGs in TL-1, TL-3, TL-8, and TL-11 exhibited two transition points at both 10 and 15 DAP. qRT-PCR analysis of 15 genes, including 13 TF and 2 zein genes, was performed to further confirm the dynamics of differential gene expression (Fig 5 and S2 Table). The qRT-PCR results revealed similar expression trends compared with the RNA-seq results. Additionally, the DEGs in the A, D, E, H, I, J, K, L and O clusters identified in qRT-PCR showed a single transition point at 15 DAP, whereas those in the B, C, F, G, M and N clusters showed two transition points at both 10 and 15 DAP. (Fig 5). These results facilitate the identification of co-expressed gene sets associated with regulatory nodes that are involved in the temporal control of maize endosperm development.

Stringent GO enrichment analysis of the DEGs in these clusters revealed that those in TL-2, TL-6, TL-7, TL-10, TL-13 and TL-15 predominantly participated in the response to monocarboxylic acid metabolic process, defense response and lipid metabolic process, glucan biosynthetic process and cellular carbohydrate biosynthesis, translation, oligopeptide transport, and cellular nitrogen compound metabolic process, respectively (Table 3 and S14 Table). Additionally, some DEGs exhibited similar expression patterns and thus may be involved in the same biological process, for example, a fraction of the TL-1 and TL-8 DEGs exhibited a down-up-down expression pattern at three transition points and were enriched for translation and nucleosome assembly (Table 3 and S14 Table). As the previous study, histone family genes have been shown to be crucial for the packaging of DNA and cell cycle regulation [40]. Compared with other clusters, the DEGs in TL-3, TL-4, TL-5, TL-9, TL-11, TL-12 and TL-14 were not significantly enriched in a specific GO biological process, while they were significantly enriched in diverse molecular functions: TL-4 (three-step: down-up-up) was enriched in 2 iron, 2 sulphur cluster binding; TL-5 (three-step: down-down-up) was enriched in macromolecular complex; TL-9 (three-step: up-down-down) was enriched in catalytic activity;

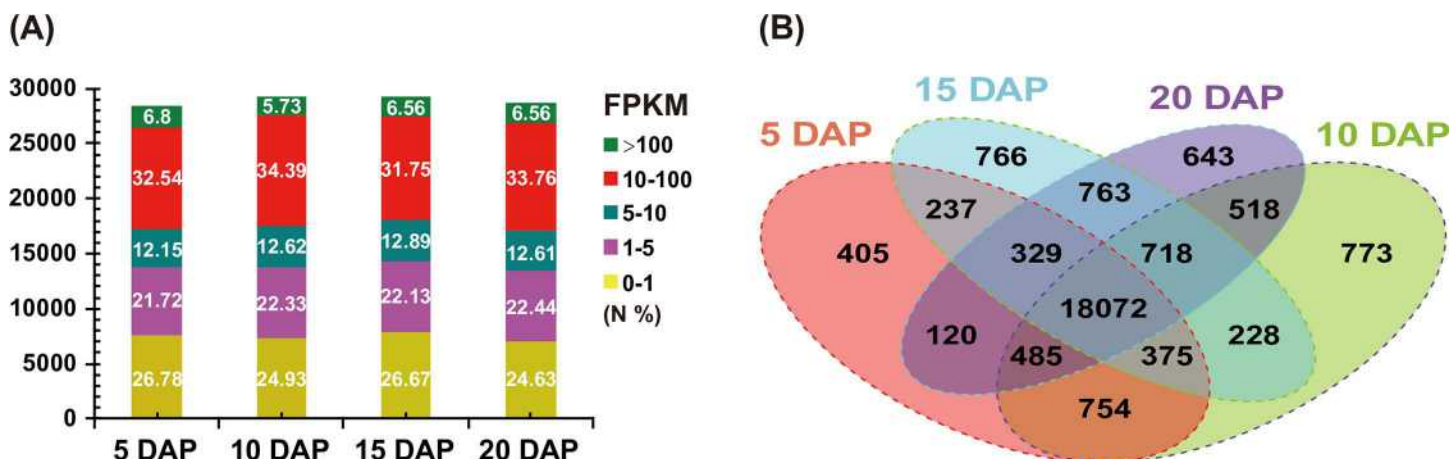


**Fig 3. Analysis of global gene expression based on FPKM values among different endosperm developmental stages.** (A) Distribution of the transcripts at five expression levels based on the FPKM values are shown, and the expression values from 10 to 100 correspond with the most highly represented transcripts at the four developmental stages. The vertical axis represents the number of transcripts; and 'N' is the percentage of transcripts expressed at the corresponding level. (B) A total of 25,186 genes (FPKM value  $\geq 1$ ) were expressed during the four stages. Genes with shared and specific expression were detected during these stages.

doi:10.1371/journal.pone.0163814.g003



**Table 2. Differentially expressed genes among four endosperm developmental stages in maize.**

Comparison	DEG number	Up-regulated	Down-regulated	No.
5 DAP vs 10 DAP	2803	1679 (59.9%)	1124 (40.1%)	D10_5
5 DAP vs 15 DAP	3402	1956 (57.5%)	1446 (42.5%)	D15_5
5 DAP vs 20 DAP	3490	2255 (64.6%)	1235 (35.4%)	D20_5
10 DAP vs 15 DAP	3566	1676 (47.0%)	1890 (53.0%)	D15_10
10 DAP vs 20 DAP	2938	1454 (49.5%)	1484 (50.5%)	D20_10
15 DAP vs 20 DAP	2802	1716 (61.2%)	1086 (38.8%)	D20_15

doi:10.1371/journal.pone.0163814.t002

TL-12 (three-step: up-up-down) was enriched in monooxygenase activity; TL-14 (three-step: up-up-up) was enriched in serine-type endopeptidase activity; while TL-3 and TL-11 (three-step: up-down-up) was especially enriched in nutrient reservoir activity, which occurs primarily in the starchy endosperm [6] (S14 Table). The largest proportion of up-regulated genes was identified in the comparison between 5 and 20 DAP, whereas the largest proportion of down-regulated genes was detected in the comparisons between 10 and 15 DAP and between 10 and 20 DAP (Fig 6A). These results indicate that the gene expression patterns change dramatically during maize endosperm development from 5–20 DAP.

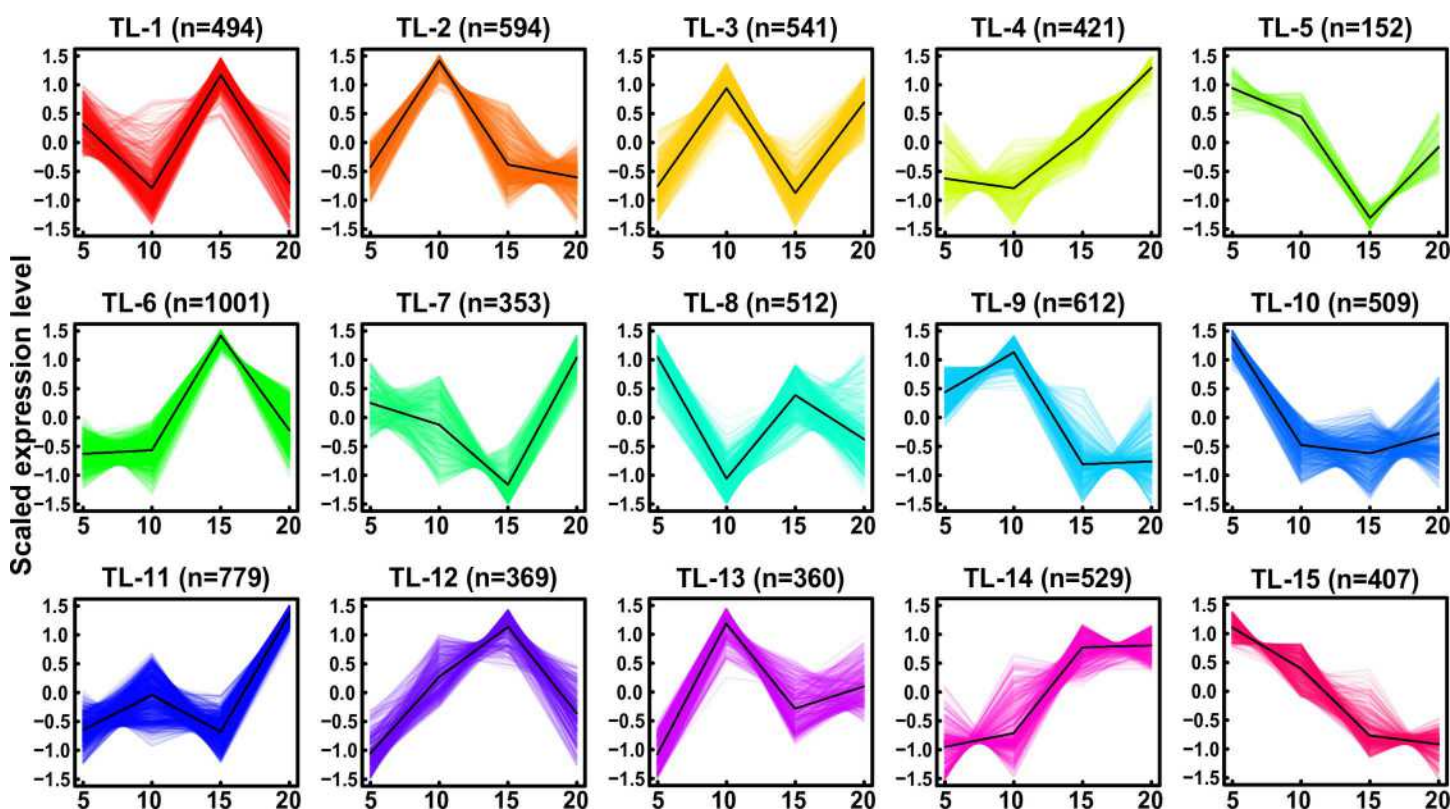


**Fig 4. Expression patterns of DEGs in developing maize endosperm.** Fifteen expression patterns were characterized by the fluctuating expression of gene sets at 5, 10, 15 and 20 DAP. The DEG sets showed different trends of transition from down- to up-regulated states or from up- to down-regulated states over the developmental stages (TL-14 and 15). The up- and down-regulated gene sets are staggered or are depicted consecutively over the developmental stages of maize endosperm. The scaled expression levels of the DEGs are provided on the y-axis, the developmental stages are shown on the x-axis, the coloured lines represent the individual gene expression clusters, and the trend in expression of each gene set is depicted as a black line. 'n' represents the number of DEGs.

doi:10.1371/journal.pone.0163814.g004

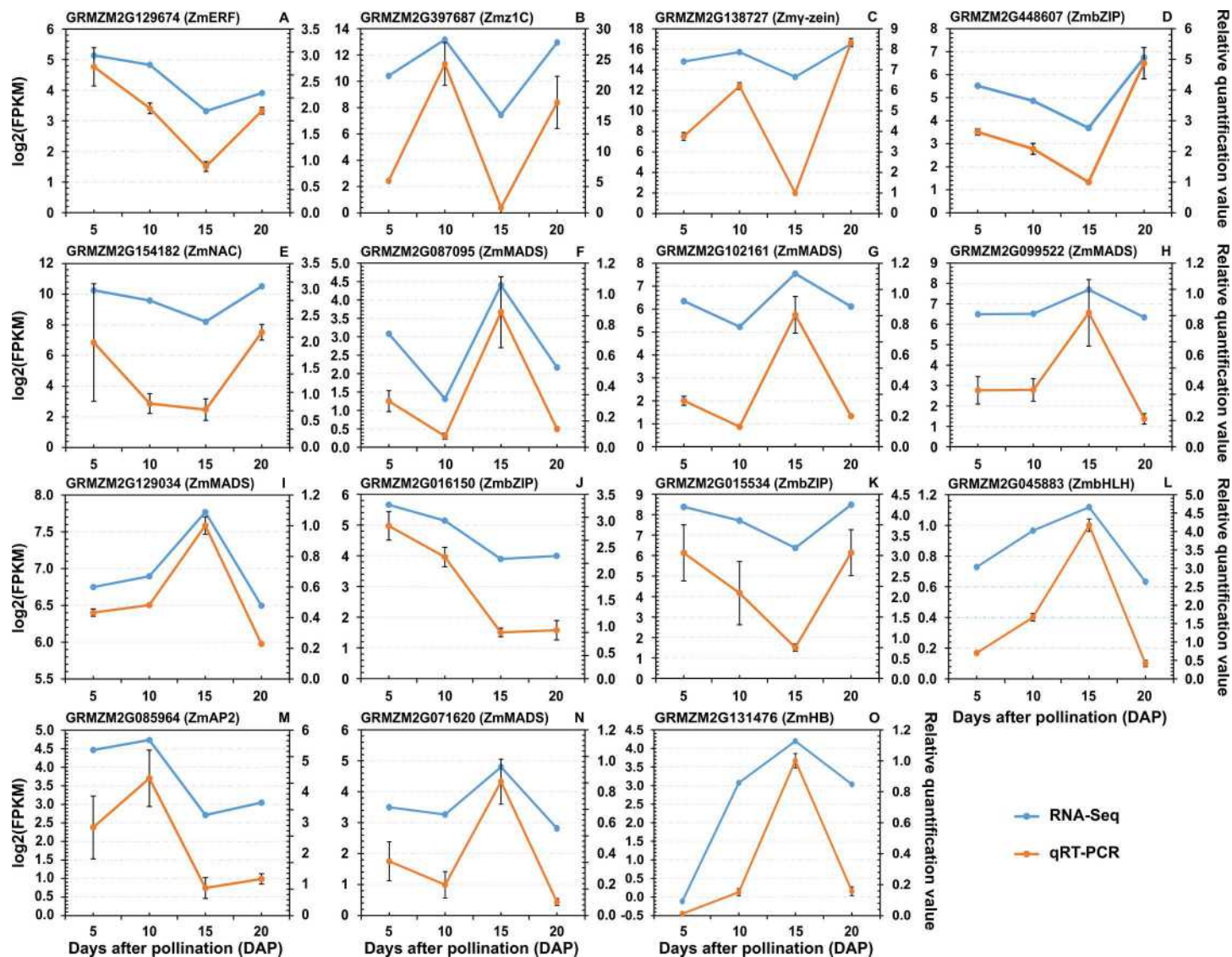


**Fig 5. Expression pattern analysis of 13 TF and 2 zein genes by qRT-PCR and RNA-seq.** The y-axis shows the mRNA levels. The scale on the right indicates gene expression level based on RNA-Seq. The scale on the left shows relative gene expression levels based on qRT-PCR. The x-axis indicates the day of endosperm sampling after pollination. The letters correspond to the genes. The blue lines correspond with RNA-seq; and the gold lines correspond with qRT-PCR.

doi:10.1371/journal.pone.0163814.g005

## Dynamic expression of TFs during maize endosperm development

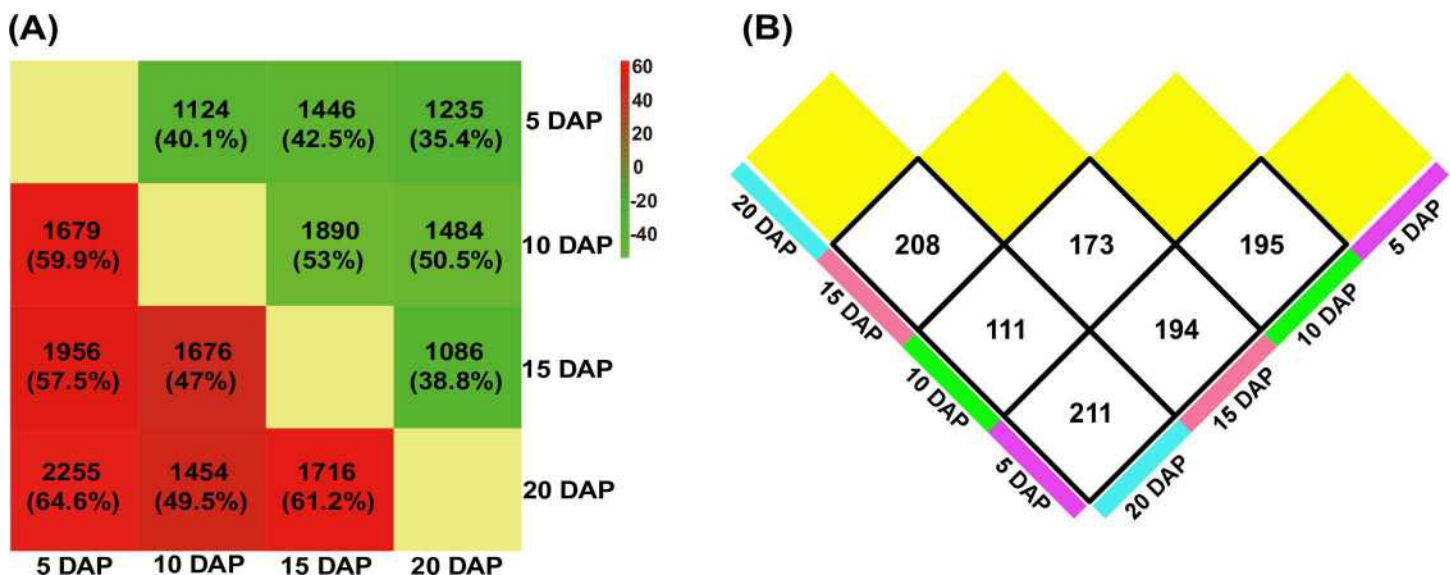
A total of 1,945 maize TFs were found to be expressed in at least one of the four developmental stages (S15 Table); of them, 473 TFs were differentially expressed (S16 Table). Furthermore, more than 100 TFs were found to be differentially expressed in each of the six comparisons (Fig 6B). The most highly differentially expressed genes were members of the *bZIP* family. A representative example is *OPAQUE2* (O2; GRMZM2G015534), a *bZIP* TF with FPKM values of 333.47, 210.00, 82.90 and 357.73 at 5, 10, 15 and 20 DAP, respectively. The expression pattern of O2 was consistent with that observed in the qRT-PCR validation experiments. O2 plays an important role in the regulation of seed carbon and nitrogen metabolism and activates  $\alpha$ - and  $\beta$ -*prolamin* genes in the synthesis of storage proteins during endosperm development [41–44].



**Table 3. Functional category enrichment analysis of genes in fifteen major clusters.**

Cluster	GO_acc	GO Term	Query	Background	p-value	FDR
			Item/total	Item/total		
TL-1	GO:0006412	translation	77/324	1071/25,288	2.50E-34	1.80E-31
	GO:0034645	cellular macromolecule biosynthesis	113/324	3777/25,288	9.50E-19	2.40E-16
	GO:0006334	nucleosome assembly	20/324	206/25,288	1.20E-11	7.70E-10
TL-2	GO:0032787	monocarboxylic acid metabolic process	11/324	188/25,288	4.30E-05	2.60E-02
TL-3	GO:0045735	nutrient reservoir activity	10/313	118/25,288	4.10E-06	1.30E-03
TL-4	GO:0051537	2 iron, 2 sulfur cluster binding	5/136	40/25,288	4.20E-06	7.80E-04
TL-5	GO:0032991	macromolecular complex	13/74	2352/25,288	1.90E-02	1.00E+00
TL-6	GO:0006952	defense response	10/534	82/25,288	2.10E-05	1.50E-02
	GO:0006629	lipid metabolic process	32/534	674/25,288	3.30E-05	1.50E-02
TL-7	GO:0009250	glucan biosynthetic process	8/196	88/25,288	7.90E-07	2.00E-04
	GO:0034637	cellular carbohydrate biosynthesis	10/196	168/25,288	1.30E-06	2.00E-04
TL-8	GO:0006412	translation	78/326	1071/25,288	6.00E-35	4.30E-32
	GO:0006333	chromatin assembly or disassembly	27/326	244/25,288	1.70E-16	3.20E-14
	GO:0006334	nucleosome assembly	25/326	206/25,288	3.20E-16	3.20E-14
TL-9	GO:0003824	catalytic activity	122/205	11249/25,288	1.20E-05	3.30E-03
TL-10	GO:0006412	translation	27/268	1071/25,288	3.90E-05	1.40E-02
TL-11	GO:0045735	nutrient reservoir activity	12/407	118/25,288	1.10E-06	5.20E-04
TL-12	GO:0004497	monooxygenase activity	11/213	429/25,288	1.30E-03	4.20E-01
TL-13	GO:0006857	oligopeptide transport	5/210	65/25,288	2.80E-04	9.00E-02
TL-14	GO:0004252	serine-type endopeptidase activity	7/182	213/25,288	1.10E-03	3.90E-01
TL-15	GO:0034641	cellular nitrogen compound metabolic	11/139	373/25,288	9.00E-06	3.30E-03

doi:10.1371/journal.pone.0163814.t003

**Fig 6. Distributions of the numbers of DEGs and DETFs.** (A) Identification of the dynamic distribution of DEGs (fold change (FC)  $\geq 2$  (for up-regulation) or FC  $\leq 0.5$  (for down-regulation)) in developing endosperm via comparison of two stages; the red colour represents up-regulation, and green represents down-regulation. The scale bar depicts the percentages of DEGs in both directions (up and down). (B) A semi-matrix showing the dynamic changes in the DETFs, as determined by pair-wise comparisons of their expression at different developmental stages.

doi:10.1371/journal.pone.0163814.g006

The DETFs were distributed among 50 TF families; of them, 40% (20/50) contained DETFs in each cluster (Fig 7A). In contrast, 60% (30/50) of the TF families included relatively fewer DETFs, with most exhibiting either up- or down-regulation at specific stages of endosperm development (Fig 7A).

The dynamic expression of DETFs was demonstrated by hierarchical clustering analysis (Fig 7B). A total of 473 DETFs could be grouped into 12 clusters; of these DETFs, 39 (R2, R5, R7-9 and R11), 44 (R1-5), 40 (R1, R6-7 and R12) and 44 (R1, R4-5, R8 and R10-12) were highly expressed specifically at 5, 10, 15 and 20 DAP, respectively (Fig 7B and S17 Table). GO enrichment analysis showed that the DETFs that were highly expressed at 5 DAP were mainly involved in binding processes, such as water, ice, zinc ion, protein, cation, ion, metal ion and transition metal ion binding, as well as nucleus and ligand-dependent nuclear receptor activity (S18 Table). Specifically, TFs in the *C3H*, *FAR1*, *GATA*, *GeBP* and *ZF-HD* families are key regulators of the above biological processes. The DETFs at 10 DAP were involved in various immune responses, signalling, binding and lumen development, as well as other biological functions (S18 Table). In particular, *Dof*, *E2F/DP*, *GATA*, *GRF*, *SRS*, *WOX* and *ZF-HD* family members have important roles in regulating the above functions, and the functions of some of

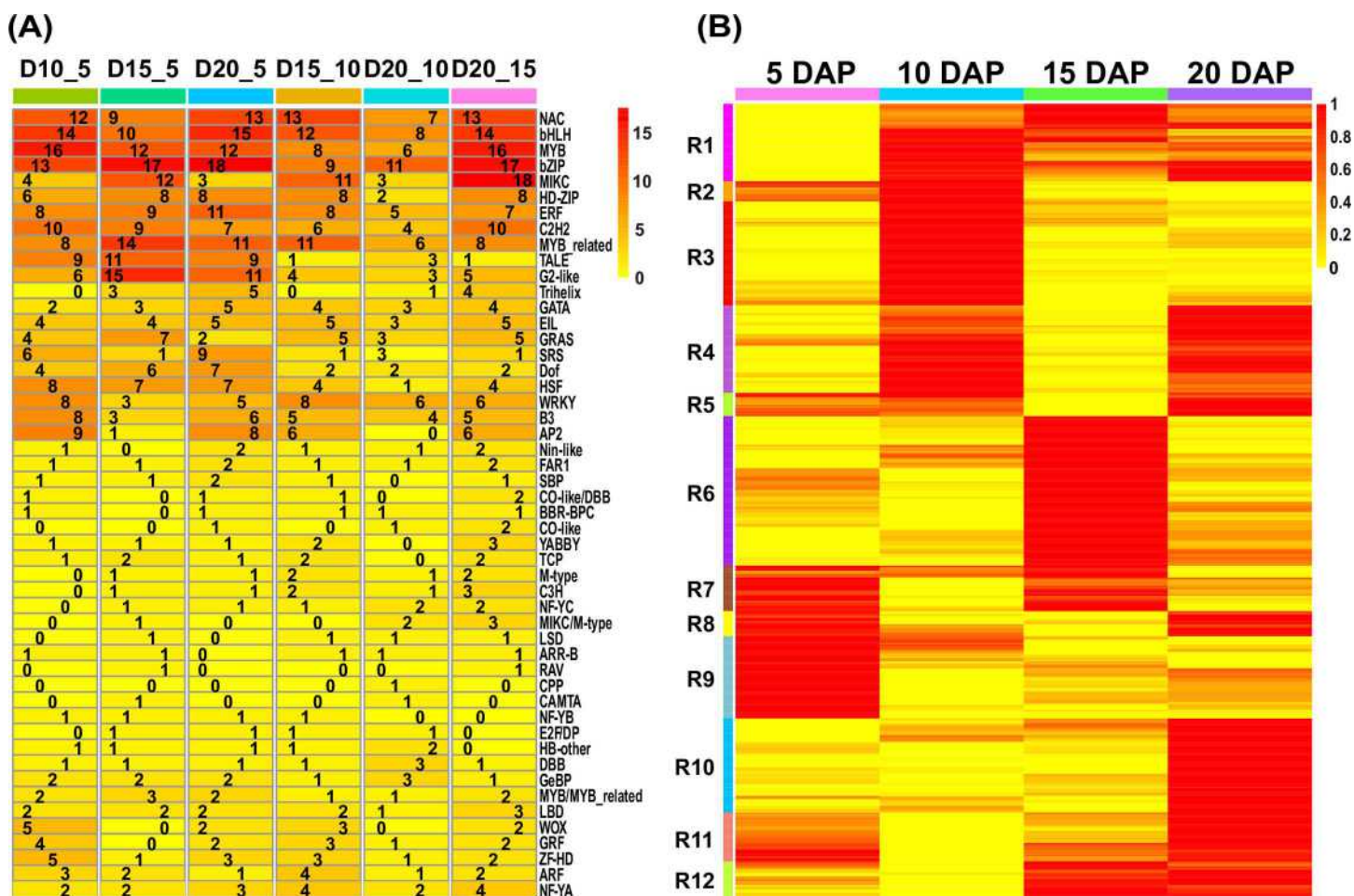


**Fig 7. Enrichment and expression analysis of DETFs during maize endosperm development.** (A) Pair-wise comparisons identified the dynamic distribution of the numbers of DETFs from 50 TF families. The scale bar represents the number of DETFs. (B) Heat map of DETFs identified at the time point of their peak expression based on normalised FPKM values. Twelve modules are classified according to normalised FPKM values of more than 0.5. The scale bar shows the normalised FPKM values.

doi:10.1371/journal.pone.0163814.g007



these TFs have been reported in previous studies [14,45–46]. In addition, the *GRF* members differentially expressed at 10 DAP are mainly involved in the regulation of nucleotide binding in the endosperm. To a certain extent, many biological processes overlapped at 15 and 10 DAP, but the different DETFs at 15 DAP showed significant enrichment for protein metabolic processes and cytoplasmic localisation. These biological processes were found to involve several DETF families, such as *CAMTA*, *Dof*, *GeBP*, *MIKC/M-type*, *M-type*, *SRS* and *WOX* (S18 Table), and DETFs exhibiting high expression in the R6 cluster were also identified at specific stages. Although the biological functions regulated by the DETFs at 20 DAP were similar to those regulated at the other stages, many of the DETFs at 20 DAP were involved in the responses to various stimuli, binding, and formation of the lumen and were components of organelles, the membrane, and the nucleoplasm in contrast with those at 15 DAP (S18 Table). DETFs in the *BBR-BPC*, *CO-like*, *E2F/DP* and *ZF-HD* families showed the greatest contribution to these biological processes, whereas those in R10 were specifically observed at 20 DAP.

Overall, these results indicate that members of these 50 TF families either play important roles in regulating the entire developmental process or act as regulatory nodes to control endosperm development at specific times.

## Discussion

In the present study, we performed high-throughput transcriptome sequencing to study the transcriptome dynamics during maize endosperm development from 5 to 20 DAP. These findings further enrich the existing research literature.

First, analysis of the RNA-seq data resulted in the identification of 44,973 AS events in 11,010 protein-coding genes. ES was found to be a predominant AS event in maize endosperm development (Fig 1A), in contrast with the reported findings of a low level of ES (<5%) in *Arabidopsis thaliana* [38–39]. Further, unlike previous studies of AS events [12–18], dynamic AS events were observed in the present study (Figs 1C and 2). These AS events were not only stage-specific but also underwent dynamic changes, and the biological diversity of gene function was affected by single and multiple AS events. As exemplified in *GRMZM2G050933* and *GRMZM2G310069*, to a certain extent, AS events resulted in the addition or removal of protein domains, as well as the rearrangement of sequences, allowing for the comprehensive examination of the biological diversity of gene function. GO enrichment analysis revealed that although the biological functions of genes with single or multiple AS events differed, these genes participated in developmentally related pathways (S5 and S7 Tables). Thus, the AS data represent a valuable resource for identification of candidate genes involved in endosperm development, especially because approximately 40% of maize genes have not yet been functionally annotated in the Ensembl Plant database (<http://plants.ensembl.org/>). A representative candidate is the uncharacterized gene *GRMZM2G310069*, which exhibited a different AS type in each of the four developmental stages (Fig 2D). The above results and previous studies suggest that AS plays an important role in the transition between developmental stages during endosperm development.

Second, differential expression analysis indicated that the gene expression programmes changed dramatically during maize endosperm development between 5 and 20 DAP. A total of 7,633 DEGs in fifteen clusters were identified through pair-wise comparisons between each of the four developmental stages (Fig 4). DEGs in 73.33% (11/15) of the clusters exhibited transition points at 10 and/or 15 DAP, and these points were confirmed by qRT-PCR (Fig 5 and S2 Table). These findings demonstrate the importance of these two time points during maize endosperm development. This observation is supported by the results of previous studies showing that at approximately 10 DAP, endosperm cells asynchronously and gradually switch

to an endoreduplication cell cycle, with notable accumulation of spherosomes and protein bodies, and the cytoplasm becomes dense, rapidly filling the seed cavity, resulting in a change in cell shape [7,11]. Several important developmental changes, such as storage protein and starch accumulation and an abrupt increase in the IAA concentration, begin at approximately 10 DAP [47]. In addition, many significant metabolic changes, including changes in cyclin proteins activity, starch accumulation and GA signalling pathway activity, occur at 15 DAP [11,22,48].

A detailed investigation of the expression patterns of the DEGs was performed to elucidate the differences in biological functions within and among of 15 AS gene sets. In contrast with previous studies [6,49], trend analysis performed here allowed for determination of the expression trends of various functional gene sets, including zein genes, which account for 70% of corn endosperm proteins and affect the translucency of the mature kernel [50,51]. In addition, “up-and-down” oscillating expression patterns were identified in zein gene subfamilies. Almost all of the DEGs among *19-kD α-zein*, *22-kD α-zein*, *15-kD β-zein*, *16-kD*, *27-kD γ-zein* and *50-kD γ-zein* exhibited “up-down-up” oscillating expression patterns in the TL-2, -3, -9, -11 and -13 clusters; these findings are consistent with those of a previous study [49]. These oscillating expression patterns were also confirmed by qRT-PCR for *22-kD α-zein* (GRMZM2G397687) and *27-kD γ-zein* (GRMZM2G138727) (Fig 5 and S2 Table). Nevertheless, two *19-kD α-zein* genes (GRMZM2G053120 and GRMZM2G404459) in TL-10 and an *18-kD δ-zein* (GRMZM2G100018) gene in TL-7 exhibited “down-up-down” and “down-down-up” oscillating expression patterns. The oscillating expression patterns of these zein genes are likely related to their positional expression in maize endosperm. For example, *19-kD α-zein* and *22-kD α-zein* are expressed in a narrow vertical strip on the adgerminal side of the endosperm at 10 DAP. By 15 DAP, *22-kD α-zeins transcripts* are detectable in most regions; conversely, *10-kD σ-zeins transcripts* are only observed on the adgerminal and abgerminal sides of the endosperm, and *19-kD B1α-zein transcripts* are enriched in peripheral, central and starchy endosperm cells. At 20 DAP, *19-kD B1α-zein transcripts* are present in most regions, *22-kD α-zein transcripts* are enriched in the peripheral regions of the endosperm, and *15-kD β-zein transcripts* are enriched in the border region of the abgerminal side of the endosperm [52]. Obviously, further investigation of the expression patterns of DEGs is necessary to delineate the mechanisms that control gene expression programmes during maize endosperm development.

Finally, the differential regulation of TFs occurred during endosperm development. A total of 473 DETFs from 50 families were identified during the four developmental stages of maize endosperm (Fig 6B and S16 Table), most of which have been identified to be involved in the regulation of plant development (S9 Fig). A representative example, a *bZIP* TF termed OPAQUE2 (O2; GRMZM2G015534), was expressed at a high level and exhibited a consistent expression pattern between RNA-seq and qRT-PCR results in our study (Fig 5 and S2 Table). Previous reports have also shown that O2 mainly participates in the regulation of carbon and nitrogen metabolism and activates the  $\alpha$ - and  $\beta$ -prolamin genes in the synthesis of storage proteins during endosperm development [41–44]. Furthermore, the present study revealed that *WRKY* family members were involved mainly in the physiological programmes of senescence, pathogen defence and phytohormone signalling. These results are in agreement with previous reports showing that *WRKY* family members play roles in plant immunity and plant senescence, as well as salicylic acid- and abscisic acid-mediated plant defence and abiotic stress tolerance [53,54]. Although the differentially expressed members of the *ARR-B*, *GeBP* and *ARF* families were expressed at relatively low levels, these TFs are involved in hormone signalling, including cytokinin signalling (*ARR-B* and *GeBP*) and auxin signalling (*ARF*). Moreover, some of the changes in the biological functions of these DETF family members were specific to only one of the four stages of endosperm development (Fig 7A). Fig 7B shows the results of



complete analysis of the DETF expression patterns, with the highly expressed DETFs depicted according to the specific developmental stages. Further functional analysis revealed the potential regulatory roles of several DETFs in the transition between developmental stages ([S18 Table](#)). These findings may facilitate the generation of a stage-specific regulatory network and delineation of the regulatory mechanisms involved in maize endosperm development.

## Supporting Information

**S1 Fig. Typical morphologies of maize kernel and endosperm at four days after pollination (DAP).**

(TIF)

**S2 Fig. Read coverage for the four time points studied.** A, B, C and D show reads mapped to maize reference genome sequences at 5, 10, 15 and 20 DAP, respectively. The boxes in red depict the differing coverage of the reads mapped to the maize genome sequences across the four stages.

(TIF)

**S3 Fig. Reads mapped to the reference gene model.** A, an example illustrating reads mapped to the gene (*GRMZM2G050933*) model, with a single AS event observed at 5 DAP. B, an example showing reads mapped to a gene (*GRMZM2G310069*) model, with multiple AS events observed at 10 DAP. The different colours represent different bases, and the coloured areas indicate the regions in which AS events occurred. Corresponding to [Fig 2B and 2D](#).

(TIF)

**S4 Fig. Exon skipping (ES) identification.** A and B, an example illustrating a newly identified transcribed regions, *GRMZM2G412075*, showing reads mapped to the gene model, with a single AS event observed at 15 DAP. The different colours represent different bases, and the coloured areas indicate the regions in which ES occurred.

(TIF)

**S5 Fig. Alternative 5' splice site (Alt.5') identification.** A and B, an example illustrating newly identified transcribed regions of *GRMZM2G036619*, showing reads mapped to the gene model, with a single AS event observed at 5 DAP. The different colours represent different bases, and the coloured areas are regions with an A5SS.

(TIF)

**S6 Fig. Alternative 3' splice site (A3SS) identification.** A and B, an example illustrating newly identified transcribed regions of *GRMZM2G053588*, showing reads mapped to the gene model, with a single AS event observed at 5 DAP. The different colours represent different bases, and the coloured areas are regions with an A3SS.

(TIF)

**S7 Fig. Validation of alternative splicing events by RT-PCR.** The capital letters indicate types of AS events. Corresponding to [S1 Table](#).

(TIF)

**S8 Fig. Gene Ontology (GO) enrichment analysis of genes with AS events in maize endosperm.** A, Enrichment of biological process-related GO terms of genes with a single AS event. B, Enrichment of biological process-related GO terms of genes with multiple AS events.

(TIF)

**S9 Fig. Gene Ontology (GO) enrichment analysis of differentially expressed transcription factors (DETFs).** Enrichment of biological process-related GO terms of DETFs from four

developmental stages of maize endosperm.  
(TIF)

**S1 Table. Primer pair sequences and domain information for genes with an AS event.**  
(XLS)

**S2 Table. qRT-PCR analysis of 15 genes.**  
(XLS)

**S3 Table. Alternative splicing (AS) types of genes.**  
(XLS)

**S4 Table. Single alternative splicing (AS) events in genes.**  
(XLS)

**S5 Table. GO annotation of genes with a single alternative splicing (AS) event.**  
(XLS)

**S6 Table. Multiple alternative splicing (AS) events in genes.**  
(XLS)

**S7 Table. GO annotation of genes with multiple alternative splicing (AS) events.**  
(XLS)

**S8 Table. Cufflinks analysis of putative genes.**  
(XLS)

**S9 Table. Functional annotation of putative genes.**  
(XLS)

**S10 Table. Gene expression at four developmental stages.**  
(XLS)

**S11 Table. GO annotation of genes differentially expressed at specific stages.**  
(XLS)

**S12 Table. Differentially expressed genes.**  
(XLS)

**S13 Table. Differentially expressed gene clustering.**  
(XLS)

**S14 Table. GO annotation of differentially expressed gene clusters.**  
(XLS)

**S15 Table. Transcription factor (TF) expression at four developmental stages.**  
(XLS)

**S16 Table. Differentially expressed transcription factors (DETFs).**  
(XLS)

**S17 Table. Clustering of differentially expressed transcription factors (DETFs).**  
(XLS)

**S18 Table. GO annotation of differentially expressed transcription factors (DETFs) at a specific stage.**  
(XLS)

## Acknowledgments

The authors thank Min Wang for providing technical assistance. The RNA-seq data has been deposited in NCBI's SRA database under the BioProject accession number PRJNA299361.

## Author Contributions

**Conceptualization:** JZQ DWG CM.

**Data curation:** JZQ.

**Formal analysis:** JZQ.

**Funding acquisition:** DWG.

**Investigation:** JZQ.

**Methodology:** JZQ CM.

**Project administration:** JZQ DWG JQX CM.

**Resources:** JQX DWG.

**Software:** JZQ CM.

**Supervision:** DWG JQX CM STX RHZ XHZ.

**Validation:** JZQ CM DWG JQX.

**Visualization:** JZQ CM.

**Writing – original draft:** JZQ.

**Writing – review & editing:** JZQ CM DWG JQX STX JJF YBL LW FFL RHZ XHZ.

## References

1. Godfray HC, Beddington JR, Crute IR, Haddad L, Lawrence D, Muir JF, et al. (2010). Food security: the challenge of feeding 9 billion people. *Science* 327: 812–818. doi: [10.1126/science.1185383](https://doi.org/10.1126/science.1185383) PMID: [20110467](https://pubmed.ncbi.nlm.nih.gov/20110467/)
2. Lopes MA, Larkins BA. (1993). Endosperm origin, development, and function. *Plant Cell* 5: 1383–1399. doi: [10.1105/tpc.5.10.1383](https://doi.org/10.1105/tpc.5.10.1383) PMID: [8281040](https://pubmed.ncbi.nlm.nih.gov/8281040/)
3. Leroux BM, Goodyke AJ, Schumacher KI, Abbott CP, Clore AM, Yadegari R, et al. (2014). Maize early endosperm growth and development: from fertilization through cell type differentiation. *Am. J. Bot* 101: 1259–1274. doi: [10.3732/ajb.1400083](https://doi.org/10.3732/ajb.1400083) PMID: [25104551](https://pubmed.ncbi.nlm.nih.gov/25104551/)
4. Rousseau D, Widiez T, Di Tommaso S, Rositi H, Adrien J, Maire E, et al. (2015). Fast virtual histology using X-ray in-line phase tomography: application to the 3D anatomy of maize developing seeds. *Plant Methods* 11: 55. doi: [10.1186/s13007-015-0098-y](https://doi.org/10.1186/s13007-015-0098-y) PMID: [26688690](https://pubmed.ncbi.nlm.nih.gov/26688690/)
5. Sabelli PA, Larkins BA. (2009). The development of endosperm in grasses. *Plant Physiol* 149: 14–26. doi: [10.1104/pp.108.129437](https://doi.org/10.1104/pp.108.129437) PMID: [19126691](https://pubmed.ncbi.nlm.nih.gov/19126691/)
6. Li G, Wang D, Yang R, Logan K, Chen H, Zhang S, et al. (2014). Temporal patterns of gene expression in developing maize endosperm identified through transcriptome sequencing. *Proc. Natl Acad. Sci. U S A* 111: 7582–7587. doi: [10.1073/pnas.1406383111](https://doi.org/10.1073/pnas.1406383111) PMID: [24821765](https://pubmed.ncbi.nlm.nih.gov/24821765/)
7. Olsen OA. (2001). ENDOSPERM DEVELOPMENT: cellularization and cell fate specification. *Annu. Rev. Plant Physiol. Plant Mol. Biol* 52: 233–267. doi: [10.1146/annurev.arplant.52.1.233](https://doi.org/10.1146/annurev.arplant.52.1.233) PMID: [11337398](https://pubmed.ncbi.nlm.nih.gov/11337398/)
8. Olsen OA. (2004). Nuclear endosperm development in cereals and *Arabidopsis thaliana*. *Plant Cell* 16: S214–S227. doi: [10.1105/tpc.017111](https://doi.org/10.1105/tpc.017111) PMID: [15010513](https://pubmed.ncbi.nlm.nih.gov/15010513/)
9. Sabelli PA, Larkins BA. (2009). The contribution of cell cycle regulation to endosperm development. *Sex Plant Reprod* 22(4): 207–219. doi: [10.1007/s00497-009-0105-4](https://doi.org/10.1007/s00497-009-0105-4) PMID: [20033442](https://pubmed.ncbi.nlm.nih.gov/20033442/)



10. Becraft PW. (2001). Cell fate specification in the cereal endosperm. *Semin. Cell Dev. Biol* 12: 387–394. doi: [10.1006/scdb.2001.0268](https://doi.org/10.1006/scdb.2001.0268) PMID: [11535047](https://pubmed.ncbi.nlm.nih.gov/11535047/)
11. Dante RA, Sabelli PA, Nguyen HN, Leiva-Neto JT, Tao Y, Lowe KS, et al. (2014). Cyclin-dependent kinase complexes in developing maize endosperm: evidence for differential expression and functional specialization. *Planta* 239: 493–509. doi: [10.1007/s00425-013-1990-1](https://doi.org/10.1007/s00425-013-1990-1) PMID: [24240479](https://pubmed.ncbi.nlm.nih.gov/24240479/)
12. Keren H, Lev-Maor G, Ast G. (2010). Alternative splicing and evolution: diversification, exon definition and function. *Nat. Rev. Genet* 11: 345–355. doi: [10.1038/nrg2776](https://doi.org/10.1038/nrg2776) PMID: [20376054](https://pubmed.ncbi.nlm.nih.gov/20376054/)
13. Kalsotra A, Cooper TA. (2011). Functional consequences of developmentally regulated alternative splicing. *Nat. Rev. Genet* 12: 715–729. doi: [10.1038/nrg3052](https://doi.org/10.1038/nrg3052) PMID: [21921927](https://pubmed.ncbi.nlm.nih.gov/21921927/)
14. Lu X, Chen D, Shu D, Zhang Z, Wang W, Klukas C, et al. (2013). The differential transcription network between embryo and endosperm in the early developing maize seed. *Plant Physiol* 162: 440–455. doi: [10.1104/pp.113.214874](https://doi.org/10.1104/pp.113.214874) PMID: [23478895](https://pubmed.ncbi.nlm.nih.gov/23478895/)
15. Black DL. (2003). Mechanisms of alternative pre-messenger RNA splicing. *Annu. Rev. Biochem* 72: 291–336. doi: [10.1146/annurev.biochem.72.121801.161720](https://doi.org/10.1146/annurev.biochem.72.121801.161720) PMID: [12626338](https://pubmed.ncbi.nlm.nih.gov/12626338/)
16. Marquez Y, Brown JW, Simpson C, Barta A, Kalyna M. (2012). Transcriptome survey reveals increased complexity of the alternative splicing landscape in Arabidopsis. *Genome Res* 22: 1184–1195. doi: [10.1101/gr.134106.111](https://doi.org/10.1101/gr.134106.111) PMID: [22391557](https://pubmed.ncbi.nlm.nih.gov/22391557/)
17. Zou X, Jiang Y, Zheng Y, Zhang M, Zhang Z. (2011). Prolyl 4-hydroxylase genes are subjected to alternative splicing in roots of maize seedlings under waterlogging. *Ann. Bot* 108: 1323–1335. doi: [10.1093/aob/mcr223](https://doi.org/10.1093/aob/mcr223) PMID: [21969257](https://pubmed.ncbi.nlm.nih.gov/21969257/)
18. Thatcher SR, Zhou W, Leonard A, Wang BB, Beatty M, Zastrow-Hayes G, et al. (2014). Genome-wide analysis of alternative splicing in Zea mays: landscape and genetic regulation. *Plant Cell* 26: 3472–3487. doi: [10.1105/tpc.114.130773](https://doi.org/10.1105/tpc.114.130773) PMID: [25248552](https://pubmed.ncbi.nlm.nih.gov/25248552/)
19. Lai J, Dey N, Kim CS, Bharti AK, Rudd S, Mayer KF, et al. (2004). Characterization of the maize endosperm transcriptome and its comparison to the rice genome. *Genome Res* 14: 1932–1937. doi: [10.1101/gr.2780504](https://doi.org/10.1101/gr.2780504) PMID: [15466291](https://pubmed.ncbi.nlm.nih.gov/15466291/)
20. Chen J, Zeng B, Zhang M, Xie S, Wang G, Hauck A, et al. (2014). Dynamic transcriptome landscape of maize embryo and endosperm development. *Plant Physiol* 166: 252–264. doi: [10.1104/pp.114.240689](https://doi.org/10.1104/pp.114.240689) PMID: [25037214](https://pubmed.ncbi.nlm.nih.gov/25037214/)
21. Zhan J, Thakare D, Ma C, Lloyd A, Nixon NM, Arakaki AM, et al. (2015). RNA sequencing of laser-capture microdissected compartments of the maize kernel identifies regulatory modules associated with endosperm cell differentiation. *Plant Cell* 27: 513–531. doi: [10.1105/tpc.114.135657](https://doi.org/10.1105/tpc.114.135657) PMID: [25783031](https://pubmed.ncbi.nlm.nih.gov/25783031/)
22. Liu X, Fu J, Gu D, Liu W, Liu T., Peng Y, et al. (2008). Genome-wide analysis of gene expression profiles during the kernel development of maize (*Zea mays* L.). *Genomics* 91: 378–387. doi: [10.1016/j.ygeno.2007.12.002](https://doi.org/10.1016/j.ygeno.2007.12.002) PMID: [18280698](https://pubmed.ncbi.nlm.nih.gov/18280698/)
23. Zhang W, Yan H, Chen W, Liu J, Jiang C, Jiang H, et al. (2014). Genome-wide identification and characterization of maize expansin genes expressed in endosperm. *Mol. Genet. Genomics* 289: 1061–1074. doi: [10.1007/s00438-014-0867-8](https://doi.org/10.1007/s00438-014-0867-8) PMID: [25213600](https://pubmed.ncbi.nlm.nih.gov/25213600/)
24. Trapnell C, Pachter L, Salzberg SL. (2009). TopHat: discovering splice junctions with RNA-Seq. *Bioinformatics* 25: 1105–1111. doi: [10.1093/bioinformatics/btp120](https://doi.org/10.1093/bioinformatics/btp120) PMID: [19289445](https://pubmed.ncbi.nlm.nih.gov/19289445/)
25. Langmead B, Trapnell C, Pop M, Salzberg SL. (2009). Ultrafast and memory-efficient alignment of short DNA sequences to the human genome. *Genome Biol* 10: R25. doi: [10.1186/gb-2009-10-3-r25](https://doi.org/10.1186/gb-2009-10-3-r25) PMID: [19261174](https://pubmed.ncbi.nlm.nih.gov/19261174/)
26. Rogers MF, Thomas J, Reddy A S, Ben-Hur A. (2012). SpliceGrapher: detecting patterns of alternative splicing from RNA-Seq data in the context of gene models and EST data. *Genome Biol* 13: R4. doi: [10.1186/gb-2012-13-1-r4](https://doi.org/10.1186/gb-2012-13-1-r4) PMID: [22293517](https://pubmed.ncbi.nlm.nih.gov/22293517/)
27. Thorvaldsdóttir H, Robinson JT, Mesirov JP. (2013). Integrative genomics viewer (IGV): high-performance genomics data visualization and exploration. *Brief. Bioinform* 14: 178–192. doi: [10.1093/bib/bbs017](https://doi.org/10.1093/bib/bbs017) PMID: [22517427](https://pubmed.ncbi.nlm.nih.gov/22517427/)
28. Finn RD, Coghill P, Eberhardt RY, Eddy SR, Mistry J, Mitchell AL, et al. (2016). The Pfam protein families database: towards a more sustainable future. *Nucleic Acids Res* 44: D279–D285. doi: [10.1093/nar/gkv1344](https://doi.org/10.1093/nar/gkv1344) PMID: [26673716](https://pubmed.ncbi.nlm.nih.gov/26673716/)
29. Trapnell C, Williams BA, Pertea G, Mortazavi A, Kwan G, van Baren MJ, et al. (2010). Transcript assembly and quantification by RNA-Seq reveals unannotated transcripts and isoform switching during cell differentiation. *Nat. Biotechnol* 28: 511–515. doi: [10.1038/nbt.1621](https://doi.org/10.1038/nbt.1621) PMID: [20436464](https://pubmed.ncbi.nlm.nih.gov/20436464/)
30. Leng N, Dawson JA, Thomson JA, Ruotti V, Rissman AI, Smits BM, et al. (2013). EBSeq: an empirical Bayes hierarchical model for inference in RNA-seq experiments. *Bioinformatics* 29: 1035–1043. doi: [10.1093/bioinformatics/btt087](https://doi.org/10.1093/bioinformatics/btt087) PMID: [23428641](https://pubmed.ncbi.nlm.nih.gov/23428641/)

31. Benjamini Y., Hochberg Y., Controlling the false discovery rate: a practical and powerful approach to multiple testing. *J. R. Stat. Soc. B* 57 (1995) 289–300. <http://www.jstor.org/stable/2346101>.
32. Du Z, Zhou X, Ling Y, Zhang Z, Su Z. (2010). agriGO: a GO analysis toolkit for the agricultural community. *Nucleic Acids Res* 38: W64–W70. doi: [10.1093/nar/gkq310](https://doi.org/10.1093/nar/gkq310) PMID: [20435677](https://pubmed.ncbi.nlm.nih.gov/20435677/)
33. Supek F, Bošnjak M, Škunca N, Šmuc T. (2011). REVIGO summarizes and visualizes long lists of gene ontology terms. *PLOS ONE* 6: e21800. doi: [10.1371/journal.pone.0021800](https://doi.org/10.1371/journal.pone.0021800) PMID: [21789182](https://pubmed.ncbi.nlm.nih.gov/21789182/)
34. Calinski T, Harabasz J. (1974). A dendrite method for cluster analysis. *Comm. in Stats.—Theory & Methods* 3: 1–27. doi: [10.1080/03610927408827101](https://doi.org/10.1080/03610927408827101)
35. Sekhon RS, Lin H, Childs KL, Hansey CN, Buell CR, de Leon N and Kaeppler SM. (2011). Genome-wide atlas of transcription during maize development. *The Plant journal: for cell and molecular biology* 66: 553–563. doi: [10.1111/j.1365-3113X.2011.04527.x](https://doi.org/10.1111/j.1365-3113X.2011.04527.x) PMID: [21299659](https://pubmed.ncbi.nlm.nih.gov/21299659/)
36. Livak KJ, Schmittgen TD. (2001). Analysis of relative gene expression data using real-time quantitative PCR and the 2<sup>-</sup>(Delta Delta C(T)) method. *Methods* 25: 402–408. doi: [10.1006/meth.2001.1262](https://doi.org/10.1006/meth.2001.1262) PMID: [11846609](https://pubmed.ncbi.nlm.nih.gov/11846609/)
37. Teoh KT, Requesens DV, Devaiah SP, Johnson D, Huang X, Howard JA, et al. (2013). Transcriptome analysis of embryo maturation in maize. *BMC Plant Biol* 13: 19. doi: [10.1186/1471-2229-13-19](https://doi.org/10.1186/1471-2229-13-19) PMID: [23379350](https://pubmed.ncbi.nlm.nih.gov/23379350/)
38. Ner-Gaon H, Halachmi R, Savaldi-Goldstein S, Rubin E, Ophir R, Fluhr R. (2004). Intron retention is a major phenomenon in alternative splicing in Arabidopsis. *Plant J* 39: 877–885. doi: [10.1111/j.1365-3113X.2004.02172.x](https://doi.org/10.1111/j.1365-3113X.2004.02172.x) PMID: [15341630](https://pubmed.ncbi.nlm.nih.gov/15341630/)
39. Kim E, Goren A, Ast G. (2008). Alternative splicing: current perspectives. *BioEssays* 30: 38–47. doi: [10.1002/bies.20692](https://doi.org/10.1002/bies.20692) PMID: [18081010](https://pubmed.ncbi.nlm.nih.gov/18081010/)
40. Marzluff WF, Duronio RJ. (2002). Histone mRNA expression: multiple levels of cell cycle regulation and important developmental consequences. *Curr. Opin. Cell Biol* 14: 692–699. doi: [10.1016/S0955067402003873](https://doi.org/10.1016/S0955067402003873) PMID: [12473341](https://pubmed.ncbi.nlm.nih.gov/12473341/)
41. Vincentz M, Bandeira-Kobarg C, Gauer L, Schlögl P, Leite A. (2003). Evolutionary pattern of angiosperm bZIP factors homologous to the maize Opaque2 regulatory protein. *J. Mol. Evol* 56: 105–116. doi: [10.1007/s00239-002-2386-1](https://doi.org/10.1007/s00239-002-2386-1) PMID: [12569427](https://pubmed.ncbi.nlm.nih.gov/12569427/)
42. Wei K, Chen J, Wang Y, Chen Y, Chen S, Lin Y, et al. (2012). Genome-wide analysis of bZIP-encoding genes in maize. *DNA Res* 19: 463–476. doi: [10.1093/dnares/dss026](https://doi.org/10.1093/dnares/dss026) PMID: [23103471](https://pubmed.ncbi.nlm.nih.gov/23103471/)
43. Jin Z, Xu W, Liu A. (2014). Genomic surveys and expression analysis of bZIP gene family in castor bean (*Ricinus communis* L.). *Planta* 239: 299–312. doi: [10.1007/s00425-013-1979-9](https://doi.org/10.1007/s00425-013-1979-9) PMID: [24165825](https://pubmed.ncbi.nlm.nih.gov/24165825/)
44. Wang X, Wu F, Liu L, Liu X, Che Y, Keller NP, et al. (2015). The bZIP transcription factor PfZipA regulates secondary metabolism and oxidative stress response in the plant endophytic fungus *Pestalotiopsis fici*. *Fungal Genet. Biol* 81: 221–228. doi: [10.1016/j.fgb.2015.03.010](https://doi.org/10.1016/j.fgb.2015.03.010) PMID: [25847004](https://pubmed.ncbi.nlm.nih.gov/25847004/)
45. Le BH, Cheng C, Bui AQ, Wagmaister JA, Henry KF, et al. (2010). Global analysis of gene activity during Arabidopsis seed development and identification of seed-specific transcription factors. *Proceedings of the National Academy of Sciences of the United States of America* 107: 8063–8070. doi: [10.1073/pnas.1003530107](https://doi.org/10.1073/pnas.1003530107) PMID: [20385809](https://pubmed.ncbi.nlm.nih.gov/20385809/)
46. Agarwal P, Kapoor S and Tyagi AK. (2011). Transcription factors regulating the progression of monocot and dicot seed development. *Bioessays* 33: 189–202. doi: [10.1002/bies.201000107](https://doi.org/10.1002/bies.201000107) PMID: [21319185](https://pubmed.ncbi.nlm.nih.gov/21319185/)
47. Lur HS, Setter TL. (1993). Role of auxin in maize endosperm development (timing of nuclear DNA endoreduplication, zein expression, and cytokinin). *Plant Physiol* 103: 273–280. doi: [10.1186/1471-2229-14-142](https://doi.org/10.1186/1471-2229-14-142) PMID: [12231934](https://pubmed.ncbi.nlm.nih.gov/12231934/)
48. Lian T, Guo W, Chen M, Li J, Liang Q, Liu F, et al. (2015). Genome-wide identification and transcriptional analysis of folate metabolism-related genes in maize kernels. *BMC Plant Biol* 15: 204. doi: [10.1186/s12870-015-0578-2](https://doi.org/10.1186/s12870-015-0578-2) PMID: [26283542](https://pubmed.ncbi.nlm.nih.gov/26283542/)
49. Feng L, Zhu J, Wang G, Tang Y, Chen H, Jin W, et al. (2009). Expressional profiling study revealed unique expressional patterns and dramatic expressional divergence of maize alpha-zein super gene family. *Plant Mol. Biol* 69: 649–659. doi: [10.1007/s11103-008-9444-z](https://doi.org/10.1007/s11103-008-9444-z) PMID: [19112555](https://pubmed.ncbi.nlm.nih.gov/19112555/)
50. Wu Y, Messing J. (2014). Proteome balancing of the maize seed for higher nutritional value. *Front. Plant Sci* 5: 240. doi: [10.3389/fpls.2014.00240](https://doi.org/10.3389/fpls.2014.00240) PMID: [24910639](https://pubmed.ncbi.nlm.nih.gov/24910639/)
51. Wu Y, Holding DR, Messing J. (2010). γ-Zeins are essential for endosperm modification in quality protein maize. *Proc. Natl Acad. Sci. U S A* 107: 12810–12815. doi: [10.1073/pnas.1004721107](https://doi.org/10.1073/pnas.1004721107) PMID: [20615951](https://pubmed.ncbi.nlm.nih.gov/20615951/)
52. Woo YM, Hu DW., Larkins BA, Jung R. (2001). Genomics analysis of genes expressed in maize endosperm identifies novel seed proteins and clarifies patterns of Zein gene expression. *Plant Cell* 13: 2297–2318. doi: [10.1105/tpc.010240](https://doi.org/10.1105/tpc.010240) PMID: [11595803](https://pubmed.ncbi.nlm.nih.gov/11595803/)

53. Pandey SP, Somssich IE. (2009). The role of WRKY transcription factors in plant immunity. *Plant Physiol* 150: 1648–1655. doi: [10.1104/pp.109.138990](https://doi.org/10.1104/pp.109.138990) PMID: [19420325](https://pubmed.ncbi.nlm.nih.gov/19420325/)
54. Schluttenhofer C, Yuan L. (2015). Regulation of specialized metabolism by WRKY transcription factors. *Plant Physiol* 167: 295–306. doi: [10.1104/pp.114.251769](https://doi.org/10.1104/pp.114.251769) PMID: [25501946](https://pubmed.ncbi.nlm.nih.gov/25501946/)



# 证书

陕审玉 2015006 号

品种名称：陕单 618

育种单位：西北农林科技大学

品种来源：KA105×KB081

主要育种人：薛吉全 张兴华 郝引川 郭东伟 路海东

适宜区域：适宜陕西关中灌区夏播种植。

二〇一六年一月八日





# 证书

陕审玉 2015040 号

品种名称：陕单 622

育种单位：西北农林科技大学

品种来源：91227 × KB102

主要育种人：张兴华 郝引川 张仁和 郭东伟 薛吉全

适宜区域：适宜陕南海拔 900 米以下春玉米地区种植。





# 主要农作物品种 审定证书

审定编号：陕审玉 2017033 号

品种名称：陕单 623

品种来源：91227×KB092

申请者：西北农林科技大学

育种者：西北农林科技大学

审定意见：经陕西省农作物品种审定委员会第五十次会议审定通过，  
适宜陕南夏播玉米区种植。

公告号：陕农业发〔2017〕64号

证书编号：2017-64-0046

2017年07月26日





# 主要农作物品种 审定证书

审定编号：陕审玉 2017027 号

品种名称：陕单 636

品种来源：KA103×KB043

申请者：西北农林科技大学

育种者：西北农林科技大学

审定意见：经陕西省农作物品种审定委员会第五十次会议审定通过，  
适宜陕北、渭北春玉米区机械化籽粒收获。

公告号：陕农业发〔2017〕64号

证书编号：2017-64-0040

2017年07月26日





# 陕西省农业厅文件

陕农业发〔2017〕64号

---

## 陕西省农业厅 关于公布第五十次农作物品种 审定结果的通知

各设区市农业局（委），杨凌示范区农业局，韩城市农林局：

陕西省农作物品种审定委员会于2017年6月19日召开第50次品种审定会议，会议审定通过了玉米、水稻、棉花和大豆等四种农作物品种53个。经农业部种子管理局在中国种业信息网上公示，未有异议，现予以公布（见附件）。望各级农业部门根据新品种特点和适宜种植区域，做好宣传推广工作。另外，第48次品种审定委员会审定通过的玉米品种衡远Y4038，育种权



人达到一致，申请撤销了育种人异议，省品种审定委员会同意将该品种一并公布。

附件：1. 陕西省第 50 次审定会通过审定品种目录

2. 品种介绍



2017 年 7 月 26 日



陕西省第 50 次审定会通过审定品种目录

序号	作物 种类	品种 名称	品种来源	育种单位	适宜地区	审定编号
1	水稻	泰丰优 7 号	泰丰 A × 华恢 7 号	陕西华盛种业科技有限公司 广东省农业科学院水稻研究所	适宜陕南海拔 800 米以下的浅山 丘陵稻区和关中平原稻区种植	陕审稻 2017001 号
2		双亚黑一号	“黑帅”变异株优选	陕西双亚粮油工贸有限公司	适宜陕南海拔 650 米以下稻区种植	陕审稻 2017002 号
3		广 8 优 5 号	广 8A × 康恢 115	安康市农业科学研究所 广东省农业科学院水稻研究所 汉中现代农业科技有限公司	适宜陕南汉中、安康海拔 700 米 以下稻区种植	陕审稻 2017003 号
4		川香 145	川 106A × 康恢 1145	安康市农业科学研究所 四川省农业科学院作物研究所 汉中现代农业科技有限公司	适宜陕南汉中、安康海拔 650 米 以下稻区种植	陕审稻 2017004 号
5		糯优 748	香糯 518A × 糯恢 748	四川达丰种业科技有限责任公司 成都南方杂交水稻研究所	适宜在陕南海拔 650 米以下坝区 种植	陕审稻 2017005 号
6		泰优 037	泰香 22A × R037	汉中现代农业科技有限公司	适宜陕南海拔 650 米以下稻区种 植	陕审稻 2017006 号
7		陕农优 206	陕农 1A × 陕恢 206	汉中市农业科学研究所	适宜陕南汉中、安康海拔 650 米 以下的丘陵、平川稻区种植	陕审稻 2017007 号
8		泰丰优 2098	泰丰 A × 福恢 2098	福建省农业科学院水稻研究所 广东省农业科学院水稻研究所	适宜在陕南海拔 650 米以下稻区 种植	陕审稻 2017008 号
1	大豆	陕垦豆 4 号	98D-1-4-1/晋大 70	陕西农垦大华种业有限责任公司	适宜陕西夏播区种植	陕审豆 2017001 号
2		秦豆 2014	96E218/濮豆 10 号	陕西省杂交油菜研究中心	适宜陕西夏播区种植	陕审豆 2017002 号
3		金豆 228	秦豆 8 号变异株/中 黄 13	陕西高农种业有限公司	适宜陕西夏播区种植	陕审豆 2017003 号
1	棉花	中棉所 98	中 9018/sGK958	中国农业科学院棉花研究所 中棉种业科技股份有限公司	陕西关中春播棉区	陕审棉 2017001 号



序号	作物 种类	品种 名称	品种来源	育种单位	适宜地区	审定编号
1	玉米	德单 123	CA24 × BB31	北京德农种业有限公司	适宜关中夏播玉米区种植	陕审玉 2017001 号
2		伟育 187	WY583 × WY712	河南宝景农业科技有限公司	适宜关中夏播玉米区种植	陕审玉 2017002 号
3		秋丰 526	G123P × G6-123	洛阳秋丰种业有限公司	适宜关中夏播玉米区种植	陕审玉 2017003 号
4		博赞 88	DW2 × J555	洛阳金益农种子有限公司	适宜关中夏播玉米区种植	陕审玉 2017004 号
5		秋润 90	CCE62 × Fih6	陕西高农种业有限公司	适宜关中夏播玉米区种植	陕审玉 2017005 号
6		先玉 1366	PH1JYA × PH1N2D	铁岭先锋种子研究有限公司	适宜关中夏播玉米区种植	陕审玉 2017006 号
7		延科 158	C9330 × C382	延安延丰种业有限公司	适宜关中夏播玉米区种植	陕审玉 2017007 号
8		泓丰 707	京 X005 × 京 707	北京新实泓丰种业有限公司 北京市农林科学院玉米研究中心	适宜关中夏播玉米区种植	陕审玉 2017008 号
9		渭单 203	WZ031 × WZ048	陕西天丞禾农业科技有限公司	适宜关中夏播玉米区种植	陕审玉 2017009 号
10		渭研 6000	WZ31b × WZ068	陕西天丞禾农业科技有限公司	适宜关中夏播玉米区种植	陕审玉 2017010 号
11		华农 866	B280 × 京 66	北京华农伟业种子科技有限公司	适宜关中夏播玉米区种植	陕审玉 2017011 号
12		榆单 2275	0033 × 0589	陕西大地种业有限公司	适宜关中夏播玉米区种植	陕审玉 2017012 号
13		五谷 563	WG3511 × WG3151	甘肃五谷种业股份有限公司	适宜关中夏播玉米区种植	陕审玉 2017013 号
14		兴民 35	SY-M × XM1-24	陕西兴民种业有限公司	适宜关中夏播玉米区种植	陕审玉 2017014 号



序号	作物 种类	品种 名称	品种来源	育种单位	适宜地区	审定编号
15	玉米	大唐 220	G16 × G13	陕西大唐种业股份有限公司	适宜关中夏播玉米区种植	陕审玉 2017015 号
16		秦鑫 1708	鑫选 A-1 × 鑫选 9-3	西安鑫丰农业科技有限公司	适宜关中夏播玉米区种植	陕审玉 2017016 号
17		新单 66	新 QS258 × 新 798	河南省新乡市农业科学院	适宜关中夏播玉米区种植	陕审玉 2017017 号
18		九和玉 1 号	ppc12 × Zdk26	河南九和通种业有限公司	适宜关中夏播玉米区种植	陕审玉 2017018 号
19		鳳单 588	GW758 × GW3	陕西鑫鳳禾农业发展有限公司	适宜关中夏播玉米区种植	陕审玉 2017019 号
20		农丰 171	MX14 × NF128	孟州市农丰种子科技有限公司	适宜关中夏播玉米区种植	陕审玉 2017020 号
21		西农 233	XN672-305 × PH5AD	西北农林科技大学农学院	适宜关中夏播玉米区种植	陕审玉 2017021 号
22		中榆 968	S-1/P-1	榆林盛大种业有限责任公司	适宜陕西春播玉米区种植	陕审玉 2017022 号
23		正玉 998	P11 × N12	河南正粮种业有限公司 平顶山市农业科学院	适宜陕西春播玉米区种植	陕审玉 2017023 号
24		A1589	D1798Z × B2340Z	中种国际种子有限公司	适宜陕北、渭北春播玉米区种植	陕审玉 2017024 号
25		陕单 628	KA203 × KB102	西北农林科技大学	适宜陕北、渭北春播玉米区种植	陕审玉 2017025 号
26		润丰 101	W02 × W029	西安市户县润丰种苗有限公司	适宜陕北、渭北春播玉米区种植	陕审玉 2017026 号
27		陕单 636	KA103 × KB043	西北农林科技大学	适宜陕北、渭北春玉米区机械化 籽粒收获	陕审玉 2017027 号
28		华盛玉 882	HS3187 × HS81B	汉中华盛种业科技有限公司	适宜陕南春播玉米区种植	陕审玉 2017028 号
29		安科 106	R08 × AY369	安康市农业科学研究所	适宜陕南海拔 700 米以下地区春 播种植	陕审玉 2017029 号
30		兴民 20	SY-M × 1-27-3	陕西兴民种业有限公司	适宜陕南春播玉米区种植	陕审玉 2017030 号



序号	作物 种类	品种 名称	品种来源	育种单位	适宜地区	审定编号
31	玉米	高玉 14022	KNL1088 × FL306	湖北康农种业股份有限公司 四川高地种业有限公司	适宜陕南春播玉米区种植	陕审玉 2017031 号
32		禾盛玉 818	改 4 × 380	湖北省种子集团有限公司	适宜陕南春播玉米区种植	陕审玉 2017032 号
33		陕单 623	91227 × KB092	西北农林科技大学	适宜陕南夏播玉米区种植	陕审玉 2017033 号
34		彩甜糯 9 号	N633 × T106	榆林市金日种业有限公司	适宜陕西鲜食玉米区种植	陕审玉 2017034 号
35		陕 K512	M419/4 × F414	陕西省生物农业研究所(陕西省科学院 酶工程研究所)	适宜陕西鲜食玉米区种植	陕审玉 2017035 号
36		陕 K818	SNT8 × J18	陕西省生物农业研究所(陕西省科学院 酶工程研究所) 西安市农业技术推广中心	适宜陕西鲜食玉米区种植	陕审玉 2017036 号
37		五鲜 1 号	nsc47 × nse898	陕西五行种业有限公司	适宜陕西鲜食玉米区种植	陕审玉 2017037 号
38		五糯 3 号	东 48 × 东 32	陕西五行种业有限公司	适宜陕西鲜食玉米区种植	陕审玉 2017038 号
39		华亦 1204	Q101 × Q102	钱自更	适宜陕西青贮玉米区种植	陕审玉 2017039 号
40		先玉 1267	PH1DP8 × PH1N2D	铁岭先锋种子研究有限公司	适宜陕西青贮玉米区种植	陕审玉 2017040 号
41		兴民 28	XMG-1 × XM-1-13	陕西兴民种业有限公司	适宜陕西青贮玉米区种植	陕审玉 2017041 号
42		衡远 Y4038	衡远 YZ079 × 衡远 YZ009	深圳衡达涌金种业高科技有限公司	适宜关中夏播玉米区种植	陕审玉 2017042 号



月 20 日 ~ 5 月 10 日，每亩适宜密度 4500 ~ 5000 株，建议氮、磷、钾配合施用，氮肥分施、重施攻穗期肥，及时防治病虫害。

6、适宜地区及产量水平：适宜陕北、渭北春播玉米区种植。两年区试平均亩产 802.95 公斤。

### 玉米 润丰 101

1、审定编号：陕审玉 2017026 号

2、育种单位：西安市户县润丰种苗有限公司

3、主要育种人：王权龙、王香梅、刘博策、屈欣、李茜

4、品种来源：W02×W029

5、特征特性：两年区试平均生育期 122.9 天左右，幼苗芽鞘紫色，叶片上挺，苗势强壮，叶色深绿，总叶片数 21 片；株高 275 厘米，穗位高 105 厘米，株型紧凑，雄花分枝 10 ~ 12 个，外颖绿色，花丝绿色、花药粉黄色，果穗筒型，穗轴白色，穗长 20 厘米，穗粗 5.1 厘米，穗行数平均 16 ~ 18 行，行粒数 40 粒，籽粒黄色，马齿型，百粒重 36 克，出籽率 88.6%。

经抗病性鉴定：抗丝黑穗病、穗腐病、小斑病和茎腐病，中抗大斑病。

经品质检测：容重 741 克/升，粗蛋白 9.49%，粗脂肪 3.77%，粗淀粉 76.41%。

6、栽培技术要点：春播宜在 4 月下旬至 5 月初播种；适宜种植密度每亩 4000 株；每亩底施硝酸磷肥 40 公斤，追施尿素 25 公斤；种衣剂包衣种子，预防地下害虫和苗期病害。

7、适宜地区及产量水平：适宜陕北、渭北春播玉米区种植。两年区试平均 751.5 公斤。

### 玉米 陕单 636



1、审定编号：陕审玉 2017027 号

2、选育单位：西北农林科技大学

3、主要育种人：薛吉全、张兴华、郝引川、郭东伟、张仁和

4、品种来源：KA103×KB043

5、特征特性：两年区试生育期平均 119.5 天，较对照 122.8 早 3.3 天。幼苗叶鞘绿色，子叶长圆形，叶色浅绿。成株株型半紧凑，叶片稀疏、叶上挺，全株叶片数 17 片。成株株高 233.8 厘米，穗位高 74.8 厘米。雄花分枝 6~8 个，雄花护颖绿色，花药浅紫色，花丝浅红色。果穗筒型，穗长 19.4 厘米，穗行数 16~18 行，籽粒浅黄色、马齿型，穗轴浅红色，百粒重 35.5 克，成熟期籽粒含水量 22.4%，籽粒脱水快。

经抗病性鉴定：抗穗腐病，感茎腐病、丝黑穗病和大斑病。

经品质检测：容重 716 克/L，粗蛋白 9.97%，粗脂肪 3.53%，粗淀粉 75.59%。

6、栽培技术要点：在中等肥力以上地块栽培，适宜播种期 4 月中、下旬，足墒播种，一播全苗，每亩适宜密度 5000~5500 株，提倡氮磷配合，氮肥分次施用，重施攻穗期肥，酌施攻粒肥，及时防治病虫害。

7、适宜地区及产量水平：适宜陕北、渭北春玉米区机械化籽粒收获。两年平均亩产 729.8 公斤。

### 玉米 华盛玉 882

1、审定编号：陕审玉 2017028 号

2、选育单位：陕西华盛种业科技有限公司

3、主要选育人：雷秀安、张友军、郑少荣、李春元

4、品种来源：HS3187×HS81B



			中农绝早	备注
--	--	--	------	----

5、特征特性：两年区试平均生育期 124.5 天；幼苗生长势强，幼苗叶鞘紫色，叶片绿色，全株 20~21 片叶，植株半紧凑。株高 290 厘米，穗位高 125 厘米，雄穗中等大小，一级分枝 9~15 个，花药紫色，护颖紫色，花粉量中等，花丝红色。果穗筒型，穗长 23.6 厘米，穗粗 5.6 厘米，穗行数 17.4 行，穗轴白色，行粒数 40 左右，籽粒黄白色，半马齿型，出籽率为 87% 左右，百粒重 37.6 克。

经抗病性鉴定：高抗纹枯病、穗腐病和小斑病，抗丝黑穗病，中抗茎腐病和大斑病。

经品质检测：容重 765 克/L，粗蛋白（干基）11.01%，粗脂肪（干基）3.80%，粗淀粉（干基）72.78%。

#### 6、栽培技术要点：

（1）亩留苗 2800~3200 株，与洋芋套种亩密度 2400~2600 株。

（2）直播清明至谷雨播种，营养钵育苗移栽可提前到 3 月 15 日。

（3）合理施肥：施足底肥，早施追肥，重施喇叭口肥，增施锌肥。根据玉米需肥规律，进行三次施肥。第一次（底肥），沟施氮、磷、钾 5~20 公斤/亩，播种时一次性完成；第二次（苗期），4~6 片展开叶时追施尿素 10~15 公斤/亩；第三次（穗肥），12~13 片展开叶（大喇叭口期），施尿素 20~25 公斤/亩。施肥后及时浇水。

（4）除草及病虫害防治：采取土壤封闭的方法进行化学除草。苗期用菊酯类或有机磷类农药进行叶面喷雾，及时防治地老虎等害虫危害，避免缺苗断垄；玉米大喇叭口期，在玉米心叶中丢施呋喃丹颗粒剂，有效地防治玉米螟和蚜虫危害。

7、适宜地区及产量水平：适宜陕南春播玉米区种植。两年区试平均亩产 601.6 公斤。



厘米，筒型果穗，穗长 19.4 厘米，穗行数 15.1 行，行粒数 37.6 粒，籽粒黄色，马齿型，红轴。出籽率 83.6%，千粒重 328 克。两年区试平均生育期 123.8 天。

经抗病性鉴定：高抗纹枯病，抗穗腐病，中抗丝黑穗病，茎腐病，大斑病和小斑病。

经品质检测：容重 742 克/升，粗蛋白（干基）9.84%，粗脂肪（干基）4.29%，粗淀粉（干基）71.55%。

#### 6、栽培技术要点：

（1）播期播量：陕南春播一般在 3 月下旬至 4 月初播种，亩播量 2 公斤左右。

（2）种植密度：每亩 2800~3300 株。

（3）病虫害防治：及时防治蚜虫，玉米螟等病虫害。

（4）注意灌水保证出苗，抽穗前注意灌好杨花灌浆水。

7、适宜地区及产量水平：适宜陕南春播玉米区种植。两年区试平均亩产 614.6 公斤。

### 玉米 陕单 623

1、审定编号：陕审玉 2017033 号

2、选育单位：西北农林科技大学

3、主要育种人：张兴华、张仁和、郝引川、郭东伟、薛吉全

4、品种来源：91227×KB092

5、特征特性：两年区试生育期平均 108.3 天，比对照郑单 958 晚 0.9 天，需有效积温 2300℃左右。幼苗叶鞘紫色，叶片深绿色，叶缘紫色，雄花分枝 9~10 个，花药浅紫色，颖壳紫色。株型半紧凑，叶片稀疏、叶上挺，成株叶片数 19 片。花丝红色。株高 246 厘米，穗位高 106 厘米。果穗筒型，穗长 18.4 厘米，穗行数平均 14.9 行，穗轴白色，籽粒黄色、半马偏硬，百粒重 27



# 主要农作物品种 审定证书

审定编号：陕审玉 2018020 号

品种名称：陕单 620

品种来源：KA105×KB106

申请者：西北农林科技大学

育种者：西北农林科技大学

审定意见：经陕西省农作物品种审定委员会第五十一次会议审定通过，  
适宜陕北、渭北春播玉米区，关中夏播机械化籽粒收获。


公告号：陕农业发【2018】45 号

证书编号：2018-45-0044





# 陕西省主要农作物品种审定申请表

作物种类	玉米		品种名称	陕单 620	
品种来源	KA105×KB106		申请组别	关中灌区夏玉米机收粒区试	
申请 者	西北农林科技大学（加盖公章）				
地 址	陕西省杨陵示范区邠城路 3 号			邮政编码	712100
联 系 人	薛吉全	固定电话	029-87082934	移动电话	13709129113
传 真	029-87082934	电子邮件	Xjq2934@163.com		
育 种 者	薛吉全 张兴华 郝引川 张仁和 郭东伟			国 籍	中国
地 址	陕西省杨陵示范区邠城路 3 号			邮政编码	712100
联 系 人	薛吉全	固定电话	029-87082934	移动电话	13709129113
传 真	029-87082934	电子邮件	Xjq2934@163.com		
品种 保护 情况	<input type="checkbox"/> 已获授权	新品种保护名称	品种权号	亲本组合	
	<input type="checkbox"/> 保护申请中	申请公告暂定名称	申请公告号	亲本组合	
	<input checked="" type="checkbox"/> 未申请保护				
是否 转基因	<input type="checkbox"/> 是	转基因生物名称	转基因安全证书编号	亲本组合	
	<input checked="" type="checkbox"/> 否				
品种选育单位意见：					
该品种在 2014-2015 年多点联合试验中表现突出，推荐参加陕西夏玉米联合体区试。					
<div style="text-align: center;">  <p>年      月      日</p> </div>					



# 主要农作物品种 审定证书

审定编号：陕审玉 2018001 号

品种名称：陕单 619

品种来源：KA105×KB020

申请者：西北农林科技大学

育种者：西北农林科技大学

审定意见：经陕西省农作物品种审定委员会第五十一次会议审定通过，  
适宜关中夏播玉米区种植。

公告号：陕农业发【2018】45 号

证书编号：2018-45-0025



# 陕西省主要农作物品种审定申请表

作物种类	玉米		品种名称	陕单 619	
品种来源	KA105×KB020		申请组别	关中夏玉米	
申请 者	西北农林科技大学农学院 (加盖公章)				
地 址	陕西杨凌邠城路 3 号			邮政编码	712100
联 系 人	薛吉全	固定电话	029-87082934	移动电话	13709129113
传 真	029-87082934	电子邮件	xjq2934@163.com		
育 种 者	薛吉全 张兴华 郝引川 郭东伟 张仁和 路海东 赵崇耀 徐淑兔 刘建超			国 籍	中国
地 址	陕西杨凌邠城路 3 号			邮政编码	712100
联 系 人	薛吉全	固定电话	029-87082934	移动电话	13709129113
传 真	029-87082934	电子邮件	Xjq2934@163.com		
品种 保护 情况	<input type="checkbox"/> 已获授权	新品种保护名称	品种权号	亲本组合	
	<input type="checkbox"/> 保护申请中	申请公告暂定名称	申请公告号	亲本组合	
	<input checked="" type="checkbox"/> 未申请保护				
是否 转基因	<input type="checkbox"/> 是	转基因生物名称	转基因安全证书编号	亲本组合	
	<input checked="" type="checkbox"/> 否				
品种选育单位意见:					
该品种已按规定完成区域试验和生产试验, 符合审定标准, 同意申报。					
 2015 年 2 月 26 日					



# 主要农作物品种 审定证书

审定编号：陕审玉 2019051 号

品种名称：陕单 625

品种来源：KA106×KB102

申请者：西北农林科技大学

育种者：西北农林科技大学

审定意见：经陕西省农作物品种审定委员会第五十二次会议审定通过，  
适宜陕西陕南春玉米区种植。


公告号：陕农业发〔2019〕58号

证书编号：2019-58-0082

2019年07月02日



# 陕西省主要农作物品种审定申请表

作物种类	玉米		品种名称	陕单 625	
品种来源	KA106×KB102		申请组别	陕南春播玉米区试	
申请者	西北农林科技大学（加盖公章）				
地 址	陕西省杨陵示范区邠城路 3 号			邮政编码	712100
联 系 人	张兴华	固定电话	029-87082934	移动电话	13325481061
传 真	029-87082934	电子邮件	Zhxx4569@163.com		
育 种 者	西北农林科技大学（张兴华 薛吉全 郝引川 张仁和 郭东伟）			国 籍	中国
地 址	陕西省杨陵示范区邠城路 3 号			邮政编码	712100
联 系 人	张兴华	固定电话	029-87082934	移动电话	13325481061
传 真	029-87082934	电子邮件	Zhxx4569@163.com		
品种 保护 情况	<input type="checkbox"/> 已获授权	新品种保护名称	品种权号	亲本组合	
	<input type="checkbox"/> 保护申请中	申请公告暂定名称	申请公告号	亲本组合	
	<input checked="" type="checkbox"/> 未申请保护				
是否 转基因	<input type="checkbox"/> 是	转基因生物名称	转基因安全证书编号	亲本组合	
	<input checked="" type="checkbox"/> 否				
品种选育单位意见：					
<p>该品种在 2014-2015 年联合试验中表现突出，推荐参加陕南春播区试。</p> <div style="text-align: right;">  <p>年 月 日</p> </div>					



# 主要农作物品种 审定证书

审定编号：陕审玉 2019013 号

品种名称：陕单 650

品种来源：KA105×KB024

申请者：西北农林科技大学

育种者：西北农林科技大学

审定意见：经陕西省农作物品种审定委员会第五十二次会议审定通过，  
适宜关中灌区夏玉米机械化籽粒收获区种植。


公告号：陕农业发〔2019〕58 号

证书编号：2019-58-0044

2019 年 07 月 02 日



# 陕西省主要农作物品种审定申请表

作物种类	玉 米		品种名称	陕单 650	
品种来源	KA105×KB024		申请组别	关中灌区夏玉米机收组	
申 请 者	西北农林科技大学（加盖公章）				
地 址	陕西省杨陵示范区邠城路 3 号			邮政编码	712100
联 系 人	薛吉全	固定电话	029-87082934	移动电话	13709129113
传 真	029-87082934	电子邮件	Xjq2934@163.com		
育 种 者	薛吉全 张兴华 郝引川 张仁和 郭东伟			国 籍	中国
地 址	陕西省杨陵示范区邠城路 3 号			邮政编码	712100
联 系 人	薛吉全	固定电话	029-87082934	移动电话	13709129113
传 真	029-87082934	电子邮件	Xjq2934@163.com		
品种 保护 情况	<input type="checkbox"/> 已获授权	新品种保护名称	品种权号	亲本组合	
	<input type="checkbox"/> 保护申请中	申请公告暂定名称	申请公告号	亲本组合	
	<input checked="" type="checkbox"/> 未申请保护				
是否 转基因	<input type="checkbox"/> 是	转基因生物名称	转基因安全证书编号	亲本组合	
	<input checked="" type="checkbox"/> 否				
品种选育单位意见：					
该品种在 2014-2015 年多点联合试验中表现突出，推荐参加关中灌区夏玉米机收组区试。					
<div style="text-align: right;">               2017 年 04 月 12 日           </div>					



# 主要农作物品种 审定证书

审定编号：陕审玉 2019001 号

品种名称：陕单 658

品种来源：KA105×KB025

申请者：西北农林科技大学

育种者：西北农林科技大学

审定意见：经陕西省农作物品种审定委员会第五十二次会议审定通过，  
适宜关中夏播玉米区种植。

公告号：陕农业发（2019）58 号

证书编号：2019-58-0032



# 陕西省主要农作物品种审定申请表

作物种类	玉 米		品种名称	陕单 658	
品种来源	KA105×KB025		申请组别	关中灌区夏玉米区试	
申 请 者	西北农林科技大学（加盖公章）				
地 址	陕西省杨陵示范区邠城路 3 号			邮政编码	712100
联 系 人	薛吉全	固定电话	029-87082934	移动电话	13709129113
传 真	029-87082934	电子邮件	Xjq2934@163.com		
育 种 者	薛吉全 张兴华 郝引川 张仁和 郭东伟			国 籍	中国
地 址	陕西省杨陵示范区邠城路 3 号			邮政编码	712100
联 系 人	薛吉全	固定电话	029-87082934	移动电话	13709129113
传 真	029-87082934	电子邮件	Xjq2934@163.com		
品种 保护 情况	<input type="checkbox"/> 已获授权	新品种保护名称	品种权号	亲本组合	
	<input type="checkbox"/> 保护申请中	申请公告暂定名称	申请公告号	亲本组合	
	<input checked="" type="checkbox"/> 未申请保护				
是否 转基因	<input type="checkbox"/> 是	转基因生物名称	转基因安全证书编号	亲本组合	
	<input checked="" type="checkbox"/> 否				
品种选育单位意见：					
该品种在 2015-2016 年多点联合试验中表现突出，推荐参加陕西关中夏玉米区试。					
 2017 年 04 月 12 日					



# 主要农作物品种 审定证书

审定编号：陕审玉 2019048 号

品种名称：陕单 668

品种来源：KA106×KB135

申请者：西北农林科技大学

育种者：西北农林科技大学


审定意见：经陕西省农作物品种审定委员会第五十二次会议审定通过，  
适宜陕北、渭北春播玉米区种植。

公告号：陕农业发〔2019〕58 号

证书编号：2019-58-0079



# 陕西省主要农作物品种审定申请表

作物种类	玉米		品种名称	陕单 668	
品种来源	KA106×KB135		申请组别	陕西春玉米联合体区试	
申请 者	西北农林科技大学（加盖公章）				
地 址	陕西省杨陵示范区邠城路 3 号			邮政编码	712100
联 系 人	郝引川	固定电话	029-87082934	移动电话	13488319696
传 真	029-87082934	电子邮件	h.ychuan@163.com		
育 种 者	西北农林科技大学（郝引川 张兴华 薛吉全 张仁和 郭东伟）			国 籍	中国
地 址	陕西省杨陵示范区邠城路 3 号			邮政编码	712100
联 系 人	郝引川	固定电话	029-87082934	移动电话	13488319696
传 真	029-87082934	电子邮件	h.ychuan@163.com		
品种 保护 情况	<input type="checkbox"/> 已获授权	新品种保护名称	品种权号	亲本组合	
	<input type="checkbox"/> 保护申请中	申请公告暂定名称	申请公告号	亲本组合	
	<input checked="" type="checkbox"/> 未申请保护				
是否 转基因	<input type="checkbox"/> 是	转基因生物名称	转基因安全证书编号	亲本组合	
	<input checked="" type="checkbox"/> 否				
品种选育单位意见：					
该品种在 2015-2016 年多点联合试验中表现突出，推荐参加陕西春玉米联合体区试。					
					





# 陕西省科学技术奖 证书

为表彰陕西省科学技术奖获得者，  
特颁发此证书。

项目名称：高产优质多抗玉米品种陕单 609 选育  
及应用

奖励等级：壹等

获奖者：郭东伟



2017年2月4日

证书号：2016-1-02-R9



# 2016年度陕西省科学技术奖专业评审建议奖励项目

## 一等奖建议奖励项目（39项）

序号	受理编号	项目名称	主要完成单位	主要完成人	推荐单位
1	S2016JLJS0505	陕产枣类及沙棘等药食两用资源的绿色产业链构建与示范应用	陕西中医药大学、南京中医药大学、陕西海天制药有限公司、延安常泰药业有限责任公司、陕西汇源健康食品有限公司	唐志书、段金殿、郭盛、白吉庆、宋忠兴、刘启明、王梅、王春、张严磊、师宗臣、刘红波	咸阳市科学技术局
2	S2016JLJS0172	高产优质多抗玉米品种陕单609选育及应用	西北农林科技大学	薛吉全、张兴华、严勇敢、郝引川、王荣成、张仁和、马向峰、路海东、郭东伟、徐淑兔、李凤艳	杨凌农业高新技术产业示范区管理委员会
3	S2016JLJS0470	西北旱区豆科植物根瘤菌资源多样性及其生态适应性研究	西北农林科技大学	韦革宏、陈卫民、丑敏霞、王莉	杨凌农业高新技术产业示范区管理委员会
4	S2016JLJS0300	设施番茄与甜瓜水肥需求机理研究与技术示范	西北农林科技大学	李建明、胡晓辉、邹志荣、甄爱、丁明、张智、杨建军、赵晓民、刘荣强、黄天平、曹源	陕西省农业厅
5	S2016JLJS0476	山杏种质资源及综合利用关键技术与应用	西北农林科技大学	赵忠、李科友、魏安智、马希汉、朱海兰、尉芹、杨途熙、李巨秀、齐高强、苗兴军、李明	杨凌农业高新技术产业示范区管理委员会
6	S2016JLJS0461	奶牛性控关键技术研究集成与示范应用	西北农林科技大学、杨凌职业技术学院、大庆市田丰生物工程有限公司、西安现代农业综合开发总公司、新疆西部牧业股份有限公司	咎林森、李青旺、田万强、胡建宏、刘世明、秦海鹏、徐义民、张开展、赵宪林、林清、茹彩霞	杨凌农业高新技术产业示范区管理委员会
7	S2016JLJS0147	中厚煤层国产综采装备智能化无人开采技术研究与应用	陕西陕煤黄陵矿业有限公司、北京天地玛珂电液控制系统有限公司、西安煤矿机械有限公司、天地科技股份有限公司	范京道、师永贵、唐恩贤、梁平、徐建军、黄曾华、袁建平、毛明仓、符大利、孙永锋、宋智鹰	陕西煤业化工集团有限责任公司
8	S2016JLJS0203	浅埋煤层开采岩层控制理论及其应用	西安科技大学	黄庆享、张沛、陈杰、张文忠、陈苏社、邵水才、蔚保宁、刘腾飞、黄克军	陕西省教育厅
9	S2016JLJS0437	陕北黄土塬地区油气勘探地震关键技术的突破与应用	中国石油天然气股份有限公司长庆油田分公司	王大兴、席胜利、赵玉华、张盟勃、王学刚、高利东、王永刚、窦玉坛、陈娟、赵德勇、潘玉	中国石油天然气股份有限公司长庆油田分公司
10	S2016JLJS0026	陕北黄土高原地质灾害调查、发生规律与风险管控技术	中国地质调查局西安地质调查中心、长安大学、西北大学	张茂省、黄玉华、唐亚明、薛强、武文英、李同录、王家鼎、曾磊、李政国、孙萍萍、李林	陕西省国土资源厅



CH ?

http://kry.nwsuaf.edu.cn/epstar/web/swms/mainframe/home'

西北农林科技大学

科研管理信息系统

网址导航

百度一下, 你就知道

毒霸网址大全

金山猎豹游戏中心

镇魔曲网页版

最新小说

好货商城

科研管理信息系统

科研管理信息系统

你好:郭东伟,欢迎访问科研管理信息系统! 当前身份科研人员

清除缓存

快捷菜单设置

注销

隐藏菜单

纵向项目

项目申报

立项登记

变更申请

结题申请

过程报告

过程查询

横向项目

校级项目

成果登记

基地管理

学术活动

个人查询

添加科研项目

从申报项目引入

搜索

操作	校内编号	项目名称	项目类别	开始日期	结束日期	合同经费(万元)	项目状态	审核状态
<a href="#">查看</a> <a href="#">收回</a>		全省种质资源保护利用	陕西省厅局项目	2017-07-01	2018-12-31	45	在研	已提交
<a href="#">查看</a>	201502011430	玉米种质资源创新与新品种选育	陕西省科技厅	2015-01-01	2017-12-31	70	在研	校审通过
<a href="#">查看</a>	201416000686	高直链淀粉玉米轮回改良群体的构建	其它	2014-10-01	2016-09-30	20	在研	校审通过
<a href="#">查看</a>	201401070684	西部地区抗逆转基因玉米新种质创...	农业部	2014-07-01	2015-06-30	34.75	在研	校审通过
<a href="#">查看</a>	201382041086	玉米种质资源保护	陕西省厅局项目	2013-01-01	2013-12-31	30	在研	校审通过
<a href="#">查看</a>	201301040882	玉米胚乳细胞内复制调控的分子机...	国家自然科学基金...	2014-01-01	2014-12-31	15	在研	校审通过
<a href="#">查看</a>	20080201083	小麦染色体流式分选新方法的研究	陕西省科技厅	2008-01-01	2010-12-31	6	结题	校审通过

第 1 页,共 1 页

10:52

2020/4/6

起始年度: 2017

起始月份: 01

截止年度: 2020

截止月份: 04

部门项目信息: (00100)农学院/(K3330217015)全省种质资源保护利用

摘要:

是否包含往来款: ☒是 ☐否

是否包含未复核: ☒是 ☐否

类型: 所有

查询

导出

打印

汇总数据		报表								
凭证日期	凭证编号	科目编号	科目名称	摘要	项目支出	项目收入	项目借款	项目还款	余额	凭证信
				年初余额						
				期初余额						
2017-12-11	项目00075	410201	中央科研经费拨款	郭东伟收塞亚军内转科研经费		360,000.00			360,000.00	凭证信
2018-06-06	南00929	5002-3021101	科研事业支出-差旅费	农学院张永科报李玲君海南陵水育种基地差旅费	18,674.00				341,326.00	凭证信
2018-06-06	南01159	5002-30214	科研事业支出-租赁费	农学院吴权明报农耕地租赁费	19,900.00				321,426.00	凭证信
2018-06-08	南01750	5002-30202	科研事业支出-印刷费	农学院张永科报资料印刷	1,323.00				320,103.00	凭证信
2018-07-06	南02050	5002-3022702	科研事业支出-测试分析费	农学院钟雨越报测试费	9,449.00				310,654.00	凭证信
2018-08-29	南00081	121501	个人借款	农学院郭东伟借出版费			11,760.00		298,894.00	凭证信
2018-09-29	南06822	5002-3029903	科研事业支出-版面费	研究生院渠建洲报版面费	11,760.00				287,134.00	凭证信
2018-09-29	南06822	121501	个人借款	冲农学院郭东伟借出版费				11,760.00	298,894.00	凭证信
2018-10-26	南06609	5002-3021801	科研事业支出-实验材料费	研究生院张政权报种子袋	1,580.00				297,314.00	凭证信
2018-11-01	南00072	5002-30214	科研事业支出-租赁费	农学郭东伟报温室租用费(2018.12-2.20.11)	3,900.00				293,414.00	凭证信



# 2018 年农业国际交流与合作项目 总结报告

项目任务： 中哈农业科技示范园建设

项目单位： 西北农林科技大学

联系电话： 029-87082103

联系人： 郭东伟

填制日期： 2019-01-31



# 中哈农业科技示范园建设项目总结报告

## 一、功能分类总结主要内容

(一) 项目基本情况 (包括项目立项、实施情况、经费安排和使用情况等。)

### 1、项目立项

为了响应国家“一带一路”倡议，在丝路农业教育科技创新联盟框架下，西北农林科技大学联合哈萨克斯坦北哈州立大学等单位联合建设农业科技示范园，以发挥学校长期躬耕旱区的农业科技优势和立足杨凌国际农业自贸区以及陕西省丝绸之路桥头堡的区位优势，充分体现学校响应国家一带一路建设，落实丝路联盟框架协议，推动我国农业走出去，服务于跨国企业的责任与担当。项目依托哈萨克斯坦土地资源丰富、绿色生产的特点，联合建设立足于哈国，面向中亚，服务于丝路沿线国家典型旱作农业区的综合性农业科技示范园。以创新性研究、高效生产技术集成与示范、农业科技人才培养为主要功能；采取灵活多样的方式，吸纳各类组织机构建立长期稳定的合作关系，统筹丝路联盟成员单位的科技力量和科技成果，根据中亚地区生态环境特点和农业产业特色，开展新品种、新产品研发、



生产以及绿色种养、加工技术的创新集成与示范推广，加强农业科技培训，为走出去的国内企业提供技术支撑；最终将科技示范园最终建设成为“一带一路”倡议在中亚地区农业科技合作和人才培养的重要支点，在实现提升当地农业产业科技水平，促进域内居民收入的同时，提高我国粮油的供应安全和质量安全的保障能力，同时发展与丝路沿线国家的睦邻友好合作关系，为中华民族的再次复兴创造良好的国际环境，实现双赢。

建设期限 1 年主要用于：

### 1) 新品种引种和品种比较试验

大范围征集春小麦、春油菜、玉米、马铃薯以及小宗粮豆作物品种 50 个，在北哈萨克斯坦园区开展以春小麦、春油菜小宗粮豆和马铃薯为主的品种适应性试验和品种比较试验，每个作物筛选 1-2 个适宜当地种植的品种，用于下一步推广种植。

### 2) 小麦新品种培育研究

收集当地优良作物种质资源，将国内优良品种与哈萨克斯坦当地优良小麦品种进行杂交，配置组合 50 个，为下一步两地三方穿梭育种，选育优良新品系以及更进一步的科学研究奠定基础。

### 3) 作物高效栽培技术集成与示范

以示范园为平台，开展垄沟集雨（雪）、宽窄行、宽行条

播、秸秆还田等栽培技术试验研究，熟化 1-2 项适合当地生态条件的高产高效栽培技术，用于下一步的推广应用。适当施用保水剂，种植短季节品种，耐旱品种，采取高留茬垄沟集雪栽培，提高作物春季抗旱能力，对综合技术进行示范推广。

#### 4) 农业生产技术培训

以示范园为平台，为爱菊粮油集团公司培训具备国际贸易和粮油收储质量监控能力的技术人才；与北哈萨克斯坦州立大学农学院联合培养能够进行作物育种、种质资源评价和作物高产栽培技术与推广的科技骨干，并在此基础上为企业订单农户进行生产技术培训。

### 2、实施情况

项目执行一年来团队成员精诚合作，分别进行了作物新品种引种试验，小麦新品种培育研究，栽培技术集成与示范，技术培训等四类活动，全面完成了年度合同指标，在部分数量指标上超额完成任务。

### 3、经费安排和执行情况

项目获批总经费 60 万元，包括：委托业务费 5.6 万元，专用材料费 4.4 万元，差旅费 3.6 万元，涉外培训费 8.6 万元，出国费 30 万元，间接费 7.8 万元。

截止 2018 年 12 月 31 日项目经费共支出 39.78 万元，主要用于运输、报关等业务委托 9.61 万元，材料费 1.12 万元，



差旅费 5.66 万元，国际合作交流费 23.39 万元；结余经费 20.22 万元。

## （二）主要做法

1. 工作开展情况。（包括工作部署、支撑条件建设、组织管理措施，具体执行情况、方式、规模等，其中具有创新性的做法或措施，请进行详细描述。）

1) 工作部署：自 2018 年初，双方协商建设农业科技示范园以来，校级层面均给予了高度重视，哈方由该校科研副校长 Yelbov 任示范园建设小组组长，农学院院长 Altyn 为建设小组副组长，另外为小麦、油菜、马铃薯、小杂粮各配备一位对接专家。中方则由农学院院长单卫星教授任组长、副院长郭东伟任副组长，同时配备小麦育种家 2 名，油菜、马铃薯、小杂粮、作物栽培学、作物区划学专家各 1 名，形成共计 9 人的建设团队。设定作物种植计划，每年 5 月中下旬、7 月上、8 月中旬、9 月中旬，均有专家赴示范园进行工作指导。

2) 支撑条件：哈方为示范园无偿提供 5 公顷核心试验地，土地距北哈州立大学约 4 公里，示范园配备有部分农业机械和灌溉设施，每年学校为示范园配套少量经费，用以维持示范园的日常田间管理、种子清关以及运输等开支；西北农林科技大学为示范园每年提供约 20 万元的配套经费，



网上查询系统V6.0



返回 >> 项目预算执行

起始年度: 2015 起始月份: 01 截止年度: 2020 截止月份: 04

部门项目信息: (00100)农学院/(A213021707)一带一路 - 中哈农业科技示范园建设

摘要:

是否包含往来款: ☒是 ☐否

是否包含未复核: ☒是 ☐否

类型: 所有

查询

导出

打印

汇总数据		报表								
凭证日期	凭证编号	科目编号	科目名称	摘要	项目支出	项目收入	项目借款	项目还款	余额	凭证信息
				年初余额						
				期初余额						
2017-10-09	预算00001	6002	预算分配	国际交流处划拨17年"一带一路"合作项目经费		100,000.00			100,000.00	凭证信息
2017-11-21	南05272	5002-3021101	科研事业支出-差旅费	农学院黄镇报郭东伟等3人北京差旅费	6,456.50				93,543.50	凭证信息
2017-11-21	南05327	5002-3021103		农学院黄镇报4人哈萨克斯坦出国费	49,609.72				43,933.78	凭证信息
2017-11-21	南05333	5002-3021101	科研事业支出-差旅费	农学院黄镇报3人北京差旅费	7,137.50				36,796.28	凭证信息
2017-11-23	预算00041	6002	预算分配	收回国际合作与交流经费	36,796.28					凭证信息
2018-03-13	预算00026	6002	预算分配	返还2017年收回国际合作项目结余资金		36,796.28			36,796.28	凭证信息
2018-04-02	南00045	5002-30201	科研事业支出-办公费	农学院潘小东报办公用品	1,760.00				35,036.28	凭证信息
2018-04-02	南00045	5002-30202	科研事业支出-印刷费	农学院潘小东报打印复印费	3,526.00				31,510.28	凭证信息
2018-04-11	南01650	5002-3023901	科研事业支出-租用费	农学院郭东伟报租车费	12,950.00				18,560.28	凭证信息
2018-05-24	南04741	5002-3020701	科研事业支出-邮寄费	农学院郭东伟报种子邮寄费	2,818.00				15,742.28	凭证信息
2018-05-29	南05527	5002-3021101	科研事业支出-差旅费	农学院潘小东报西安差旅费	650.72				15,091.56	凭证信息
2018-05-29	南05531	5002-3021101	科研事业支出-差旅费	农学院潘小东报西安差旅费	650.71				14,440.85	凭证信息
2018-05-29	南05535	5002-3021101	科研事业支出-差旅费	农学院潘小东报西安差旅费	650.74				13,790.11	凭证信息
2018-05-29	南05537	5002-3021101	科研事业支出-差旅费	农学院潘小东报西安差旅费	650.71				13,139.40	凭证信息
2018-05-29	南05543	5002-3021101	科研事业支出-差旅费	农学院潘小东报省农业厅报送文件差旅费	650.73				12,488.67	凭证信息
2018-06-21	会计00192	5002-3024099	科研事业支出-其他税费	支农学院郭东伟农业部国际合作交流项目增值税	12,488.67					凭证信息
2018-10-29	预算00053	6002	预算分配	划拨农业部中哈科技农业示范园建设经费		600,000.00			600,000.00	凭证信息
2018-11-19	南03995	5002-3021202	科研事业支出-业务出国(境)费用	农学院郭东伟报哈萨克斯坦签证费	1,842.00				598,158.00	凭证信息

共76行

首页 上一页 1 2 3 4 下一页 尾页 1 跳转

陕西杨凌

制度体质, 想瘦多少瘦多少! 广告

快剪辑 每日关注 热点资讯





# 杨凌示范区发展和改革局 杨凌示范区国际合作局 文件 杨凌示范区财政局

杨管发改发〔2017〕220号

---

## 关于下达 2017 年丝绸之路经济带-杨凌现代农业国际交流合作专项资金计划的通知

各项目单位：

为加快推动中国（陕西）自由贸易试验区杨凌片区和丝绸之路经济带现代农业国际交流合作中心建设，根据《关于征集 2017 年丝绸之路经济带-杨凌现代农业国际交流合作专项资金项目的通知》（杨管发改发〔2017〕16 号）要求，经党工委管委会研



究同意，现将 2017 年丝绸之路经济带-杨凌现代农业国际交流合作专项资金计划下达给你们，并就有关事项通知如下：

一、请各项目单位 12 月 5 日前签订《杨凌示范区 2017 年丝绸之路经济带-杨凌现代农业国际交流合作专项资金项目实施协议书》，并严格按照批准项目的名称、内容和规模进行建设，不得擅自变更。

二、本次下达资金支持方式为无偿资助，首批拨付 30%，项目验收后拨付剩余的 70%。财政资金必须专款专用，严禁截留挪用、滞留不用和浪费建设资金，确保资金安全，充分发挥投资效益。

三、项目单位要落实好配套资金、建设条件和相关工作；项目实施过程中要加强项目管理，落实好项目法人责任制、招标投标制、合同管理制、工程监理制，确保工程质量安全。

四、各项目单位要明确专人负责，于每季度前 3 日前将上年度项目进展情况分别报送示范区发改局和国际合作局，年终报送项目实施情况专项报告。一次逾期不报者予以提醒，二次逾期不报者予以警告，三次逾期不报者等同于项目终止，在收回已拨资金的同时，纳入陕西省公共信用信息平台“黑名单”信息系统。项目建成后，各项目单位要及时向示范区发改局申请项目验收。

六、请各项目建设单位，按照有关规定及时与示范区财政对接，办理资金拨付手续。



附件：2017年丝绸之路经济带-杨凌现代农业国际交流合作  
专项资金项目计划表（总表不发各项目单位）



2017年11月28日

附件:

2017年丝绸之路经济带-杨凌现代农业国际交流合作专项资金项目计划表

序号	项目名称	建设单位	主要建设规模和内容	实施地点	实施期限	总投资(万元)	支持额度(万元)
1	丝路沿线国家农业科技人才培训提升项目	西北农林科技大学	以西北农林科技大学专家教授为技术依托,以杨凌示范区丝路沿线国家农业科技示范园为基地,校企合作,针对丝路沿线国家当地科技需求和人才状况,在杨凌和丝路沿线国家当地进行科技提升培训,计划年培训国际留学生、交流访学生、丝路国家农业科技青年学术骨干和农业技术骨干等30-50人,不断提升杨凌示范区农业技术推广能力和扩大农业技术辐射范围。	杨凌,中亚五国,土耳其、俄罗斯、巴基斯坦等	2017-2020	200	30
合计							30





网上查询系统 V6.0



返回 >> 项目预算执行

起始年度: 2017 起始月份: 01

截止年度: 2020

截止月份: 04

部门项目信息: (00100)农学院/(A279021802)丝路沿线国家农业科技人才培训提升

摘要:

是否包含往来款: ☒ 是 ☐ 否

是否包含未复核: ☒ 是 ☐ 否

类型: 所有

查询

导出 打印

汇总数据		报表								
凭证日期	凭证编号	科目编号	科目名称	摘要	项目支出	项目收入	项目借款	项目还款	余额	凭证
2019-09-09	南00464	720102-3023901	科研支出-租用费	农学院郭东伟报租车费(榆林,定边)	5,620.00				37,903.35	凭证
2019-09-09	南00476	720102-3021101	科研支出-差旅费	农学院郭东伟报郭东伟南洛查看玉米材料差旅费用	1,600.00				36,303.35	凭证
2019-10-09	南00408	121801-3029903	应收个人款项-版面费	农学院郭东伟借<教育教学论坛>版面费			5,200.00		-	凭证
2019-10-09	南00408	720102-3029903	科研支出-版面费	农学院郭东伟借<教育教学论坛>版面费	5,200.00				31,103.35	凭证
2019-10-18	会计00231	66010203	陕西地方拨款	收杨凌示范区管委会丝路沿线国际农业科技培训经费		210,000.00			241,103.35	凭证
2019-11-01	南00032	720102-3021101	科研支出-差旅费	农学院郭东伟报北京渭南项目汇报玉米区考察差旅费用	4,227.00				236,876.35	凭证
2019-11-14	南04045	720102-3021804	科研支出-试剂药品费	农学院郭东伟报试剂	2,384.00				234,492.35	凭证
2019-11-14	南04046	121801-3029903	应收个人款项-版面费	冲农学院郭东伟借<教育教学论坛>版面费				5,200.00	-	凭证
2019-11-20	南06094	720102-3021101	科研支出-差旅费	农学院郭东伟报郭东伟南京杭州差旅费用	4,049.00				230,443.35	凭证
2020-03-16	南00541	720102-3021801	科研支出-实验材料费	农学院郭东伟报去离子水	600.00				224,955.35	凭证
2020-03-16	南00541	720102-3021101	科研支出-差旅费	农学院郭东伟报孟加拉国退票费	1,600.00				223,355.35	凭证
2020-03-16	南00541	720102-3020701	科研支出-邮寄费	农学院郭东伟报快递费	100.00				223,255.35	凭证
2020-03-24	南01333	720102-3021101	科研支出-差旅费	农学院郭东伟报郭东伟西安差旅费用	235.00				223,020.35	凭证
2020-03-24	南01339	720102-3022602	科研支出-临时聘用人员工资	农学院郭东伟发放海南聘用人员工资	4,515.00				218,505.35	凭证
负责人: 郭东伟		A279021802/丝路沿线国家农业科技人才培训提升 合计			81,494.65	300,000.00	5,200.00	5,200.00	218,505.35	
总计		总计			81,494.65	300,000.00	5,200.00	5,200.00	218,505.35	

共37行

首页 上一页 1 2 下一页 尾页 2 跳转

陕西杨凌

# 杨凌种子产业园种子质量检验检测及 研发平台建设初步设计合同书



项目名称：杨凌种子产业园种子质量检验检测及研发  
平台建设初步设计

工程地点：杨凌种子产业园种业综合服务中心

委 托 人：陕西杨凌农科集团公司

设 计 人：西北农林科技大学

签订日期： 2019 年 10 月 12 日



# 实验室建设初步设计合同书

委托方：（以下简称甲方）陕西杨凌农科集团有限公司

设计方：（以下简称乙方）西北农林科技大学（郭东伟教授团队）

依照《中华人民共和国合同法》及有关法律、法规的规定，结合种子质量检验检测以及种业研发实验室设计的特点，双方在平等、自愿、协商一致的基础上，就杨凌种子产业园农作物种子质量检验检测及种业研发实验室建设初步设计的有关事宜，达成如下合同：

## 1 本合同依据下列文件签订

1.1 《中华人民共和国合同法》、《实验室生物安全通用要求》（GB 19489-2008）等。

1.2 国家及行业有关实验室建设法规和规章等。

1.3 行业发展需求及项目申报可行性研究报告。

## 2 本合同设计项目名称及工程地点

2.1 设计项目名称：杨凌种子产业园种子质量检验检测及研发平台建设初步设计

2.2 工程地点：杨凌种子产业园种业综合服务中心（杨凌种子大厦）B座7-8层。

## 3 本合同设计项目内容

3.1 设计总体要求

3.1.1 充分考虑实验室业务的发展前景，既要有前瞻性，预留一定发展空间，又要考虑经济性，不能无限制扩大。按照流程化、科学化、人性化的需求开展设计。

3.1.2 为施工图设计单位提供实验室功能布局图以及实验室设计所包含的管综工程、水电工程、通风、通气、废气废水处理、弱电系统等的需求指标（必需满足实验设备安装、使用的各项条件要求）。

3.1.3 依据实验室设计目标进行设备选型，并提供选型依据以及进行设备采购所需的型号、参数等招标文件。

### 3.2 农作物种子质量检验检测平台设计

3.2.1 根据《农作物种子检验规程》（GB/T35431-35437-1995）、农业部关于印发《农作物种子质量检验机构考核准则》等文件的通知、《农作物种子质量检验机构考核管理办法》（农业部令 2013 年第五号修订）要求开展设计。使实验室具备开展作物种子转基因检测、纯度检测和身份检测等能力。

3.2.2 设计内容：实验室布局、水电及研发设备选型。

3.2.3 编制开展种子质量检测机构资格认证所需的全部文件资料，配合实验室完成资格认证。

### 3.3 种业研发实验室设计

3.3.1 设计目标：使实验室具备开展作物转基因、基因编辑、SNP 筛查、诱变育种、生理育种、品质育种及相关检测的能力。

3.3.2 设计步骤：总体规划、分步实施。

3.3.3 设计内容：实验室布局、水电及研发设备选型。



### 3.4 设计资质及资料数量

提供具有设计甲级资质单位盖章的初步设计报告。设计完成经甲方审定后，乙方为甲方提供 5 套完整的设计方案纸质版及电子版 1 套。

## 4 设计费用、期限及支付方式

4.1 设计费用：本次设计总费用为贰拾肆万元整（¥：240000 元）。

4.2 设计期限：本次设计期限为 30 天，即 2019 年 10 月 10 日至 2019 年 11 月 10 日。（农作物种子质量检验检测平台的资格认定以工作实际开展日期为准）。

4.3 付款方式：分三次支付，具体支付方式如下：

合同签订后 7 个工作日内，甲方支付乙方设计总费用的 30%，即柒万贰仟元整（¥：72000 元）；

完成初步设计，通过甲方的验收评审后，甲方支付乙方设计总费用的 30%，即柒万贰仟元整（¥：72000 元）。

完成农作物种子质量检验机构资格认定，甲方支付乙方设计总费用的 40%，即玖万陆仟圆整（¥：96000 元）；

甲方每次支付后，乙方提供相应金额的发票。

乙方开户银行名称、开户名称和账户号码为：

开户银行：中国银行杨凌农业高新技术产业示范区支行

开户名称：西北农林科技大学

账户号码：102810820826

## 5 双方责任

## 5.1 委托人责任

5.1.1 在规定的时间内向设计人提交基础资料及文件，并对其完整性、正确性及时限负责。

5.1.2 委托人变更委托设计项目、规模、条件或因提交的资料错误，或所提交资料作较大修改，以致造成设计人设计需返工时，双方另行协商签订补充合同、重新明确有关条款。一般性设计变更，已包含在设计费中，乙方不再另计取费用。当变更要求全部设计要推倒重来、重新设计时，甲方与乙方协商，按原合同价的 50%收取设计费用，并另行签订补充合同。

5.1.3 委托人要求设计人比合同规定时间提前交付设计文件时，如果设计人能够做到，应根据甲方要求尽量提前完成工作量，甲方不再向设计人支付赶工费。

5.1.4 委托人应保护设计人的设计方案、文件、资料图纸、数据和计算软件等。未经设计人同意，委托人对设计人交付的设计资料及文件不得擅自修改、复制或向第三人转让或用于本合同外的项目。如发生以上情况，委托人应负法律责任，设计人有权向委托人提出索赔。

## 5.2 设计人责任

5.2.1 设计人应按国家规定技术规范、标准、规程及委托人提出的设计要求，进行设计，按合同规定的进度要求提交质量合格的设计资料，并对其负责。

5.2.2 设计人采用的主要技术标准是：国家现行的法律、法规及行业规范。



5.2.3 设计人交付设计资料及文件后，按规定参加有关的设计审查，并根据审查结论负责对所交付的设计资料进行设计变更和说明。

5.2.4 设计人按合同规定时限交付设计资料及文件，并在该项目开始施工中，免费向委托人及施工单位进行设计交底、技术咨询、技术变更、处理有关设计问题和参加竣工验收等。

## **6 违约责任**

6.1 在合同履行期间，委托人要求终止或解除合同，设计人未开始设计工作的，不退还委托人已付的定金；已开始设计工作的，委托人应根据设计人已完成的实际工作量，已完成的比例，双方协商后按比例支付设计费。

6.2 委托人应按本合同第 4 条规定的金额和时间向设计人支付设计费，每逾期支付一天，应承担支付金额千分之二逾期违约金。逾期超过 60 天以上时，设计人有权暂停履行下阶段工作，并书面通知委托人。

6.3 设计人对设计资料及文件出现的遗漏或错误负责修改或补充。

6.4 由于设计单位自身原因，延误了按本合同第 4 条规定的设计资料及设计文件的交付时间，每延误一天，应减收该项目应收设计费的千分之二。

## **7 其他约定**

7.1 由于不可抗力因素致使合同无法履行时，双方应及时协商解决。

7.2 本合同在履行过程中发生的争议，由双方当事人协商解决，协商不成的按下列第（2）种方式解决：





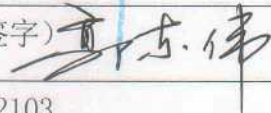
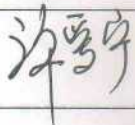
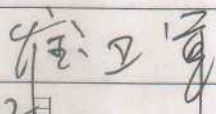
（1）提交     /     仲裁委员会仲裁；

（2）依法向委托人所在地人民法院起诉。

7.3 本合同份数：本合同共计八份，正本两份，副本六份，委托人与设计人各执正本一份，委托人执副本四份，设计人执副本两份，正副本具有同等法律效力。

7.4 本合同经双方签字盖章后生效。

7.5 本合同未尽事宜，双方可签订补充合同，有关合同及双方认可的来往电报、传真、会议纪要等，均为本合同组成部分，与本合同具有同等法律效力。

甲 方	乙 方
	
地址：杨凌示范区杨扶路中段现代农业创新园	地址：西北农林科技大学
邮编：712100	邮编：712100
法定代表人：	法定代表人： 
被授权代表：(签字) 	被授权代表：(签字) 
电话：029-87037345	电话：029-87082103
传真：029-87097950	传真：029-87082103
 伏晓兴	开户银行：中国银行杨凌农业高新技术产业示范区支行
	帐号：102810820826
日期：2019年10月12日	日期：2019年10月12日



# 荣誉证书

HONORARY CREDENTIAL

授予：

郭东伟同志2018年度杨凌示范区“农业

科技示范推广工作先进个人”荣誉称号。



二〇一九年三月





# 荣誉证书

## HONORARY CREDENTIAL

西北农林科奖证字 (2019) 第 014 号

郭东伟 同志:

你参加完成的“优质早熟抗寒抗赤霉病  
小麦新品种西农 979 的选育与应用”成果，  
获 2019 年度国家科学技术进步 贰 等奖。

特发此证。



二〇二〇年一月十三日





# 科技推广工作掠影



2017 年春在阿拉木图示范园参加播种



2018 年夏中哈专田间调查作物生长



共同研究制定试验工作方案





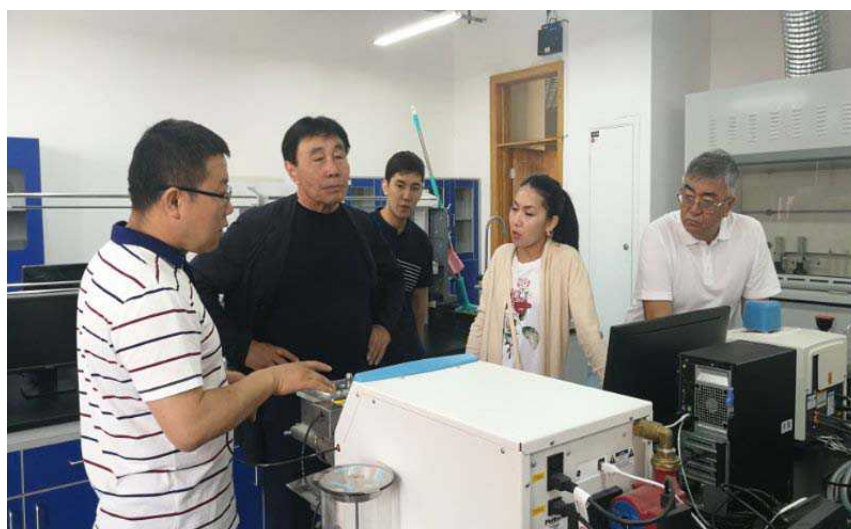
利用哈国小麦种质资源开展小麦杂交育种与田间调查



中哈研究生联欢晚会



中国驻阿拉木图总领馆郭兴桥副总领接见我校代表团一行



向来访专家介绍农学院科研平台





深入田间调查作物长势



接受中国日报、光明日报、经济日报等 8 家媒体采访



举办丝绸之路粮油加工与国际贸易培训班



组织举办陕西省农作物学会年会





组织筹备丝绸之路小麦创新联盟成立大会



克明面业安东种植基地



北哈州农业企业查看当地油菜病害



爱菊海外人才培养基地



北哈州农业科技示范园察看作物生长情况



# DB6111

## 杨凌农业高新技术产业示范区地方标准

DB 6111/T 127—2015

---

### 西农 979 小麦-玉米两熟区 优质高产栽培技术规程

Technical Specification for High-quality and High-yield cultivation of the Wheat

Variety XiNong979 in Area of Maize-wheat Rotation

2015 - 07 - 31 发布

2015 - 09 - 01 实施

杨凌示范区质量技术监督局 发布

## 前 言

本规程依据GB/T 1.1-2009给出的规则起草。

本规程由杨凌农业标准化专业技术委员会提出并归口。

本规程起草单位：西北农林科技大学、杨凌现代农业产业标准化研究推广服务中心。

本规程主要起草人：刘 杨、闵东红、李学军、孙道杰、张玲丽、冯 毅、郭东伟、王辉、杨 静、孙亚莉。

本规程首次发布。



# 西农 979 小麦-玉米两熟区优质高产栽培技术规程

## 1 范围

本规程规定了小麦-玉米两熟区西农979小麦优质高产栽培的术语与定义、产地环境、播前准备、播种、田间管理、收获贮藏。

本规程适用于杨凌示范区西农979小麦优质高产栽培。陕西关中麦区、黄淮南部麦区等同类生态区的杨凌示范基地可参考执行。

## 2 规范性引用文件

下列文件对于本文件的应用是必不可少的。凡是注日期的引用文件，仅所注日期的版本适用于本文件。凡是不注日期的引用文件，其最新版本（包括所有的修改单）适用于本文件。

GB 4285-1989 农药安全使用标准

GB 4404.1-2008 粮食作物种子 第1部分：禾谷类

GB/T 17320-2013 小麦品种品质分类

NY/T 496-2010 肥料合理使用准则 通则

NY/T 851-2004 小麦产地环境技术条件

NY/T 1276-2007 农药安全适用范围 总则

## 3 术语与定义

下列术语和定义适用于本文件。

### 3.1

#### 优质

指小麦品质符合GB/T 17320-2013规定的强筋小麦要求：粗蛋白质含量（干基） $\geq 14.0\%$ ，湿面筋含量（ $14\%$ 水分基） $\geq 30.5\%$ ，吸水率 $\geq 60\%$ 、稳定时间 $\geq 10.0\text{ min}$ ，最大拉伸阻力Rm.E.U.（参考值） $\geq 450$ ，拉伸面积 $\geq 100\text{ m}^2$ 。

### 3.2

#### 高产

指产量 $550\text{ kg}/667\text{ m}^2 \sim 650\text{ kg}/667\text{ m}^2$ 。

## 4 产地环境

西农979小麦优质高产栽培的产地环境选择应符合NY/T 851-2004小麦产地环境技术条件。

## 5 播前准备

### 5.1 基肥施用

5.1.1 根据土壤的肥力基础,测土平衡施肥。在秸秆还田、增施有机肥  $3\text{ m}^3/667\text{ m}^2 \sim 5\text{ m}^3/667\text{ m}^2$  的基础上,施氮肥(纯氮)  $8\text{ kg}/667\text{ m}^2 \sim 10\text{ kg}/667\text{ m}^2$ 、磷肥(五氧化二磷)  $6\text{ kg}/667\text{ m}^2 \sim 10\text{ kg}/667\text{ m}^2$ 、钾肥(氧化钾)  $5\text{ kg}/667\text{ m}^2 \sim 8\text{ kg}/667\text{ m}^2$ 。

5.1.2 有机肥、磷肥、钾肥作底肥,犁地时深翻施入。产量  $550\text{ kg}/667\text{ m}^2 \sim 650\text{ kg}/667\text{ m}^2$  的麦田,氮肥 50 %作底肥犁地时施入,50 %作追肥,其中 30 %作拔节期,20 %作孕穗肥追施。

5.1.3 使用氮磷钾肥料前,要测试肥料养分含量,并根据含量折算出实物量。使用复合肥料,可按 5.1.1 规定的氮肥、磷肥、钾肥施用量折算,并扣除其他养分含量的施用量,不得重复施肥。

### 5.2 种子准备

#### 5.2.1 种质要求

符合 GB 4404.1-2008 良种种子指标的西农979小麦种子。

#### 5.2.2 种子处理

##### 5.2.2.1 播前晒种

播种前将小麦种子以 5 cm~7 cm 厚度,晾晒 1 d~2 d,每隔 1 h~2 h 翻动一次。注意勿在水泥地、铁板、石板和沥青路面晒种,以防高温烫伤种子,降低发芽率。

##### 5.2.2.2 种子包衣

种子包衣剂应含有杀虫剂、杀菌剂主要活性成分。小麦种子包衣剂种类、杀虫剂和杀菌剂的使用应符合 GB 4285 和 NY/T 1276-2007 的规定。包衣剂参见附录 A.1。

##### 5.2.2.3 拌种

根据不同需求按下列方法操作:

- 纹枯病、根腐病、茎基腐病和黑穗病:用 6 % 的戊唑醇拌种剂 10 mL 加水 0.4 kg~0.5 kg,拌种 25 kg~30 kg;或使用 2.5 % 咯菌腈、或 3 % 苯醚甲环唑悬浮种衣剂单剂、或复配剂按 1:500 (药:种) 拌种。拌种剂的使用参见附录 A.1。
- 小麦全蚀病:用 12.5 % 的硅噻菌胺悬浮种衣剂 20 mL 加水 100 mL 处理麦种 10 kg;或利用 2.5 % 的咯菌腈悬浮种衣剂 20 mL 加 3 % 的苯醚甲环唑悬浮种衣剂 40 mL,加水 60 mL 处理麦种 10 kg。拌种剂的使用参见表 A.1。
- 地下害虫:用 3 % 的辛硫磷颗粒剂  $2\text{ kg}/667\text{ m}^2 \sim 3\text{ kg}/667\text{ m}^2$ ,耕地时撒施;或 50 % 的辛硫磷乳油  $15\text{ mL}/667\text{ m}^2 \sim 20\text{ mL}/667\text{ m}^2$  加水 600 mL~800 mL 拌种 10 kg。拌种剂的使用参见附录 A.1。
- 病、虫混发田块,可用上述杀虫剂和杀菌剂混合拌种或包衣。

### 5.3 整地

#### 5.3.1 土壤处理

地下害虫发生严重的地块,可用 3 % 辛硫磷颗粒或 2.5 % 的甲基异柳磷颗粒  $2\text{ kg}/667\text{ m}^2 \sim 3\text{ kg}/667\text{ m}^2$  拌细土 25 kg,耕地后均匀撒施于地面,随耙地翻入土中。



### 5.3.2 整地

玉米秸秆还田的地块，应机械粉碎还田，耕深25 cm左右，耙耱压实，或用深松机深松30 cm左右，并浇塌墒水，补施尿素5 kg/667m<sup>2</sup>，加速秸秆腐解。

## 6 播种

### 6.1 播期与播量

杨凌示范区及陕西关中西部适播期10月5日~15日，播量8 kg/667m<sup>2</sup>~10 kg/667m<sup>2</sup>；关中中部和东部适播期10月10日~12日播种，播量10 kg/667m<sup>2</sup>~12 kg/667m<sup>2</sup>。在适播期以后播种，每推迟一天，播种量应增加0.25 kg/667m<sup>2</sup>。播种深度3 cm~5 cm。

### 6.2 播种

采用精量播种机播种，播深3 cm~5 cm。高产田块采用等行距播种(18 cm~20 cm)，或宽窄行播种(24 cm×16 cm)，或采用宽幅播种方式播种(幅宽8 cm，行距12 cm)；中低产田采用20 cm~23 cm等行距播种。

## 7 田间管理

### 7.1 前期管理

#### 7.1.1 冬前管理

##### 7.1.1.1 查苗补种

出苗后及早检查，对缺苗断垄严重的地段于二叶期前用同品种种子浸种催芽后补种。

##### 7.1.1.2 化学除草

11月中下旬~12月上旬日平均气温在10℃以上时化学除草。

- a) 阔叶杂草 用75%的确隆0.001 kg/667m<sup>2</sup>，或15%的噻磺隆0.01 kg/667m<sup>2</sup>，兑水30 kg喷雾；或用5.8%的双氟磺草胺悬浮剂10 mL/667m<sup>2</sup>，或20%的氯氟吡氧乙酸乳油50 mL/667m<sup>2</sup>~60 mL/667m<sup>2</sup>，兑水30 kg喷雾。除草剂的种类及防治对象参见附录A.2。
- b) 单子叶杂草 用3%甲基二磺隆乳油30 mL/667m<sup>2</sup>，兑水30 kg喷雾；野燕麦、看麦娘等禾本科杂草用6.9%精恶唑禾草灵水乳剂60 mL/667m<sup>2</sup>~70 mL/667m<sup>2</sup>或10%精恶唑禾草灵乳油30 mL/667m<sup>2</sup>~40 mL/667m<sup>2</sup>，兑水30 kg喷雾。除草剂的种类及防治对象参见附录A.2。

### 7.1.2 早春管理

#### 7.1.2.1 水肥管理

秸秆还田、旋耕播种，土壤悬空不实，冬前降水不足，土壤墒情差的麦田，应在日平均气温 $3^{\circ}\text{C}\sim 5^{\circ}\text{C}$ 夜冻日消时适时冬灌，当耕层土壤含水量在50 %时，灌水 $40\text{ m}^3/667\text{m}^2\sim 50\text{ m}^3/667\text{m}^2$ 。浇水后及时划锄。小麦起身期可趁墒穴施或结合浇水追施 $7\text{ kg}/667\text{m}^2\sim 12\text{ kg}/667\text{m}^2$ 尿素。壮苗，在拔节期以中耕除草为主，到拔节末期基部第一节间固定、第二节间伸长1 cm以上，开始出现分蘖两极分化时，结合浇水追尿素 $5\text{ kg}/667\text{m}^2\sim 10\text{ kg}/667\text{m}^2$ 。旺苗类麦田，拔节以后酌情增减追肥用量。

#### 7.1.2.2 预防倒春寒

在寒流到来前及时浇水，一旦发生冻害，应结合浇水追施速效化肥或叶面追肥等措施补救。

#### 7.1.2.3 预防倒伏

返青群体超过100 万个/ $667\text{m}^2$ 的麦田，应及早采取化控防倒措施，陕西关中西部在3月1日~3月10日以前，关中中部和东部在2月25日~3月5日以前，用15 %的多效唑可湿性粉剂 $30\text{ g}/667\text{m}^2\sim 50\text{ g}/667\text{m}^2$ 兑水50 kg喷洒，喷洒时要注意选择日平均温度在 $10^{\circ}\text{C}$ 左右、晴天无风的天气；或深锄7 cm~10 cm断根控长。

### 7.2 中、后期管理

#### 7.2.1 病虫害防治

##### 7.2.1.1 返青期-抽穗期

在返青期至抽穗期，重点防治小麦锈病、白粉病和、纹枯病以及蚜虫和红蜘蛛。

- 纹枯病、茎基腐病：用12.5 %的烯唑醇可湿性粉剂 $0.03\text{ kg}/667\text{m}^2$ ，加50 %的多菌灵可湿性粉剂 $0.08\text{ kg}$ ，兑水 $30\text{ kg}\sim 45\text{ kg}$ ，对准茎基喷雾。
- 锈病、白粉病：用15 %的三唑酮可湿性粉剂 $0.08\text{ kg}/667\text{m}^2\sim 0.1\text{ kg}/667\text{m}^2$ ，或12.5 %的烯唑醇可湿性粉剂 $0.03\text{ kg}/667\text{m}^2$ ，兑水 $45\text{ kg}\sim 60\text{ kg}$ 喷雾。
- 红蜘蛛：虫口达到单行600头/m时，用15 %的哒螨灵乳油1500~2000倍液喷雾，或1.8 %的阿维菌素6000倍液喷雾。
- 蚜虫：虫口达到每株5头时，用50 %抗蚜威可湿性粉剂 $0.01\text{ kg}/667\text{m}^2$ 兑水 $30\text{ kg}\sim 40\text{ kg}$ 喷雾。参见附录A.3。

##### 7.2.1.2 抽穗期-成熟期

抽穗-成熟期要注意防治赤霉病，灌浆后期注意防治白粉病、锈病、叶枯病、黑胚病及蚜虫。

- 赤霉病 小麦齐穗期用50 %的多菌灵可湿粉剂 $0.08\text{ kg}/667\text{m}^2$ ，或40 %的多菌灵胶悬剂 $0.1\text{ kg}$ ，或25 %的氰烯菌酯悬浮剂 $100\text{ mL}/667\text{m}^2$ ，兑水 $40\text{ kg}\sim 60\text{ kg}$ ，对穗部均匀喷雾。
- 白粉病、锈病、叶枯病：用12.5 %的烯唑醇可湿性粉剂 $0.03\text{ kg}/667\text{m}^2\sim 0.05\text{ kg}/667\text{m}^2$ ，或25 %的丙环唑 $30\text{ mL}/667\text{m}^2$ ，兑水 $30\text{ kg}\sim 40\text{ kg}$ 均匀喷雾。
- 蚜虫：虫口密度达到每株5头时，用10 %的吡虫啉可湿性粉剂 $0.02\text{ kg}/667\text{m}^2$ ，或50 %的抗蚜威可湿性粉剂 $0.01\text{ kg}/667\text{m}^2$ ，或3 %的啶虫脒可湿性粉剂 $0.03\text{ kg}/667\text{m}^2\sim 0.04\text{ kg}/667\text{m}^2$ ，兑水 $30\text{ kg}\sim 50\text{ kg}$ 喷雾。



### 7.2.2 叶面喷肥

扬花期后7 d~10 d, 结合“一喷三防”用磷酸二氢钾500 g/667m<sup>2</sup>+尿素0.5 kg/667m<sup>2</sup>~1 kg/667m<sup>2</sup>, 兑水30 kg~50 kg叶面喷施。防治措施参见附录A.3。

### 7.2.3 水分管理

抽穗至灌浆期, 耕层土壤相对含水量低于50 %时, 应选择无风天气, 及时补灌。成熟前15 d之内禁止浇水。

## 8 收获与储存

应在蜡熟末期, 及时收获, 单收、单运、单晒、单储。

## 附录 A (资料性附录)

### 西农 979 小麦病虫害防治方法

#### A.1 病虫害防治对象及种衣剂种类

防治对象及小麦种衣剂种类参见表A.1。

表A.1 防治对象及种衣剂种类

单位: mL/10 kg种子

防治对象	药剂种类
全蚀病	12.5 %硅噻菌胺 FS、2.5 %咯菌腈 FS、3 %苯醚甲环唑 FS
纹枯病、根腐病、茎基腐病、黑穗病	6 %戊唑醇 FS、2.5 %咯菌腈 FS、3 %苯醚甲环唑 FS
地下害虫	3 %辛硫磷颗粒剂、60 %吡虫啉 FS、50 %辛硫磷乳油 EC

#### A.2 草害防治对象及化学除草剂种类

草害防治对象及化学除草剂种类参见表A.2。

表A.2 防治对象及化学除草剂种类

单位: 株/m<sup>3</sup>

防治对象	药剂种类	防治时期	防治指标	喷施部位
播娘蒿、荠菜、猪殃殃、野油菜和繁缕等阔叶杂草	苯磺隆、噻磺隆、双氟磺草胺悬浮剂、氯氟吡氧乙酸乳油	秋苗期、返青期	30	叶面喷施
野燕麦、硬草、看麦娘等单子叶杂草	精恶唑禾草灵、甲基二磺隆炔草酸(炔草酯、炔草酯)			
禾本科杂草和阔叶杂草混生	氟唑磺隆、甲氧磺草胺、阔世玛, 或者精恶唑禾草灵与苯磺隆混用、炔草酸与苯磺隆混用			

#### A.3 病虫害防治对象及常用药剂

病虫害防治对象及常用药剂参见表A.3。

表A.3 病虫害防治防治对象及常用药剂

防治对象	药剂种类	防治时期	防治指标
纹枯病、茎基腐病	12.5 %烯唑醇可湿性粉剂、50 %多菌灵可湿性粉剂	返青拔节期	病茎率 15%



表A.4 表 A.3 病虫害防治防治对象及常用药剂(续)

防治对象	药剂种类	防治时期	防治指标
锈病、白粉病、 叶枯病	15 %三唑酮可湿性粉剂、烯唑醇(禾果利) 可湿性粉剂、12.5 %烯唑醇可湿性粉剂	返青拔节期	病叶率 5 %~10 %或病情指数 15 以上
红蜘蛛	15 %哒螨灵乳油、1.8 %阿维菌素		虫口密度达到单行 600 头/m 及以 上
蚜虫	50 %抗蚜威可湿性粉剂		虫口密度达到每株 5 头以上
赤霉病	50%多菌灵可湿性粉剂、40 %多菌灵胶悬剂、 25%氰烯菌酯悬浮剂	抽穗至成熟 期	遇多雨、连阴雨天气,小麦齐穗期 喷药预防
粘虫、蚜虫、 麦叶蜂	10 %吡虫啉可湿性粉剂、50 %抗蚜威可湿性 粉剂		苗蚜百株 100 头、穗蚜百茎 500 头
麦蜘蛛	虫螨克乳油、甲氰菊酯乳油、马拉硫磷乳油、 阿维菌素乳油		单行 600 头/m
吸浆虫	吡虫啉可湿性粉剂、顺式氯氰菊酯、高效氯 氰菊酯乳油		每方(10 cm×10 cm×20 cm) 5 头,10 网复次 10 头以上成虫

# DB6111

## 杨凌农业高新技术产业示范区地方标准

DB 6111/T 128—2015

---

### 西农 979 水稻-小麦两熟区 优质高产栽培技术规程

Technical Specification for High-quality and High-yield cultivation of the Wheat  
Variety XiNong 979 in Area of Rice-wheat Rotation

2015 - 07 - 31 发布

2015 - 09 - 01 实施

杨凌示范区质量技术监督局 发布



## 前 言

本规程依据GB/T 1.1-2009给出的规则起草。

本规程由杨凌农业标准化专业技术委员会提出并归口。

本规程起草单位：西北农林科技大学、杨凌现代农业产业标准化研究推广服务中心。

本规程主要起草人：刘 杨、郭东伟、闵东红、李学军、孙道杰、张玲丽、冯 毅、王辉、杨 静、孙亚莉。

本规程首次发布。

# 西农 979 水稻-小麦两熟区优质高产栽培技术规程

## 1 范围

本规程规定了水稻-小麦两熟区西农979小麦优质高产栽培的术语与定义、产地环境、播前准备、播种、田间管理、收获贮藏。

本规程适用于杨凌示范区西农979小麦优质高产栽培。陕西关小麦区、黄淮南部麦区等同类生态区的杨凌示范基地可参考执行。

## 2 规范性引用文件

下列文件对于本文件的应用是必不可少的。凡是注日期的引用文件，仅所注日期的版本适用于本文件。凡是不注日期的引用文件，其最新版本（包括所有的修改单）适用于本文件。

GB 4285-1989 农药安全使用标准

GB 4404.1-2008 粮食作物种子 第1部分：禾谷类

GB/T 17320-2013 小麦品种品质分类

NY/T 496-2010 肥料合理使用准则 通则

NY/T 851-2004 小麦产地环境技术条件

NY/T 1276-2007 农药安全适用范围 总则

## 3 术语与定义

下列术语和定义适用于本文件。

### 3.1

#### 优质

指小麦品质符合GB/T 17320-2013规定的强筋小麦要求：粗蛋白质含量（干基） $\geq 14.0\%$ ，湿面筋含量（ $14\%$ 水分基） $\geq 30.5\%$ ，吸水率 $\geq 60\%$ 、稳定时间 $\geq 10.0\text{ min}$ ，最大拉伸阻力Rm.E.U.（参考值） $\geq 450$ ，拉伸面积 $\geq 100\text{ m}^2$ 。

### 3.2

#### 高产

指目标产量为 $450\text{ kg}/667\text{ m}^2 \sim 500\text{ kg}/667\text{ m}^2$ 。

## 4 产地环境

产地环境选择应符合NY/T 851-2004小麦产地环境技术条件。



## 5 播前准备

### 5.1 基肥

轻施基肥，重施有机肥，氮、磷、钾结合（详见7.1）。

### 5.2 种子

符合GB 4404.1-2008 良种指标的西农979小麦种子。

### 5.3 种子处理

#### 5.3.1 播前晒种

播种前将小麦种子以5 cm~7 cm厚度，晾晒1 d~2 d，每隔1 h~2 h翻动一次。注意不宜在水泥地、铁板、石板和沥青路面晒种。

#### 5.3.2 种子包衣与拌种

应结合当地病虫害种类，选用杀虫剂、杀菌剂的包衣剂进行种子拌种或包衣。小麦种子包衣剂种类杀虫剂和杀菌剂的使用应符合GB 4285和NY/T 1276-2007的规定。

——根腐病、纹枯病、黑穗病病区，用40 %的辛硫磷 100 mL 或 2 %戊唑醇 150 g，加水 5 kg，拌种 100 kg，闷种 4 h~8 h，晾干后备播。

——全蚀病病区，在上述配方中另加 12.5 %的硅噻菌胺 200 mL/667m<sup>2</sup>。

——蝼蛄、蛴螬、金针虫等地下害虫多发区，可用 40 %辛硫磷乳油药剂拌种。

### 5.4 整地开沟

#### 5.4.1 整地

前茬作物收获后，根据农时和墒情，结合施用基肥进行耕翻整地。秸秆还田视实际情况适宜加大旋耕深度，秸秆还田量大时，基肥应增施尿素5 kg/667 m<sup>2</sup>~10 kg/667 m<sup>2</sup>。

#### 5.4.2 开沟

田间外三沟在前茬水稻收获后人工清理开挖，沟系配套，逐级加深，排水沟深 100 cm 以上。田内三沟（畦沟、腰沟、田边沟）于播种后机械或人工开挖，每 2.5 m~3 m 开挖一条竖沟，沟深别达到 0.2 m、0.25 m、0.35 m 左右。距田块两端横埂 2 m~3 m，各挖一条横沟，沟深 30 cm~40 cm，田块超过 100 m 的应加挖腰沟，沟深 30 cm~40 cm，内外沟配套相同。

## 6 播种

### 6.1 播期与播量

播种期以10月15~25日为宜，播量12 kg/667m<sup>2</sup>~15 kg/667m<sup>2</sup>，基本苗宜14 万株/667m<sup>2</sup>~16万株/667m<sup>2</sup>。抢茬早播，适迟播后每推迟1 d，播量增加0.25kg/667m<sup>2</sup>。

### 6.2 播种方式

免耕机条播，宽幅播种，一次完成旋耕、开沟、播种、覆土、镇压等工序。行距25 cm，播深3 cm~5 cm。播深适宜、深浅一致，出苗均匀、苗量合理。

出苗后要进行查缺补漏，可浸种催芽补苗。

## 7 田间管理

### 7.1 施肥

#### 7.1.1 基肥

施有机肥1000 kg/667m<sup>2</sup>，纯氮(N) 14 kg/667m<sup>2</sup>~16 kg/667m<sup>2</sup>，P<sub>2</sub>O<sub>5</sub> 6 kg/667m<sup>2</sup>~8 kg/667m<sup>2</sup>，K<sub>2</sub>O 8 kg/667m<sup>2</sup>~10 kg/667m<sup>2</sup>。N:P<sub>2</sub>O<sub>5</sub>:K<sub>2</sub>O = 5:3:3。氮肥施用以基肥：壮蘖肥：拔节肥：孕穗肥=5:1:2:2为宜(纯氮)，结合整地底肥施用尿素15~17kg/667m<sup>2</sup>，P<sub>2</sub>O<sub>5</sub> 6 kg/667m<sup>2</sup>~8 kg/667m<sup>2</sup>，K<sub>2</sub>O 8 kg/667m<sup>2</sup>~10 kg/667m<sup>2</sup>。

#### 7.1.2 壮蘖肥

越冬初期宜施尿素3.0 kg/667m<sup>2</sup>~3.5 kg/667m<sup>2</sup>。

#### 7.1.3 拔节肥

小麦基部第一节间接近定长，宜施尿素6.0 kg/667m<sup>2</sup>~7.0 kg/667m<sup>2</sup>、复合肥7 kg/667m<sup>2</sup>~10 kg/667m<sup>2</sup>。

#### 7.1.4 孕穗肥

小麦叶龄余数为0.5时，施尿素6 kg/667m<sup>2</sup>~7 kg/667m<sup>2</sup>。

### 7.2 灌水

#### 7.2.1 齐苗水

播后1 d~2 d，耕层土壤相对含水量低于60 %应补灌齐苗水。

#### 7.2.2 越冬水

底墒不足(耕层土壤相对含水量≤50 %)应及时冬灌，浇水后及时划锄，增温保墒。

#### 7.2.3 拔节孕穗水

结合拔节孕穗肥施用，在3月下旬，灌水40 m<sup>3</sup>/667m<sup>2</sup>~50 m<sup>3</sup>/667m<sup>2</sup>。

#### 7.2.4 排水

冬春注意清沟理墒，保持沟系畅通，并及时培土。遇苗情干旱时及时镇压。

### 7.3 病虫草害防治

#### 7.3.1 防倒

为建立合理群体，防止倒伏。群体一般控制在42 万穗/667m<sup>2</sup>~45 万穗/667m<sup>2</sup>。

#### 7.3.2 化学除草



根据草相、草龄、墒情等选择药剂，重点做好冬前除草。在播后苗前或者杂草1~2叶时用异丙隆25%可湿性粉剂250 g/667m<sup>2</sup>~300 g/667m<sup>2</sup>喷雾。2月中旬约返青期时，宜用精恶唑禾草灵60 ml/667m<sup>2</sup>~100 ml/667m<sup>2</sup>加75%苯磺隆1.5 g，兑水50 kg均匀喷雾。防治方法及使用药剂参见附录A.2。

### 7.3.3 地下害虫

播种前药剂拌种（详见5.3.2），土壤处理采用毒饵或毒土法，用炒香麦麸、豆饼、米糠等饵料2 kg，50%辛硫磷乳油25 ml，加适量水稀释农药制作毒饵，傍晚撒于田间幼苗根际附近，每隔一定距离一小堆，15 kg/667m<sup>2</sup>~20 kg，或用50%辛硫磷200 ml/667m<sup>2</sup>拌细土30 kg~40 kg，耕翻时撒施；喷雾法，用50%辛硫磷乳油250 ml稀释1500倍，顺麦垄喷施；或用48%毒死蜱乳油100 ml稀释1500倍，顺麦垄喷施，喷药液40 kg/667m<sup>2</sup>。防治方法及使用药剂参见附录A.1。

### 7.3.4 纹枯病

在小麦返青拔节时，当病株率达20%时，可用5%井冈霉素水剂300 ml/667m<sup>2</sup>~400 ml/667m<sup>2</sup>，兑水100 kg，均匀喷雾。防治方法及使用药剂参见附录A.3。

### 7.3.5 白粉病、锈病

早春发病时用15%的三唑酮（粉锈宁）可湿性粉剂20 g/667m<sup>2</sup>~30 g/667m<sup>2</sup>，兑水50 kg喷雾防治。防治方法及使用药剂参见附录A.3。

### 7.3.6 赤霉病

在扬花期宜施50%的多菌灵可湿性粉剂100 g/667m<sup>2</sup>对水50 kg均匀喷雾。防治方法及使用药剂参见附录A.3。

### 7.3.7 蚜虫

小麦扬花至灌浆初期，用吡虫啉可湿性粉剂30 g/667m<sup>2</sup>，或者50%抗蚜威粉剂10 g/667m<sup>2</sup>~15 g/667m<sup>2</sup>兑水50 kg均匀喷雾。防治方法及使用药剂参见附录A.3。

结合病虫害防治进行叶面喷施磷酸二氢钾（100 kg/667m<sup>2</sup>）、尿素（浓度1%~1.5%）或者过磷酸钙浸出液等以提高千粒重，预防早衰。

## 8 收获贮藏

小麦蜡熟末期及时收割，避开烂场雨，防治穗发芽。脱粒后及时晾晒3~4个晴天，使得籽粒含水量降至13%以下，贮藏于通风干燥处。

## 附录 A

(资料性附录)

## 西农 979 小麦病虫害防治方法

## A.1 小麦种衣剂种类及防治对象

小麦种衣剂种类及防治对象参见表A.1。

表A.1 小麦种衣剂种类及防治对象

单位: mL/10 kg种子

药剂种类	防治对象	用 量
12.5 %硅噻菌胺	全蚀病	20
2.5 %咯菌腈	纹枯病、黑穗病、根腐病	20
15 %粉锈宁 50 g/667m <sup>2</sup> ~60g/667m <sup>2</sup>	白粉病、锈病	4
40%毒死蜱乳油	地下害虫、蚜虫	10
50 %辛硫磷	地下害虫	20

## A.2 小麦化学除草剂种类及防治对象

小麦化学除草剂种类及防治对象参见表A.2。

表A.2 小麦化学除草剂种类及防治对象

单位: 株/m<sup>2</sup>

药剂种类	防治对象	防治时期	防治指标	喷施部位
唑草酮、苯磺隆、氯氟吡氧乙酸、 苄嘧磺隆、噻吩磺隆	播娘蒿、荠菜、猪殃殃、 野油菜和繁缕	秋苗期、返青期	30	叶面喷施
精恶唑禾草灵、炔草酸(炔草酸酯、 炔草酯)、甲基二磺隆	野燕麦、硬草、看麦娘	秋苗期、返青期	30	
氟唑磺隆、甲氧磺草胺、阔世玛, 或者精恶唑禾草灵与苯磺隆混用、炔草 酸与苯磺隆混用	禾本科杂草和阔叶杂草混 生	秋苗期、返青期	30	

## A.3 小麦病虫害防治常用药剂及防治对象

小麦病虫害防治常用药剂及防治对象参见表A.3。

表A.3 小麦病虫害防治常用药剂及防治对象

药剂种类	防治对象	防治时期	防治指标
12.5 %烯唑醇可湿性粉剂、50 %多菌 灵可湿性粉剂	纹枯病、茎基 腐病	返青拔节期	病茎率 15%



表 A.3 小麦病虫害防治常用药剂及防治对象(续)

药剂种类	防治对象	防治时期	防治指标
15 %三唑酮可湿性粉剂、烯唑醇(禾果利)可湿性粉剂、12.5 %烯唑醇可湿性粉剂、25 %环丙唑	锈病、白粉病、叶枯病	返青拔节期	病叶率 5 %~10 %或病情指数 15 以上
15 %哒螨灵乳油、1.8 %阿维菌素	红蜘蛛		虫口密度达单行长虫量 $\geq 600$ 头/m
50 %抗蚜威可湿性粉剂	蚜虫		虫口密度达到每株 5 头以上
50 %多菌灵可湿性粉剂、40 %多菌灵胶悬剂、25 %氰烯菌酯悬浮剂	赤霉病	抽穗至成熟期	遇多雨、连阴雨天气,小麦齐穗期喷药预防
10 %吡虫啉可湿性粉剂、50 %抗蚜威可湿性粉剂	粘虫、蚜虫 麦叶蜂		苗蚜百株 100 头、穗蚜百茎 500 头
虫螨克乳油、甲氧菊酯乳油、马拉硫磷乳油、阿维菌素乳油	麦蜘蛛		虫口密度达到单行长虫量 $\geq 600$ 头/m
吡虫啉可湿性粉剂、顺式氯氰菊酯、高效氯氰菊酯乳油	吸浆虫		每方(10cm $\times$ 10cm $\times$ 20cm) 5 头,10 网复次 10 头以上成虫